SYNTHESIS, CHARACTERIZATION AND IN VITRO INVESTIGATION OF NANOCELLULOSE REINFORCED CHITOSAN HYDROGEL FOR ENHANCING BIOAVAILABILITY OF CURCUMIN

THENNAKOON MUDIYANSELAGE SAMPATH UDENI GUNATHILAKE

FACULTY OF ENGINEERING
UNIVERSITY OF MALAYA
KUALA LUMPUR

2019

SYNTHESIS, CHARACTERIZATION AND IN VITRO INVESTIGATION OF NANOCELLULOSE REINFORCED CHITOSAN HYDROGEL FOR ENHANCING BIOAVAILABILITY OF CURCUMIN

THENNAKOON MUDIYANSELAGE SAMPATH UDENI GUNATHILAKE

THESIS SUBMITTED IN FULFILMENT OF THE REQUIREMENTS FOR THE DEGREE OF DOCTOR OF PHILOSOPHY

FACULTY OF ENGINEERING
UNIVERSITY OF MALAYA
KUALA LUMPUR

2019

UNIVERSITY OF MALAYA

ORIGINAL LITERARY WORK DECLARATION

Name of Candidate: Thennakoon Mudiyanselage Sampath Udeni Gunathilake

Matric No: KHA 150058

Name of Degree: Doctor of Philosophy

Title of Thesis: Synthesis, Characterization and In Vitro Investigation of Nanocellulose Reinforced Chitosan Hydrogel for Enhancing Bioavailability of Curcumin

Field of Study: Advance Materials/Nanomaterials

I do solemnly and sincerely declare that:

(1) I am the sole author/writer of this Work;
(2) This Work is original;
(3) Any use of any work in which copyright exists was done by way of fair dealing and for permitted purposes and any excerpt or extract from, or reference to or reproduction of any copyright work has been disclosed expressly and sufficiently and the title of the Work and its authorship have been acknowledged in this Work;
(4) I do not have any actual knowledge nor do I ought reasonably to know that the making of this work constitutes an infringement of any copyright work;
(5) I hereby assign all and every rights in the copyright to this Work to the University of Malaya ("UM"), who henceforth shall be owner of the copyright in this Work and that any reproduction or use in any form or by any means whatsoever is prohibited without the written consent of UM having been first had and obtained;
(6) I am fully aware that if in the course of making this Work I have infringed any copyright whether intentionally or otherwise, I may be subject to legal action or any other action as may be determined by UM.

Candidate's Signature Date:

Subscribed and solemnly declared before,

Witness's Signature Date:

Name:

Designation:

SYNTHESIS, CHARACTERIZATION AND IN VITRO INVESTIGATION OF NANOCELLULOSE REINFORCED CHITOSAN HYDROGEL FOR ENHANCING BIOAVAILABILITY OF CURCUMIN

ABSTRACT

A unique biodegradable, superporous, swellable and pH sensitive nanocellulose reinforced chitosan hydrogel with dynamic mechanical properties was prepared for enhancing bioavailability of curcumin. Rod-shaped cellulose nanocrystals (CNCs) that were approximately 200–300 nm in length and 40–50 nm in width were prepared from microcrystalline cellulose via sulfuric acid hydrolysis. CNC ratios of 0%, 0.5%, 1%, 1.5%, 2%, and 2.5% were selected to study the effects of CNCs on the mechanical properties and swelling behavior of the chitosan hydrogel. The crosslinking reaction between chitosan and glutaraldehyde was confirmed by the presence of a –C═N stretching group at 1548 cm^{-1} in the Fourier transform infrared spectrum of chitosan hydrogel. The crosslinking degree of the chitosan hydrogel was 83.6%. The X-ray diffraction patterns confirmed that adding CNCs induced a combination of amorphous and crystalline regions in the hydrogel matrix. Mechanical tests showed that the maximum compression of the chitosan hydrogel increased from 25.9 ± 1kPa to 50.8 ± 3kPa with increasing CNC content from 0%−2.5%. Field emission scanning electron microscope images revealed that the pore size significantly increased with the formation of widely interconnected porous structure in gas foamed hydrogels. The in vitro degradation rate of hydrogel decreased with the increase of CNC concentration of the hydrogel. Differential scanning calorimetry (DSC) results showed that the thermal stability of the hydrogel increased with the addition of nanocellulose due to the strong interfacial linkage between nanostructured cellulose and chitosan. All the hydrogels showed maximum swelling ratios greater than 300% in distilled water. CNC-chitosan hydrogels exhibited excellent pH sensitivity and producing the maximum swelling ratio

under acidic condition (pH 4.01). As a result of its pH-responsiveness, the CNC/chitosan hydrogel has been evaluated as drug delivery vehicle to the stomach. Curcumin, a less water-soluble drug was used in this study, due to the fact that the fast swellable, superporous hydrogel could release a water-insoluble drug to a great extent. FTIR spectrum indicated that there is no interaction between drug and ingredients present in the hydrogels. The drug release data showed good fitting to Ritger-Peppas model. 0.5% CNC-chitosan hydrogel showed the highest increase of drug encapsulation efficiency and drug release after gas foaming at 40 °C, which was from 41% to 68% and from 0.74 mg/L to 1.61 mg/L, respectively. At the later part of this study, curcumin was extracted using turmeric and incorporated into 0.5% CNC-chitosan hydrogel with a nonionic surfactant (Tween 20), using in situ loading method. The drug release of hydrogel increased from 0.21% ± 0.02% to 54.85% ± 0.77%, with the increase of Tween 20 concentration from 0% to 30% (w/v), after 7.5 h. Moreover, the results revealed that the drug maintained its chemical activity after in vitro release. According to the results of this study, CNC reinforced chitosan hydrogel can be suggested to improve the bioavailability of curcumin for the absorption from stomach and upper intestinal tract.

Keywords: Hydrogel, Chitosan, Nanocellulose, Curcumin

SINTESIS, KARAKTERISASI DAN INVESTIGASI DALAM VITRO KITOSAN HIDROGEL YANG DIPERKUATKAN OLEH NANOSELULOSA UNTUK MENINGKATKAN KETERSEDIAAN BIO TERHADAP CURCUMIN

ABSTRAK

Hidrogel yang unik, biorosot, superporous, mampu bengkak dan sensitif terhadap pH serta mempunyai ciri ciri mekanikal yang dinamik telah disediakan untuk meningkatkan ketersediaan bio terhadap curcumin didalam kitosan yang diperkukuh dengan nanoselulosa. Nanocrystals selulosa (CNCs) yang berbentuk batang, kira-kira 200-300 nm panjang dan 40-50 nm lebar, telah disediakan daripada selulosa microcrystalline melalui asid sulfurik hidrolisis. CNC yang bernisbah 0%, 0.5%, 1%, 1.5%, 2%, dan 2.5% telah dipilih dalam kajian ini untuk mengkaji kesan CNCs atas ciri-ciri mekanikal dan kelakuan bengkak hidrogel kitosan. Curcumin, ubat yang kurang larutan di dalam air digunakan sebab hidrogel yang cepat membengkak dan superporous boleh melepaskan ubat yang bukan air larutan ke tahap yang hebat. Tindak balas silang antara kitosan dan glutaraldehyde telah disahkan oleh kehadiran ─C═N kumpulan regangan di 1548 cm^{-1} dalam spektrum Fourier transformasi inframerah hidrogel kitosan. Tahap penyilangan hidrogel kitosan adalah sebanyak 83.6%. Corak pembelauan sinar-X mengesahkan bahawa penambahan CNCs mendorong gabungan kawasan amorfus dan kristal dalam matriks hidrogel. Ujian mekanikal menunjukkan bahawa mampatan maksimum hidrogel kitosan meningkat dari 25.9 ± 1kPa kepada 50.8 ± 3kPa dengan meningkatkan kandungan CNC dari 0% kepada 2.5%. Pelepasan imej imbasan mikroskop elektron menunjukkan bahawa peningkatan saiz liang yang ketara dengan pembentukan struktur berliang meluas saling di Hidrogel gas berbusa. Kadar degradasi in vitro oleh hidrogel menurun dengan peningkatan kepekatan CNC hidrogel tersebut. Keputusan DSC menunjukkan peningkatan kestabilan terma hidrogel selepas panambahan nanoselulose disebabkan kekuatan interaksi antara selulosa nanostruktur

dan kitosan. Semua Hidrogel menunjukkan nisbah bengkak maksimum yang tinggi daripada 300%. Hidrogel CNC-kitosan mempamerkan sensitiviti kepda pH yang sangat baik dan menghasilkan nisbah bengkak maksimum di bawah keadaan berasid (pH 4.01). Disebabkan oleh pH responsif, CNC/kitosan hidrogel telah dinilai sebagai kenderaan penghantaran ubat ke perut. Curcumin adalah ubat yang kurang melarut dalam air telah digunakan dalam kajian ini. Ini disebabkan keupayaan hidrogel membengkak dengan cepat dan sangat berliang menyababkan ubat yang tidak melarut dalam air dapat dikelurkan dengan laju. Spektrum FTIR menunjukkan bahawa tidak ada interaksi antara ubat-ubatan dan bahan-bahan di dalam Hidrogel. Data pelepasan ubat menunjukkan kesesuai yang baik untuk model Ritger-Peppas. Selepas gas hidrogel berbuih pada suhu yang tinggi, kecekapan pemuatan ubat meningkat daripada 41% kepada 68% dan pengeluaran ubat meningkat daripada 0.74 mg/L kepada 1.61 mg/L. Pada bahagian akhir penyelidikan, curcumin telah diekstrak daripada kunyit dan telah ditambahkan ke dalam CNC-kitosan hidrogel bersama dengan Tween 20, dengan cara percampuran in situ. Selepas 7.5 jam, pengeluaran ubat dari hidrogel meningkat dari 0.21% ± 0.02% ke 54.85% ± 0.77% dengan peningkatan kandungan Tween 20 dari 0% ke 30% (w/v). Selain itu, keputusan mendedahkan bahawa ubat mengekalkan aktiviti kimia selepas pelepasan dalam vitro. Menurut hasil kajian ini, kitosan hidrogel yang diperkukuh dengan CNC boleh dicadangkan untuk meningkatkan bioavailabiliti curcumin untuk penyerapan dari perut dan usus atasan.

Kata kunci: Hidrogel, Kitosan, Nanoselulosa, Curcumin

ACKNOWLEDGEMENTS

Firstly, I would like to express my sincere gratitude to my supervisor Assoc. Prof. Ir. Dr. Ching Yern Chee for the continuous support, patience, motivation, and guidance through the completion of this research study. Your advice and guidance have been of enormous importance to make my PhD program productive and exciting. Further, I would like to thank Prof. Dr. Chuah Cheng Hock for his insightful comments and encouragement. Without his constructive advice and guidance this would not have been completed.

My gratefulness goes to University of Malaya for providing me resources, facilities and the financial aid throughout this research. I would like to thank the technical staffs at faculty of engineering and faculty of science for providing me the assistance and facilities to carry out my research.

I deeply appreciate and thank for the support given from my lab mates and for the great time I have had with them.

Finally, deepest and greatest gratitude goes to my family for their patience, all the dedication and their blessings.

TABLE OF CONTENTS

LIST OF FIGURES

LIST OF TABLES

LIST OF SYMBOLS AND ABBREVIATIONS

AMP	:	2-acrylamido-2-methyl propanesulfonic acid
BMP	:	Bone morphogenetic protein
BSA	:	Bovine serum albumin
CAD	:	Computer-aided design
CMC	:	Carboxymethyl chitosan
CNC	:	Cellulose nanocrystal
EC	:	Ethyl cellulose
FTIR	:	Fourier transform infrared spectroscopy
GA	:	Glutaraldehyde
HA	:	Hyaluronic acid
HPMC	:	Hydroxylpropyl methylcellulose
HPN	:	Hybrid polymer networks
IGF	:	Insulin-like growth factor
IPN	:	Interpenetrating
MBA	:	(N,N-methylenebisacrylamide)
MCC	:	Microcrystalline cellulose
NMR	:	Nuclear magnetic resonance
PAA	:	Poly(acrylic acid)
PBS	:	Phosphate buffered saline
PCL	:	Poly(-caprolactone)
PDI	:	polydispersity index
PDLA	:	Poly(D-lactic acid)
PEO	:	Poly(ethylene oxide)
PLA	:	Poly(lactic acid)

PLGA	:	Poly(lactic-co-glycolic acid)
PLLA	:	Poly(L-lactic acid)
PVA	:	Poly(vinyl alcohol)
RP	:	Rapid prototyping
SA	:	Sodium alginate
SGF	:	Simulated gastric fluid
SPH	:	Super-porous hydrogels
TEMPO	:	2,2,6,6-tetramethyl-piperidinyl-1-oxyl
TGA	:	Thermogravimetric analysis
TOBC	:	TEMPO mediated oxidized bacterial cellulose
UV-Vis	:	Ultraviolet–visible
XRD	:	X-ray diffraction

CHAPTER 1: INTRODUCTION

1.1 Overview

Biopolymers and their derivatives are abundant, varied, and important for living beings; they exhibit special properties and have greater importance for miscellaneous applications. There are primarily two classes of biopolymers, namely, natural biopolymers and synthetic biopolymers. Natural biopolymers are obtained from living organisms (e.g. micro-organisms, plants and animals) and synthetic biopolymers are chemically synthesized from biological starting materials (e.g. starch, sugars, natural fats or oils, etc) (Othman, 2014). Biocomposite materials are materials made from two or more constituent biomaterials that result in significant properties than those of the characteristics of individual components. Biopolymers are generally biocompatible, nontoxic and biodegradable. The properties of environmental friendliness and prospects for sustainable development make them a popular initiative in industrial applications. Many of the applications of biopolymers can be found in the medical field, such as drug delivery systems, surgical implant devices, wound closure and healing products due to possessing of certain properties like, biocompatibility, biodegradation to non-toxic end products, high bio-activity, low antigenicity, ability to support cell growth and proliferation with appropriate mechanical properties, processability to complex shapes with appropriate porosity, as well as maintaining mechanical strength. The introduction of porosity into a biomaterial broadens the scope of applications. Porous materials made from biopolymers having properties such as biocompatibility and biodegradability are of special interest for medical, cosmetic, pharmaceutical, and other applications. Three-dimensional scaffolds for tissue engineering, "green" packaging, delivery matrices and eco-friendly insulating materials are only a few examples of these applications (Gavillon & Budtova, 2007).

Biopolymers can be obtained in different forms (e.g. hydrogels, mesoporous materials, etc). Among them, hydrogels are one of the most interesting since they have the remarkable ability to swell in water or aqueous solvents without dissolution and therefore facilitate the applications such as tissue engineering, drug delivery, wound dressing, hygiene products etc. It‘s not compulsory for life changing developments to be high-tech devices with out-of-sight expectations. Sometimes the simplest contrivance can lead to a greater progress than expensive and advanced technologies. This is true for hydrogels, too. This group of materials has loads of applications that exploit their exceptional ability of loading, retaining and releasing of fluids. They are used for various domestic applications such as diapers, perfume delivery, cosmetics, watering beads for plants; biomedical applications (e.g.plastic surgeries, immunotherapy, vaccine, culture of organs-on chips, tissue engineering, bone regeneration, cardiac applications, dental applications, drug delivery, wound healing, soft contact lenses); applications in electronics (e.g. high-performant cheap capacitors etc.); separation applications (e.g. electrophoresis, bioseparations, proteomic and chromatography); environmental applications (e.g. removal of pollutants such as organic pollutants, heavy metals); microbiological applications (e.g. holding purifying microorganisms for purification of water, holding microorganisms for production of biomolecules). When various types of hydrogels are concerned, biopolymer-based hydrogels may own predominant properties (Gritsch, Motta, Chirani, & Faré, 2015). In general, biopolymers are nontoxic, biocompatible and biodegradable. Therefore, these hydrogels are particularly attractive in green applications (most often used in biomedical applications such as drug delivery and regenerative medicine) (Ahmadi, Oveisi, Samani, & Amoozgar, 2014).

Control of intricate hydrogel features such as porosity and microarchitecture plays a key role toward guiding the development of hydrogel platform for required application.

There are many techniques developed to fabricate porous microarchitecture in the polymer matrices. In this study, gas foaming is being used to fabricate the polymers with high porosity without using any organic solvent (Liu & Ma, 2004). The three basic steps in the gas foaming process are: (1) plasticization due to CO_2 diffusion into the polymer matrix at high pressure; (2) nucleation due to supersaturated gas and depressurization; and (3) gas bubbles growth due to the gas diffusion from the surrounding polymer (Annabi, Fathi, Mithieux, Weiss, & Dehghani, 2011). Skin layer formation and poor pore interconnectivity are common issues in porous fabrication technique. However, these can be overcome by fabrication of polymer matrices using gas foaming method (Dehghani & Annabi, 2011). By tuning the process conditions such as operating pressure, depressurization rate and temperature, the final structure of the product can be modified as required. The porous structure is generated when the discontinuous dispersed gas phase is removed from the continuous phase of polymer. These polymeric foams have low kinetic stability due to the significant difference between the densities of the gas and liquid. The liquid phase tends to move down while the gas tends to move upwards, which leads to the formation of interconnected porous structure with highly porous top surface (Dehghani & Annabi, 2011). The results of the previous studies showed that the solubility of CO_2 dramatically increases as the pressure is increased (0.077 mol CO_2/kg H_2O solubility at 1 bar increases to around 30-fold at 50 bar) (Dodds, Stutzman, & Sollami, 1956; Ji, Annabi, Khademhosseini, & Dehghani, 2011).

Chitosan is a linear polysaccharide produced commercially by deacetylation of chitin, a naturally occurring biopolymer in the exoskeleton of insects, crustaceans and cell walls of fungi. Due to the biological and mechanical properties of chitosan, it has been used to produce powder, hydrogels, membranes, fibers, porous scaffolds and beads that have been investigated with various biological and medical applications. The

process of deacetylation involves the removal of acetyl groups from chitin, leaving behind a reactive amino group ($–NH_2$) and the high adaptability of chitosan for a vast range of applications is mainly due to this highly reactive amino groups (Hussain, Iman, & Maji, 2013). The structure of chitosan is very similar to that of cellulose, except the presence of acetylamino group in place of the hydroxyl group at C–2 position of the cellulose structure. The high viscosity of chitosan solutions is because of the presence of intra- and intermolecular hydrogen bonding interactions between chitosan chains formed by amine and hydroxyl groups (Patel, Prajapati, & Patel, 2007). According to the studies of chain flexibilities of chitosan molecules by Chen, Lin, and Yang (1994), the degree of deacetylation of chitosan that determine the number of intermolecular hydrogen bonds, was found to affect the rigidity of the polymer material. At low pH values, the hydrogen bonding dissociates due to the protonation of the amine groups leading to higher swelling degrees.

Chitosan hydrogels can be fabricated via either physical or chemical crosslinking methods. Chemically crosslinked networks have permanent junctions formed by covalent bonds between polymer chains. There are four types of chemically crosslinked chitosan hydrogels, namely chitosan crosslinked systems, interpenetrating polymer networks (IPN), semi interpenetrating polymer networks (Semi-IPN) and hybrid polymer networks (HPN). The type of crosslinking and the degree of crosslinking influence many of the hydrogel properties such as swelling, mechanical properties and transport of molecules. Physical hydrogels are formed by physical crosslinks include reversible links such as ionic interactions, polyelectrolyte complexes and secondary interactions like networks namely entangled chitosan hydrogels and grafted chitosan hydrogels.

Different types of particles and fibers are reinforced into hydrogels to improve the poor mechanical properties (Chandramohan & Marimuthu, 2011). Previous studies have been carried out in which different particles and fibers have been reinforced to chitosan hydrogel to enhance the thermal, mechanical and biological properties. Nanocelluloses have attracted a considerable attention as a reinforcing agent due to its high crystallinity and high mechanical strength when compared with natural cellulose. The highly crystalline regions of cellulose microfibrils can be extracted using appropriate combination of mechanical, chemical, and enzymatic treatments. Strong acid hydrolysis is typically used to produce CNCs given that strong acids can easily penetrate and hydrolyze amorphous regions, thereby leaving crystalline regions unaffected (George & Sabapathi, 2015). Rod-shaped nanocellulose that is approximately 250–300 nm in length and 10–20 nm in width can be obtained from microcrystalline cellulose via acid hydrolysis (Khoo, Ismail, & Chow, 2016).

Many of the applications of chitosan hydrogel can be found in the medical field, such as drug delivery systems, tissue engineering, tissue repair, wound closure and healing products. Chitosan hydrogel is an attractive matrix for oral drug delivery applications due to its physiochemical properties, biocompatibility and mild gelation properties. Cationic hydrogel like chitosan swells greater at acidic medium due to protonation of free amino groups. The protonated groups cause repulsion between polymer chains and hence are responsible for swelling. This property of hydrogel has been used for the delivery of drugs such as clarithromycin, amoxicillin, metronidazole, ranitidine hydrochloride, curcumin and etc., to the stomach during ulceritis or as an injectable drug delivery carrier (Chavda & Patel, 2010; Majithiya & Murthy, 2005; Rizwan et al., 2017; Yadav, Satish, & Shivakumar, 2007).

Curcumin is a lipophilic, phenolic compound, which is derived from rhizomes of *Curcuma longa*, usually a mixture of three curcuminoids (curcumin, demethocycurcumin, and bisdemethoxycurcumin) (Madhavi & Kagan, 2014). Recent studies indicated that curcumin has a broad range of biological activities such as antimicrobial, antitumor, anti-inflammatory and antioxidant effects. It can suppress the growth of a variety of parasite bacteria and pathogenic fungi, such as *Plasmodium falciparum, Helicobacter pylori***,** *Bacillus subtilis*, *e.t* (Sarkar, De, & Mukhopadhyay, 2016). Among all former studies on the antibacterial activity of curcumin, the most promising result showed against *Helicobacter pylori* (Zorofchian Moghadamtousi et al., 2014). *H. pylori* is a microaerophilic bacterium, which lives in the sticky mucus that lines the stomach. It has attracted great attention as a main cause of peptic ulcer disease. International agency for research on cancer defined *H. pylori* as a group I carcinogenic agent of human gastric cancer (De et al., 2009).

1.2 Problem statement

The use of natural hydrogels in many applications is limited because of their relatively poor mechanical properties (Hoare & Kohane, 2008; Shapiro & Oyen, 2013). The mechanical properties of hydrogels as scaffolds for tissue-engineering can have significant influence on the bioactivity of encapsulated cells. The scaffold should have sufficient mechanical strength to facilitate the initial stages of the growth of tissue (Vazquez, Avila, Díaz, & Hernandez, 2016). Also, adequate mechanical strength is desirable for hydrogels as drug delivery systems (Amin, Rajabnezhad, & Kohli, 2009; Wen, Li, Li, Yin, & Li, 2017). Improved mechanical strength can withstand the pressure during gastric contraction and prolong the gastric retention time (Gupta & Singh, 2012). The gastric forces calculated from high-resolution pill tracking by Laulicht, Tripathi, Schlageter, Kucera, and Mathiowitz (2010) reported that the average cumulative stress summed over the 30 min period prior to gastric emptying is 160,000 ±

70,000 dynes/cm^2 (16 ± 7 kPa) fasted and 520,000 ± 270,000 dynes/cm^2 (52 ± 27 kPa) fed. Hydrogels with less mechanical strength can become fragmented after repetitive gastric contractions and alter the drug release profile.

Tailoring the crosslinking degree is commonly used to control the mechanical properties of the hydrogel. Many crosslinking agents have been proven the ability to enhance mechanical properties of chitosan hydrogel (most often by glutaraldehyde). Recently, nanomaterials have been used as reinforcing agents to improve the mechanical strength and stability of polymer hydrogels (Chang, van Spreeuwel, Zhang, & Varghese, 2010; Park, Lee, & Hyun, 2015). Cellulose nanocrystals (CNCs) have received considerable attention as reinforcing agent because of their favorable properties, such as large surface area, high mechanical strength, low density, non-toxic nature, high aspect ratio, biocompatibility and biodegradability (Ahmed, 2015; Park et al., 2015; Yang et al., 2012; Yang, Bakaic, Hoare, & Cranston, 2013).

In this study, physical reinforcement of cellulose nanocrystal in hydrogel matrix offers a new perspective for the fabrication of chitosan hydrogel with exceptional mechanical properties that may be important for biomedical applications where high strength is required. Nanocellulose reinforced chitosan hydrogel forms a semi-interpenetrating polymer network (semi-IPN) via the diffusion of linear polymer chains into a preformed polymer network. One constituent of the semi-IPN hydrogel is a crosslinked polymer, and the other is a non-crosslinked polymer. The constituent polymers of the semi-IPN can be separated, in principle, from the polymer network without breaking the chemical bonds. A semi-IPN structure improves the mechanical properties of hydrogel and controls its swelling behavior (Shivashankar & Mandal, 2012).

Curcumin (diferuloylmethane) a natural polyphenolic nutraceutical, is a major component of turmeric (*Curcuma longa*) that has been associated with antioxidant, anticancer, anti-inflammatory, antiviral, and antibacterial activities as indicated by over 6,000 citations and over one hundred clinical studies (Prasad, Tyagi, & Aggarwal, 2014). *Helicobacter pylori* (H. pylori) a gram-negative bacterium, is reported as etiologic factor in the development of the chronic gastritis, ulcers and gastric adenocarcinoma. Many studies highlighted the potential of curcumin as a promising antibacterial agent having property to restore and repair the gastric damage caused by *H. pylori* infection. The poor solubility and low bioavailability of curcumin have been highlighted as the major problem that can lead to loss of local therapeutic action in the stomach (Anand, Kunnumakkara, Newman, & Aggarwal, 2007). However, many attempts have been made to improve the pharmacotherapy of the stomach through local drug release, leading to high drug concentration at the gastric mucosa, making it possible to treat stomach and duodenal ulcer, gastritis and esophagitis (Ali, Pandit, Jain, & Dhar, 2014; Arya & Pathak, 2014; Gupta & Aggarwal, 2008; Mahattanadul, 2016; Ridhima, Shweta, & Upendra, 2012; Treesinchai, Puttipipatkhachorn, Pitaksuteepong, & Sungthongjeen, 2016).

Chitosan/CNC hydrogels have been used for various drug delivery applications. Previous studies had reported the use of chitosan/CNC hydrogels as potential drug carrier for procaine hydrochloride and formation of polyelectrolyte-macroion complexes (Akhlaghi, Berry, & Tam, 2013; Wang & Roman, 2011). However, nanocellulose reinforced chitosan hydrogel is not yet investigated or reported for its application as drug delivery system for curcumin. In this study, we used nanocellulose reinforced chitosan hydrogel with improved mechanical properties for oral administration of curcumin. Oral administration is a noninvasive and convenient drug delivery route most preferred by patients. However, poor solubility and low

bioavailability of hydrophobic drugs has greatly limited their oral administration. In this study, we investigated the effect of nanocellulose content and the processing parameters (temperature and pressure) of hydrogel fabrication process (gas foaming) on the drug delivery behavior of the hydrogel. Nanocellulose possesses hydroxyl groups which can form hydrogen bonds with curcumin molecules. It will apparently lead to increase the entrapment efficiency of the hydrogel. Increasing the pressure of the gas forming process will cause higher nucleation density and improvement of porous nature. Gas foaming at high temperature will improve the diffusion rate of gas into the hydrogel matrix forming larger interconnected pore structures. Due to the improvement of porous nature of the hydrogel, greater number of water molecules will enter the hydrogel network, cause swelling, and release of higher amount of drug. Curcumin is a hydrophobic drug which is poorly soluble in aqueous media often has insufficient dissolution and consequently has poor bioavailability after oral administration. If solubility is low there may be incomplete absorption of the drug causing less bioavailability. Therefore, in this study, a non-ionic surfactant (Tween 20) (various concentrations) is incorporated in to the hydrogel to improve the solubility of curcumin in gastric medium and studies are carried out to investigate the effect of Tween 20 on curcumin delivery from the hydrogel. Tween 20, a nonionic surfactant with high HLB value will improve the solubility of hydrophobic drug and drug release as these surfactants are more hydrophilic and water soluble (Sathali & Rajalakshmi, 2010).

1.3 Objectives of research

The main objective of this research is to prepare nanocellulose reinforced chitosan hydrogel with improved mechanical properties and focus on its use for curcumin drug delivery. Two different aspects are focused upon, that are (1) to improve the mechanical strength of the chitosan hydrogel using nanocellulose as reinforcement and (2) to

improve the bioavailability of less water-soluble curcumin using nanocellulose reinforced chitosan hydrogel.

To achieve these objectives, the research design includes the synthesis of nanocellulose reinforced chitosan hydrogel, characterization of the hydrogel and the studies on the drug (curcumin) delivery behavior of the hydrogel in simulated gastric conditions.

The specific objectives of this work are:

1. To prepare nanocellulose reinforced chitosan hydrogel by chemical crosslinking method.
2. To obtain interconnected larger pore structures of the hydrogel using carbon dioxide gas foaming method.
3. To study the mechanical properties, thermal behavior, swelling degree, crystal structure, morphology, crosslinking degree, in vitro degradation behavior of nanocellulose reinforced chitosan hydrogel.
4. To investigate the effect of nanocellulose content and processing parameters (pressure and temperature) of the gas foaming process on the drug (curcumin) delivery behavior of the hydrogel.
5. To investigate the effect of a nonionic surfactant (Tween 20) on the solubility of curcumin and drug (curcumin) delivery behavior of the hydrogel.

1.4 Scope of study

The scope of the study is to prepare nanocellulose reinforced chitosan hydrogel with improved mechanical properties for potential use as a carrier for curcumin drug delivery. Nanocellulose prepared by acid hydrolysis of microcrystalline cellulose was used as reinforcement in the chitosan hydrogel. Nanocellulose reinforced chitosan hydrogel was synthesized using glutaraldehyde as the cross-linking agent. The

crosslinking process of the hydrogel was identified using Fourier transform infrared spectroscopy (FTIR). The dispersion of nanocellulose in the hydrogel matrix was examined by field emission scanning electron microscopy (FESEM).

Large/interconnected pores of the hydrogel were obtained using carbon dioxide gas foaming method. Various pressure and temperature conditions of the gas foaming process was used to improve the porous structure of the hydrogel. The morphology of the gas foamed hydrogel was studies using field emission scanning electron microscopy (FESEM).

The mechanical properties of the hydrogels were analyzed by compression test using a universal/tensile tester. X-ray diffraction studies were carried out to evaluate the crystal structure of the hydrogel. The swelling studies of the hydrogels were carried out in distilled water and in buffer solutions (with pH values of 4.01, 7, and 10.01). The thermal behavior of the hydrogel was investigated using differential scanning calorimetry. In vitro degradation studies of the hydrogels were carried out in phosphate-buffered saline. The degree of crosslinking was determined by undissolved proportion of the hydrogel in acetic acid solution.

The drug (curcumin) was incorporated into the hydrogel via post-loading method and in vitro drug release studies were carried out in simulated gastric medium. The drug content of the release medium was analyzed using UV-Vis spectrophotometer. The effect of nanocellulose content on the drug delivery behavior was studied with varying the nanocellulose concentration of the hydrogel. Also, different pressure and temperature conditions of the gas foaming process was used to fabricate the hydrogel. The effect of hydrogel processing condition on the drug delivery property of the hydrogel was studied by varying the pressure and temperature of the gas foaming process. The interaction between the curcumin and the hydrogel matrix was studied

using FTIR spectroscopy. The drug activity of the hydrogel was studied using UV-Vis spectroscopy.

At the later part of the research, curcumin was extracted from dried rhizomes of *curcuma longa* using methanolic extraction. Extracted curcumin with a nonionic surfactant (Tween 20) was incorporated in to the 0.5% CNC-chitosan hydrogel using in situ loading method. The effect of nonionic surfactant (Tween 20) on the drug delivery behavior of the hydrogel was investigated by varying the nonionic surfactant concentration in the hydrogel formulation. The in vitro drug release studies were carried out in simulated gastric medium. The drug content of the release medium was determined using UV-Vis spectrophotometer.

The improvement of the mechanical properties of the hydrogel confirmed the strong adhesion and interaction between two polysaccharides because of the chemical similarity between their molecules. Gas foaming is used to fabricate superporous hydrogel with large and widely interconnected pore structures. Due to the fast swelling property the super porous hydrogels are widely used for the delivery of poorly water-soluble drugs. A large extent of chitosan matrix swelling is found to occur in acidic medium, hence the drug molecules are expected to diffuse extensively through the swollen gel in to the exterior medium at gastric pH levels. The solubility of a drug is a fundamental parameter in terms of promoting any effect impacting the therapeutic effect of the drug. Nonionic surfactant will facilitate dissolution of the drug by partitioning of drug into the aqueous phase of gastric fluid. On the basis of the findings from this study, the stimuli sensitive, fast swellable, nonionic surfactant incorporated chitosan/nanocellulose hydrogel can be suggested as promising candidate for stomach specific drug delivery of curcumin.

1.5 Outline of the thesis

The thesis consists of five chapters and is organized to describe the background of the study, literature review, methodology, results with data analysis, discussion and conclusions. The details concerning each chapter are summarized below:

Chapter 1 provides a basic introduction about the background and motivation of the study. The problems to be studied are also highlighted in this chapter. The chapter ends with specific research objectives that aim to resolve the identified problems.

Chapter 2 presents a detail literature review about biopolymers, hydrogel, fabrication methods of hydrogel, chitosan hydrogel, reinforcement of chitosan hydrogel, cellulose nanocrystals and curcumin drug delivery systems. This helps to understand the subject matter presented in this research, to identify the problem statement and establishing the objectives and research methodology.

Chapter 3 describes the research methodology of this study, includes the materials, apparatus use for the synthesis, characterization and drug delivery studies of the hydrogel. This chapter also describes the procedures for the synthesis and the characterization of the nanocellulose reinforced chitosan hydrogel (gas foamed hydrogel and hydrogel formed at atmospheric condition). It also includes the detailed testing methods employed for the drug delivery studies of the atmospheric formed hydrogel, gas foamed hydrogel and nonionic surfactant incorporated hydrogel.

Chapter 4 presents the results and its discussion on the characterization of the hydrogel and curcumin drug delivery. The characterization results are presented into two sections. Section one (1) reports the results of the characterization of hydrogels formed at atmospheric condition, and section two (2) presents the results of the characterization of gas foamed hydrogel. The results of drug delivery are divided in to

four sections. Section one (1) explains the results of the drug delivery studies of hydrogels formed at atmospheric condition, and section two (2) shows the results of the drug delivery studies of gas foamed hydrogels (Gas foamed at room temperature). Section three (3) presents the results of the drug delivery studies of gas foamed hydrogels (Gas foamed at 40 °C), then section four (4) indicates the results for the investigation of the effect of a nonionic surfactant on the drug delivery from the hydrogel.

Chapter 5 concludes the findings of this study and recommendations for the future work pertaining to this research.

CHAPTER 2: LITERATURE REVIEW

2.1 Biopolymers

Biopolymers are generally considered an eco-friendly alternative to fossil fuel based polymers due to the renewable resources used to produce them and their biodegradability. Their properties and the possibility of formation of these substances using renewable resources make biopolymers a popular initiative in industrial applications. In recent years, there has been an increasing interest in the use of biodegradable materials for packaging, medicine, agriculture, and other areas (Vroman & Tighzert, 2009).

Biopolymers consist of monomeric units covalently bonded to form larger structures. There are primarily two classes of biopolymers, namely, natural biopolymers and synthetic biopolymers. Natural biopolymers are obtained from living organisms and the synthetic biopolymers represent the long-chain molecules synthesized with biomolecules. Natural biopolymers are further divided into polysaccharides, proteins, polynucleotides, polyisoprenes, and polyesters. Synthetic biopolymers can be classified according to the way of preparation such as, biopolymers synthesized by addition and condensation polymerization reaction are listed separately. Biocomposite materials are materials made from two or more constituent biomaterials that result in significant properties than those of the characteristics of individual components. Biodegradability and other properties of biopolymers strongly depend on the polymer structure. The properties of a polymer can be categorized into three broad classes: (1) intrinsic properties, which are inherent to the polymer itself; (2) processing properties, which refer to the behavior of material during forming; and (3) product properties in principle determined by combinations of intrinsic and processing properties. The practitioner needs more detailed information about processing properties such as viscosity, melt strength, melt flow index at the various stages of production (Othman, 2014).

2.1.1 **Natural biopolymers**

Natural biopolymers are polymers that obtained from living organisms and further divided into polysaccharides, proteins, polynucleotides, polyisoprenes, and polyesters.

2.1.1.1 Cellulose

Cellulose is the most abundant organic polymer on earth. It is an important structural component of the primary cell wall of plant cells and tissues (Pauly & Keegstra, 2008). The building block of the cellulose polymer is monosaccharide glucose molecules. Polymer consists of repeated glucose units attached together by β-1,4 glycosidic linkages as shown in Figure 2.1. β-1,4 glycosidic bond is formed by covalent bonding of oxygen to the C1 of one glucose ring and the C4 of the connecting ring. Three hydroxyl groups containing in the repeating unit and their ability to make hydrogen bonds between cellulose chains responsible for the physical properties of cellulose (Synytsya & Novak, 2014).

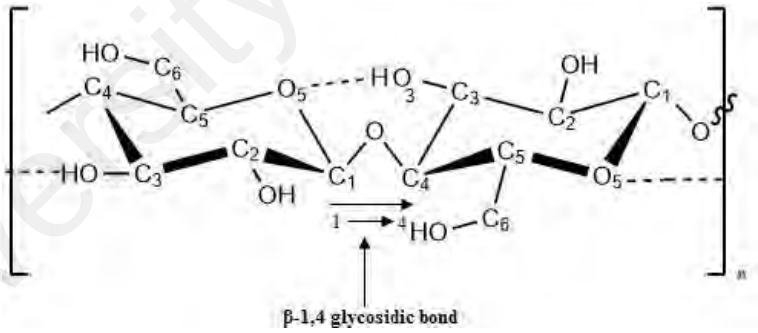

Figure 2.1: β-1,4 glycosidic bond of a cellulose unit

Cellulose can be also synthesized by some species of bacteria (*Acetobacter xylinum*). Bacterial cellulose is similar to plant cellulose in chemical structure, but the lack of contaminant molecules (lignin and hemicelluloses). Hence, it does not require intensive purification methods. Due to the significance of mechanical strength and biocompatibility, cellulose is widely used in tissue engineering applications (Lynd, Weimer, Van Zyl, & Pretorius, 2002).

Cellulose is used as a raw material in industries such as veterinary, foods, fibers, textile, wood, paper, cosmetic and pharmaceuticals. Derivatives of cellulose also play a major role in the applications of fibers, textiles, coatings, thermoplastic films, pharmaceutical technologies and as food additives (El-Sakhawy, Kamel, Salama, & Sarhan, 2014). Development of highly porous structure in cellulose is important because of their potential uses in biomedical applications, filtration, controlled flow of fluids, aircraft, automotive, building and packaging industries (Medina-Gonzalez, Camy, & Condoret, 2012).

2.1.1.2 Collagen

Collagen is the most abundant structural protein in the vertebrate body and major component of bone, connective tissues, skin, cartilage, and tendons. Moreover, collagen is the most abundant protein type of the extracellular matrix of connecting tissues, which provides structural integrity and conferred the mechanical and biochemical properties. At present, 28 types of collagen have been identified, and among these, the dominant collagen present in extracellular matrix, in tissues such as skin, tendon and bone is type I collagen. Type II collagen found in cartilage and type III occurs in adult skin (Chang, Shefelbine, & Buehler, 2012; Shoulders & Raines, 2009).

Collagen protein has a complex hierarchy of structural order in primary, secondary, tertiary and quaternary structures. In primary structure, every third amino acid is a glycine, with strict repeating as shown in Figure 2.2a. About 35% of the non-glycine positions in the repeating unit are consist of proline, can be mostly found in x-position and 4-hydroxyproline, predominant in y-position. In secondary structure, glycine and hydroxyproline units lead to form a helical macromolecule. In tertiary structure, three helical units twist to form a right-handed triple-helical collagen molecule as shown in Figure 2.2b. In quaternary structure, triple-helical collagen molecules stagger into

with various biological and medical applications. High adaptability of chitosan for a vast range of applications is due to a high degree of chemical reactive amino groups present in D-glucosamine residues. When compared with the higher deacetylate chitosan scaffolds, lower deacetylate chitosan scaffolds possess smaller pore sizes, higher mechanical strength, moderate swelling properties and greater cellular activities (Nwe, Furuike, & Tamura, 2009). The chemical structure of chitosan shows in Figure 2.3.

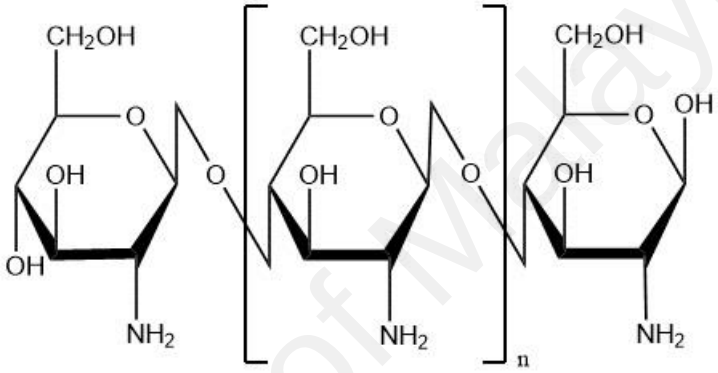

Figure 2.3: Chemical structure of chitosan [poly-(*β*-1/4)-2-amino-2-deoxy-D-glucopyranose]

Chitin may exist in three polymorphic states, the α, β and γ forms, depending on its source. Rhombic α-chitin resembles alternating antiparallel arrangement of polysaccharide chains with strong intermolecular hydrogen bonds found in shells of shrimps, crabs, and other arthropods. β-chitin is mainly found in squid pens and diatoms, characterized by an alternating antiparallel arrangement of polysaccharide chains with weak intermolecular hydrogen bonds (Youn, No, & Prinyawiwatkul, 2013). γ- chitin forms with two parallel polysaccharide chains statistically alternating with an antiparallel chain, which is a combination of α- and β-chitin and found in fungal microorganisms (Zamani & Taherzadeh, 2012).

Molecular weight of chitosan determines its number of biological and physicochemical properties such as biodegradability, viscosity, hydrophilicity,

swellability, crystallinity, tensile strength, moisture content and mucoadhesion. Molecular weight represents an average value of all the molecules present in the sample. Depending on the source of raw material and the processing method the molecular weight of chitosan is in the range of 10–100,000 kDa (Szymańska & Winnicka, 2015; Yuan, Chesnutt, Haggard, & Bumgardner, 2011). There is no a specific standard to define molecular weight, but it has been demonstrated that the molecular weight lower than 50 kDa as low molecular weight chitosan, the molecular weight between 50 - 150 kDa as medium molecular weight and the molecular weight higher than 150 kDa as high molecular weight chitosan (Goy, Britto, & Assis, 2009).

The average molecular weight is determined by number of methods such as light scattering, osmometry, NMR, viscometric assay or chromatographic techniques. The average molecular weight may vary according to these methods and also by the process of deacetylation. In order to ensure chitosan‘s uniformity and proper functionality in the final product, the distribution of the polymer chain weight is determined by polydispersity index (PDI). It is the ratio of weight average molecular weight to number average molecular weight. This gives an idea about the homogeneity of a polymer. The PDI value between 0.85 and 1.15 is considered as having good polymer homogeneity (Szymańska & Winnicka, 2015).

Chitin is a hard, inelastic nitrogenous polysaccharide that is usually insoluble in most of the solvents due to its compact form (Mogilevskaya, Akopova, Zelenetskii, & Ozerin, 2006). Hence, the deacetylation is performed to remove acetyl groups to form a deacetylated derivative called chitosan (Chen, Wang, & Ou, 2004). Deacetylation of chitosan is controlled by processing of native polymer with alkali treatment for different time periods. The degree of deacetylation is the ratio of average number of D-glucosamine units to average number of N-acetylglucosamine units and D-glucosamine

units in the chain. Several methods have been developed to determine the degree of deacetylation such as UV-Vis spectroscopy, infrared spectroscopy, elemental analysis, 1H NMR spectroscopy and 13C NMR spectroscopy (Yuan et al., 2011).

The N-atom of the structure of chitosan unshared electron pair which can potentially donate. At lower pH, the protonation of amino groups cause, with no possibility of donating electrons. Due to the presence of large quantity of amino groups, the pKa value of chitosan is about 6.2-7.0. Therefore, it shows a pH-dependent solubility: it readily soluble in dilute acid solutions and very difficult to dissolve in water or alkaline solution. Chitosan is soluble in many dilute inorganic acids such as HCl, HBr, HI, HNO_3, and $HClO_4$. But, it is slightly soluble in dilute phosphoric acid and sparingly soluble in sulphuric acid at room temperature. The organic acids commonly used for dissolving chitosan are acetic, formic, and lactic acid. 1% acetic acid solution at about pH 4.0 is widely used as a reference. However, the solubility depending on the degree of deacetylation and it is assumed that it must be at least 85% deacetylated in order to achieve the desired solubility (Anusha & Fleming, 2016; Van Toan & Hanh, 2013).

For the commercial production of chitosan, crab shells and shrimp are used as raw materials, which require high production cost and multiple chemical processes such as deproteinization, decolourization and demineralization. Gladius of squid is another rich source of chitosan, which is transparent and a waste material from seafood processing industries. Production of chitosan from gladius is cost-effective due to the absence of coloured compounds. Low impurities of gladius prevent the usage of excess acids and alkaline pollutants. In addition, chitosan from gladius is more soluble, reactive, and swellable than from other sources due to weaker molecular hydrogen bonding (Anusha & Fleming, 2016).

Various grades of chitosan are commercially available depend on the purity, molecular weight and degree of deacetylation, Processing conditions and wide range of chitosan sources can affect the quality and the properties of final product. This might cause deviation of the product from pharmaceutical specifications. Also, the specification data provided by suppliers are often incomplete and it can mislead the pharmaceutical technologies. During the production of chitosan, it may contaminate with impurities, such as heavy metals, ash, or proteins. The purity level of chitosan has an impact on the biological properties such as immunogenicity and biodegradability as well as the solubility and stability. Furthermore, the microbiological contamination may enhance the chitosan degradation via enzymatic hydrolysis. Therefore, in order to comply with the required specifications of specific application, chitosan should be of high purity and free from contaminants and foreign matter (Szymańska & Winnicka, 2015).

2.1.2 **Synthetic biopolymers**

Synthetic biopolymers are chemically synthesized from biological starting materials such as sugars, starch, natural fats or oils (Othman, 2014). Synthetic biopolymers can be classified according to the way of preparation such as, biopolymers synthesized by addition and condensation polymerization reaction are listed separately.

2.1.2.1 Poly(lactic acid)

Among the biobased materials, poly(lactic acid) (PLA) is one of the most promising biomaterials and has remarkable properties, which make it suitable for different applications. It is cheaper and commercially available with wide range of grades. Since the basic monomer unit (lactic acid) synthesized by the fermentation of renewable resources (carbohydrates), PLA complies the concept of sustainable development and is

classified as an eco-friendly material (Jamshidian, Tehrany, Imran, Jacquot, & Desobry, 2010).

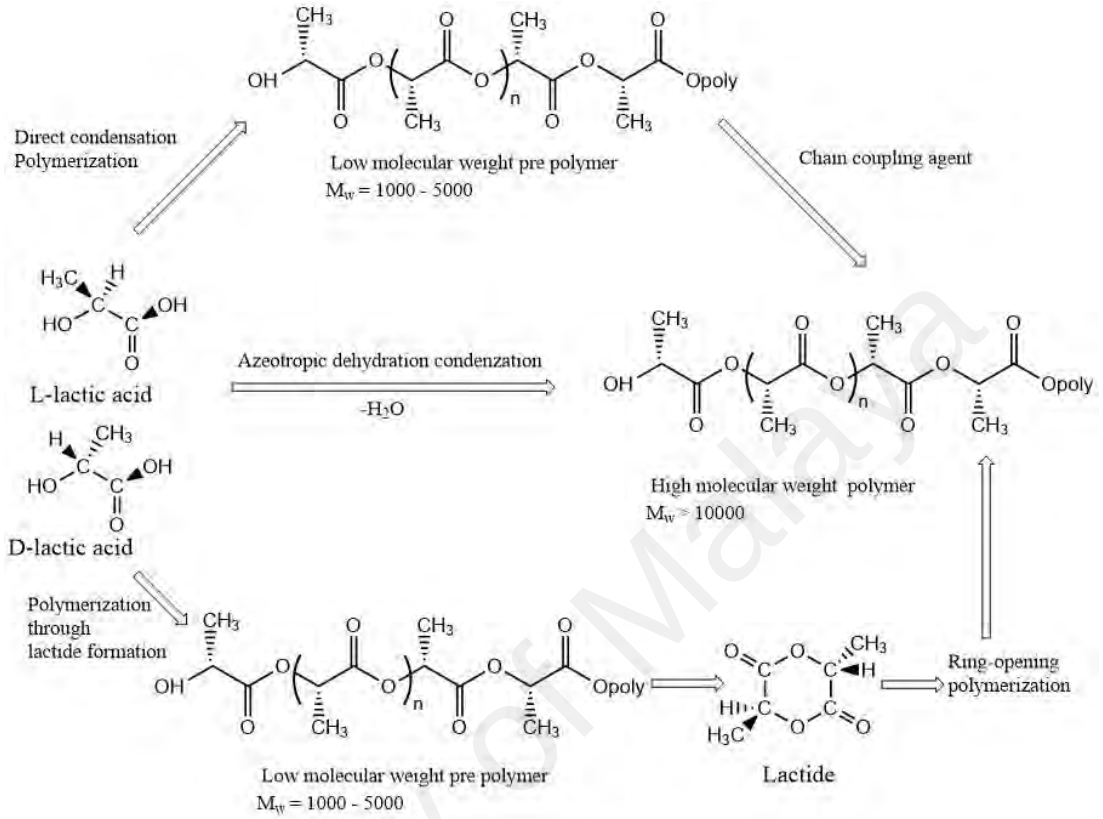

Figure 2.4: Three main routes for obtaining high molecular weight PLA

Figure 2.4 shows the three main routes for the synthesis of PLA. In the first step, lactic acid is condensation-polymerized to form low molecular weight prepolymer and employed with chain coupling agent to increase chain length and to form high molecular weight PLA. The second step involves with azeotropic dehydrative condensation, a one-step process to form high molecular weight PLA from the monomer unit. Third and the main process is a ring-opening process of lactide into high molecular weight PLA which is patented by Cargill (US) in 1992 (Auras, Harte, & Selke, 2004).

2.1.2.2 Poly(lactic-co-glycolic acid)

Poly(lactic-co-glycolic acid) PLGA is synthesized by ring-opening co-polymerization of poly(lactic acid) (PLA) and poly(glycolic acid) (PGA). PLGA also can be prepared by different ratios of its monomeric units. Different types of PLGA can be obtained by the different ratios of monomer units. These are identified according to the ratio of two types of monomers. For instance, PLGA 75:25 refers to a copolymer consists of 75% lactic acid and 25% glycolic acid (Makadia & Siegel, 2011). Figure 2.5 shows the structure of PLGA and its constituent monomers, lactic and glycolic acid.

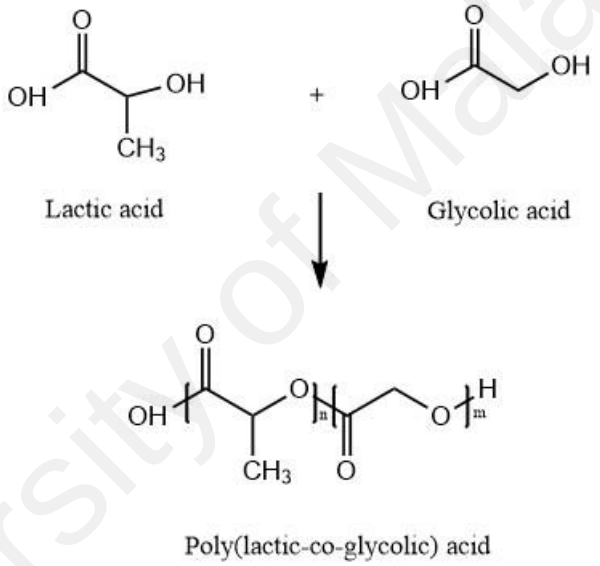

Figure 2.5: PLGA and its constituent monomers, lactic and glycolic acid

Unlike the two types of monomers, PLGA dissolved in a wide range of common solvents such as tetrahydrofuran, chlorinated solvents acetone or ethyl acetate. PLGA degrades by hydrolysis in aqueous environments and produces lactic acid and glycolic acid as byproducts. The degradation rates depend on the molecular weight of the polymer, the ratio of glycolic acid to lactic acid, stereochemistry (depends on the D and L-lactic acid monomers), and end group functionalization (polymers end capped with esters degrades slowly than the presence of free carboxylic acid groups at the end). Since the T_g is above 37 °C, PLGA shows a glassy behavior in nature. It is reported T_g

decreases with decreasing the amount of lactic acid present in the copolymer (Gentile, Chiono, Carmagnola, & Hatton, 2014).

Due to biocompatibility, tailored biodegradation, potential to modify surface properties and ease of fabrication into porous structures, PLGA has considered and are being investigated for a wide range of biomedical applications (Gentile et al., 2014). They are mainly used in pharmaceutical industry to develop drug delivery systems, as a sutures for wound closure and as scaffolding materials for tissue engineering (Azimi, Nourpanah, Rabiee, & Arbab, 2014).

2.1.3 Biocomposite materials

Composite material is a material made from two or more constituent materials that result in significant properties than those of the characteristics of individual components. Composites can be produced with the view of tailoring physical, chemical, or mechanical properties, to fulfill the requirements of different applications such as automotive, aeronautic, naval, and so on (Salernitano & Migliaresi, 2003; Verma, Gope, Maheshwari, & Sharma, 2012).

In view of their potential for high performance, composite biomaterials have been studied and tested for various kinds of applications. To be considered as biocomposite material, each constituent of the composite must be biocompatible. Extreme modifications of the properties of biomaterials can be improved by incorporation of nanosized filler. This properties improvement depends on both nanofiller geometry and on the surface (interface) area. There are three types of nanofillers namely, spherical, layered and acicular, based on their aspect ratio and geometry. A wide range of nanobiocomposites has been produced by introducing nanosized fillers and tested to overcome the conventional drawbacks of biopolymer (Chivrac, Pollet, & Avérous, 2009).

To be successful for the applications, any biomaterial requires a wide range of study about its fabrication and properties. Fabrication of porous structures in biocomposites with various material combinations has become an increased research interest due to their wide range of applications in areas such as tissue engineering, nanocomposites, drug delivery systems, packaging and the automotive industry (Kumar, Negi, Choudhary, & Bhardwaj, 2014).

2.1.3.1 Chitosan/PLA composite materials

PLA is biocompatible and undergoes scission in the body to form lactic acid, which is a natural intermediate in the process of metabolic conversion of carbohydrates. These characteristics make this polymer compatible for use in biomedical applications. However, PLA has several drawbacks such as acidic degradation product, past biodegradation, and hydrophobicity. Chitosan is another biodegradable and biocompatible material, hydrophilic and alkaline in nature, which is widely used in biomedical applications. Acidic byproduct produced by PLA can be readily neutralized due to the alkaline nature of chitosan when using these two polymers as biocomposite material (Li, Ding, & Zhou, 2004).

2.1.3.2 PLA/cellulose nanocomposites

Due to the biocompatibility, PLA is widely used in biomedical applications. The degradation product, lactic acid is also biocompatible due to the possibility of incorporation into the carbohydrate metabolism. However, due to the poor mechanical properties of PLA, various types of fillers such as carbon fibers, carbon nanotubes, hydroxyapatite and cellulose nanocrystals have been introduced for the reinforcement of the polymer (Luo et al., 2014). Cellulose nanocrystals, also known as nanowhiskers, have been introduced as filler for the polymers due to exceptional mechanical properties, high aspect ratio, and large specific surface area. Cellulose nanowhisker can

be obtained from plant cellulose as well as bacterial cellulose. They are exceptionally hydrophilic and show high tensile strength properties (A. Kumar et al., 2014).

2.1.3.3 Cellulose/chitosan composite materials

Cellulose is polysaccharide made from glucose subunits and chitosan is made from amino polysaccharide subunits. The chemical structure of chitosan backbone is very similar to that of cellulose. Therefore, studies have been done to test the miscibility of chitosan with cellulose and introduction of amino groups to cellulose to improve the physical, chemical, mechanical and biological properties of developed composites (Nguyen, Chung, & Park, 2011).

2.1.3.4 Chitosan/ PLGA composite materials

Due to the hydrophobic characteristics of PLGA, it is difficult to apply alone as a biopolymer in many applications like tissue engineering. To overcome these difficulties, composite materials have been made with PLGA by mixing with a hydrophilic biopolymer. Due to the presence of β-(1-4)-linkages between *N*-acetyl-*D*-glucosamine and *D*-glucosamine and the ability of *D*-glucosamine to immobilization of ligands and glycoproteins through covalent bonding, chitosan has been widely used to mix with PLGA to make biocomposite materials, especially related to tissue engineering applications (Kim et al., 2013).

2.1.3.5 Chitosan/collagen composite material

Collagen is a one of promising biomaterial used in tissue engineering applications due to its superior biocompatibility and biodegradability. The main difficulty with collagen as a tissue engineering scaffold is rapid degradation upon exposure to body fluids and cell culture media. Chitosan has been widely used in biomedical applications due to many advantageous such as antibacterial activity, wound healing property, and accelerating tissue regeneration. In addition, chitosan can function as a bridge to

improve the mechanical strength of collagen scaffolds due to the presence of a large number of amino groups attached to its backbone (Peng, Cheng, Wang, Xu, & Wang, 2006).

2.2 Hydrogel

Hydrogels can be defined in many different ways. Among these the most popular one is that hydrogel is a swellable, crosslinked polymeric network that is synthesized by the simple reaction of one or more monomers. Besides that, it is defined as a polymeric network capable of swell and holding significant amount of water within its structure, without undergoing dissolution (Ahmed, 2015). Hydrogel forming polymers have certain hydrophilic groups in their polymeric structure namely amine, hydroxyl, amide and sulphate, which help to absorb more water results in hydrogel expansion, the process which is known as swelling. During the swollen state, crosslinks will prevent the separation of polymer molecules and will prevent dissolution and destruction of the hydrogel. Hydrogels are three-dimensional network structures. Thereby, the driving forces for molecular aggregation are observed. They are called ‗physical' or ‗reversible' gels if the molecular entanglements and/or driving forces are basically bonds based on non-covalent bonds such as hydrogen-bonds, van der Waals, charge transfer, dipole-dipole, π-π stacking and coordination interactions. In chemical or permanent gels, adjacent macromolecular chains are bonded to each other by network of covalent bonds. This can be achieved by crosslinking of polymer in dry state or in solution (Caló & Khutoryanskiy, 2015). Hydrogels have a solid-like appearance due to the entrapment of large amount of liquid (major component of the hydrogel) in the interstices of a solid 3D-matrix with large surface area (minor component of the hydrogel), usually through surface tension and capillary forces. The solid 3D-matrix of the hydrogel is formed by the entanglement of 1D-polymeric consecutive strands of either macromolecules or low molecular weight molecules via covalent or non-covalent

interactions. In general, the diameters of the strands are in the nanometer range and lengths in micrometer range. Consequently, these networks show immobilization of up to 10^5 liquid molecules per gelator molecule (a substance capable of forming a gel, usually with molecular weight lower than 3000 g mol^{-1}) and thereby, enhance the viscosity of the gel by a factor of 10^{10} (Carrillo et al., 2015).

2.2.1 Biopolymer hydrogel

Biopolymers can be obtained in different forms (e.g. hydrogels, mesoporous materials, etc). Among them, hydrogels are one of the most interesting since they have the remarkable ability to swell without dissolution.

2.2.1.1 Chitosan hydrogel

Chitosan, a natural cationic polysaccharide, which exhibits properties that make it desirable for the preparation of hydrogel structures. The polymers commonly used in the preparation of hydrogels have hydrophilic functional groups in their polymeric structure such as amine, amide, hydroxyl and sulphate (Ahmadi et al., 2014). Chitosan is produced by alkaline deacetylation of naturally available chitin, found in exoskeletons of crustaceans, insects and fungi. The deacetylation of chitin involves the removal of acetyl group from the polymer chain of chitin and thereby introducing amino group to the polymer chain. Increase in deacetylation degree of chitin results in higher amount of amino groups and its aqueous solubility (Hussain et al., 2013).

Chitosan hydrogels can be prepared into different formulations, shapes and geometries including liquid gels, beads, tablets, powders, capsules, microspheres, films, microparticles, sponges (porous scaffolds), nanofibrils, textile fibers, and inorganic composites. In each formulation of chitosan is either chemically or physically crosslinked to form the hydrogel (Bhattarai, Gunn, & Zhang, 2010). Chitosan hydrogel has found attention in many different fields such as pharmaceutical, medical,

agricultural, cosmetics and food industries. The biomedical applications of chitosan hydrogel include drug and gene delivery, tissue repair, tissue engineering and wound dressing. The use of chitosan hydrogel in tissue engineering and drug delivery applications is limited due to its low solubility in certain physiological conditions and hydrophilic property. Different properties of chitosan can be achieved via modification at the amino groups or hydroxyl groups. Such modifications have been done through covalent crosslinking, ionic crosslinking, grafting and polyelectrolyte complexes (Giri, Thakur, Alexander, Badwaik, & Tripathi, 2012).

2.2.1.2 Cellulose hydrogel

Cellulose hydrogels can be obtained via physical crosslinking of cellulose solution. Due to the presence of hydroxyl groups, cellulose can arrange into linked hydrogen bond network easily. However, it is less soluble in solutions as a result of its highly extended hydrogen bonded network structure. Recent studies have been introduced new solvents such as ionic liquids , N-methylmorpholine-N-oxide and alkali/urea (or thiourea) aqueous systems, to dissolve the cellulose, providing more possibilities to prepare cellulose hydrogels. Biocompatible water soluble cellulose derivatives such as methyl cellulose, hydroxypropyl cellulose, hydroxypropylmethyl cellulose and carboxymethyl cellulose have been widely used to prepare cellulose-based hydrogels via chemical or physical crosslinking methods. These hydrophobically modified celluloses are substituted partly by hydroxylpropyl or methyl groups, thereby formations of some hydrogen bonds are prevented and the resultant cellulose derivatives become water soluble. In physical crosslinked cellulose gels, hydrogel network is formed via non-covalent bonds such as hydrogen bonding, associative polymer-polymer interaction or ionic bonding. In chemical cross-linked hydrogels, two or more polymer chains crosslink with a functionalized crosslinker or under UV light irradiation to form the network structure (Shen, Shamshina, Berton, Gurau, & Rogers, 2016).

Cellulose-based hydrogels widely used in the applications such as control delivery systems, tissue engineering application, sensor, blood purification, water purification, as well as agriculture and chromatographic supports. Moreover, due to the environmental friendliness and cost effectiveness, it will provide another sustainable alternative for petroleum-based products in near future (Ma, Li, & Bao, 2015).

Bacterial cellulose produced by some microorganism has been used as an attractive candidate for the preparation of cellulose based hydrogels, especially for biomedical applications. Bacterial cellulose is a highly crystalline material with high water-holding capacity, mechanical properties and high biocompatibility. Based on these properties, bacterial cellulose based hydrogels are widely used in biomedical field such as tissue engineering scaffold, dental implant and meniscus implant (Chang & Zhang, 2011).

2.2.1.3 Collagen hydrogel

Collagen hydrogels are popular in many applications because of their biodegradability, low immunogenicity and superior biocompatibility. Although collagen gels consists of three-dimensional network, the use of collagen hydrogel is limited due to poor mechanical strength, rapid biodegradation rate and low thermal stability. Different types of crosslinking agents have been used to improve the mechanical properties and structural integrity of collagen hydrogel. Formaldehyde, dialdehyde, starch, glutaraldehyde, genipin and epoxy compound are the effective crosslinking agents which used for the preparation of collagen hydrogel (Naito et al., 2013).

Glutaraldehyde is commonly used to prepare collagen hydrogel due to its high reactivity, high solubility and low cost. It is often assumed that the aldehyde groups of glutaraldehyde react with ε-amino groups of hydroxylysine or lysine of collagen, forming the corresponding Schiff bases. Previous studies have shown that the viscosity, resistance to deformation, flow and storage modulus of glutaraldehyde-crosslinked

collagen dispersions increased with increasing the concentration of glutaraldehyde (Tian, Liu, & Li, 2016).

Collagen hydrogel has been widely used in cell culture studies (Naito et al., 2013), tissue engineering applications (Hesse et al., 2010), wound dressing applications (Chikazu et al., 2010) and as drug delivery systems (Potdar et al., 2008).

2.2.1.4 Gelatin hydrogel

Gelatin is composed of mixture of fibrous proteins synthesized by acid or alkaline hydrolysis of collagen. Gelatin possesses biomedically favorable properties such as biodegradability, low cytotoxicity, low immunogenicity, and great capacity for potential modification at the level of amino acids. It alone can form physical hydrogels by physical crosslinking in water when exceeding the concentration around 2% w/v and the temperature below 30 ~ 35 °C. During the process of physical gel formation, gelatin molecules aggregate and undergo a conformational transition from a random coil to a triple helix (Bode, da Silva, Drake, Ross-Murphy, & Dreiss, 2011). However, gelatin hydrogels have poor chemical stability and mechanical strength. These properties can be improved by introducing irreversible chemical crosslinks into the gelatin matrix using crosslinking agents such as carbodiimides, glutaraldehyde, and formaldehyde. These crosslinking agents can couple the carboxyl and amine groups by forming stable amide bonds (Foox & Zilberman, 2015).

The restrictions on the application of gelatin in many applications have been overcome by the introduction of other polymers such as oxidized cellulose nanowhiskers, poly(lactic-co-glycolic acid) into the gelatin. However, it is reported that this will cause decrease in superb non-immunogenic property of gelatin. Since gelatin is denatured product of collagen, it may contains divalent metal ions such as calcium, zinc, copper and iron that can form ionic bonds with the carboxylic acid groups of gelatin

molecules which affect the organization of the gelatin network. It is expected that the removal of these metal ions will free the carboxylic acid groups. It will increase the electrostatic interactions between the carboxylic acid groups and amine groups, and improve the crosslinking density upon chemical crosslinking, thereby improving the stability and mechanical strength of the hydrogel (Xing et al., 2014).

Gelatin hydrogels have been widely studied as tissue engineering scaffolds (Zhao et al., 2016), drug delivery carrier (Raafat, 2010), food additive (Baziwane & He, 2003) and packaging material (Kavoosi, Dadfar, Dadfar, Ahmadi, & Niakosari, 2014).

2.2.1.5 Alginate hydrogel

Alginate, also called algin or alginic acid is a naturally occurring anionic polysaccharide found in seaweed, and has been widely used for biomedical applications, due to its low toxicity, biocompatibility, relatively low cost, ability to gel under mild conditions by introducing cations such as Ca^{2+} (Lee & Mooney, 2012). Alginate hydrogels can be formed through ionotropic gelation alginate with multivalent cations (Mg^{2+}, Ca^{2+}, Sr^{2+} and Ba^{2+}). However, ionically crosslinked alginate hydrogel has low mechanical strength, stiffness and toughness, which limits their use in many applications. Therefore, alginate has to be modified via chemical or physical crosslinking process to improve the mechanical performance of the hydrogel (Kaklamani, Cheneler, Grover, Adams, & Bowen, 2014). Thermoresponsive phase transition has also been used for the preparation of alginate hydrogel. Thermosensitive hydrogels can be obtained by the addition of poly(N-isopropylacrylamide) (PNIPAAm) in to alginate hydrogel backbone. The mechanism of phase separation of PNIPAAm is thermally induced release of water molecules bound to the isopropyl side groups above its lower critical solution temperature, causing inter and intra-molecular hydrophobic interactions between isopropyl groups. Covalently crosslinked hydrogels can be

prepared by covalently conjugating methacrylate groups onto the alginate backbone, under UV light and in the presence of a photoinitiator (Andersen, Auk-Emblem, & Dornish, 2015).

Due to the structural similarity to extracellular matrices components of living tissues, alginate hydrogels have been widely used for the applications such as cell transplantation, drug delivery matrices and wound healing applications. Controlled drug delivery systems based on alginate have been used to deliver small chemical drugs to macromolecular proteins, depending on the method of crosslinking and the type of crosslinkers (Eldin, Kamoun, Sofan, & Elbayomi, 2015). Alginate wound dressing materials maintain a physiological moist microenvironment and minimize bacterial infection that promotes wound healing (Qin, 2004). Alginate hydrogels are also promising candidates as scaffolds in tissue engineering applications (Kuo & Ma, 2001).

2.2.1.6 Elastin hydrogel

Protein-based hydrogels are promising candidates for various biomedical applications due to their biocompatibility, amino acid composition and ease of handling in the in vivo environment. Elastin-like polypeptides possess unique characteristics such as reversible thermoresponsive nature, mechanical properties, modular designs and biocompatibility, which make them promising candidates for different applications such as tissue engineering, thermal purification components, thermoresponsive drug delivery matrices and self-assembly building blocks. Elastin hydrogels can be synthesized by physical or chemical crosslinking methods. Elastin-like polypeptides agglomerates above the lower critical solution temperature forming viscous liquids, that can be used as cell injectable delivery systems or as cell carriers. More stable hydrogels can be formed by chemical crosslinking of elastin-like polypeptides. Chemical crosslinking can be achieved by chemical functionalization of polypeptide sequence using carbodiimide

reactions, glutaraldehyde crosslinking or via the reaction of carboxyl or amine groups in the protein molecule (Y. N. Zhang et al., 2015).

Elastin based hydrogels have been used as tissue engineering scaffolds for lung tissue engineering (Dunphy, Bratt, Akram, Forsyth, & El Haj, 2014), cardiac tissue engineering (Bozzini et al., 2011) and vascular tissue engineering (Annabi et al., 2013) due to its elasticity, biocompatibility and high mechanical properties. Elastin based hydrogel systems have been utilized for wound dressing applications, which require a combination of flexibility and elasticity properties to adjust to wounds with moving tissue parts or complex geometry (Vasconcelos, Gomes, & Cavaco-Paulo, 2012; Zeng et al., 2016).

2.3 Fabrication methods of porous hydrogel

The introduction of porosity into a biomaterial broadens the scope of applications. Porous materials made from biopolymers having properties such as biocompatibility and biodegradability are of special interest for medical, cosmetic, pharmaceutical, and other applications. Three-dimensional scaffolds for tissue engineering, wound healing materials, "green" packaging, delivery matrices and eco-friendly insulating materials are only a few examples of these applications (Gavillon & Budtova, 2007).

Total porosity is one of the important structural parameters of a matrix to be used as a porous biomaterial. Total porosity is defined as the ratio of the total pore volume, to the overall (or bulk) volume. However, for certain applications, total porosity alone does not have a direct impact on its features. Pore size and pore interconnectivity is more important. Usually, high total porosity accomplished by poor mechanical properties. Inside a porous biopolymer, there may be closed (isolated) pores and open (connected) pores. Pore interconnectivity is important for the accessible of gas, liquid, and particulate suspensions. Pore interconnectivity is defined as the ratio of the pore

homogeneous interconnected pores structures of the scaffold are required for the development of scaffold for tissue engineering applications. Ideal pore sizes vary for different cells and tissues. Porous controlled-release systems should contain pores that are sufficiently large to enable diffusion of the drug (Dhandayuthapani, Yoshida, Maekawa, & Kumar, 2011).

Fabrication methods for biobased porous materials are more related to the choice of material. This can be classified into three main types. First, natural polymers, such as collagen and chitosan, are heat sensitive, so freeze-drying is mainly used to produce porosity, although electrospinning is also possible. Secondly, synthetic polymers, such as PLGA and PLA, often known as thermoplastics, so they can be fabricated by a wide variety of techniques. Bioceramics, such as hydroxyapatite and tricalcium phosphate usually introduce as additives into polymeric matrices since pure ceramic matrices suffer from low hardness. Freeze-drying can be used to fabricate pure ceramic biomaterials, but this needs the use of sintering as a post-processing step which leads to additional porosity within the matrix walls (Ashworth, Best, & Cameron, 2014).

Porous fabrication techniques can be categorized into two categories, designed manufacturing techniques and non-designed manufacturing techniques. Designed manufacturing techniques include 3D printing, rapid prototyping of solid free-form technologies. Non-designed manufacturing techniques include freeze-drying or emulsion freezing, solvent casting or particulate leaching, gas foaming, phase separation, electrospinning and combination of these techniques.

2.3.1 Solvent casting and particulate leaching

Solvent casting and particulate leaching is one of easy and cheapest way of porous scaffold fabrication. Figure 2.7 shows the detailed process of solvent casting-particulate leaching fabrication technique. The polymer is first dissolved in an organic solvent.

Particles, mainly water-soluble salts (e.g. sodium chloride, sodium citrate) with specific dimension are then added to the solution. After that, the mixture is poured into a mold of the desired shape. Next, the solvent is removed either by lyophilization or evaporation and allowed salt particles leached into the polymer matrix. Finally, the mold is dipped in a water bath for sufficient time to dissolve the salt particles, leached inside the polymer matrix. Porosity and pore size can be easily controlled by the amount and the size of salt particles added to the matrix. Though, difficulty confronted in the removal of leached salt particles from the matrix limits the thickness of the matrix to 0.5-2 mm (Mallick, Tripathi, & Srivastava, 2015).

Interconnected porous chitosan scaffold was prepared using sodium acetate particulate leaching method. Sodium acetate was mixed with chitosan solution and injected into the mold. Then mold was freeze dried and lyophilized to evaporate the solvent. After that, washed with series of ethanol solution (100, 90, 80, 70 and 50% v/v) sequentially for 2 h each and salt-leached in distilled water for 48 h. Finally, freeze-dried at −70 °C for 24 h and lyophilized for 24 h. It was observed that the porosity and pore interconnectivity increased with increasing the ratio of sodium acetate. Moreover, with 90 % sodium acetate, many minute pores (7– 30 μm) were formed between the main pores (200–500 μm) (Lim, Lee, Shin, & Lim, 2011).

structures (Yang, Wu, Liang, Wan, & Xu, 2013). The advantages of this method are simplicity of the process, high reproducibility, low defects rate, high porosity and narrow pore size distribution (Kim, Kim, Lee, & Drioli, 2016).

Nano-hydroxyapatite/poly(L-lactic acid) composite scaffold was developed using phase separation technique for bone tissue engineering applications. The porosity more than 90% was easily achieved and the pore sizes were able to adjust by varying the phase separation parameters (Wei & Ma, 2004).

PLLA/PLA scaffolds were prepared via thermally induced phase separation starting from ternary systems where dioxane as the solvent and water as the non-solvent. The porosity was within the range from 87% to 92%. Average pore size, pore distribution, pore interconnectivity and mechanical properties were dependeded on the combination of the operating conditions such as solvent/non-solvent ratio, polymer concentration, remixing temperature and time (La Carrubba, Pavia, Brucato, & Piccarolo, 2008).

2.3.3 Gas foaming

Gas foaming is being used to fabricate the polymers with high porosity without using any organic solvent (Liu & Ma, 2004). This technique uses high-pressure CO_2 for saturation of the polymer in an isolated chamber for a certain period of time. It needs high-pressure CO_2 (800 psi) to saturate the polymer with gas (Sachlos & Czernuszka, 2003). When the polymer is saturated with CO_2 at high-pressure, intermolecular interactions between CO_2 and the polymer molecules become higher and causes a reduction of glass transition temperature of the polymer. Rapid depressurization causes thermodynamic instability and leads to form nucleated gas cells creating pores inside the polymer matrix. This technique is suitable for amorphous and semicrystalline polymers having relatively low T_g or Tm and high affinity for CO_2 (Poursamar et al.,

2015). Instead of carbon dioxide, nitrogen gas can also be used for this method. Figure 2.8 displays the schematic diagram of a CO_2 gas foaming device.

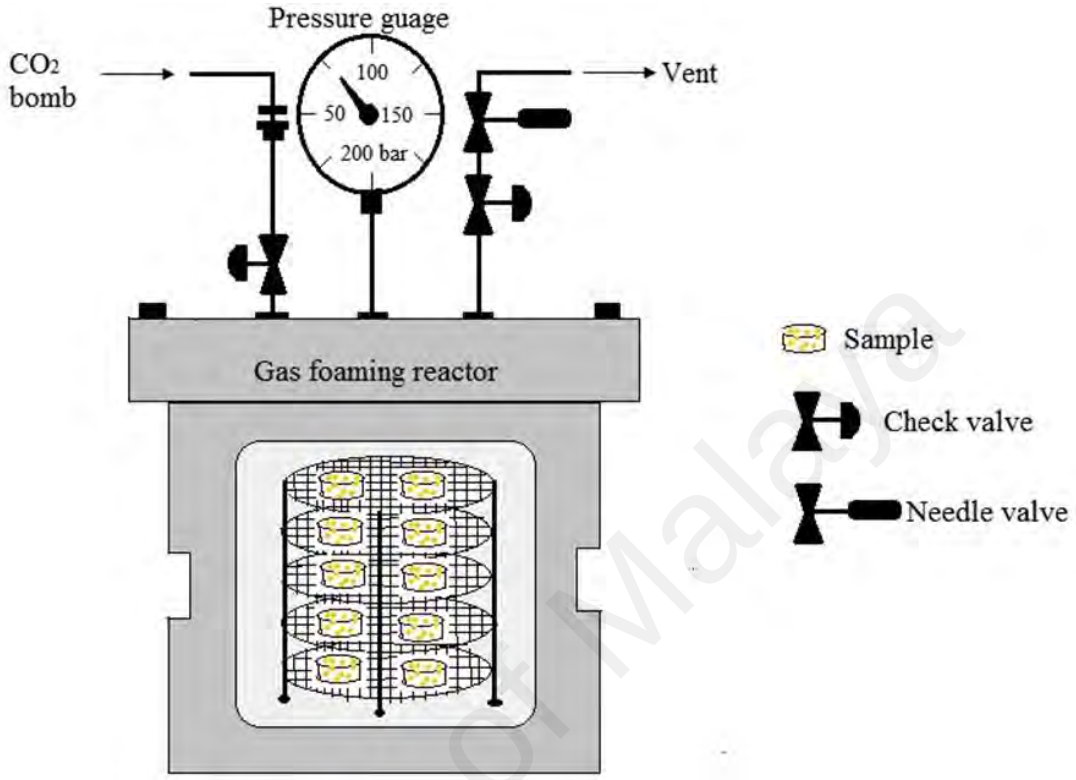

Figure 2.8: The schematic diagram of CO_2 gas foaming device

The effect of high-pressure CO_2 on the characteristics of elastin-based hybrid hydrogel was investigated. Compared to fabrication at atmospheric pressure condition, fabrication at high-pressure CO_2 eliminated the skin-like layer formation on top of the hydrogel and formed larger pores with an average pore size of 78 ± 17 μm. However, the swelling ratio of the hydrogels fabricated at high-pressure CO_2 decreased due to the higher degree of crosslinking. In addition, dense gas CO_2 substantially increased the compressive and tensile modulus of fabricated hydrogels (Annabi, Mithieux, Weiss, & Dehghani, 2010).

2.3.4 Emulsion freeze-drying

In this method polymer is dissolved in its solvent and water is added and then polymer solvent solution and water homogenized to form an emulsion. Before the

2.3.5 Rapid prototyping technique

Rapid prototyping, generally known as solid freeform fabrication technique and one of the most promising techniques for designing and producing scaffolds with 100% interconnected pores, fully computer controlled architecture with high porosities (Sobral, Caridade, Sousa, Mano, & Reis, 2011; Torabi, Farjood, & Hamedani, 2014). The inherent limitations such as long fabrication periods, incomplete removal of residual chemicals or volatile porogenic elements, labor intensive processes, poor repeatability, insufficient interconnectivity of pores and thin wall structures, irregularly shaped pores, of the conventional methods have led to use the rapid prototyping techniques to customize design and fabricate 3D porous scaffolds (Alvarez & Nakajima, 2009; Hoque, Chuan, & Pashby, 2012). All current rapid prototyping techniques are based on the use of computer-aided design information that is converted to a stereo lithography type file format. Rapid prototype machine software processes this file to produce a solid model by a variety of processes. Starting from the bottom, the first layer of the physical model is created. The next layer is glued or bonded to the previous layer. This process is continued until the whole model is completed. Any supports are removed from the finished surface model and cleaned (Stanek et al., 2012). Figure 2.10 displays the schematic diagram of rapid prototyping technique. Main advantages of rapid prototyping process are rapid processing time, customization and efficiency (Peltola, Melchels, Grijpma, & Kellomäki, 2008). Limitations of this techniques are high machine cost, high processing temperatures limiting the ability to process temperature-sensitive polymers, and need of multidisciplinary collaboration (Abdelaal & Darwish, 2011).

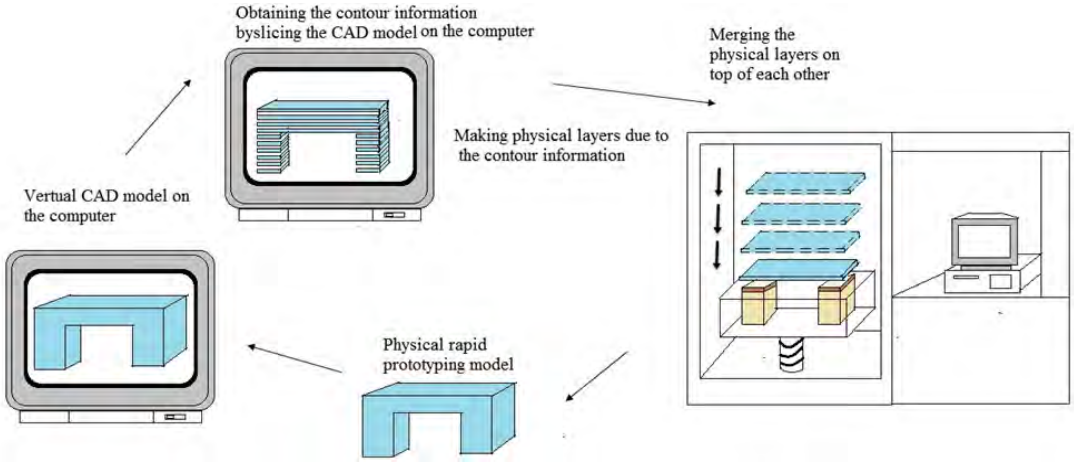

Figure 2.10: The schematic diagram of rapid prototyping technique

Hybrid poly(l-lactide)/chitosan scaffolds were developed using the rapid freeze prototyping technique. It was found that the mechanical properties of the scaffolds depend on the ratio of chitosan microspheres to poly(l-lactide) and cryogenic temperature used in the rapid freeze prototyping fabrication process. The results showed that the scaffolds possessed greater porosity and enhanced pore size distribution compared to dispensing-based rapid prototyping technique (Zhu, Li, Cooper, & Chen, 2011).

2.3.6 3D printing

3D printing, also known as additive manufacturing, and inkjet printing liquid binder is used to make a three-dimensional object from digital model data. This technique involves printing liquid binder to bind the loose powder to create 3D objects. Since biomaterials widely exist as solid or liquid form, most of them can be directly utilized in this technology. The first step of 3D printing is modeling of virtual model from computer-aided design (CAD) or animation modeling software. The machine uses these data as a guideline to print (Li et al., 2014). Then, a thin layer of powder is deposited onto the building platform. In the printing step, the machine reads the design from digital model data and a printer head selectively lay down liquid binder solution onto a powder bed to form the 2D pattern. This process is repeated layer by layer until the

material/binder layering is completed and the final 3D model has been printed. Final objects are extracted from the powder bed by removing or dissolving the unbound powder (Cox, Thornby, Gibbons, Williams, & Mallick, 2015). Pore size and the spacing can be controlled by the pattern used. The advantage of 3D printing is the control of pore size and distribution. Both rapid prototyping (RP) and 3D printing technologies build models layer by layer using computer-aided design. But, there are still some differences such as 3D printers usually make smaller parts, 3D printing costs less, less material choices for 3D printers, 3D printers are less complex and easier to use than rapid prototyping machines. Figure 2.11 displays the schematic diagram of rapid prototyping technique.

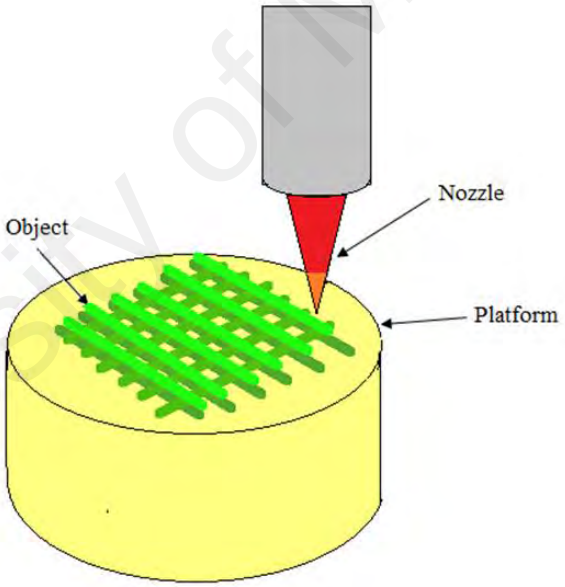

Figure 2.11: The schematic diagram of 3D printing technique

Cylindrical scaffolds of five different designs were fabricated using a unique blend of starch-based polymer powders (cornstarch, dextran and gelatin) by 3D printing process. It was observed that the scaffold porosity corresponded to the designed porosities. A unique microporosity resulted due to the voids formed between granules or particles of the bulk material. Microporosity of the scaffolds of all designs were found to be within the range of 0.335-0.590. A highly interconnected porous network with

suitable mechanical properties was fabricated using 3D printing process (Lam, Mo, Teoh, & Hutmacher, 2002).

Indirect 3D printing protocol was employed to overcome the limitations of the direct technique for the preparation of porous scaffolds. 3D structures were fabricated by inkjet printing liquid binder droplets onto particulate matter. In indirect 3D printing protocol, molds are printed and the final materials are cast into the mold cavity. Scanning electron micrographs showed that well interconnected, highly open, uniform pore architecture (~100–150 μm), which is essential for uniform cell seeding, proliferation, growth, and migration in three dimensions (Lee, Dunn, & Wu, 2005).

2.3.7 Electrospinning technique

A combination of two techniques namely electrospray and spinning is applied in electrospinning technique to form loosely connected 3D porous mats with high porosity and high surface area. A high electric field is applied to a fluid or melt which may extrude from a metallic syringe needle and acts as one of the electrodes as shown in Figure 2.12. When the electrostatic forces overcome the liquid surface tension forces, the droplet comes to the end of the needle and deformed (Shi et al., 2015). Then a fine, charged jet of the polymer solution is ejected from the tip of the needle to the counter electrode leading to the formation of continuous fibers. The fiber diameter and porosity of the matrix depend on the parameters such as voltage, polymer flow rate, the distance between the needle and the plate, and polymer concentration in the solution (Agarwal, Wendorff, & Greiner, 2008). A wide range of polymers can be used in this technique such as synthetic polymers, natural polymers or a blend of both. The most important thing in electrospinning is that it can be used with various polymers, both in solution and in melt form. In melt electrospinning, it does not require the dissolution of the polymer in organic solvent, therefore it is environmentally safe and no mass loss due to

Electrospun poly(-caprolactone)/chitosan nanofibers were prepared to study the effects of chitosan concentration on the bovine serum albumin (BSA) protein release behavior. Poly(-caprolactone) (PCL) and chitosan nanofibers with different ratios of chitosan were electrospun with using formic acid/acetic acid solvent system. Based on the scanning electron micrograph images a higher fiber diameter and pore size exhibited with increasing the chitosan content in nanofiber. In addition, compared to PCL/chitosan nanofibers, PCL/chitosan/BSA nanofibers showed higher fiber diameter and larger pore size. Results showed that the chitosan ratio affected significantly in the protein release profile from the PCL/chitosan/BSA blend (Roozbahani, Sultana, Almasi, & Naghizadeh, 2015).

2.4 Chitosan hydrogel

Preparation of hydrogels from bio-based materials offer certain advantages over synthetic polymers in terms of biocompatibility and biodegradability. The hydrogels prepared from chitosan have been the most commonly used biomaterials in biomedical field such as tissue engineering scaffolds, enzyme immobilization, wound healing materials and drug delivery matrices (Grijalvo, Mayr, Eritja, & Díaz, 2016). Chitosan hydrogel can be categorized in to two different classes based on the method of chitosan crosslinking and preparation, namely physical or chemical hydrogels. Chemically crosslinked networks have permanent junctions, formed by covalent bonding between polymer chains. There are four types of chemically crosslinked chitosan hydrogels, namely chitosan crosslinked systems, hybrid polymer networks (HPN), interpenetrating polymer networks (IPN), and semi interpenetrating polymer networks (Semi-IPN).

In hybrid hydrogel networks, the crosslinking occurs between chitosan chains and the other polymer units, even if crosslinking of two structural units of the same type and/or belonging to the same polymeric chain cannot be excluded (Rodrigues, de

Camargo Forte, Azambuja, & Castagno, 2007). In order to obtain required mechanical and biological properties, combinations of natural and synthetic polymers have been widely used for the preparation of HPN hydrogels.

Crosslinked polymer networks can be further strengthen by interlacing secondary polymers within the crosslinked networks. In IPN hydrogels, at least one network is synthesized and/or crosslinked in the presence of the other. IPNs are synthesized in order to confer the key properties of one of the components while maintaining the critical attributes of another. Sometimes surprising properties are observed by the IPN which are not exhibited in either of the two single components alone. In semi-IPNs, where only one of the polymer networks is crosslinked, while the second polymer remains in its linear state (Bhattarai et al., 2010; Myung et al., 2008). There are several chitosan-based semi-IPNs have been formed with polyether (Lee, Kim, & Lee, 2000; Yao et al., 1998), silk (She et al., 2008), poly(ethylene oxide) (Gupta & Kumar, 2001) and poly(vinyl pyrrolidone) (Risbud, Hardikar, Bhat, & Bhonde, 2000). This technique can be used to select polymers which can complement the deficiencies of one another. With the development of IPN-based hydrogels, the hydrogel porosity, crosslinking density, and gel stiffness can be controlled based on the requirement of the targeted application (Bhattarai et al., 2010).

Chemical crosslinked chitosan networks can be synthesized using the available amine and hydroxyl groups situated in chitosan chains. Specifically, these types of crosslinking can occur via crosslinkers or photopolymerization reaction. Many bifunctional small molecules have been utilized to crosslink chitosan polymers include dialdehyde compounds such as glutaraldehyde and other reagents like genipin, palladium cation, diisocyanate, and acrylic acid diglycidyl ether. Chemically crosslinked chitosan hydrogels possess high mechanical strength compared to physical

hydrogels. The biocompatibilities of some crosslinkers are unknown, while others have been found to be relatively toxic (Ahmadi et al., 2014; Bhattarai et al., 2010).

Genipin, is a naturally derived chemical crosslinker obtained from the gardenia, widely used for tissue fixation, drug delivery and food industries due to its less toxicity and higher biocompatibility when compared to other crosslinkers such as glutaraldehyde. Genipine-crosslinked chitosan hydrogels exhibit slower degradation rate than their glutaraldehyde crosslinked counterpart (Bhattarai et al., 2010). The reaction mechanisms of crosslinking between chitosan and genipin are pH dependent. Under alkaline conditions, the ring-opening reaction is initiated by nucleophilic attack on C-1 of deoxyloganin aglycone by hydroxyl ions in aqueous solution, followed by opening the dihydropyran ring, which subsequently undergoes an aldol condensation. At neutral and acidic conditions, genipin reacts with primary amino groups on chitosan, followed by opening the dihydropyran ring and attacked by the secondary amino group on the newly formed aldehydo group (Muzzarelli, 2009). Crosslinking reaction between genipin and chitosan can be characterized by Fourier-transform infrared spectroscopy (FTIR). By comparison of the FTIR spectra of uncrosslinked and genipin crosslinked chitosan, Mirzaei, Faridi-Majidi, Shokrgozar, and Asghari Paskiabi (2014) indicated the appearance of new broad peak around 1415 cm^{-1} in genipin crosslinked chitosan spectrum, which was due to the presence of ring stretching of heterocyclic amine. Mi, Tan, Liang, Huang, and Sung (2001) reported that the crosslinking of chitosan with genipin decreased the swelling ratio, tensile strain and degradability of chitosan membrane. Chiono et al. (2008) showed that the optimal compositions of genipin crosslinked chitosan/gelatin blends supported the neuroblastoma cell adhesion and proliferation. Studies on controlled release bovine serum albumin by Karnchanajindanun, Srisa-ard, and Baimark (2011) demonstrated that genipin

crosslinked chitosan microspheres could be successfully use for protein drug delivery systems.

Glutaraldehyde, the most widely used crosslinking agent, due efficient stabilization of biomaterials, easy accessibility, and the effective crosslinking ability of its aqueous solutions with biomaterials (Reddy, Reddy, & Jiang, 2015). It has been commonly used to crosslink biopolymers for medical use such as for synthesis of hydrogel, enzyme and cell immobilization. The dialdehyde groups of glutaraldehyde are highly reactive and forms covalent bonds with reactive functional groups such as thiols, amines, hydroxyl, phenols and imidazoles (Migneault, Dartiguenave, Bertrand, & Waldron, 2004). The active aldehyde groups of glutaraldehyde easily, covalently crosslink with amine functional groups of chitosan. The mechanism involves the formation of imine, or Schiff base via nucleophilic attack by amines of chitosan on the electrophilic C atoms of aldehydes, which displaces C═O bond by a C═N bond. Crosslinking reaction between glutaraldehyde and chitosan can be identified by Fourier-transform infrared spectroscopy (FTIR) (Kildeeva, Perminov, Vladimirov, Novikov, & Mikhailov, 2009). By comparison of the FTIR spectra of uncrosslinked and glutaraldehyde crosslinked chitosan, B. Li et al. (2013) indicated the appearance of new sharp peak at 1610 cm^{-1} in the FTIR spectrum of glutaraldehyde crosslinked chitosan, due to the stretching vibrations of C═N in Schiff base formed due to the reaction between glutaraldehyde and chitosan. Jameela and Jayakrishnan (1995) prepared chitosan microspheres crosslinked with glutaraldehyde for controlled release of antineoplastic agent, mitoxantrone. They found that the drug release could be effectively controlled by the extent of cross-linking. From the studies of antibacterial activity of glutaraldehyde crosslinked chitosan, B. Li et al. (2013) investigated that glutaraldehyde crosslinked chitosan markedly inhibited the growth of antibiotic resistant bacterial species. Besides

that, Kawase et al. (1997) showed that glutaraldehyde crosslinked chitosan can be used as a scaffold for hepatocyte attachment.

The other method of synthesis of covalently crosslinked chitosan hydrogel is photochemical processes of photopolymer crosslinking, initialized by visible or UV irradiation. UV or visible light can interact with photoinitiator molecules to create free radicals which initiates photo polymerization to form crosslinked hydrogel (Ahmadi et al., 2014). The main advantage of this method is that in situ formation of hydrogels from aqueous precursors, which can be used in vivo for several biomedical applications such as tissue adhesive in punctures, subcutaneous injection or in different surgeries. Photopolymerization can be used to overcome the limitations associated with chemical crosslinkers such as toxicity of most monomers and organic solvents. Since the photopolymerization conditions are sufficiently mild (low organic solvent levels, low light intensity, physiological temperature and short irradiation time), the crosslinking reaction can be carried out in the presence of cells and tissues. Moreover, the polymeric reaction can be adjusted by controlling the distance and duration of exposure of UV or visible light (Nguyen & West, 2002).

Physical hydrogels are synthesized by physical crosslinks including reversible links such as polyelectrolyte complexes, ionic interactions and secondary interactions like networks named entangled chitosan hydrogels or grafted chitosan hydrogel networks. Chitosan is a cationic polyelectrolyte polysaccharide with ionizable amine groups. Anions are often introducing as ionic crosslinkers to prepare ionically crosslinked chitosan hydrogels (e.g. phosphate bearing molecules like tripolyphosphate) (Bhattarai et al., 2010). The protonated amine groups of chitosan interact with anionic groups of other polymers and form complex polyelectrolyte hydrogels. Since chitosan is positively charged, negatively charged polymers from natural origin such as alginate,

pectin, chondroitin sulfate, xanthan gum, carrageenan, dextran sulfate or hyaluronic acid or polymers from synthetic origin like polylactic acid, polyphosphoric acid or polyacrylic acid have been used to form polyelectrolyte complexes. However, the main limitation of the formation of polyelectrolyte complex hydrogels is that both polymers need to be ionized and oppositely charged. Solubility of the resulting complex also depends on the net charge. If the net charge is zero, the precipitation of the polyelectrolyte complex is quite common (Hamman, 2010).

2.4.1 Applications of chitosan hydrogel

Many of the applications of chitosan hydrogel can be found in the medical field, such as drug delivery systems, tissue engineering, tissue repair, wound closure and healing products due to the possessing of certain properties like, biocompatibility, biodegradation to non-toxic end products, high bio-activity, low antigenicity, ability to support cell growth and proliferation with appropriate mechanical properties as well as processability to complex shapes with appropriate porosity (Cheung, Ng, Wong, & Chan, 2015).

2.4.1.1 Tissue engineering

Disease, injury, or trauma can damage tissues, and treatments are needed to facilitate the repair, replacement, or regeneration of damaged tissues in the human body. Typical treatments include tissue transplantation from one site of the body to another or from one individual to another. Major problems associated with these techniques are painful operation, high cost, risk of refusal by the patient‘s immune system, and risk of introducing infection or disease from the donor to the patient. Tissue engineering aims to regenerate damaged tissues without replacing them and by combining body cells on a highly porous scaffold biomaterial, which acts as a template for tissue regeneration. These templates should not only possess biodegradability, biocompatibility and other

scaffold and help provide physical support for the seeded cells (Murphy & O'Brien, 2010).

Table 2.1: Optimal pore size for cell/tissue ingrowth

Cell/tissue type	Optimal pore size (μm)
Blood vessels	5 μm
Hepatocytes	20 μm
Bone	100-350 μm
Osteoid	40-100 μm
Fibroblast	5–15 μm
Adult mammalian skin	20–125 μm
Fibrovascular tissue	> 500 μm

Recently, chitosan hydrogels have been widely used as scaffolds for tissue engineering due to their non-toxic, biodegradable and biocompatible nature. This polymer has hydrophilic nature with the ability of degradation via human enzymes like lysozyme which results in biocompatibility and biodegradability, the biological properties commonly needed for tissue engineering applications (Ahmadi et al., 2014). It is reported that the rate of degradation of chitosan into non-toxic residues is related to the molecular mass of the polymer and its deacetylation degree (Croisier & Jérôme, 2013). Besides that, chitosan exhibits other remarkable properties such as ability to form complicated shapes with appropriate porosity, mechanical and swelling properties. Tissue engineering needs scaffolds with adequate mechanical properties to withstand the physiological loads (Hung, Hutton, & Grayson, 2013). Swelling of scaffold facilitates absorption of extracellular fluids as well as transport of cell nutrients and metabolites inside the scaffold (Maji, Dasgupta, Pramanik, & Bissoyi, 2016). Crosslinking can be used to tailoring of swellability, stability and mechanical properties of chitosan hydrogel (Rohindra, Nand, & Khurma, 2004; Subramanian & Lin, 2005).

Chitosan is a popular biomaterial in clinical medicine, especially in plastic reconstructive surgery and dermatology. Chitosan scaffolds were prepared by crosslinking with glutaraldehyde for cultivation of human dermal fibroblasts. The porosity and the pore size of the scaffolds were controlled by varying the freezing rate to form ice crystals of varying sizes. With this technique, the pore size was 40–140 μm, and the average porosity was about 93% ± 12.57% (Hilmi et al., 2013).

Nwe et al. (2009) reported that porosity of the chitosan scaffolds produced by fungal mycelia was greater than that of the chitosan obtained from crab shells and squid bone plates. Chitosan from shrimp shells possessed the lowest porosity. It was reported that the molecular alignment disappeared when chitosan dissolved with acetic acid. Also, the formation of hydrogen bonds between polymer chains caused interconnecting of a network of pores during freeze-drying step. It was also observed that polygonal pores resulted when low molecular weight chitosan was used and elongated pores ensued from chitosan with high molecular weight. Porosity, pore size, and distribution pattern of pores highly affected on the mechanical properties, water absorption, and water vapor permeability of the scaffold.

3D micro-porous chitosan scaffolds were produced by dissolving chitosan in acetic acid, followed by stirring and finally adding the solution into a NaOH solution. Here the foaming was achieved by mechanical stirring, without adding a chemical foaming agent. It was mentioned that the pore diameter of chitosan scaffold decreased with increasing the stirring rate of the sample due to the high shear force of the homogenizer‘s cutting head. Also, the pore diameter decreased with decreasing the concentration of chitosan in the solution. Lower concentrations of chitosan (less than 1%), lowered the sample‘s viscosity for foaming and on the other hand concentrations

greater than 3%, caused sample‘s viscosity too high and stick to the homogenizer‘s cutting heads which resulted in difficulties in mixing (Hsieh, Chang, & Lin, 2007).

Formation of a nonporous skin layer is a barrier to the cell growth in tissue engineering scaffolds. Chitosan hydrogels were fabricated with dense gas CO_2 and porous structure on top, bottom surface and in cross sections were obtained without formation of a nonporous skin layer. Due to the high porosity, the crosslinked chitosan hydrogel fabricated under dense gas conditions showed higher equilibrium swelling ratio than the samples fabricated under atmospheric conditions. Hydrogels exhibited equilibrium swelling ratios of 17.2 ± 0.8 and 10.3 ± 0.4 at the dense gas condition and atmospheric condition, respectively (Ji et al., 2011).

The low viscosity and high diffusivity of supercritical CO_2 offers fabrication of highly porous tissue engineering scaffolds. Chitosan hydrogel was fabricated using supercritical CO_2 for the implantation of osteoblast cells. Hydrogel fabricated under 250 bar, 45 °C, 2 h at 5 g/min CO_2 flow rate yielded 87.03% porosity which was similar to lyophilization (88.68%) operated at 55 °C for 48 h. Even though the porosity is similar for both conditions, the fabrication using supercritical CO_2 found to be more time and energy efficient (Ozdemir, Sendemir-Urkmez, & Yesil-Celiktas, 2013).

Macroporous chitosan scaffolds were developed to load either with bone morphogenetic proteins (BMP-2) or insulin-like growth factor (IGF-1) to study the bone healing property in vivo. Porosity was developed by mechanical stirring the chitosan solution using homogenizer and transferring the bubbled solution into sodium hydroxide solution to conduct liquid hardening process. Chitosan scaffold with pore sizes from 70-900 μm was obtained using liquid hardening method. The absorption efficiency of IGF-1 and BMP-2 was found to be 90 ± 2% and 87 ± 2%, respectively. In vivo studies revealed that chitosan scaffolds loaded with IGF-1 showed significant

osteoblastic differentiation than BMP-2-loaded chitosan scaffolds (Sivashankari & Prabaharan, 2016).

2.4.1.2 Wound healing

Selecting a proper dressing material is one important aspect of healing chronic wounds. An ideal wound dressing material should allow gaseous exchange, absorb exudates and toxic compounds, maintain high humidity at the applied surface, provide thermal insulation, protect the wound from bacterial contamination, be nontoxic, be removed easily, be easily handled without any damages, be sterilizable and be free from leaving foreign particles in the wound (Ghosh & Jassal, 2002).

Depending on the required property, the hydrophilicity, swelling ratio, porosity, and degradation of a wound dressing material are controlled using bioactive hydrogels to regulate the rate of fluid passage from the wound, enhance the diffusion of encapsulated drug, and release the by-products into the wound and help in tissue regeneration, respectively (Piraino & Selimović, 2015).

Chitosan hydrogels generally use for wound healing applications as a wound dressing material and hemostatic agent to promote the process of wound healing. Chitosan exhibits properties such as biodegradability, biocompatibility, antimicrobial activity and low immunogenicity which make it as a suitable candidate for wound dressing material. Also, chitosan hydrogel provides a three-dimensional matrix for tissue growth, activate macrophage activity that results in further events such as release of biological mediators. Chitosan slowly degrades to release N-acetyl-β-D-glucosamine units which stimulates fibroblast proliferation and collagen synthesis. Additionally, it exhibits antimicrobial properties which initiates host cell defense and offers protection to wounds at risk of infection which is particularly beneficial for wound treatment (Cheung et al., 2015; Chhabra, Tyagi, Bhatnagar, Mittal, & Kumar, 2016).

Hydrogels are crosslinked polymer matrices with several hydrophilic groups or domains. Although these materials are hydrophilic, the presence of chemical or physical bonds between polymer chains prevent the dissolution of hydrogel in water. Binding of polymer chains is achieved either by noncovalent physical associations and physical entanglements or by covalent crosslinkages (Bhattarai et al., 2010).

Porous materials are highly attractive as controlled drug delivery matrices because of their controllable pore size, high surface area with narrow distribution, and favorable surface properties. Mesoporous, microporous, and nanoporous structures of polymer matrices control the passage between the external and internal surfaces of a solid, allowing materials to pass in or out of the solid (Ahuja & Pathak, 2009). Drugs are incorporated into hydrogel in two ways. One is through post-loading, wherein a drug is loaded after hydrogel networks are formed. If the hydrogel system is inert, diffusion is the major driving force for drug uptake and release. In the presence of drug-binding ligands in the hydrogel, drug–polymer interaction and drug diffusion must both be considered in any model description of release. The other is through in situ loading, wherein drugs or drug–polymer conjugates are introduced to polymer precursor solution. In this method, hydrogel formation and drug encapsulation occur simultaneously. In such cases, drug release depends on hydrogel swelling, diffusion, reversible drug–polymer interactions, or degradation of labile covalent bonds (Lin & Metters, 2006).

When the pore size of a hydrogel is greater than the molecular size of the drug, the diffusion coefficient can be related to the porosity and tortuosity of the hydrogel. For hydrogels with pore sizes closer to the drug molecular size or nonporous hydrogels, drug diffusion coefficients are decreased because of the steric hindrance of polymer chains. In such cases, the average free volume for drug molecules is decreased and the

hydrodynamic drag toward the drug is increased, causing increased drug diffusion path length compared with hydrogels with pore sizes much larger than that of the encapsulated drug (Lin & Metters, 2006).

Chitosan is a highly swellable, pH responsive and biocompatible polymer which can be used to deliver drugs to specific sites of gastrointestinal tract. The pH-sensitive swelling and releasing behavior of hydrogels are useful for the design of oral drug delivery carrier. Chitosan is a linear ubiquitous polysaccharide and heteropolymer consists of glucosamine and N-acetyl-glucosamine units. Amino groups of chitosan have a pKa value of around 6.5. At pH below this pKa value, the amino groups of chitosan get ionized and positively charged $-NH_3^+$ groups are distributed among hydrogel network. This leads to the repulsion of polymer chains within the hydrogel and allowing more water intake into the hydrogel network (Szymańska & Winnicka, 2015). Cationic nature of chitosan in acidic medium increases the retention of the hydrogel at the site of application and readily binds to negatively charged surfaces such as mucosal membranes. Mucoadhesive ability could result in formulations containing chitosan being retained in the mucosal surface such as gastric mucosa due to the acidic environment of the stomach. Due to the high degree of swelling and mucoadhesive properties in acidic medium, chitosan-based hydrogels have been used as a carrier for stomach-specific drug delivery systems (Ali et al., 2014; Dubey, Verma, & Verma, 2015; Hejazi & Amiji, 2002; Majithiya & Murthy, 2005; Patel & Amiji, 1996; Thakur, Monga, & Wanchoo, 2014).

Majithiya and Murthy (2005) developed chitosan-based mucoadhesive microspheres for delivery of clarithromycin to treat stomach ulcers. An emulsification technique with glutaraldehyde as the crosslinking agent was used to prepare microspheres. Their results showed the entrapment efficiency up to 74%. It was reported that the swelling ability

decreased with increasing the crosslinking degree. In addition, the extent of crosslinking exhibited inverse correlation with drug release and linear relationship with mucoadhesion. Also, the results showed a good mucoadhesion of microspheres with the stomach mucosa, higher drug accumulation and sustained release of drug.

Yassin, Alsarra, and Al-Mohizea (2006) developed a gastroretentive drug delivery system of verapamil using chitosan beads. The beads were synthesized by adding dropwise solution that contains chitosan and verapamil to a solution containing tripolyphosphate using a syringe pump. Beads were further crosslinked using glutaraldehyde. Beads showed a very good spherical geometry and drug loading efficiency of 42%. Beads formed from medium molecular weight chitosan showed good floating characteristics (buoyancy more than 6 hours) and slowest release of drugs. The beads with the ability of in vitro floating for more than 6 hours were suggested as possible candidates for delivery of drugs with very poor alkaline solubility and for the absorption from upper small intestine.

Semi-interpenetrating polymer network (semi-IPN) hydrogel was prepared by crosslinked chitosan and poly(ethylene oxide) (PEO) for site-specific antibiotic delivery in the stomach. Release studies of amoxicillin and metronidazole was carried out in simulated intestinal fluid and simulated gastric fluid at 37 °C. Freeze-dried chitosan-PEO semi-IPN showed extensive swelling properties when compared to the air-dried hydrogel. It was observed that more than 65% of the encapsulated amoxicillin and 59% of metronidazole were released from the freeze-dried chitosan-PEO semi-IPN in simulated gastric fluid. According to the results, the study suggested that freeze-dried chitosan-PEO semi-IPN can be used for site-specific delivery of antibiotics in the acidic environment of the stomach (Patel & Amiji, 1996).

Bioadhesive superporous hydrogel composite particles were prepared from hydroxypropyl-methylcellulose and chitosan biopolymers using gas blowing for intestinal drug delivery. Composite particles with a pore size of 100–1000 μm and a porosity of 47.11% ± 1.80% were obtained for drug (metoprolol succinate) delivery studies. The particles showed more than 80% drug loading and drug release up to 10 h (Chavda, Modhia, Mehta, Patel, & Patel, 2013).

Chitosan was crosslinked with different amount of glutaraldehyde to prepare appropriate hydrogels to be used as drug delivery of amoxicillin trihydrate. Crosslinked hydrogels were freeze-dried and used for drug delivery studies. It was observed that the pore size increased from 100 μm to 500 μm with increasing the crosslinking agent from 1:0.068 to 1:0.30. Hydrogel with 20 mol% crosslinker showed the best swelling behavior for drug release (Mirzaei B, Ramazani SA, Shafiee, & Danaei, 2013).

2.5 Reinforcement of chitosan hydrogel

Composites are new materials, with enhanced material properties, formed with a combination of materials. Generally, a composite is composed of two component materials with different properties, such that one of the materials is inserted in to the other. The insert material is of discrete nature, which is known as reinforcement. The material which receives the insert is of continuous nature and commonly called matrix. The matrix component can be metallic, ceramic or polymer. Composites not only retain the main features of the original component materials, but also get the performances that are not shown by the original components. The form of reinforcement may be fibrous, sheet, particulate, ribbon or wire like. Different types of fibers and particles have been reinforced in biopolymer hydrogels to improve the mechanical strength (Chandramohan & Marimuthu, 2011). Previous studies have been carried out on chitosan hydrogels reinforced with different particles and fibers to enhance the mechanical, thermal, and

biological properties. Particles include bioceramics (biphasic calcium phosphate, hydroxyapatite) and nanoparticles such as carbon nanotubes, nanohydroxyapatite, Cu, Ag, Au and Zno have been used as reinforcing agents in chitosan hydrogel. (Dhivya, Saravanan, Sastry, & Selvamurugan, 2015; El-Mekawy & Jassas, 2017; Hernández, Benavides-Mendoza, Ortega-Ortiz, Hernández-Fuentes, & Juárez-Maldonado, 2017; Iviglia et al., 2016; B. Li et al., 2015; Li, Wen, Zhang, & Ju, 2013; Venkatesan, Jayakumar, Mohandas, Bhatnagar, & Kim, 2014). Different kinds of fibers such as chitin, silk, collagen and nanofibrils (cellulose, collagen and chitin) are also used as reinforcing agents in chitosan hydrogel (Chen et al., 2012; Mattioli-Belmonte et al., 2007; Mirahmadi, Tafazzoli-Shadpour, Shokrgozar, & Bonakdar, 2013; Wang, Hu, & Cai, 2010; Zhou, Fu, Zhang, Zhan, & Levit, 2014).

2.5.1 **Particle reinforced chitosan hydrogel**

Particulate reinforced composites are known as matrices which embedded with a dispersed phase in particulate form. The effect of the reinforced particles on the composite material properties depends on the particle size (Singh & Singh, 2014). From previous studies, different types of reinforcing particles such as bioceramics (biphasic calcium phosphate, hydroxyapatite) and nanoparticles (carbon nanotubes, nanohydroxyapatite, Cu, Ag, Au and Zno) have been used to improve the properties of chitosan hydrogels.

Bioceramics are biocompatible ceramic materials used in biomedical applications ranging from medical implants to biomedical pumps. It has been used as long-term hard tissue implants due to its chemical stability, chemical similarity to that of hard tissues, biocompatibility, mechanical properties, wear, inertness, and corrosion resistance. Biphasic calcium phosphate and hydroxyapatite are bioceramic compounds which are widely used in various biomedical applications, mostly in orthopaedics and dentistry

due to its close similarity with inorganic mineral component of bone and teeth. Iviglia et al. (2016) developed particle reinforced chitosan-pectin hydrogel to promote the osteoblast proliferation. The size of the reinforced biphasic calcium phosphate particles was in the range of 100–300 μm. Results showed that the addition of ceramic particles improved the mechanical strength, osteoblast adhesion and proliferation compared to chitosan-pectin hydrogel. B. Li et al. (2015) prepared chitosan/hydroxyapatite (HA) hybrid hydrogel by irradiation with ultraviolet (UV) radiation to promote bone regeneration. According to the results, the bone regeneration significantly increased in HA/chitosan hydrogel compared to the hydrogel without HA. The higher HA content in the hydrogel facilitated the acceleration of bone regeneration.

The incorporation of nanomaterials in the hydrogel matrix is an attractive approach to improve the mechanical strength of the hydrogel. The mechanical properties improve due to the increased tortuosity of the polymer molecules as a result of nanoparticle insertion and the resistance offered by the nanoparticles to any movement. Furthermore, the increased surface area-to-volume ratio of nanomaterials provides a substantial interface for them to interact with the polymer. Carbon nanotubes, nanobioceramics and inorganic nanoparticles (Cu, Au, Ag and Zno) are most commonly used reinforcing agents in chitosan hydrogel matrices. Chitosan beads embedded with carbon nanotubes (CNT) have been used for the dye removal (Congo red). The maximum compressive force at complete breakdown of chitosan/CNT hydrogel beads increased from 1.87 N to 7.62 N with the addition of CNTs. Also, the adsorption of Congo red increased from 178.32 to 423.34 mg/g with the addition of CNTs (Chatterjee, Lee, & Woo, 2009). Demirtaş, Irmak, and Gümüşderelioğlu (2017) developed a bioprintable form of chitosan/nanohydroxyapatite hydrogel for the bone tissue engineering. They observed that the addition of nanohydroxyapatite to chitosan hydrogel enhanced the cell proliferation, cell viability and osteogenic differentiation. Inorganic nanoparticles

reinforced chitosan hydrogels have been widely used for the inhibition of pathogenic microorganisms. Antimicrobial release system was prepared using copper nanoparticles/chitosan gel nanocomposites and antimicrobial activity was tested against *Aggregatibacter actinomycetemcomitans* by halo inhibition assay on semisolid agar medium. Nanocomposite material inhibited the growth of *A. actinomycetemcomitans*, showed higher stability in saliva and exhibited controlled and sustained release of bactericidal copper concentrations. Chitosan hydrogels containing silver nanoparticles were developed to study the impact on the growth of a selected strain of bacteria (*Escherichia coli*). Results showed that the chitosan based hydrogels modified with nanosilver did not negatively affect on epidermal cells. However, they inhibited the growth of *Escherichia coli.*

2.5.2 **Fiber reinforced chitosan hydrogel**

Fiber reinforced biopolymer hydrogels have been developed to have high porosity with desired mechanical properties based on the fiber-matrix interactions and the arrangement of fibers. It is reported that both strength and stiffness can be improved extensively by reinforcing fibers to the hydrogel. The mechanical properties of these matrices are affected by the binding strength of matrix, fiber orientation, fiber aspect ratio and volume fraction. Studies have been carried out using different kinds of fibers such as chitin, silk, collagen and nanofibrils (cellulose, collagen and chitin) as reinforcing agents in chitosan hydrogel.

The addition of natural fibers such as silk, chitin and collagen have been widely used to improve the mechanical properties of hydrogel scaffolds, while maintaining their biocompatibility and biodegradability. Due to the superior biocompatibility and degradability, natural silk can be used as a reinforcement material to improve the performance of the hydrogel for remolding and repairing the cartilage tissue. Mirahmadi

et al. (2013) prepared thermosensitive chitosan hydrogel using electrospun silk fibers for cartilage tissue engineering. Their findings revealed that the addition of silk fibers significantly improved the mechanical properties of the hydrogel. According to the compressive test results, the stiffness of silk-containing scaffolds (dispersion of silk and electrospun fiber layers) improved by 1.9 and 3.1 times than the pure chitosan hydrogel. From the studies of collagen fiber/chitosan hydrogel for tissue engineering by Wang et al. (2010) indicated that the stiffness of collagen-containing materials was approximately 3 times greater than the pure chitosan.

Nanofibril is a material containing fibrils with width in the nanometric range and length in the micrometer range. The incorporation of nanofibrils in hydrogels is an attractive method for preparing biomaterials with tailored functionality. The formation of interactions between fibrils and percolating networks lead to useful properties in hydrogels. The fibrils obtained from natural fibers such as cellulose, chitin and collagen have been widely used as reinforcing agents for chitosan hydrogel. Cellulose nanofibrils can be synthesized by enzymatic or mechanical processing to obtain the fibrils with high aspect ratios and having a width in the nanometer range. Spagnol et al. (2012) showed that the swelling ratio and average dimension of porous structures of superabsorbent hydrogel composite (made of cellulose nanofibrils and chitosan-graft-poly(acrylic acid)) increased with increasing the cellulose nanofibril content in the gel. Mattioli-Belmonte et al. (2007) reported that the chitin nanofibril/chitosan glycolate gels were more effective as an aesthetic factor and for repairing shallow lesions. Wang, Sang, Luo, and Li (2011) obtained different types of nanofibrous structures in collagen/chitosan hybrid gels using two different methods: thermally triggered cofibrillogenesis and glutaraldehyde crosslinking treatment. Their results revealed that the tensile strength of lyophilized scaffolds improved from 248.2 ± 19.7 to 361.2 ± 32.3 kPa with increasing the chitosan/collagen ratio from 0.2 to 0.8. This value

for collagen/chitosan scaffold formed by glutaraldehyde crosslinking treatment was about 300 kPa.

2.6 Cellulose nanocrystals

Cellulose nanocrystals (CNC) or nanocrystalline cellulose (NCC) are unique nanomaterials extracted from the most abundant natural polymer on earth. Cellulose nanocrystals have better mechanical strength and high crystallinity when compared with natural cellulose. In bulk natural cellulose, ordered (crystalline) and disordered (amorphous) regions of cellulose molecular chains are found with varying their proportions according to the type of its source. Figure 2.15 shows the closely interacted crystalline regions and regularly distributed amorphous regions. A suitable combination of mechanical, chemical and enzymatic treatments can be used to extract highly crystalline regions of the cellulose microfibrils. It is reported that the chemical methods are much better than the mechanical methods due to producing rod-shaped short nanocrystals and less energy consumption. Strong acid hydrolysis is mostly applied method to preparation of cellulose nanocrystals as they can easily penetrate into the amorphous region and hydrolyze without affecting to crystalline region (George & Sabapathi, 2015; Rubentheren, Ward, Chee, & Nair, 2015).

The theoretical Yong‘s modulus along the chain axis of perfect cellulose nanocrystals is estimated to be 167.5 GPa, which is theoretically greater than the Yong‘s modulus of steel. The hydroxyl groups present on the surface of CNCs can be easily modified with different chemical groups to facilitate the incorporation and dispersion within different polymer matrices (Habibi, Lucia, & Rojas, 2010).

CNCs are popular reinforcing materials for various kind of polymers due to their properties such as large surface area, high mechanical strength, high aspect ratio, lower

2.6.1.1 Chemical hydrolysis

The acid hydrolysis methods have been extensively used for nanocellulose extraction from various natural sources such as microcrystalline cellulose, wood fiber, plant fiber, tunicate, bacteria and algae (Chirayil, Mathew, & Thomas, 2014). The process preferentially hydrolyzes the less dense, amorphous parts of native cellulose and leaving crystalline particles with shorter chains unaffected (Usov et al., 2015). Different nanocelluloses have different morphologies based on the source of native cellulose broken down. Different acids, such as hydrobromic, sulfuric, hydrochloric, phosphoric, and maleic acids have been widely used for acid hydrolysis method. Concentrated sulfuric acid is most commonly used acid for the acid hydrolysis method. The reaction between surface hydroxyl groups of cellulose and sulfuric acid causes the formation of surface charged sulfate ester groups on the cellulose chains, facilitating the dispersion of CNCs in aqueous systems (Mascheroni et al., 2016). In the acid hydrolysis method, initially, the purified cellulose source is mixed into deionized water with given concentration of acid. After reacting for a set period of time, the mixture is diluted with deionized water to terminate the reaction. After that, the mixture is washed with deionized water using filtration or repeated centrifuge cycles to remove excess acid from the suspension. Then, the slurry is kept in dialysis membranes and dialyzed for set period of time. After that, it is dipped into distilled water until a neutral pH is achieved. Subsequently, the nanocellulose suspension can be exposed to ultrasound treatment to facilitate dispersion of cellulose nanocrystals in the suspension (Moon, Martini, Nairn, Simonsen, & Youngblood, 2011).

A high yield of CNCs can be achieved by using ammonium persulfate, instead of using concentrated inorganic acids as oxidizing agents. Ammonium persulfate is highly water soluble strong oxidant and able to remove in situ lignin, pectin, hemicelluloses and other cellulose contaminants present in different cellulose sources. The time need

for the cleavage of cellulose is comparatively higher when compared to acid hydrolysis but it results in uniform crystals with high crystallinity (Li, Mascheroni, & Piergiovanni, 2015).

Mascheroni et al. (2016) obtained CNCs starting from cotton linters by two different methods: treatment with ammonium persulfate and sulfuric acid hydrolysis. CNCs obtained by ammonium persulfate treatment method showed higher crystallinity, charge densities (due to the carboxylic groups formed during the process), and clarity of the solution when compared to sulphuric acid hydrolysis method.

Sadeghifar, Filpponen, Clarke, Brougham, and Argyropoulos (2011) used hydrobromic acid hydrolysis in the production of CNCs from cotton fibers. Ultrasonic energy was applied for 5 minutes at every 60-minute time interval during acid hydrolysis to improve the yield of CNCs. The optimum conditions for this reaction were found to be 2.5 M of hydrobromic acid at 100 °C for 3 h. Highly crystalline cellulose with the lengths of 100–200 nm and transverse dimensions ranging between 7–8 nm was obtained using this method. The results showed that the yield increased with increasing the hydrobromic acid concentration from 1.5 M to 2.5 M. Furthermore, the yield increased from 23.5% to 26.6% and 39.0% to 50.1% with the concomitant application of sonic energy for 2 h and 4 h reaction time, respectively.

Krishnamachari, Hashaikeh, Chiesa, and Gad El Rab (2012) investigated the effect of acid exposure time of acid hydrolysis method on cellulose nanocrystal properties. It was observed that the samples hydrolyzed for 30 min or more had a considerably lower elastic modulus than those hydrolyzed for 20 min or less. According to thermogravimetric (TGA) studies, the onset of thermal degradation of all CNC samples occurred at a lower temperature than that of microcrystalline cellulose.

A. Kumar et al. (2014) extracted cellulose nanocrystals from sugarcane bagasse using acid hydrolysis method. Chemically purified cellulose was mixed with 64% sulfuric acid at 1:10 g/ml (cellulose/H_2SO_4) proportion and stirred at 45 °C for 60 min. It was found that the produced CNCs were rod-shaped, size in the range of 20-60 nm (diameter) and 250-480 nm (length). Produced CNCs showed higher crystallinity (72.5%) and lower thermal stability compared with native cellulose (63.5%).

Hong, Chen, and Xue (2016) characterized the cellulose nanocrystals produced from bamboo pulp. Under the optimum conditions of acid hydrolysis reaction (60% sulfuric acid, 1:8 solid-liquid ratios, 45 °C temperature and 90 minutes reaction time) the yield of CNCs reached a maximum of 32.3%. Micro-morphological studies revealed that the CNCs existed in two forms as rods and a porous network. According to FTIR studies, CNCs maintained the basic chemical structure of cellulose. In addition, the produced CNCs showed lower thermal stability compared to bamboo pulp.

2.6.1.2 Mechanical process

Mechanical processes impose high shear forces to cellulose fibers and cause transverse cleavage along the longitudinal axis of the cellulose microfibrillar structure resulting in microfibrils and microfibril aggregates with high aspect ratio called microfibrillated cellulose. Generally, cellulose materials are run in multiple passes through the mechanical treatment. After each pass, it produces particles having more uniform diameter and smaller in size, but with increased mechanical damage to the crystalline structure (Moon et al., 2011).

A filtration step is often included in microfibrillated cellulose production to remove the larger non-fibrillated and partially fibrillated fractions. Mechanical treatment can be followed by chemical treatment in order to remove non-fibrillated fractions or to chemically functionalize the particle surface. To facilitate the disintegration of cellulose

microfibrils in to thinner cellulosic nanofibers, three pretreatment steps can be applied: using never-dried cellulosic source materials, partial removal of matrix material, and chemical treatment. These pretreatments will effectively weaken the interfibrillar hydrogen bonds. During the drying of cellulosic sources, the spaces between microfibrils collapse and formation of hydrogen bonding occur between the fibrils causing difficult to separate agglomerates. Re-swelling of dried cellulosic source does not replace all the hydrogen bonds and, therefore, it does not cause same "weakening" effect. Incomplete removal of matrix material can cause inhibition of coalescence of the microfibril bundles during drying and facilitate the subsequent fibrillation of the material. The charge-imparting on fibril surface also improves the interfibrillar repulsive forces. This can be achieved either by adsorption of charged polyelectrolytes to oppositely charged (fiber) surfaces (e.g. carboxymethyl cellulose) or by oxidation (usually employing 2,2,6,6-tetramethyl-piperidinyl-1-oxyl radical (TEMPO) for region selective oxidation) (Moon et al., 2011).

2.6.1.3 Enzymatic hydrolysis

When compared to conventional acid hydrolysis, enzymatic production of CNCs is desirable because it does not require harsh chemicals, needs lower energy requirements and environmental friendly. Although it is beneficial from the environment point of view, this technology is still hindered by economical (costly cellulase enzyme) and technical (long processing) obstacles. Pretreatment such as mechanical grinding is applied before enzyme treatment, so the enzymes can have access to elementary cellulose fibrils (Lee, Hamid, & Zain, 2014).

Biologically cellulose is broken down by hydrolytic enzymes, collectively referred to as cellulases: endoglucanase, exoglucanase and beta-glucosidase. Biological process involves the hydrolysis of cellulose by an enzyme produced from microbe itself or

produced by the biological agent. Enzyme hydrolyses the cellulose from its original size down to nano-meter level. These cellulases generally help the organism to use cellulose as carbon source to support its growth and metabolism. There is a high degree of synergistic action between endoglucanases and exoglucanases which converts solid crystal of cellulose to disordered solid-liquid interface. Endoglucanases are typically active in more soluble amorphous region and cleave the internal bonds (e.g., noncovalent interaction) of cellulose. Exoglucanases hydrolyze the terminal glycosidic bond from the end of the exposed cellulose chains generated by endoglucanases. Subsequently, β-glucosidases further hydrolyze beta-1,4 glycosidic linkage of cellulose into nanocellulose or even glucose product (Lee et al., 2014; Ozioko, Ikeyi, & Ugwu, 2013). Several fungal and bacterial species such as *Aspergillus niger, Aspergillus fumigatus, Trichoderma spp*., *Pseudomonas fluorescens, Bacillus subtilis, Escherichia coli* and *Serratia marcescens* have been reported for the efficient production of cellulases (Sethi, Datta, Gupta, & Gupta, 2013).

Most industrial cellulases are produced by fungi, because the cellulases that they produce are abundant and easy to extract. The filamentous fungus *Trichoderma ressei* is a well-known efficient biological producer of cellulases (Adav, Chao, & Sze, 2012). Other fungus such as brown rot fungi degrade cellulosic sources and produce peroxidases in combination with cellulase. *Trichoderma ressei* does not produce peroxidases but only produces cellulases (Guillén, Martínez, Gutiérrez, & Del Rio, 2005). This microorganism is also popular for the production of cellulose nanocrystals due to the secretion of enzyme extracellularly in to the medium (Ng & Zeikus, 1981). The extracellular production of cellulase is affected by many key factors such as temperature, pH and substrate concentration that can be used to manipulate the controlled hydrolysis of cellulose (Ghose, 1987).

2.6.2 Nanocellulose reinforced hydrogels

2.6.2.1 Properties

Recently, cellulose nanocrystals have gained significant interest as reinforcing agents due to their favorable properties, such as high mechanical strength, large surface area, low density, high aspect ratio, biocompatibility, and biodegradability (Ahmed, 2015; Park et al., 2015; Yang et al., 2012; X. Yang et al., 2013). Nanocellulose has been incorporated in the manufacture of various kinds of hydrogels with unique properties. The incorporation of nanocellulose in different hydrogel matrices have demonstrated excellent improvement of mechanical, thermal, optical, water uptake capacity, crystallinity, solute retention or release, biocompatibility and biodegradability properties.

Nanocelluloses have been widely used to synthesize nanocomposite hydrogels with excellent mechanical thermal and swelling properties. From the studies of pH sensitive poly(acrylic acid) (PAA)/cellulose nanocrystal (CNC) hydrogel by Lim, Ahmad, and Lazim (2015) showed that the swelling ratio of PAA/CNC hydrogel was higher compared with PAA hydrogel because of hydrophilic nature of nanocellulose. Furthermore, the results of thermal analysis revealed that PAA/CNC hydrogel had high thermal stability compared to PAA hydrogel. Park et al. (2015) prepared TEMPO mediated oxidized bacterial cellulose/sodium alginate hydrogel for cell encapsulation. They found that the bacterial cellulose improved the chemical stability and mechanical properties of the sodium alginate (SA) hydrogel beads. Similarly, Domingues et al. (2015) developed an injectable hyaluronic acid (HA)/CNC hydrogel for tissue engineering applications. Results indicated that the addition of CNCs in the hydrogel led to the formation of organized and compact network structure with maximum storage modulus of 152.4 kPa for 0.25 wt% CNCs content, a 135% improvement when compared to unfilled hydrogels. Moreover, CNC reinforced poly(vinyl alcohol) (PVA)

hydrogels were prepared using glutaraldehyde (GA) as a crosslinker. Results indicated that the compressive strength of hydrogel at 60% strain increased from 17.5 kPa to 53 kPa with the introduction of 1 wt% CNCs. However, the addition of CNCs did not affect the thermal stability and swelling ratio of the hydrogel (Tanpichai & Oksman, 2016).

Biocompatibility and biodegradability are desirable properties for materials used in biomedical applications include drug delivery, tissue engineering and wound healing. Ávila et al. (2014) synthesized densified bacterial nanocellulose hydrogel with 17% cellulose for auricular cartilage regeneration. According to the biocompatibility studies the densified bacterial nanocellulose hydrogels showed non-cytotoxic properties and caused a minimal foreign body response. Zhang, Chen, Zhang, and Hong (2016) prepared nanoporous cellulose/poly(L-lactide-co-caprolactone) nanocomposite gel and studied the hydrolytic degradation behavior by immersing the nanocomposites in phosphate-buffered saline solutions at 37 °C. Nanocomposites showed faster degradation rates compared to aliphatic polyesters and neat polycaprolactone. For instance, after six weeks, the weight loss ratios of nanocomposites reached to a maximum of 10% and it was only 5 wt% for neat polycaprolactone, even after 420 days.

2.6.2.2 Applications

Hydrogel consists in a hydrophilic three-dimensional network; which can swell under biological conditions. It is an ideal class of material for biomedical applications, including wound healing, tissue engineering and drug delivery. Besides that, they have also been used as absorbents and substrates for microbial encapsulation. Most hydrogels are brittle and susceptible to failure under low deformation. Nanocellulose reinforcement in the hydrogel matrix has been widely studied to improve the chemical or physical characteristics of hydrogel nanocomposites. This will expand their

application scopes in the fields of tissue engineering, pharmaceuticals and drug delivery etc.

Mechanical strength of the hydrogel is an important parameter when designing a tissue engineering scaffold. Domingues et al. (2015) developed injectable hyaluronic acid (HA)/CNC bionanocomposite hydrogel with improved mechanical properties for tissue engineering applications. From in vitro studies, HA/CNCs hydrogel showed preferential cell supportive properties due to higher structural integrity and potential interaction of microenvironmental cues with CNC‘s sulphate groups. Yan et al. (2017) reported that the bacterial nanocellulose enhanced cell attachment to the alginate/bacterial cellulose nanocrystals/collagen composite hydrogel scaffold due to the reinforcing effect and excellent biocompatibility properties of bacterial nanocellulose. Moreover, Park et al. (2015) reported that TEMPO mediated oxidized bacterial cellulose (TOBC)/sodium alginate hydrogel beads showed more cell viability and proliferation than the cells in the sodium alginate hydrogel beads because of the 3D fibrous structure of TOBC, which was similar to the extracellular matrix.

The nanometer size dimension and the presence of free reactive hydroxyl group exposed at the surface rendered nanocellulose a good candidate for imparting different functionalities through chemical derivatization. Also, the solid carriers formed from nanocellulose and different hydrogel matrices spatially trap drug molecules and impart in regulation of drug release. Ooi, Ahmad, and Amin (2016) developed nanocellulose reinforced gelatin hydrogel and investigated the drug delivery behavior of theophylline. According to their results the storage modulus of CNC/gelatin hydrogel improved with the addition of CNC. The gelatin hydrogels with 15% nanocellulose was suggested as the best potential candidate for controlled drug delivery application. A biocompatible double-membrane CNC/sodium alginate hydrogel was prepared for controlled drug

delivery of ceftazidime hydrate and human epidermal growth factor. Results showed that the controlled release lasted for more than 6 days for the incorporated drugs (Lin, G ze, Wouessidjewe, Huang, & Dufresne, 2016).

Nanocellulose has been reported as an attractive candidate for prepare wound dressing materials due to its capability of self-assembling into 3D micro-porous structures and ability of maintaining a moist environment. Leppiniemi et al. (2017) produced 3D-printable bioactivated CNC/alginate hydrogel by ionic cross-linking using calcium ion. The hydrogel was suggested as a potential candidate for wound dressing applications due to the suitability for 3D printing, good tissue compatibility, better mechanical properties and water absorption in moist conditions. Furthermore, fabric skeleton reinforced chitosan/bacterial nanocellulose hydrogel was prepared with high mechanical properties and antibacterial properties for antibacterial wound dressing applications. The composite exhibited bacteriostatic properties against *Escherichia coli* and *Staphylococcus aureus.* According to the results of mechanical studies, composite showed excellent mechanical properties as compared to the bacterial nanocellulose sheets (Zhang et al., 2016).

Nanocellulose composite hydrogels have been considered as absorbent materials due to their relatively high swelling capacity. Mohammed, Grishkewich, Berry, and Tam (2015) synthesized CNC/alginate hydrogel beads for removal of organic dyes in aqueous solutions. It was observed that the percentage dye removal increased with increasing the CNC content. The dye removal percent of alginate beads with 1 wt% CNCs is almost three-fold higher when compared to the hydrogel beads with 0 wt% CNCs. This is because of the increased number of adsorption sites generated due to the high surface area of CNCs.

2.7 Curcumin

Curcumin (diferuloylmethane) a natural polyphenolic nutraceutical, is a major component of turmeric (*Curcuma longa*) that has been associated with antioxidant, anticancer, anti-inflammatory, antiviral, and antibacterial activities as indicated by over 6,000 citations and over one hundred clinical studies (Prasad et al., 2014). Curcumin can be extracted from dried rhizomes of turmeric (*Curcuma longa*). As shown in Figure 2.16, the chemical composition of the extracted curcumin is a mixture of curcuminoids (curcumin, demethoxycurcumin and bis-demethoxycurcumin). Curcumin has three reactive functional groups which associated with its different biological activities: one diketone moiety, and two phenolic groups. The presence of C═O groups as hydrogen acceptors and C-4 as a hydrogen donor are most important for chemical reactions associated with its biological activities (Ahmed et al., 2017).

Various health benefits of curcumin have been reported and it is well known for its antioxidant property. Antioxidant property of curcumin helps to neutralization of free radical species and balance the anti-oxidant state of the body. Curcumin shows anti-diabetic activity by increase in gene expression such as insulin-like growth factor-1 and by increase of insulin secretion and prevention or delaying of diabetic retinopathy. It also exhibits prevention of inflammatory process via modulation or inhibition of various molecular pathways. Curcumin-based therapeutics have been widely used for the treatment of liver disorders in different parts of the world. It has also been used for the treatment of cardiovascular diseases. Due to the antioxidant activity of curcumin it has been used for the neutralization of adverse effect of ultraviolet (UV) light on the skin. Beside those properties, curcumin shows various effects and activities which are important in the health management such as gastro-protective effect, neuro-protective effect, anti-obesity effect, effect on hypertension, anti-tumor activity, effect on respiratory disorder, immunomodulatory effect, anti-malarial activity, nephro-

2.7.1 **Curcumin in preventing gastric cancer**

Stomach cancer also known as gastric cancer is the third leading cause of cancer-related death in the world. These cancers spread in the innermost lining of the stomach that produces mucus. The most common early symptoms may include heartburn, loss of appetite, upper abdominal pain and nausea. Late signs of gastric cancer include yellowing of the skin, weight loss, whiten eyes, vomiting, swallowing difficulty and blood in the stool among others. Gastric cancer can spread from stomach to other body parts such as liver, lungs, lymph nodes, bones and lining of the abdomen (Zali, Rezaei-Tavirani, & Azodi, 2011).

The most common cause of gastric cancer is infection by *Helicobacter pylori* (*H. pylori*) a microaerophilic gram-negative bacterium that colonizes the gastric mucosa. Although the mechanism of *H. pylori*-induced carcinogenesis is yet to be understood the inflammation is the most commonly cited factor in the carcinogenic process. Besides the inflammation, *H. pylori* directly interacts with epithelial cells, resulting in protein modulation and gene activation. It would finally results in a _hummingbird' epithelial phenotype, epithelial motility, loss of gap junctions, and eventual epithelial cell death. Most recently, much attention has been given to the relationship between *H. pylori,* stem cells and cancer. It is reported that *H. pylori* preferentially attacks parietal cells, thus altering the maturation process of epithelial stem cells. In addition, other studies reported inflammation related to *H. pylori* recruits peripheral- or bone-marrow derived stem cells to the gastric mucosa, which then transform into the malignant clone (Herrera & Parsonnet, 2009).

Transmission of *H. pylori* is commonly from person to person via the gastric–oral or faecal–oral route due to poor sanitation and hygiene. No single antibiotic is reported to cure the *H. pylori* infection. Several antibiotic combinations have been proposed,

including triple therapies (clarithromycin, amoxicillin and metronidazole) bismuth-free therapies (clarithromycin, amoxicillin and tinidazole) and bismuth-based quadruple therapy (bismuth salts, tetracycline and metronidazole). In view of the ineffectiveness with conventional therapy due to development of resistant strains, noncompliance among the patients, undesirable side effects, and the cost of antibiotic regimens, there is an urgent need to change many drug treatment strategies for *H. pylori* infection. Curcumin, diferuloylmethane from turmeric powder, has recently been reported to arrest *H. pylori* growth. Due to the poor solubility of curcumin, various types of drug delivery systems such as liposomes, nanoparticles, microemulsions, hydrogels and polymeric implantable devices have been developed for the enhancement of bioavailability of curcumin (Bansal, Goel, Aqil, Vadhanam, & Gupta, 2011; De Francesco, Bellesia, Ridola, Manta, & Zullo, 2017).

2.7.2 **Curcumin drug delivery systems**

Various types of methods have been developed for the delivery of curcumin into body. Oral administration of curcumin shows beneficial effects such as inhibition of inflammatory molecules, effective against different types of cancer, effective for the treatment of diabetic condition, enhance wound repair and protects against the pulmonary and cardiovascular effects. However, curcumin shows poor water solubility, rapid metabolism and rapid elimination which ultimately results in poor bioavailability upon oral administration. Therefore, the advanced drug delivery systems like nanoparticles, liposomes, micellar formulations, cyclodextrin inclusion complexes microemulsions and different hydrogel based delivery systems, have been developed to circumvent their bioavailability issues (Dhivya & Rajalakshmi, 2017; Pandit, Gaikwad, Agarkar, Gade, & Rai, 2015; Petchsomrit, Sermkaew, & Wiwattanapatapee, 2017; Ratanajiajaroen & Ohshima, 2012; Yadav, Suresh, Devi, & Yadav, 2009).

Subcutaneous treatment of curcumin in animal models has been reported sustained tissue concentrations. According to previous study, single subcutaneous dose of microparticles sustained curcumin in liver for nearly a month in mice. Intraperitoneal injection of curcumin is more often applied to animals than to humans. In intraperitoneal injection the bioavailability of compound is higher than gavage. It is reported that intraperitoneal injection administration of curcumin acts against asthma, inhibits tumor growth, inflammation and collagen deposition. Intravenous injection of curcumin exhibits anticancer property in animal model. Intravenous injection of liposomal formulation of curcumin also enhanced the effect of radio and chemotherapy. However, among all types of delivery systems, oral administration is a noninvasive and convenient drug delivery route most preferred by patients (Prasad et al., 2014).

The poor dissolution and low bioavailability of curcumin have been highlighted as the major challenges of drug delivery to stomach (Ridhima et al., 2012). However, many attempts have been made from previous studies to improve the pharmacotherapy of the stomach through local drug release, leading to high amount of drug at the gastric mucosa to treat stomach and duodenal ulcer, gastritis and esophagitis (Ali et al., 2014; Chiu, Kocagöz, Larson, & Brey, 2013; Guo, Xie, & Luo, 2013; Mohammed et al., 2015; Shivashankar & Mandal, 2012; Treesinchai et al., 2016).

Ravindra et al. (2012) developed curcumin/silver nanoparticle incorporated hydrogels for antibacterial and drug delivery applications. The hydrogels were prepared by free radical copolymerization of 2-acrylamido-2-methyl propanesulfonic acid (AMP) and acrylamide (AM) using (N,N-methylenebisacrylamide) (MBA) as the crosslinker. It was observed that the drug encapsulation decreased in Ag ions loaded hydrogels because of all the AMP chains were bounded by Ag ions which caused limiting the anchoring capacity of drug into the hydrogels. According to the results of drug release

studies, plain poly(AM-co-AMPS) hydrogel showed faster release when compared to curcumin loaded silver nanocomposite hydrogels. This is due to the adsorption of high amount of drug on the silver nanoparticles together with entrapment in the hydrogels. The prolonged release of drug from curcumin loaded silver nanocomposite hydrogel suggests the usefulness of the material towards long term wound healing.

Kumar and Rai (2012) prepared floating microspheres with prolonged gastric residence time for enhancing bioavailability of curcumin. Hydroxylpropyl methylcellulose (HPMC), ethyl cellulose (EC) and Eudragit S 100 polymer in different ratios were used to prepare hydrogel by emulsion solvent diffusion method. The drug entrapment efficiency and yield of microspheres were in the ranges of 72.6 - 83.5%, and 45.5 - 82.0%, respectively. The maximum drug release was 47.1 - 81.3% for different formulations of microspheres after 20 h.

Bajpai, Chand, and Ahuja (2015) prepared chitosan/cellulose micro crystal (Ch/CMC) composite films and determined the antimicrobial activity against fungi and bacteria. Chitosan/CMC films showed prolonged release of curcumin over a time period of 36 h. The concentration of cellulose crystals dispersed within the chitosan matrix showed a negative effect on the curcumin release. This is due to the formation of additional physical crosslinks with dispersed CMCs.

Guzman-Villanueva, El-Sherbiny, Herrera-Ruiz, and Smyth (2013) prepared chitosan/alginate/carrageenan nano-microparticulate system via ionotropic gelation method for delivery of curcumin. Curcumin encapsulated nano-particles showed a homogenous drug dispersion in aqueous solution compared to the free form of curcumin. The results of drug release studies revealed that over 95% of loaded curcumin released from freeze-dried (50:50, alginate/carrageenan) microparticles in a pH 7.4

buffer solution, after 7 h incubation. Results indicated that high amount of drug release in the formulations with higher content of carrageenan.

Anitha et al. (2011) developed O–carboxymethyl chitosan (O–CMC) nanocarrier for curcumin delivery to cancer cells. The entrapment efficiency of nanocarrier system was found to be 87%. Drug release profiles indicated prolonged, sustained release of drug from the matrix. In addition, cytotoxicity studies revealed that curcumin loaded nanocarrier system was toxic to cancer cells and non-toxic to normal cells. Moreover, fluorescence-activated cell sorting studies revealed the cellular uptake of curcumin–O–CMC nanoparticles into the cancer cells.

Surfactants are used to improve the solubility of some poorly soluble drugs (Bhat, Dar, & Rather, 2008). Different types of surfactants have been utilized to improve the bioavailability of less soluble drugs in previous drug delivery systems. Based on the nature of the polar head groups of surfactants, they can be divided in to four groups: cationic, anionic, zwitterionic and nonionic (Patil, Patil, & Pratap, 2016). Among those, nonionic surfactants are more popular in drug delivery applications, due to stability, compatibility and less toxicity compared to their anionic, cationic or amphoteric counterparts (Kumar & Rajeshwarrao, 2011).

Related to the biological fate and physicochemical parameters of different nonionic surfactants, Tween a very convenient and safe choice for the improvement of drug solubilization in pharmaceutical applications (Kaur & Mehta, 2017). Tween surfactants contain hydrophobic alkyl chain and hydrophilic ethylene glycol head (Lu, Li, Yang, Zhao, & Qu, 2013). The commonly used Tween surfactants are Tween 20, 40, 60 and 80. They possess same hydrophilic head group with different length of alkyl chains. The alkyl chain length influences the hydrophile–lipophile balance (HLB) value of the surfactant, which in turn directly affect the entrapment efficiency of the drug. Low HLB

value links with high hydrophobicity. Surfactants with higher HLB values show higher water solubility (El-Ridy, Abdelbary, Essam, Abd EL-Salam, & Aly Kassem, 2011). The HLB value of Tween 20 is 16.7 and it is most hydrophilic when compared to other Tween surfactants (Mehta, Kaur, & Bhasin, 2010). Ratanajiajaroen, Watthanaphanit, Tamura, Tokura, and Rujiravanit (2012) found that the solubility of curcumin increased from 11 ng/mL to 0.767 mg/mL with the presence of 2% (v/v) Tween 20 to acetate buffer (pH 5.5) medium. Furthermore, they observed that the drug release rate increased with increasing the surfactant concentration in chitin beads. O'Toole et al. (2012) observed complete release of curcumin from the submicrometer spray-dried chitosan/Tween 20 particles in both 1% acetic acid and phosphate buffered saline solutions after 2 h. Furthermore, according to the studies on oil entrapped alginate/curcumin beads by Petchsomrit, Sermkaew, and Wiwattanapatapee (2013), the percentage curcumin release increased with increasing the Tween 80 concentration of alginate beads. Their results showed that the cumulative drug release increased up to 70% with the incorporation of 25% (w/v) of Tween 80.

2.8 Summary of the literature review

There are primarily two types of biopolymer either entirely biosynthesized by living organisms (natural) or chemically synthesized from a biological material (synthetic). Natural biopolymers such as cellulose, chitin and collagen are most abundant on earth (cellulose and chitin) and in the human body (collagen). Each biopolymer molecule has a unique primary structure. Material-specific properties are due to the unique primary structure that they possess. Poly(lactic acid) and poly(lactic-co-glycolic acid) are few examples for synthetic biopolymers that can be classified according to the way of preparation. Biocomposite materials are made up of two or more constituent materials out of which one is biogeneric in origin. Due to exhibiting biodegradable properties,

biopolymers have been widely used in biomedical applications such as tissue engineering, wound healing and drug delivery systems.

Porous fabrication techniques can be categorized into two categories, designed manufacturing techniques and non-designed manufacturing techniques. Gas foaming is being used to fabricate the amorphous and semicrystalline polymers with high porosity without using any organic solvent.

Biopolymers can be obtained in the form of hydrogel by chemical or physical crosslinking methods. The most significant feature of hydrogel is that it can hold significant amount of water within its structure, without undergoing dissolution. The most common problem associated with biopolymer hydrogel is poor mechanical properties. This has been overcome by using different types of crosslinking agents. Biopolymer hydrogels have been widely applied in biomedical applications such as gene delivery, drug delivery, tissue repair, wound dressing, and tissue engineering.

The hydrogels derived from chitosan have been the most widely used biomaterials in biomedical field. Chitosan hydrogel can be prepared using crosslinking method with different types of crosslinking agents (glutaraldehyde, genipin) by Schiff base mechanism. Chitosan hydrogel can be found in the medical field, such as drug delivery systems, tissue engineering, tissue repair, wound closure and healing products due to the possessing of certain properties like, biocompatibility, biodegradation to non-toxic end products. The use of chitosan hydrogel in many applications is limited due to poor mechanical properties. Different types of fibers and particles have been reinforced into chitosan hydrogels to improve low mechanical properties. The incorporation of nanomaterials in the hydrogel matrix is also an attractive approach to improve the mechanical properties of the hydrogel.

Cellulose nanocrystals are popular reinforcing materials which can be extracted using chemical, enzymatic or mechanical treatment method from the most abundant natural polymer available on the earth. Nanocellulose has been extensively used to prepare nanocomposite hydrogels with excellent mechanical thermal and swelling properties. Nanocellulose reinforced hydrogels have widely used for tissue engineering, control drug delivery systems and wound healing applications in previous studies.

Curcumin is a major component of turmeric, a promising antibacterial agent having property to restore and repair the gastric damage caused by *H. pylori* infection. However, the poor solubility and low bioavailability of curcumin have been highlighted as the major problems associated with curcumin drug delivery. Many attempts have been made to improve the bioavailability of curcumin through local drug release. These include curcumin loaded nanoparticle hydrogels, floating microspheres, composite films, nano-microparticulate systems and nanocarriers. Furthermore, the nonionic surfactants have been extensively used in curcumin drug delivery systems to facilitate their solubilization.

CHAPTER 3: METHODOLOGY

3.1 Synthesis and characterization of nanocellulose reinforced chitosan hydrogel

In the initial part of this study, the preparation of hydrogel including nanocellulose synthesis, synthesis of nanocellulose reinforced chitosan hydrogel and gas foaming of hydrogel is described in detail. Secondly, the tests, methods, apparatus and instruments used for the characterization of the hydrogel are described.

3.1.1 Synthesis of nanocellulose reinforced chitosan hydrogel

3.1.1.1 Materials

Medium molecular weight chitosan (viscosity 200–500 cP, 0.5% acetic acid at 20 °C), glacial acetic acid (AR grade), methanol, hydrochloric acid, sodium chloride and sulfuric acid were purchased from Friedemann Schmidt. Glutaraldehyde (25%) was obtained from Thermo Fisher Scientific. Microcrystalline cellulose and Tween 20 was purchased from R&M chemicals. Phosphate buffered saline (PBS) solutions were provided by Sigma–Aldrich. The buffer solutions (with pH values of 4.01, 7 and 10.01) were obtained from Trans Instruments Pvt Ltd. Curcumin was provided by HIMEDIA Laboratories Pvt Ltd. (Mumbai, India).

3.1.1.2 Preparation of CNCs

CNCs were prepared using the sulfuric acid hydrolysis method described by Rubentheren et al. (2015), with minor modifications. Initially, 10 g microcrystalline cellulose (MCC) was mixed with distilled water and placed into a beaker. The mixture was placed in an ice bath, and sulfuric acid was added dropwise (to avoid a spike in temperature) under constant stirring until the desired acid concentration of 64% (w/w) was reached. Subsequently, the suspension was stirred vigorously at 45 °C for 60 min. After acid hydrolysis, the suspension was added to cooled deionized water 1:10 (v/v) to

$$\text{Crosslinking degree (\%)} \quad \frac{W_d}{W_t} \quad 100 \tag{3.2}$$

Where W_d is the dry weight of post-dissolved hydrogel in acetic and W_t is the initial dry weight of the hydrogel (before dissolved in acetic acid).

3.1.2.9 In vitro degradation studies of the hydrogel in PBS solution

In vitro degradation studies of hydrogels were carried out in PBS solution for six weeks. The dried gels (0% CNC-chitosan, 0.5% CNC-chitosan, 1% CNC-chitosan, 1.5% CNC-chitosan, 2% CNC-chitosan, and 2.5% CNC-chitosan) were kept in 50 mL of PBS. The PBS was renewed every week. At predetermined time intervals, samples were taken out, thoroughly washed, blotted using filter paper and dried to constant weight at 45 °C. Dry weight of the sample was measured and weight loss was determined using Equation (3.3).

$$\text{Weight loss (\%)} \quad \frac{W_0 - W_t}{W_0} \quad 100 \tag{3.3}$$

W_o is the dry weight of the hydrogel taken initially and W_t is the dry weight at time t.

3.1.3 Characterization of gas foamed hydrogel

The swelling ratio is an important property in hydrogel drug delivery systems due to the correlation with the diffusion rates of both the penetrant into the matrix and the drug throughout the hydrogel (Carbinatto, de Castro, Evangelista, & Cury, 2014). From the hydrogels formed at atmospheric condition, 0.5% CNC-chitosan hydrogel showed the highest swelling degree. Therefore, 0.5% CNC-chitosan hydrogel formulation was selected for the gas foaming process and to study the morphology, mechanical and swelling properties of the gas foamed hydrogel.

3.1.3.1 Mechanical testing

The mechanical properties of gas foamed hydrogels (0.5% CNC-chitosan hydrogels, gas foamed at 10, 30 and 50 bar/ room temperature) were investigated by compression test using a (Shimadzu, AGS-X) universal/tensile tester (Shimadzu, Kyoto, Japan). The hydrogels were cut in to disk shapes (thickness (12 mm) and diameter (18 mm)) and allowed to equilibrate in pH 7.4 buffer solutions for 30 h. During the compressive strength tests, stress and strain responses were monitored under a load of 500 N and at a rate of 0.5 mm/min. Strain and stress were recorded using Trapezium Lite X software until maximum breaking strength was approached. Five replicates were tested to get the average and standard deviation.

3.1.3.2 Morphology studies (Before and after immersed in simulated gastric fluid)

The morphology of the gas foamed hydrogel (0.5% CNC-chitosan hydrogel, gas foamed at 50 bar/room temperature) and hydrogel (0.5% CNC-chitosan hydrogel) prepared at atmospheric condition was examined using (FE-SEM, SU8220) field emission scanning electron microscope (Hitachi, Tokyo, Japan). Morphology of both hydrogels, before and after immersed in simulated gastric fluid (SGF) were observed. Hydrogels were freeze dried using freeze dryer to remove water without disturbing the morphology. After this, the hydrogels were coated with gold in order to prevent the charging effects at an accelerating voltage of 5 kV.

3.1.3.3 Equilibrium swelling study in distilled water

The swelling ratios were measured by the immersion of gas foamed hydrogels (0.5% CNC-chitosan hydrogels, gas foamed at 10, 30 and 50 bar/ room temperature) in distilled water at 37 °C. Before the swelling test, hydrogels were cut into disk shape pieces and dried in room temperature until they reached constant weight. Dried hydrogels were weighed before immersion into the distilled water. The weight of

the swelled hydrogels after immersion in the distilled water was recorded at predetermined time intervals over 16 h. The swelling ratio of the hydrogels was calculated using Equation (3.4).

$$\text{Swelling ratio (\%)} \quad \frac{W_1 - W_0}{W_0} \quad 100 \qquad (3.4)$$

Where W_1 is the weight of swollen hydrogel in distilled water and W_0 is the initial dry weight of the hydrogel.

3.2 Drug delivery studies of nanocellulose reinforced chitosan hydrogel

3.2.1 Estimation procedure of curcumin by UV-Vis spectrophotometer

a) Absorption maxima in distilled water: The absorption maxima (λ_{max}) for curcumin in distilled water was determined by scanning the drug solution within the range of 300-800 nm using UV-Vis spectrophotometer (Shimadzu, Kyoto, Japan). It was found that the drug exhibited λ_{max} at 427 nm (Figure 3.11).

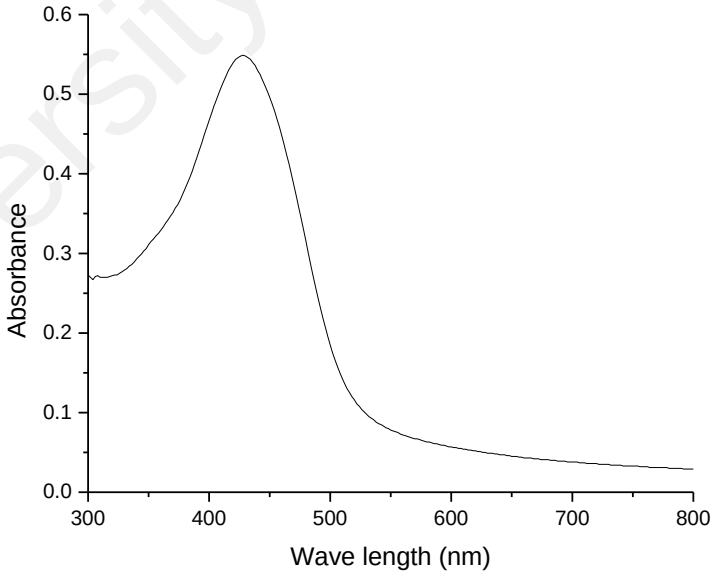

Figure 3.11: Absorption spectra of curcumin in distilled water

b) Preparation of stock solution: 100 mg of curcumin was accurately weighed and solubilized in 5 mL of methanol and the volume was made up to 100 mL with

distilled water to prepare 1000 mg/L solution. Working standards were prepared using this stock solution.

c) Preparation of working standard: 10 mL of stock solution was taken in volumetric flask (100 mL) and volume was made up with distilled water to obtain concentration of 100 mg/L. Further dilutions were made to give 0, 1, 2, 3, 4, 5, 6, 7 and 8 mg/L concentration of curcumin, respectively. These dilutions were scanned and the absorbance was measured at 427 nm using UV-Vis spectrophotometer. To obtain the standard calibration curve, the resulted absorbance values were plotted against the respective concentrations (Figure 3.12). Average values of absorbance were calculated by repeating the procedure three times (Hazra et al., 2015; Rashmi, 2014).

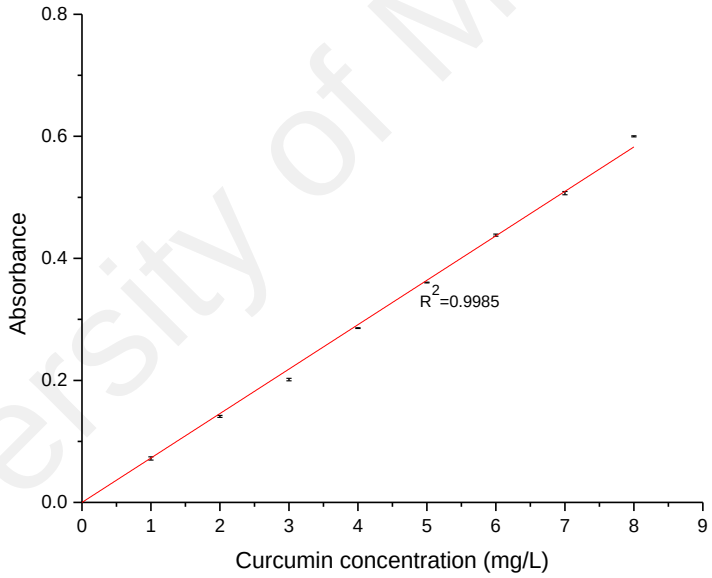

Figure 3.12: Standard calibration plot of UV absorbency of curcumin in distilled water

d) Absorption maxima in simulated gastric medium (simulated gastric medium was prepared by dissolving 2 g NaCl in 7.0 mL HCl and water up to 1000 mL): The absorption maxima (λ_{max}) for curcumin in simulated gastric medium was determine by scanning the drug solution within the range of 300-800 nm using UV-Vis spectrophotometer (Shimadzu, Kyoto, Japan). It was found that the drug exhibited λ_{max} at 427 nm (Figure 3.13).

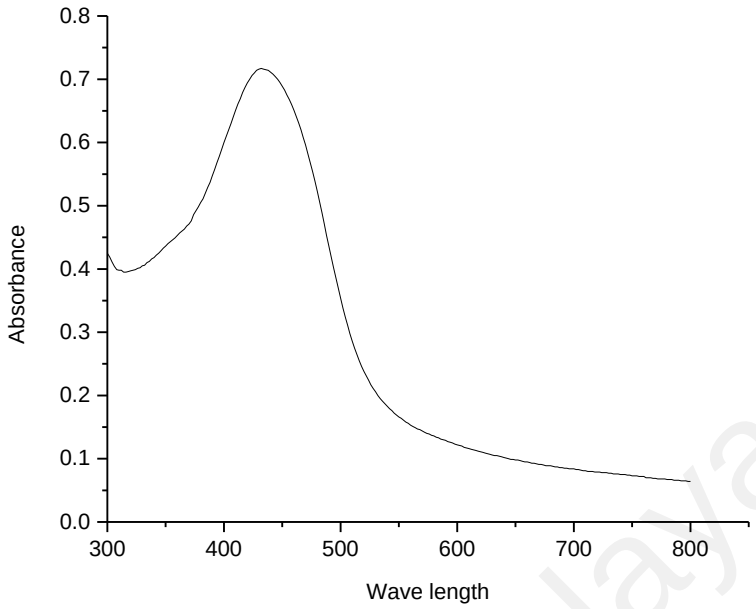

Figure 3.13: Absorption spectra of curcumin in simulated gastric medium

e) Preparation of stock solution: 100 mg of curcumin was accurately weighed and solubilized in 5 mL of methanol and the volume was made up to 100 mL with simulated gastric medium, to prepare 1000 mg/L solution. Working standards were prepared using this stock solution.

f) Preparation of working standard: 10 mL of stock solution was taken in volumetric flask (100 mL) and volume was made up with simulated gastric medium to obtain concentration of 100 mg/L. Further dilutions were made to give 0, 0.3, 0.6, 0.9, 1.2, 1.5, 1.8, 2.1 and 2.4 mg/L concentration of curcumin, respectively. These dilutions were scanned and the absorbance was measured at 427 nm using UV-Vis spectrophotometer. To obtain the standard calibration curve, the resulted absorbance values were plotted against the respective concentrations (Figure 3.14). Average values of absorbance were calculated by repeating the procedure three times (Hazra et al., 2015; Rashmi, 2014).

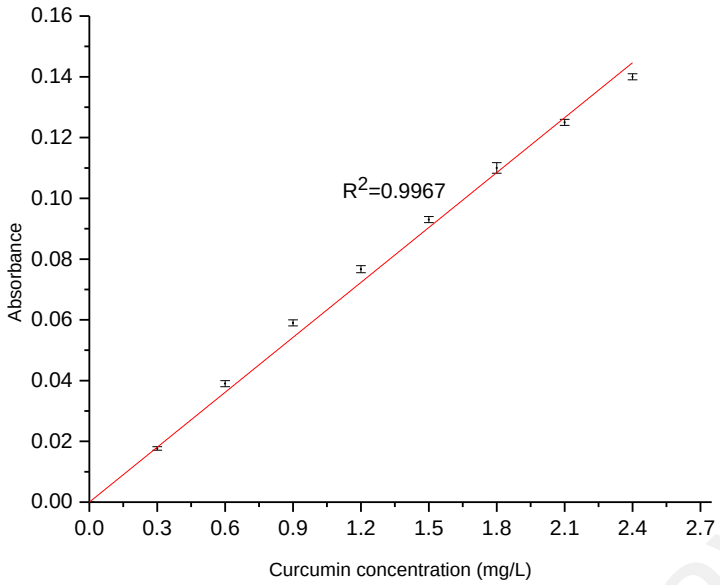

Figure 3.14: Standard calibration plot of UV absorbency of curcumin in gastric medium

g) Calibration curves (Figure 3.12 and Figure 3.14) were used to determine the concentration of curcumin present in distilled water and gastric medium, respectively.

3.2.2 Drug delivery studies of the hydrogel formed at atmospheric condition

3.2.2.1 Characterization (FTIR analysis of curcumin and curcumin loaded hydrogel)

FTIR studies of curcumin, 0.5% CNC-chitosan hydrogel and curcumin loaded 0.5% CNC-chitosan hydrogel were carried out using PerkinElmer spectrum 400 FTIR spectrometer (Shimadzu, Kyoto, Japan) over the range 3000–500 cm^{-1}.

3.2.2.2 Drug loading efficiency

Curcumin (purchased from Himedia Co.) was encapsulated into hydrogels by post loading method. Disk shaped hydrogels (0% CNC-chitosan, 0.1% CNC-chitosan, 0.2% CNC-chitosan, 0.3% CNC-chitosan, 0.5% CNC-chitosan, 0.6% CNC-chitosan, 1% CNC-chitosan, 1.5% CNC-chitosan, 2% CNC-chitosan, and 2.5% CNC-chitosan) with 18 mm diameter and 12 mm height were immersed in 30 mg/L drug solution for 24 h at room temperature. (Further increase of the drug concentration produces no significant

increase of encapsulation efficiency for all the samples. Therefore, 30 mg/L drug solution was used for the drug loading of each sample). Curcumin loaded hydrogels were removed from drug solution and rinsed with distilled water and washing was collected. Curcumin concentration remaining in the solution was determined by UV-2600, UV−Vis spectrophotometer (Shimadzu, Kyoto, Japan) at 427 nm. The experiments were repeated three times and average values were taken. The drug encapsulation efficiency was calculated using Equation (3.5).

$$\text{Encapsulation efficiency (\%)} \quad \frac{\text{Amount of curcumin in the hydrogel}}{\text{Initial drug amount in the solution}} \quad 100 \qquad (3.5)$$

3.2.2.3 In vitro drug release

In vitro drug release from hydrogel networks (0% CNC-chitosan, 0.1% CNC-chitosan, 0.2% CNC-chitosan, 0.3% CNC-chitosan, 0.5% CNC-chitosan, 0.6% CNC-chitosan, 1% CNC-chitosan, 1.5% CNC-chitosan, 2% CNC-chitosan, and 2.5% CNC-chitosan) with different drug loading contents was investigated by immersion of drug loaded hydrogels in simulated gastric medium (simulated gastric medium was prepared by dissolving 2 g NaCl in 7.0 mL HCl and water up to 1000 mL) at 37 °C (Figure 3.15). In order to study the release, 3 mL solution containing released drug was removed at predetermined time intervals and returned it back to the solution after the analysis. The concentration of released curcumin was measured at 427 nm using UV-Vis spectrophotometer (UV-2600, Shimadzu, Japan). The experiments were performed triplicates and average values were taken.

Hydrogels were gas foamed at 30 bar/40 ^{0}C and investigated the effect of processing temperature for the drug delivery behavior of the hydrogel. The drug loading efficiencies of hydrogels were determined by following the same method described in 3.2.2.2. Also the same method described in 3.2.2.3 was followed to observe the in vitro drug release behavior of these hydrogels. The drug encapsulation efficiency and release profiles of these hydrogels were compared with the hydrogels formed at 1 bar/27 ^{0}C, 1 bar/40 ^{0}C and 30 bar/27 ^{0}C.

3.2.4 **Drug activity**

In drug delivery systems, the chemical and biological activity of drug after release into the body is the most critical parameter. The drug activity of curcumin before loading and after release could be studied by using UV-Vis spectrophotometer (Bashir, Teo, Ramesh, & Ramesh, 2016). UV- visible spectra of pure drug and the drug released from the hydrogel were obtained using UV-visible spectrophotometer. Drug activity was determined through comparison between the spectra (the absorption maxima (λ_{max})) of pure drug and released drug.

3.2.5 **Investigation of the effect of a nonionic surfactant on drug delivery behavior of the hydrogel (chitosan/nanocellulose/Tween 20 hydrogel)**

From the previous results, we observed an improvement of mechanical properties of the hydrogel with physical reinforcement of nanocellulose in to the hydrogel matrix. Further, it showed that the swelling characteristics improved with the addition of low concentrations of nanocellulose and exerted highest swelling properties at acidic medium. It also showed that the chitosan hydrogel reinforced with 0.5% CNC, showed the highest swelling properties and highest cumulative release of curcumin. Therefore, in this study, 0.5% CNC-chitosan hydrogel formulation was selected for further improvement of drug delivery properties of the hydrogel. According to the previous

results, the percentage of curcumin encapsulation and the amount of curcumin release increased after the gas foaming of hydrogels (due to the formation of large interconnected pore structures). However, the poor solubility of curcumin caused less concentrations of released drug in simulated gastric medium. Therefore, in this study, a nonionic surfactant (Tween 20) was incorporated into the hydrogel as a solubilizing agent for curcumin.

The aim of this study is to evaluate the effect of a nonionic surfactant (Tween 20) on the drug (curcumin) delivery behavior of 0.5% nanocellulose reinforced chitosan hydrogel. Curcumin was extracted from dried rhizomes of *Curcuma longa* and incorporated into the hydrogel with Tween 20, using in situ loading method (drug is introduced at the time of hydrogel formulation). This part includes the characterization of curcumin extracted from turmeric, dissolution studies of curcumin in Tween 20/ simulated gastric fluid, drug loading and release studies and drug activity test.

3.2.5.1 Extraction of curcumin from turmeric

Curcumin was extracted from rhizomes of *Curcuma longa* following the method proposed elsewhere (Mohammed & Habil, 2015). Dried rhizomes were crushed in a mortar and pestle, and then extracted with methanol. They were soaked in methanol for 3 days and then filtered with Whatman filter paper (pore size 0.2 μm). After that, filtrate was poured into a Petri plate and the solvent was evaporated under vacuum to obtain semi-dry oily mass.

3.2.5.2 Preparation of curcumin loaded chitosan/nanocellulose/Tween 20 hydrogel (in situ loading method)

Cellulose nanocrystals (CNC) were prepared from microcrystalline cellulose by sulfuric acid hydrolysis method reported in our previous study. Chitosan was dissolved in 5% (v/v) aqueous acetic acid solution at room temperature and left overnight in the shaker

with the rotation rate of 250 rpm and then filtered through the filter paper to remove any insoluble matters. To prepare curcumin loaded chitosan/nanocellulose/Tween 20 hydrogel, nanocellulose, extracted curcumin and Tween 20 were added to chitosan solution and stirred (250 rpm) for one hour. After that glutaraldehyde was added and stirred (350 rpm) for 1 min at room temperature. The mixture was then poured into the mold and allowed the hydrogel to solidify at room temperature for 24 h. The composition of curcumin entrapped chitosan/nanocellulose/Tween 20 hydrogel formulations are listed in Table 3.1.

Table 3.1: Composition of curcumin entrapped chitosan/nanocellulose/Tween 20 hydrogel formulations

Formulation	Chitosan (w/v)%	Nanocellulose (w/v)%	Tween 20 (w/v)%	Glutaraldehyde (v/v)%	Curcumin (mg per 2.5 g of hydrogel disc)
CH/CNC/ TW-0%	2	0.5	0	0.2	1.5
CH/CNC/ TW-5%	2	0.5	5	0.2	1.5
CH/CNC/ TW-10%	2	0.5	10	0.2	1.5
CH/CNC/ TW-15%	2	0.5	15	0.2	1.5
CH/CNC/ TW-20%	2	0.5	20	0.2	1.5
CH/CNC/ TW-25%	2	0.5	25	0.2	1.5
CH/CNC/ TW-30%	2	0.5	30	0.2	1.5

3.2.5.3 CO_2 gas foaming of curcumin loaded-hydrogel

After mixing CNC, drug, Tween 20 and crosslinker with chitosan solution as described above, the mixture was poured in to the mold and placed inside the gas foaming apparatus. Then the apparatus was pressurized with CO_2 to predetermined

3.2.5.5 UV-Vis spectroscopic analysis of curcumin (HIMEDIA Co.) and extracted curcumin from turmeric

UV-Vis spectra of both curcumin purchased from HIMEDIA Co. and curcumin extracted from turmeric were obtained by scanning the drug solutions within the range of 350-800 nm using UV-Vis spectrophotometer (Shimadzu, Kyoto, Japan).

3.2.5.6 FTIR analysis of curcumin-loaded hydrogel

FTIR studies of curcumin extracted from turmeric, Tween 20, hydrogel and curcumin loaded hydrogel/Tween 20 were carried out using PerkinElmer spectrum 400 FTIR spectrometer (Shimadzu, Kyoto, Japan) over the range of 3000–500 cm^{-1}.

3.2.5.7 Morphology Studies

The morphology of the hydrogels was examined using field emission scanning electron microscope (FE-SEM, SU8220). Hydrogels were freeze dried using freeze dryer to remove water without disturbing the morphology. After this, the hydrogels were coated with platinum in order to prevent the charging effects at an accelerating voltage of 5 kV.

3.2.5.8 Estimation procedure of curcumin by UV-Vis spectrophotometer

The absorption maxima (λ_{max}) of curcumin was determine by scanning the drug solution within the range of 350-800 nm using UV-Vis spectrophotometer. It was found that the drug exhibited λ_{max} at 427 nm in both of the distilled water and simulated gastric medium as shown in Figure 3.17a and Figure 3.18a, respectively. The concentration of curcumin extracted from turmeric was determined by the standard calibration curve prepared (λ_{max} at 427 nm) using standard solutions of curcumin (HIMEDIA Co).

The concentration of curcumin present in distilled water was determined from the calibration curve (Figure 3.17b) prepared from standard solutions of curcumin (HIMEDIA Co.), dissolved in methanol and diluted by distilled water.

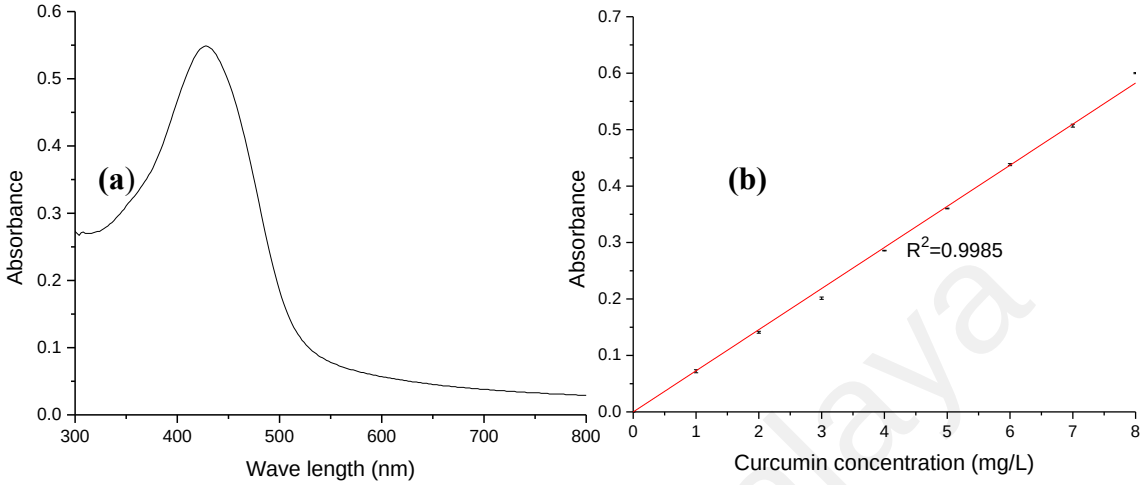

Figure 3.17: a) UV–Vis absorbance spectrum of curcumin in distilled water and b) calibration curve of curcumin

The concentration of curcumin present in simulated gastric fluid was determined from the calibration curve (Figure 3.18b) prepared from standard solutions of curcumin (HIMEDIA Co.), dissolved in methanol and diluted by simulated gastric fluid (Jansirani, Saradha, Salomideborani, & Selvapriyadharshini, 2014; Parize, Stulzer, Laranjeira, Brighente, & Souza, 2012).

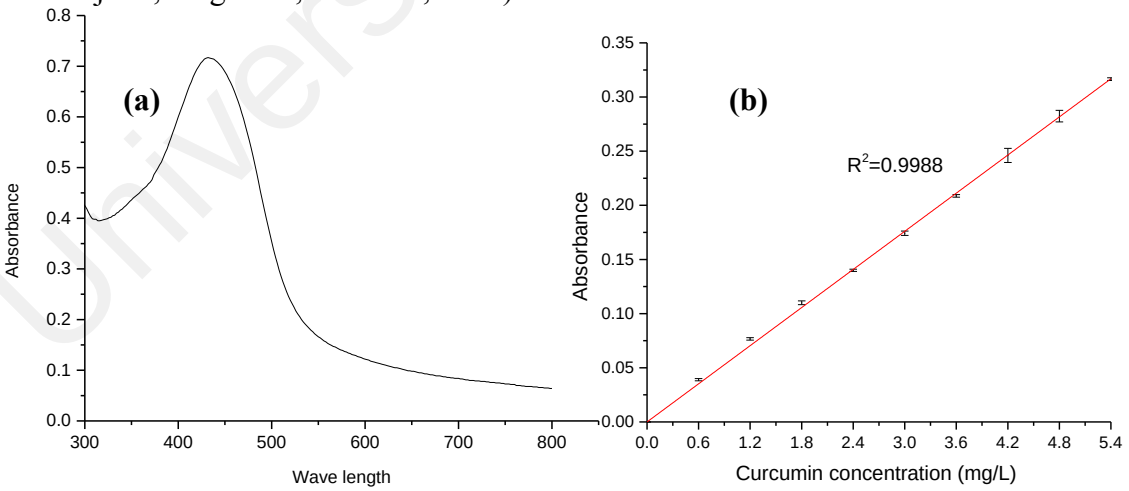

Figure 3.18: a) UV–Vis absorbance spectrum of curcumin in simulated gastric medium and b) calibration curve of curcumin.

3.2.5.9 Drug entrapment efficiency

Disc shape hydrogel (1.80 cm diameter and 1.20 cm height) was immersed in 30 mL ethanol for 24 h. Then, the solution was filtered and diluted suitably to measure the

absorbance, from which the concentration of drug was calculated using the standard calibration data. Each formulation was analyzed in triplicate and average values were taken. The drug entrapment efficiency was calculated based on the ratio of actual amount of drug present in the hydrogel to the initial amount of drug contained in the hydrogel using Equation 3.6.

$$\text{Entrapment efficiency} = \frac{\text{Actual amount of curcumin in hydrogel}}{\text{Initial amount of curcumin contained in the hydrogel}} \quad (3.6)$$

3.2.5.10 Drug release

In vitro drug release from hydrogel networks with different Tween 20 concentrations was investigated in simulated gastric medium (prepared by dissolving 2 g NaCl in 7.0 mL HCl and water up to 1000 mL) at 37 °C. In order to study the release, drug loaded hydrogel discs (1.80 cm diameter and 1.20 cm height) were immersed in simulated gastric medium; 3 mL aliquot of release medium was withdrawn at predetermined time intervals and returned it back to the solution after the analysis. The concentration of released curcumin was determined by the calibration curve prepared using the curcumin (HIMEDIA Co.) in simulated gastric fluid. The experiments were performed triplicates and average values were taken.

3.2.5.11 Drug activity

In drug delivery systems, the chemical and biological activity of drug after release into the body is the most critical parameter. The drug activity of curcumin before loading and after release could be studied by using UV-Vis spectrophotometer (Bashir et al., 2016). UV- visible spectra of pure drug and the drug released from the hydrogel formed at atmospheric condition were obtained by scanning the solutions within the range of 350-800 nm using UV-visible spectrophotometer. The drug activity was determined through comparison between the spectra (the absorption maxima (λ_{max})) of pure drug and released drug.

3.2.5.12 Curcumin solubility studies in Tween 20/simulated gastric fluid

To determine a saturated concentration of curcumin in simulated gastric fluid, an excess amount of curcumin (extracted from turmeric) was added in to 30 mL of simulated gastric fluid with different concentrations of Tween 20 (0.8%, 1.6%, 2.4%, 3.2%, 4%, 5.6% (w/v)). Then, the mixtures were stirred (350 rpm) with using magnetic stirrer at 37 °C for 12h. Samples were covered to avoid exposition to the light. After that, the solutions were centrifuged at 10,000 rpm for 10 min, supernatant was decanted and dissolved curcumin was determined using the standard calibration curve (Gowthamarajan & Singh, 2010; Kaewnopparat et al., 2009).

CHAPTER 4: RESULTS AND DISCUSSION

4.1 Synthesis and characterization of nanocellulose reinforced chitosan hydrogel

As illustrated in Figure 4.1a, b, nanocellulose reinforced chitosan hydrogel forms a semi-interpenetrating polymer network (semi-IPN) via the diffusion of linear polymer chains into a preformed polymer network. One constituent of the semi-IPN hydrogel is a crosslinked polymer, and the other is a non-crosslinked polymer. The constituent polymers of the semi-IPN can be separated, in principle, from the polymer network without breaking the chemical bonds. A semi-IPN structure improves the mechanical properties of a hydrogel and controls its swelling behavior.

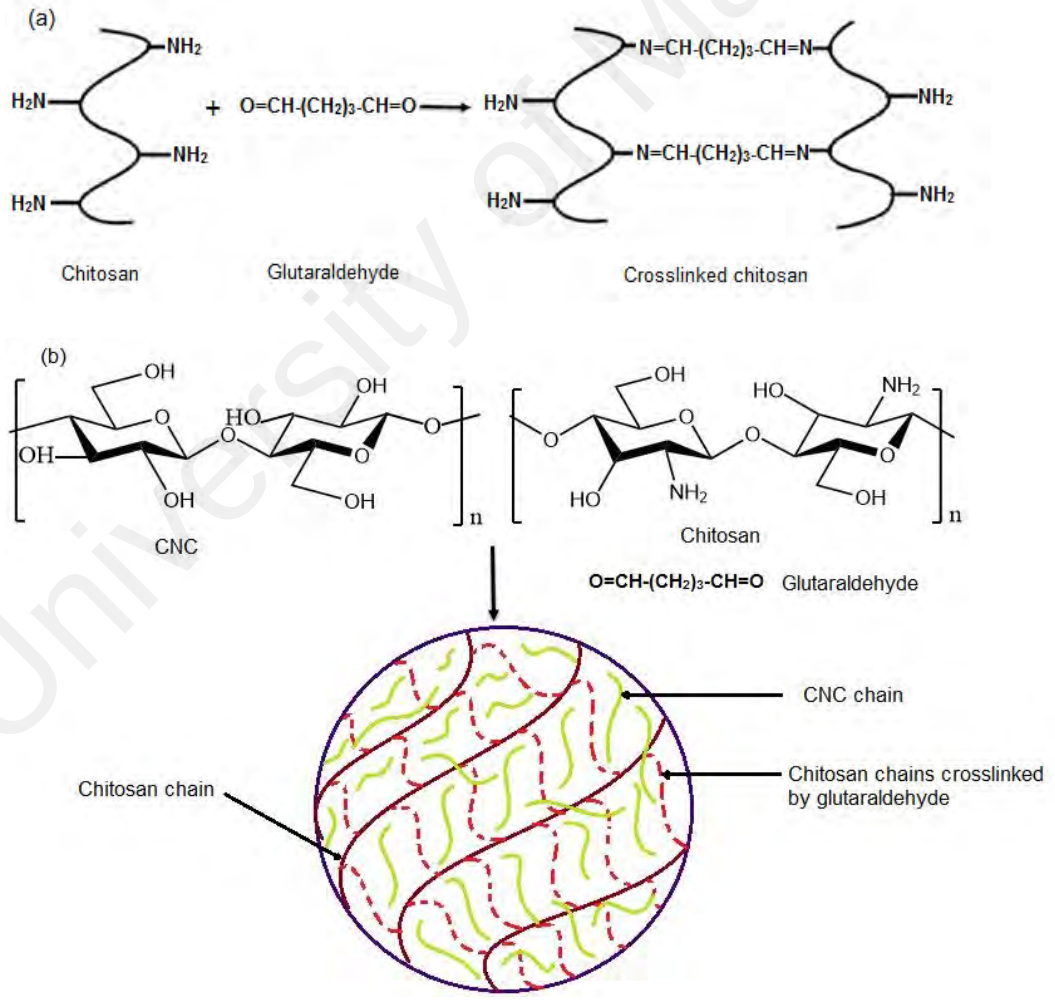

Figure 4.1: The schematic representation of the steps for the formation of CNC-chitosan hydrogel: (a) crosslinking process of chitosan with glutaraldehyde; (b) proposed mechanism for the formation of semi-interpenetrating polymer network hydrogel

4.1.1 Characterization of the hydrogel formed at atmospheric condition

4.1.1.1 Mechanical properties

Compression tests were performed to investigate the effect of nanocellulose reinforcement on the mechanical properties of the chitosan hydrogels. The compressive stress-strain curves of the hydrogels with varying CNC concentrations are shown in Figure 4.2. The magnitude of stress increased with an increase in the CNC content of the hydrogel at a given strain. This result showed that the high contents of CNCs in the hydrogels enhanced the mechanical properties of the hydrogels. The stress–strain curves became non-linear at the 30%–40% strain level for the pure chitosan hydrogel and all the CNC-chitosan hydrogels. This result indicated that plastic deformation occurred in the hydrogels at strains greater than 40%. Among the hydrogels, the pure chitosan hydrogel exhibited the lowest maximum stress (25.9 ± 1kPa). As shown in Figure 4.3, the maximum stress of the CNC-chitosan hydrogel increased from 38.4 ± 1kPa to 50.8 ± 3kPa with increasing CNC content ranging from 0.5% to 2.5%. A nearly two-fold increase in the maximum stress was observed in the 2.5% CNC reinforced chitosan hydrogel compared with the pure chitosan hydrogel.

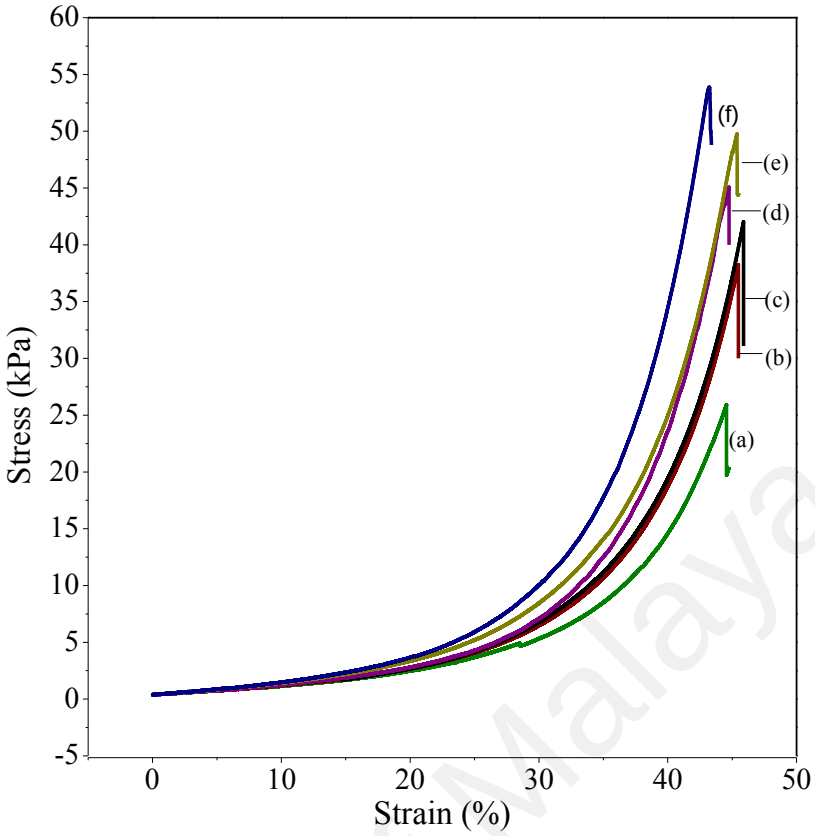

Figure 4.2: Stress-strain curves of hydrogels: (a) chitosan hydrogel; (b) 0.5% CNC-chitosan hydrogel; (c) 1% CNC-chitosan hydrogel; (d) 1.5% CNC-chitosan hydrogel; (e) 2% CNC-chitosan hydrogel; (f) 2.5% CNC-chitosan hydrogel

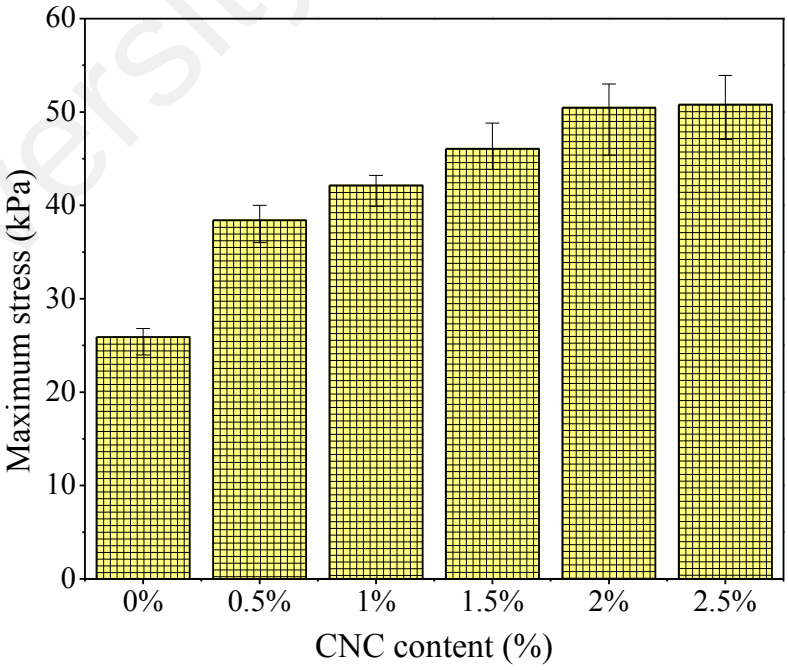

Figure 4.3: Maximum stress of hydrogels with varying CNC content

Figure 4.4 shows a comparison of the compression processes of the chitosan hydrogel and the 1.5% CNC-chitosan hydrogel. Figure 4.4a and Figure 4.4c represent the appearances of the 1.5% CNC-chitosan hydrogel and the chitosan hydrogel before the compression tests, respectively. An irreversible damage occurred in the 1.5% CNC-chitosan hydrogel because of the internal fractures induced under a maximum compression of 46.07 ± 2kPa. However, the 1.5% CNC-chitosan hydrogel completely recovered its shape after maximum compression (as shown in Figure 4.4b). By contrast, the chitosan hydrogel was brittle; it easily broke into fragments under a maximum compression of 25.9 ± 1kPa (as shown in Figure 4.4d).

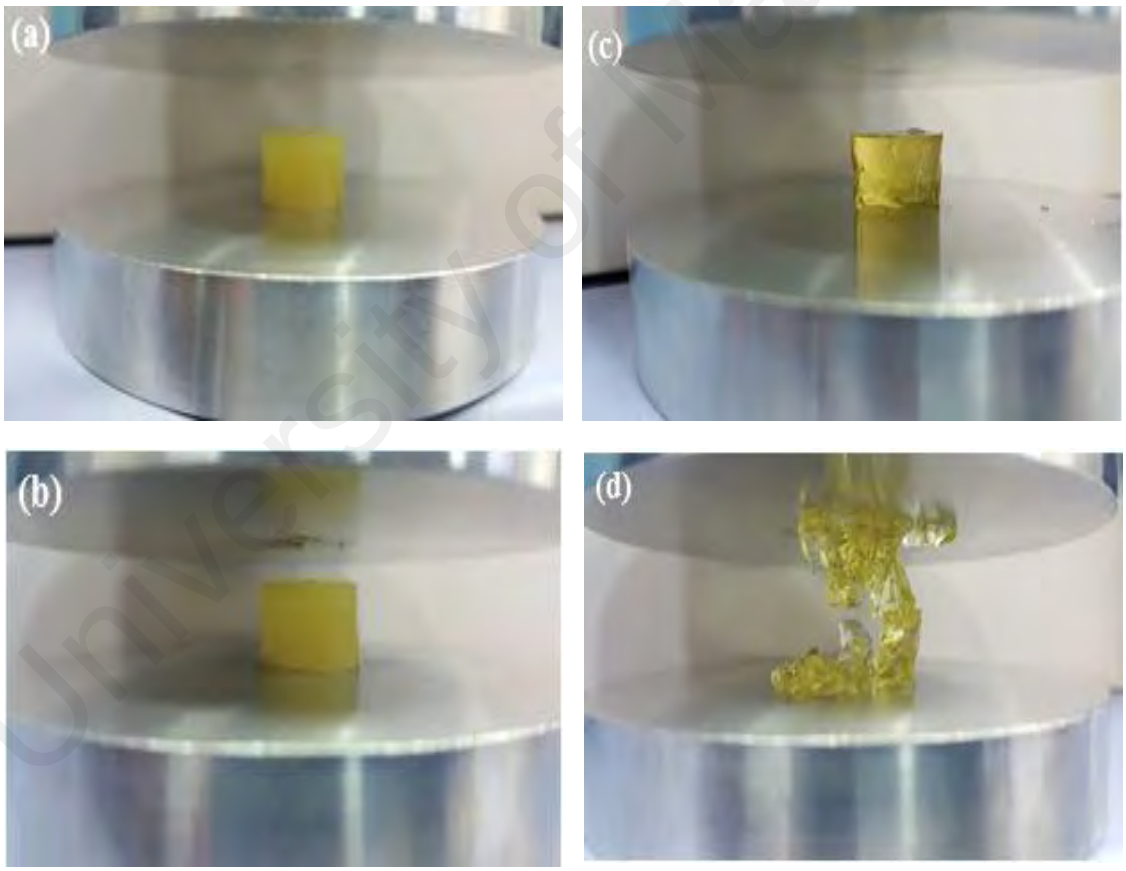

Figure 4.4: Comparison of compression process of hydrogels: (a) 1.5% CNC-chitosan hydrogel (before compression); (b) 1.5% CNC-chitosan hydrogel (after compression); (c) chitosan hydrogel (before compression); (d) chitosan hydrogel (after compression)

The results showed that maximum compression did not increase with the addition of over 2.5% CNCs to the chitosan hydrogel. The maximum compression values were 51.7 ± 6kPa and 54.4 ± 3kPa for the 5% CNC-chitosan hydrogel and 7% CNC-chitosan hydrogel, respectively. According to the previous studies, the average cumulative stress summed over the 30 min period prior to gastric emptying is 160,000 ± 70,000 dynes/cm^2 (16 ± 7 kPa) fasted and 520,000 ± 270,000 dynes/cm^2 (52 ± 27 kPa) fed. Based on the results of our compression studies, these stresses can be withstand by 5% - 7% nanocellulose reinforced chitosan hydrogels. In the previous study of Ji et al. (2011), the compressive strength of the chitosan hydrogel with 0.5% v/v of glutaraldehyde was approximately 65 kPa at 43% strain level. In our study, 0.2% v/v of glutaraldehyde was used to prepare the pure chitosan hydrogel and the CNC-reinforced chitosan hydrogels. A comparison of our results with those of Ji et al. (2011) showed that significantly enhanced mechanical properties were achieved with a lower crosslinker concentration. These results are also in good agreement with the results of previous studies in which CNC have been incorporated into several polymer matrices, such as poly(vinyl alcohol), poly(lactic acid), poly(vinylidene fluoride), natural rubber and starch (Cho & Park, 2011; González, Retegi, González, Eceiza, & Gabilondo, 2015; Mariano, El Kissi, & Dufresne, 2016; Sullivan, Moon, & Kalaitzidou, 2015; Zhang, Wu, Song, Lei, & Wu, 2015). Therefore, the mechanical strength of the chitosan hydrogel can be tailored to satisfy the specific requirements of different applications by incorporating CNCs.

CNCs exhibit high mechanical properties and crystallinity degrees compared with natural cellulose. He et al. (2014) reported that the estimated theoretical value of Young‘s modulus along the chain axis for perfect CNCs was 167.5 GPa, which was theoretically greater than the Young‘s modulus of steel. Nanoparticles typically act as decelerators which prevent cracking and retard the fragmentation of hydrogels (Han,

Lei, & Wu, 2014). By bridging cracks, nanocellulose can impede the further growth of fractures prior to the failure of the hydrogels (as shown in Figure 4.5). The optical microscopic images shown in Figure 4.5a and Figure 4.5b show the cross section and a crack in the 2.5% CNC-chitosan hydrogel, respectively. Our results indicated that incorporating CNCs into the chitosan hydrogel induced a combination of amorphous and crystalline regions in the hydrogel, thereby resulting in improved mechanical properties. Furthermore, the improvement of the mechanical properties confirmed the strong adhesion and interaction between two polysaccharides because of the chemical similarity between their molecules (Fernandes et al., 2010). The FESEM micrographs (Figure 4.6) and the increase in the maximum stress from 38.4 ± 1kPa to 50.8 ± 3kPa provide further experimental evidence of the strong interfacial adhesions between CNCs and the chitosan matrix.

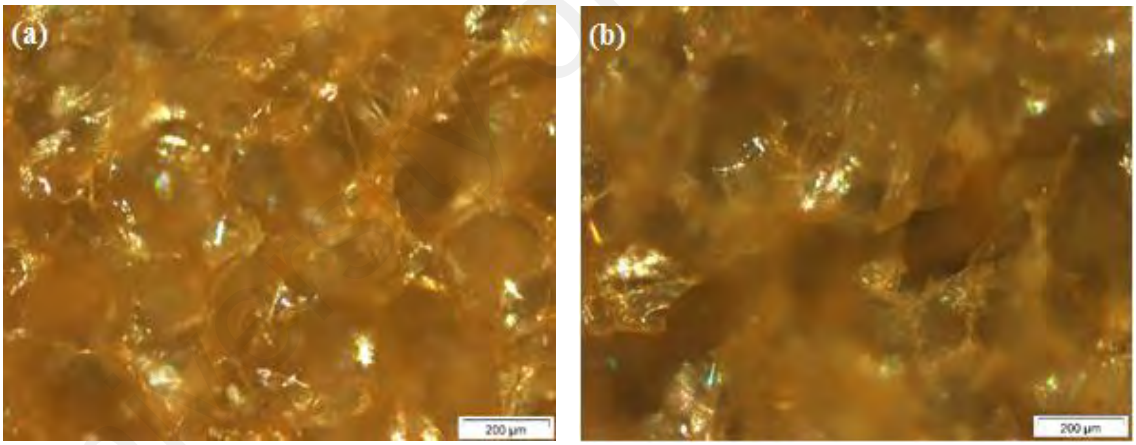

Figure 4.5: Optical microscopic images for the cross section of: (a) 2.5% CNC-chitosan hydrogel; (b) a crack in 2.5% CNC-chitosan hydrogel

4.1.1.2 Morphology studies

Prior to the FESEM observation, the hydrogels were freeze-dried to remove the water and to avoid disturbing the morphology of the hydrogels. The micrograph (Figure 4.6) was acquired at 60,000× magnification and an accelerating voltage of 5 kV. After freeze-drying, the hydrogels exhibited a highly porous network structure. The pure chitosan matrix (Figure 4.6a) exhibited a relatively smooth surface. By contrast, the

4.1.1.3 Impact of pH on swelling behavior

Swelling experiments were conducted using three different buffer solutions to investigate the effect of pH on the swelling properties of chitosan and the CNC-chitosan hydrogels. The swelling behavior of hydrogels was observed over a period of 90 h until a swelling plateau was attained. Figure 4.7 shows that in all the tested pH values, the chitosan hydrogel exhibits the highest swelling ratio followed by the 0.5% CNC-chitosan hydrogel, and then by the 1% CNC-chitosan hydrogel. The swelling ratios of the hydrogels gradually declined with increasing CNC concentration. All the CNC-reinforced chitosan hydrogels were expected to demonstrate enhanced swelling behavior because of the hydrophilic nature of CNC, which could increase the water uptake of the hydrogels. However, our results indicated unpredicted decreases in the swelling ratios. Less swelling occurred because more spaces within the hydrogel were filled-up by the CNCs as CNC content increased, as shown in Figure 4.1. This filling-up of spaces caused the formation of a rigid hydrogel structure, which consequently hindered water molecules from penetrating in to the structure (Ooi et al., 2016). Therefore, water uptake decreased, which reduced swelling ratio. This phenomenon can be proven via FESEM analysis (as shown in Figure 4.8). Figure 4.8a shows the FESEM image of the cross section of the 0.5% CNC-chitosan hydrogel, and Figure 4.8b shows that of the 2.5% CNC-chitosan hydrogel. At the same magnification of 100×, the average pore size of the 2.5% CNC-chitosan hydrogel is smaller than that of the 0.5% CNC-chitosan hydrogel. (The average pore sizes of hydrogels were calculated using ImageJ software. For pore size measurement, at least 80 pores were measured from each FESEM image of the cross section of 2.5% CNC-chitosan hydrogel and 0.5% CNC-chitosan hydrogel. The results observed from this software indicate an average pore size of 266.76 ± 42.31 μm in case of 0.5% CNC-chitosan hydrogel and 222.52 ± 41.07 μm in case of 2.5% CNC-chitosan hydrogel, respectively.)

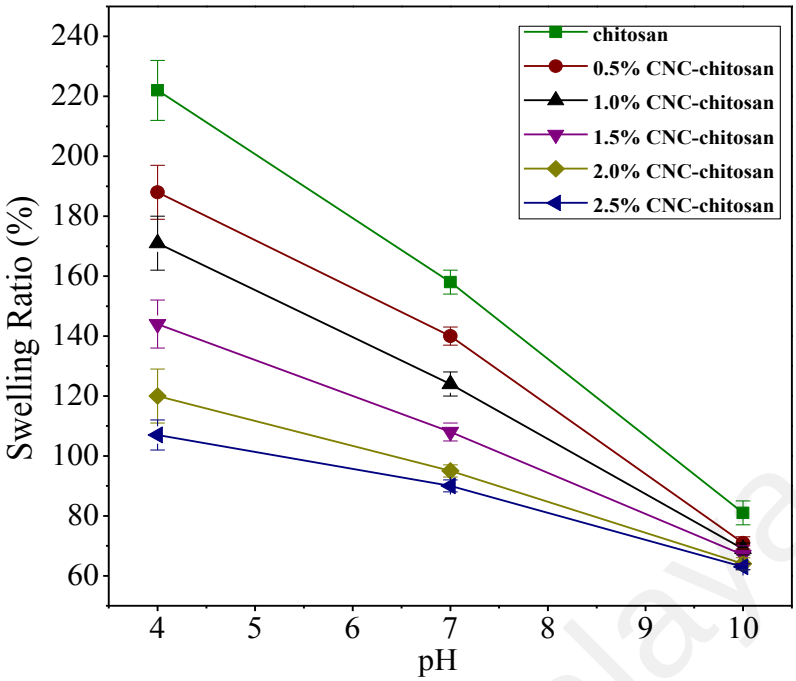

Figure 4.7: Swelling behavior of hydrogels at different pH values

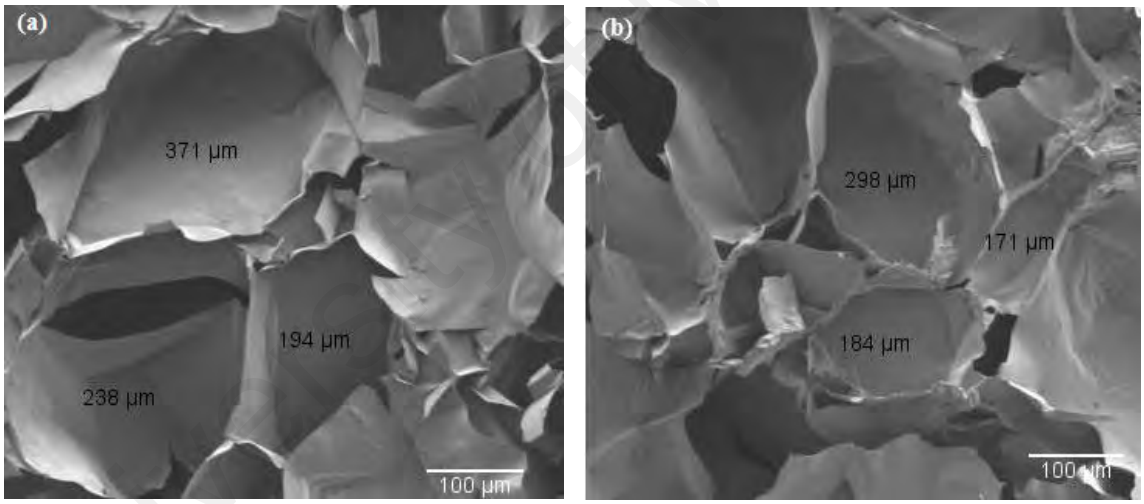

Figure 4.8: FESEM images of the cross section of hydrogels: (a) 0.5% CNC-chitosan hydrogel; (b) 2.5% CNC-chitosan hydrogel

Hydrogels are hydrophilic, polymeric materials that retain large amounts of fluids in their swollen state without dissolving the polymer matrix. Chemical crosslinking is one of the methods used to prepare a hydrogel via the covalent crosslinking of polymer chains. A low crosslinker concentration decreases the strength of a hydrogel and increases its flexibility and expandability, while absorbing its medium. Increasing the crosslinking agent can be applied to increase the crosslinking degree, this technique weakens water-retaining properties. In this work, 0.2% (v/v) glutaraldehyde was used as

4.1.1.4 Swelling ratio in distilled water

In this study, swelling experiments were carried out in distilled water for chitosan hydrogels prepared with different percentage of CNCs. As shown in Figure 4.10, swelling increases with time, first rapidly and then slowly, reaching a plateau. All the hydrogel formulations showed more than 100% swelling ratios within first 15 min. In our previous results, we found that the pore sizes of these hydrogels are in the range of several hundred micrometers. According to Ganji, Vasheghani-Farahani, and Vasheghani-Farahani (2010) the hydrogels possessing pore sizes of several hundred micrometers are classified as super-porous hydrogels (SPHs) which act as a capillary system causing a rapid water uptake into the porous structure. Such a fast swelling is because of absorption of water by capillary force rather than by simple absorption.

After the rapid swelling stage, the swelling ratio increased slowly to reach an equilibrium state. During the process of hydrogel swelling, against the favorable osmotic force, there is an opposite elasticity force, which balances the stretching of the network and prevents its deformation. At equilibrium, elasticity and osmotic forces are balanced and prevent additional swelling (Saber-Samandari & Gazi, 2015).

Referring to our previous study, all the hydrogels showed highest swelling ratio at acidic medium (pH 4.01). Results of the swelling test of this study showed that the hydrogels swelled more in distilled water than those swelled in buffer solutions (pH 4.01, pH 7 and pH 10.01). Annabi, Mithieux, Weiss, and Dehghani (2009) described that the reason for lowering of swelling ratio of elastin hydrogels in buffer solutions is due to the presence of salt in buffer solutions resulting in a contraction of the material due to water expulsion.

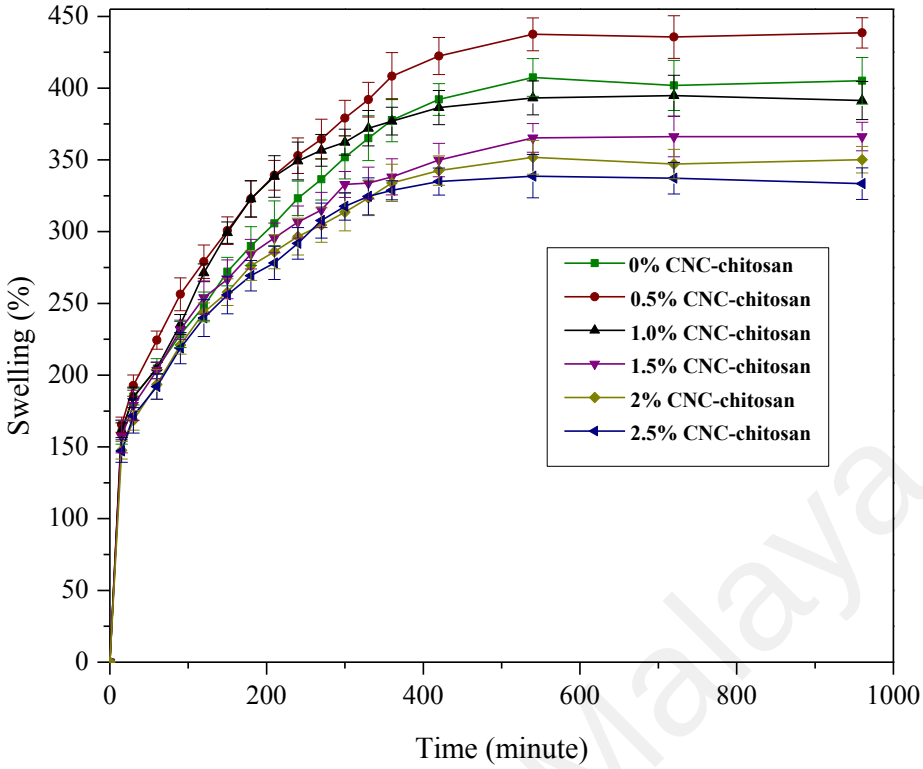

Figure 4.10: Equilibrium swelling ratio of hydrogels with varying CNC

Out of all types of hydrogels, the 0.5% CNC–chitosan hydrogel showed the highest equilibrium swelling ratio (438% ± 11%), followed by pure chitosan hydrogel (407% ± 13%) and then the 1.0% CNC–chitosan hydrogel (395% ± 14%). Initial swelling is because of water molecules forming hydrogen bonds with hydrophilic functional groups (amine ($–NH_2$) and hydroxyl groups (–OH)) present in the chitosan chains. More water molecules then orientate around the bound water to form cage like structures. Finally, excess water enters freely into the hydrogel network resulting in more swelling (Khurma, Rohindra, & Nand, 2006). All CNC–chitosan hydrogels were expected to show increased swelling ratios due to the hydrophilic property of the CNC. However, our results revealed that the 0.5% CNC–chitosan hydrogel achieved the highest equilibrium swelling ratio. Swelling ratio decreased with further increasing of CNC. Previous studies have described that the decrease of swelling occurred with increase of CNC in the hydrogel is due to the filling up of the free space of hydrogel by CNCs (Ooi et al., 2016).

4.1.1.5 X-ray diffraction analysis

The X-ray diffraction (XRD) patterns of the CNC, pure chitosan and hydrogels were investigated via powder XRD analysis. The X-ray diffractograms of the CNC, pure chitosan, chitosan hydrogel and 2.5% CNC-chitosan hydrogel shown in Figure 4.11a, b, c and d, respectively. MCC is a semi-crystalline polymer that consists of amorphous and crystalline regions in varying proportions. Acid hydrolysis was used to remove the amorphous regions of MCC while leaving the crystalline regions intact.

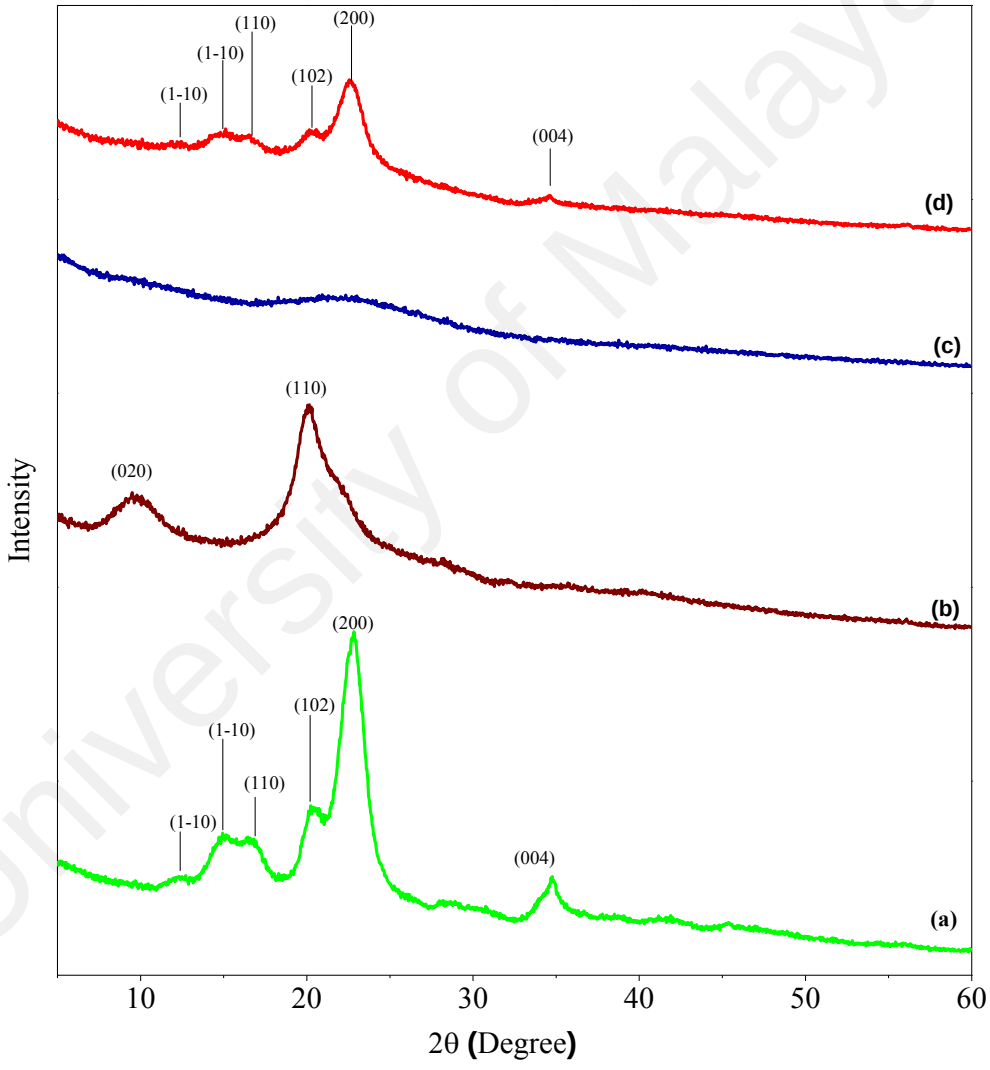

Figure 4.11: X-ray diffraction patterns of: (a) cellulose nanocrystals, (b) pure chitosan, (c) chitosan hydrogel and (d) 2.5% CNC-chitosan hydrogel

As shown in the diffractogram in Figure 4.11a, the CNC exhibited peaks around 2θ 15°, 16.5°, 20.5°, 22.5°, 34.5°, which respectively represent the (1-10), (110), (102),

(200), and (004) crystallographic planes of a typical cellulose I structure (A. Kumar et al., 2014; Novo, Bras, García, Belgacem, & Curvelo, 2015). In addition, a small peak appeared at around 2θ =12.2°, which corresponded to the (1-10) crystallographic plane of cellulose II (French & Cintrón, 2013). As shown in Figure 4.11b, two characteristic broad diffraction peaks are evident in pure chitosan; these peaks are typical fingerprints of semi-crystalline chitosan. These diffraction peaks, found at 2θ = 10°, and 2θ 20° respectively represent the diffractions from the (020) and (110) planes of the chitosan crystalline lattice (Bangyekan, Aht-Ong, & Srikulkit, 2006). However, after crosslinking with glutaraldehyde, these characteristic peaks disappeared, and a weak and broad peak appeared in the 20°–30° region (as shown in Figure 4.11c). This result could be attributed to the substitution of the amino and hydroxyl groups with the crosslinking agent. As consequences of this substitution, the intermolecular and intramolecular hydrogen bonds were deformed, and the regularity of the packing of the pure chitosan chains were destroyed. Consequently, the amorphous crosslinked chitosan (chitosan hydrogel) was formed. These results are consistent with the studies of B. Li et al. (2013) and Rahmi, Fathurrahmi, Irwansyah, and Purnaratrie (2015), who have reported on the XRD patterns of chitosan and crosslinked chitosan. Compared with the chitosan hydrogel diffraction patterns, the diffractogram of the CNC-reinforced chitosan hydrogel (Figure 4.11d) presented significantly elevated peaks because of the introduction of CNCs. The diffractogram exhibited peaks at around 2θ 15°, 16.5°, 20.5°, 22.5°, 34.5° which corresponded to crystal-type cellulose I. The minute peak around 2θ 12.2° is attributed to cellulose II structure. The characteristic broad peak of the amorphous crosslinked chitosan (chitosan hydrogel) in the 2θ = 20°–30° region, was super-positioned on the peaks of the CNC. This result shows that the CNC-chitosan hydrogel exhibits a combination of amorphous and crystalline regions.

4.1.1.6 Fourier-transform-infrared spectroscopy (FTIR)

FTIR spectroscopy was used to study the changes in the functional groups of chitosan after crosslinking and nanocellulose reinforcement (as shown in Figure 4.12). The FTIR spectra of the CNC, pure chitosan, chitosan hydrogel, and 2.5% CNC-chitosan hydrogel are presented in Figure 4.12a, b, c and d, respectively. The spectrum of the pure chitosan powder (Figure 4.12b) showed peaks at 1028 cm^{-1} and 1059 cm^{-1}, which corresponded to the C–O stretching of the C–3 position. The peak at 1150 cm^{-1} could be assigned to the asymmetric stretching of the C–O–C bridge, whereas the peak at 1321 cm^{-1} could be attributed to the C–N stretching of amide III (Fernandes Queiroz, Melo, Sabry, Sassaki, & Rocha, 2014; Khan et al., 2012; Rao, Naidu, Subha, Sairam, & Aminabhavi, 2006). The peaks at 1376 cm^{-1} and 1422 cm^{-1} corresponded to CH_2 bending and CH_3 symmetrical deformations. The bands at 1586 cm^{-1} and 1645 cm^{-1} could be assigned to the NH bending of primary amine and C═O stretching of amide I. The peak at 2876 cm^{-1} could be attributed to the C–H asymmetric stretching vibration (Brugnerotto et al., 2001; Leceta, Guerrero, & De la Caba, 2013). The broad peak at 3359 cm^{-1} was ascribed to the overlapping of the O–H stretching and N–H stretching vibrations, as well as the intramolecular hydrogen bonds (Celebi & Kurt, 2015).

However, major changes can be observed in the spectrum of the chitosan hydrogel by comparing the spectrum of pure chitosan and the chitosan hydrogel. The FTIR spectrum of chitosan hydrogel showed that the peaks assigned to the N–H and O–H stretching vibrations widened and shifted from 3359 cm^{-1} to 3340 cm^{-1}, the C–H asymmetric stretching vibration at 2876 cm^{-1} shifted to 2910 cm^{-1}, and the C═O stretching vibrations at 1645 cm^{-1} shifted to 1635 cm^{-1}. Moreover, the peaks for the CH_2 bending and CH_3 symmetrical deformation at 1376 cm^{-1} and 1422 cm^{-1} disappeared as a result of the formation of a medium-sized peak at 1407 cm^{-1}. By

contrast, the band at 1586 cm^{-1} (N–H bending) disappeared, and a sharp peak formed at 1548 cm^{-1} because of the formation of the glutaraldehyde crosslinked structure of chitosan. The crosslinking process of chitosan with glutaraldehyde was confirmed by the presence of an evident peak at 1548 cm^{-1}. This peak represents the stretching vibrations of C═N in the Schiff's base (imine bond C═N) formed as a consequence of the crosslinking reaction between the amino groups of chitosan and the aldehyde groups of glutaraldehyde (B. Li et al., 2013).

The FTIR spectra of CNC and chitosan are fairly similar because of the chemical similarity between chitosan and cellulose. In the FTIR spectrum of the CNC-chitosan hydrogel, peaks representing both the chitosan hydrogel and CNC were observed. No changes or new peaks appeared, thereby indicating that the cellulose nanoparticles were physically added to chitosan hydrogel. Both materials maintained their individual chemical structures, which provided that the CNC-chitosan hydrogel existed in the form of a semi-IPN.

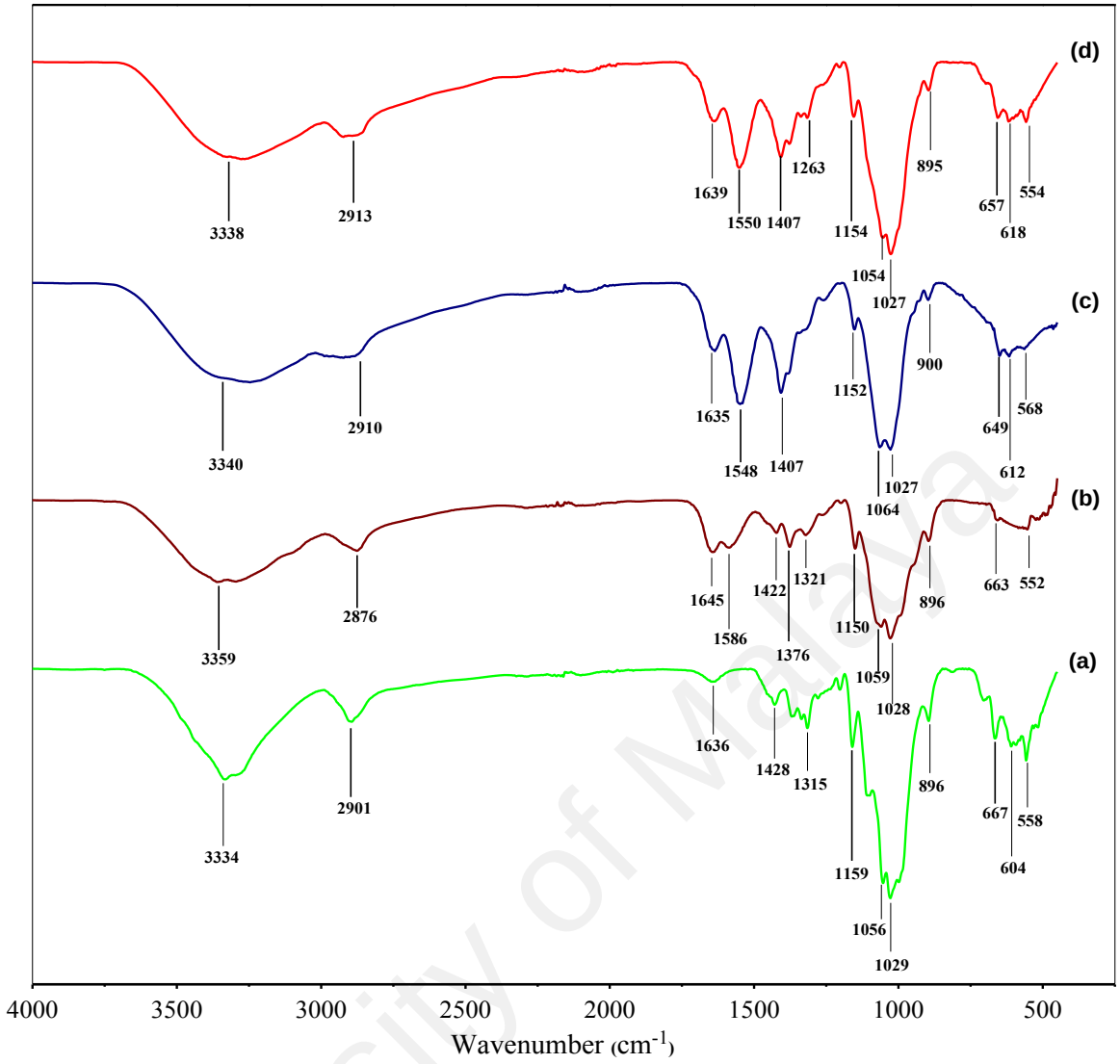

Figure 4.12: FTIR spectra of: (a) cellulose nanocrystals, (b) pure chitosan, (c) chitosan hydrogel and (d) 2.5% CNC-chitosan hydrogel

4.1.1.7 Differential scanning calorimetry

Figure 4.13 shows the DSC thermograms of chitosan, chitosan hydrogel, CNC and 1.5% CNC-chitosan hydrogel. The DSC thermograms of pure chitosan exhibited one endothermic peak in the temperature range of 80-100 ^{0}C. This might be due to the evaporation of bound water. Exothermic peak of chitosan was found at 307 °C which corresponds to decomposition of chitosan polysaccharide. This includes depolymerization, saccharide rings dehydration and decomposition of deacetylated and acetylated chitosan units. These peaks are in agreement with those reported in previous studies (Pendekal & Tegginamat, 2012; Yuan et al., 2011).

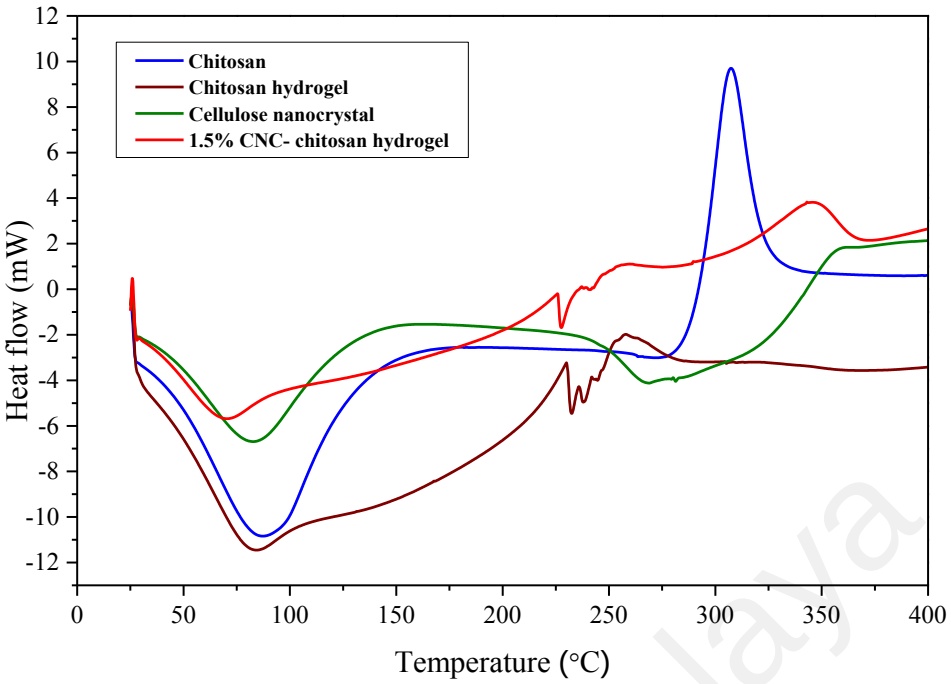

Figure 4.13: The DSC curves of chitosan, CNC, chitosan hydrogel and 1.5% CNC-chitosan hydrogel

In case of chitosan hydrogel, wide endothermic peak around 84 °C associated to the evaporation of bound water. Comparing this endothermic peak with the peak of chitosan (which corresponding to the dehydration), the endothermic peak of hydrogel was observed to broaden towards the high temperature region. Since the crosslinking reaction occurs between the glutaraldehyde and the amino groups of chitosan, it will have less amino groups available to form hydrogen bonds with water molecules. As a result, more water molecules will be bound to chitosan hydroxyl groups instead of amino groups. Since the hydrogen bonds with the hydroxyl groups are stronger than the ones with the amino groups, a higher temperature would be necessary to remove such water molecules (Yang & Su, 2011). The endothermic peaks in 232 °C, 238 °C and 246 °C, corresponding to the melting of the crystalline parts of the material. The appearance of three different endothermic melting peaks are due to the polymer chain arrangement and the formation of different crystallite sizes (Bashir et al., 2016; Dole, 1956; Ma, Liu, Liu, & Sui, 2015; Martins et al., 2015). As shown in Figure 4.13, the exothermic decomposition peak of chitosan was about 307 °C, whereas that of crosslinked chitosan hydrogel was about 258 °C. This revealed that the thermal stability of chitosan

decreased when it is crosslinked with glutaraldehyde. This might be due to the intra crosslinking reactions between chitosan chains, which interfere with previously existing attractive hydrogen bonds. Similar results have also been reported in a previous study on thermal stability of glutaraldehyde crosslinked chitosan membranes (Yang & Su, 2011).

In the curve of nanocellulose, the first endothermic peak appeared at 82 °C and can be ascribed to the evaporation of water. The surface of CNCs become sulfated because of introduction of hydrogen sulfate anion from the hydrolysis by sulfuric acid. Therefore, moisture absorption affinity greatly decreased in nanocellulose (Tan, Hamid, & Lai, 2015). Also, the evaporation of moisture occurred at lower temperatures because of small amount of loosely adsorbed moisture on the surface of the cellulose. The next endothermic peak of nanocellulose was observed around 270 °C due to the melting of CNCs and the peak was not uniform. Because of hydrolysis by sulfuric acid, CNCs have remarkable changes with respect to packing of the ultimate crystal structure as well as size of particles. Hydrolysis by sulfuric acid would sulfate both the amorphous region and accessible hydroxyl groups. Subsequently, this bulky sulfate groups will increase the interlayer spacing within the cellulose chains. As a result, crystal compactness of CNCs might be rearranged and molecular weight or degree of polymerization would decrease. Therefore, the size distribution and molecular weight of cellulose crystals would become wider (Tan et al., 2015). These could explain why there was a wider melting peak in the curve of nanocellulose. Similar results were observed by N. Ma et al. (2015) and Tan et al. (2015) for the DSC curves of nanocellulose, which produced by acid hydrolysis method.

The incorporation of CNCs in to chitosan hydrogel matrix lowered their moisture contents and the endothermic peak related to evaporation of water lowered to 70 °C.

CNC can only absorb moisture on the crystalline surfaces and is less hydrophilic than chitosan matrix (Khan et al., 2012). The crosslinked network of chitosan and the tighter network formed by interaction of the free OH groups of chitosan with nanocellulose surfaces, respectively, seem to block the active sites for absorption of moisture. Furthermore, the moisture adsorption affinity greatly decreased in sulfated CNC and therefore, the evaporation of moisture occurred at lower temperatures because of small amount of loosely adsorbed moisture on the surface of the cellulose (Tan et al., 2015). The next endothermic peak of the DSC curve corresponds to the melting of the crystalline parts of the material. It showed a more pronounced endothermic peak at 228 °C and non-pronounced endothermic peak at 243 °C. The differences in melting peaks of chitosan hydrogel and CNC/chitosan hydrogel were related to the insertion of nanocellulose in the hydrogel matrix, which promoted changes in the packing of chains related to pure chitosan hydrogel (Martins et al., 2015). As can be seen from the DSC curve, a pronounced exothermic peak appeared around 344 °C which corresponding to the decomposition of nanocellulose reinforced chitosan hydrogel. Nanocellulose reinforced chitosan hydrogel showed a higher thermal stability compared with the chitosan hydrogel, as it started to decompose at 304 °C. Normally, nanomaterials are stable and have high thermal decomposition temperature. When they are uniformly dispersed in chitosan matrix, thermal properties of the hydrogel increased, possibly due to the strong interfacial linkage between nanostructured cellulose and chitosan (as shown in Figure 4.6) (Zhou, Wang, Gu, & Xiong, 2009).

4.1.1.8 Crosslinking degree of chitosan hydrogel

In addition to the deacetylation degree of chitosan, the crosslinking degree also controls swelling, mechanical properties and rheological characteristics (Weng, Chen, & Chen, 2007). In this work, the crosslinking degree of the chitosan hydrogel was 83.6%.

This result is consistent with the findings of the study of Budianto, Muthoharoh, and Nizardo (2015). The crosslinking degree can be increased by increasing glutaraldehyde concentration. High crosslinking densities can increase the strength and density of hydrogels. In this research, we were able to improve the maximum compression of the hydrogels by increasing the CNC content at a constant crosslinker concentration.

4.1.1.9 In vitro degradation studies of the hydrogel in PBS solution

Degradation studies were carried out in PBS buffer at 37 °C for six weeks. The results of this study are presented in Figure 4.14. The hydrogels showed degradation due to the presence of −OH and $-NH_2$ groups in the chitosan backbone. These groups have the ability to interact with water. The hydrogel matrix became loose due to swelling property. Gels with low CNC content had greater ability to absorb the solvent and high swelling ability due to the presence of more void space in the hydrogel and loose network (Bashir et al., 2016). On the other hand, there may be physical crosslinks between the surface hydroxyls of cellulose crystals and –OH groups of chitosan molecules. The presence of H-bonding interactions between chitosan and cellulose restricts the relaxation of chitosan segments within the matrix. Besides that, the crystallinity is an important factor that influences the degradation of hydrogel due to the different chain packing arrangements of each polymer. Amorphous structure allows more water to penetrate in to its polymer matrix resulting faster degradation rates. In the crystalline regions, polymer chains are closely packed and resist the penetration of water molecules within the regions. CNCs are high crystalline particles with highly ordered and closely packed chains. The X-ray diffraction patters of our previous study also indicated that the addition of CNCs will induce a combination of crystalline and amorphous regions in the nanocelulose reinforced chitosan hydrogel. Several studies have also demonstrated that a small amount of CNC could lead to a remarkable decrease in the degradation rate of the composite matrix (Abou-Zeid, Hassan, Bettaieb, Khiari, &

Hassan, 2015; Paula, Mano, Duek, & Pereira, 2015). According to the results, 2.5% CNC–chitosan showed 69% weight loss as it contained high amount of CNCs, while chitosan hydrogel lost its 84% weight because it does not contain CNCs.

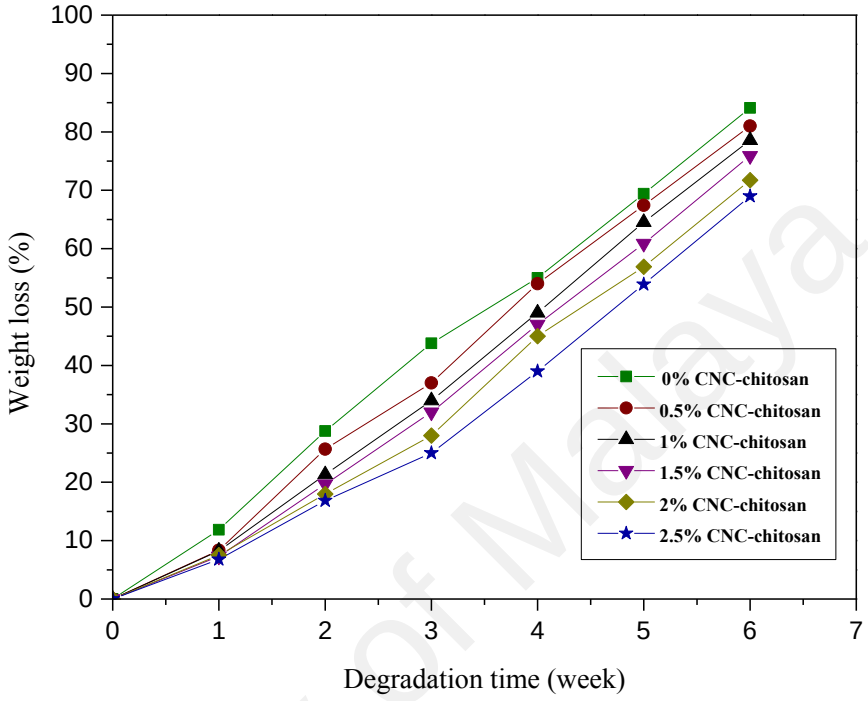

Figure 4.14: In vitro degradation study of the hydrogels with different concentration of nanocellulose

4.1.2 Characterization of gas foamed hydrogel

4.1.2.1 Mechanical properties

From the previous results, the maximum compression of CNC–chitosan hydrogel increased from 25.9 ± 1 kPa to 50.8 ± 3 kPa with increasing CNC content ranging from 0% to 2.5%. In addition, the maximum compression did not increase significantly with the addition of over 2.5% CNCs to the chitosan hydrogel. The previous results indicated a decrease in swelling ratios with increasing the CNC content of chitosan hydrogel. Within the CNC reinforced hydrogels, 0.5% CNC–chitosan hydrogel indicated the highest swelling ratio in distilled water. Therefore, 0.5% CNC–chitosan hydrogel was used for the gas foaming process and for the investigation of mechanical properties.

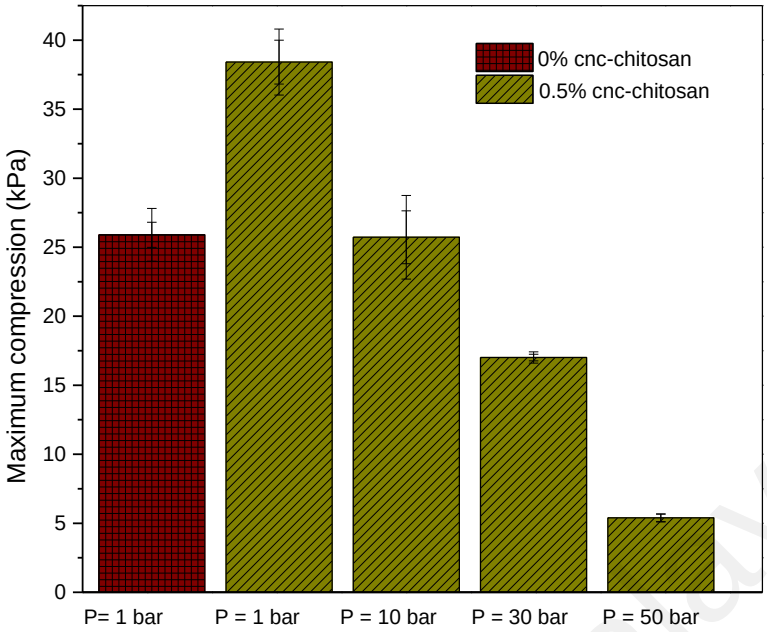

Figure 4.15: Maximum compression of hydrogels formed at different pressure conditions

As shown in Figure 4.15, the maximum compression of pure chitosan hydrogel was 25.9 ± 1 kPa and it increased to 38.4 ± 1 kPa with the introduction of 0.5% cellulose nanocrystals. The maximum compression of 0.5% CNC–chitosan hydrogel produced at atmospheric condition was 38.4 ± 1 kPa and it decreased with increasing the pressure of gas foaming process. This value for hydrogels produced at 10, 30 and 50 bar was 25.7 ± 2, 17.0 ± 0.2 and 5.4 ± 0.2 kPa, respectively. The decrease in maximum compression is due to the increase of pore size and the pore interconnectivity of CNC–chitosan hydrogel produced at gas foaming process. Several studies have also reported that the mechanical strength of hydrogels and scaffolds decreases with increase of the pore size and the pore interconnectivity (Annabi, Nichol, et al., 2010; Chiu et al., 2013; Mohammed et al., 2015). Ji et al. (2011) reported that the compressive modulus of glutaraldehyde crosslinked chitosan was more than threefold lower at CO_2 pressure of 60 bar when compared with the hydrogels produced at atmospheric condition. According to Ji et al. (2011) the maximum compression of gas foamed chitosan hydrogel is comparatively greater than the results of our study. This may be due to the

high concentration of glutaraldehyde (0.5% v/v) used for their study. According to the results of Annabi et al. (2009) the maximum compression of α-elastin hydrogel produced at dense gas CO_2 (pressure at 60 bar) was 4.3 ± 1.4 kPa; slightly lower than the results of our study, which is due to the nature of biopolymer used.

4.1.2.2 Morphology studies (Before and after immersed in simulated gastric fluid)

Prior to FESEM observation, hydrogels were freeze-dried to remove water to avoid disturbing the morphology of hydrogels. After freeze-drying, hydrogels exhibited a porous network structure (as shown in Figure 4.16). After the gas foaming (at 50 bar, room temperature), the pore size significantly increased with the formation of widely interconnected porous structure (as shown in Figure 4.16a). Gas foamed hydrogel exhibited rough cell wall structure which exposed more surface area to the drug molecules. Pore sizes of the hydrogel formed at atmospheric pressure (Figure 4.16b) was around 100 μm and it was more than 10-fold higher in gas foamed hydrogel.

Due to sudden volume expansion, the original morphological features changed in the swollen hydrogel in the drug diffusion medium. In the gas foamed hydrogel, the large pore structure disappeared and small interconnected pores formed after the immersion in simulated gastric fluid (as shown in Figure 4.16c). On the other hand, the initial porous structure of the hydrogel prepared at atmospheric condition was changed and formed a nonporous structure (Figure 4.16d).

Figure 4.16). Open capillary channels in super porous hydrogels absorb water by capillary force rather than by simple absorption resulting in faster swelling behavior (Gemeinhart, Park, & Park, 2000).

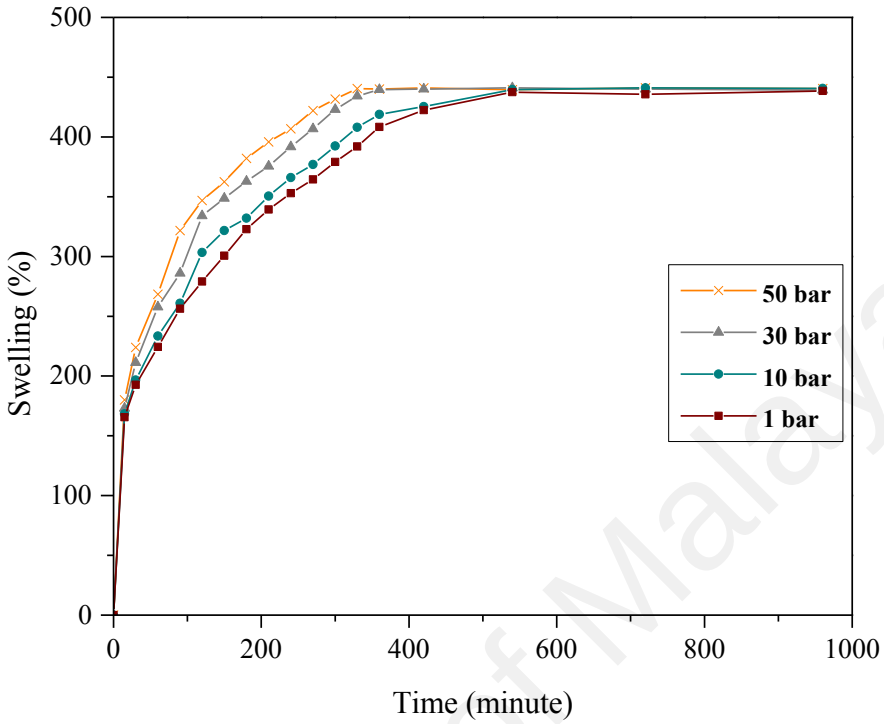

Figure 4.17: Equilibrium swelling ratio of 0.5% CNC–chitosan hydrogel formed at different pressure conditions

4.2 Drug delivery studies of nanocellulose reinforced chitosan hydrogel

4.2.1 Drug delivery studies of hydrogels formed at atmospheric condition

4.2.1.1 Characterization (FTIR analysis of curcumin and curcumin loaded hydrogel)

Figure 4.18 shows the FTIR spectra of pure chitosan hydrogel, 0.5% CNC–chitosan hydrogel, drug loaded 0.5% CNC–chitosan hydrogel and pure curcumin. Results of our previous study showed that the FTIR spectra of CNC and chitosan are fairly similar due to the chemical similarity between chitosan and cellulose. In the FTIR spectrum of the CNC–chitosan hydrogel, peaks representing both the chitosan hydrogel and CNC were observed. No change or new peak appeared in the spectrum of 0.5% CNC–chitosan hydrogel, thereby indicating that the cellulose nanoparticles were physically added to chitosan hydrogel. The spectrum of curcumin showed characteristic peaks at 1601,

1506, 1274, and 1152 cm^{-1}, which corresponded to the stretching vibrations of the benzene ring, C=C vibrations, aromatic C–O stretching, and C–O–C stretching modes, respectively (Pawar, Karde, Mundle, Jadhav, & Mehra, 2014; Zhao et al., 2015). Those characteristic peaks are not shifted significantly in curcumin loaded 0.5% CNC–chitosan hydrogel revealed that there is no interaction between drug and ingredients present in hydrogels. Thus, there is no change in the chemical composition of the drug after the loading process. However, the intensity of the bands in curcumin and curcumin-loaded hydrogel are different. The decrease in peak intensity is due to lower concentration of curcumin in the hydrogel as its concentration was not 100%. Hence, FTIR analysis provides significant evidence for the presence of curcumin in the drug-loaded hydrogel.

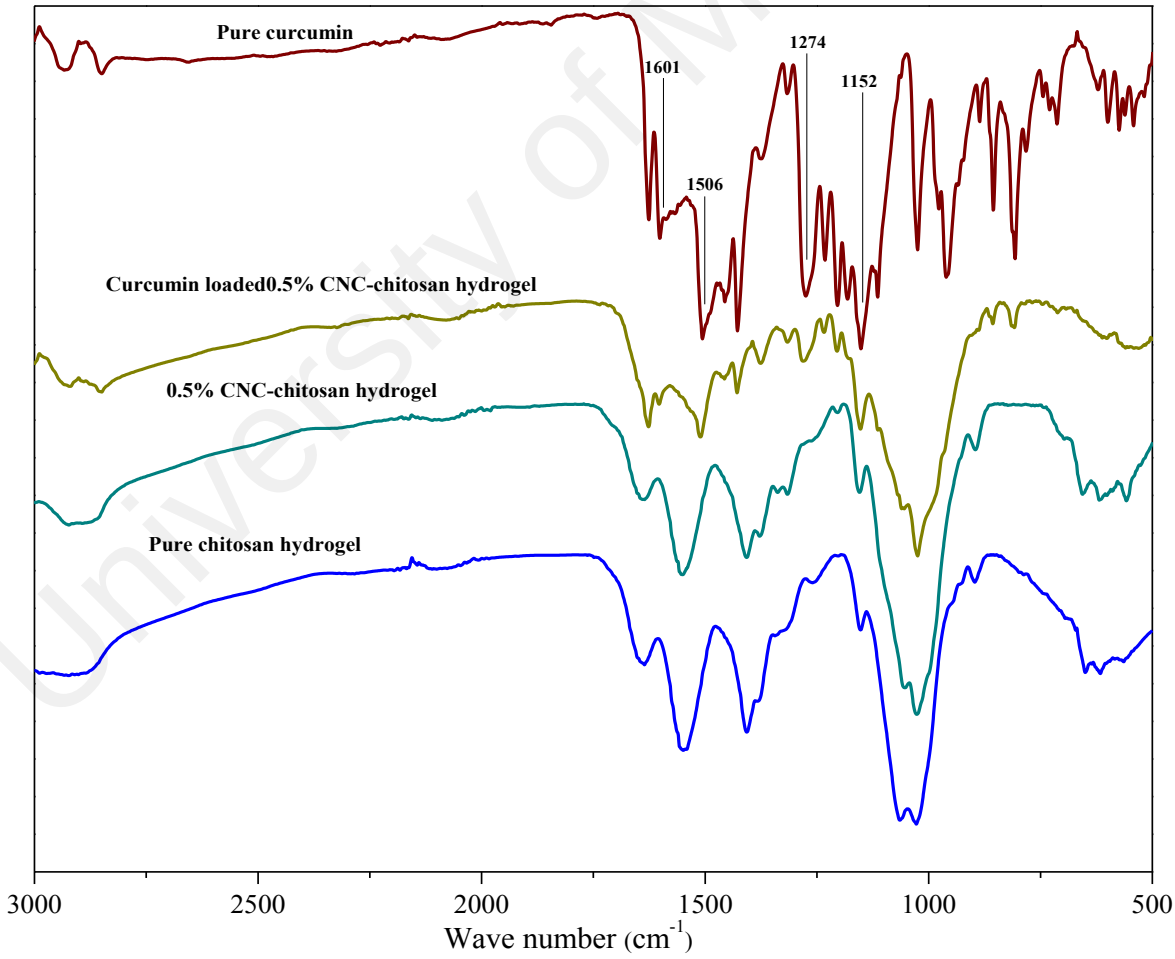

Figure 4.18: FTIR spectra of pure chitosan hydrogel, 0.5% CNC–chitosan hydrogel, curcumin loaded 0.5% CNC–chitosan hydrogel and pure curcumin

4.2.1.2 Drug encapsulation efficiency

For the curcumin molecule, intramolecular hydrogen bond is the primary interaction which consist of two hydroxyl groups (–OH) in the benzene ring and the hydroxyl near keto group (C═O) (Wegiel, Zhao, Mauer, Edgar, & Taylor, 2014). Probable interactions between curcumin and chitosan molecules are shown in Figure 4.19. The oxygen of hydroxyl on the benzene ring is an important binding site for chitosan molecules. One hydrogen bond can be formed by free hydroxyl groups of glucosamine and the other can be formed by the free amino group of glucosamine. The modeling studies of Liu, Cai, Jiang, Wu, and Le (2016) showed that the lower total energy of curcumin loaded chitosan compared to the total energy of individual molecules proved the possibility of these interactions in the drug loaded system. Thus, it is possible that an interaction will occur between drug and polymer molecules through hydrogen bonding. Results from our previous study showed that the degree of crosslinking of chitosan hydrogel was 83.6%. This reveals that more amine groups present in chitosan backbone are occupied by the crosslinking and formation of Schiff base. Therefore, it will limit the availability of free amine groups to bind with drug molecules.

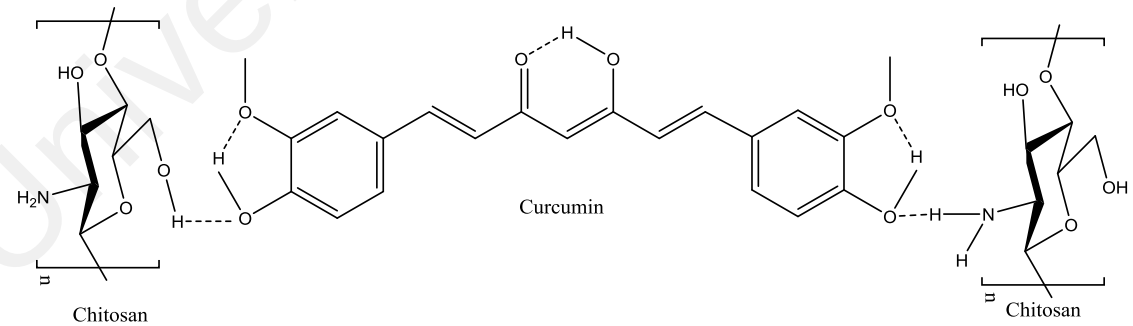

Figure 4.19: Probable interactions between curcumin and chitosan molecules

From the results showed in Figure 4.20, the maximum drug loading efficiency occurred for the 0.5% and 0.6% CNC–chitosan hydrogel which is 41% ± 2.4% and 41% ± 0.72%, respectively. This result was followed by 0.3% CNC–chitosan hydrogel (40%

± 0.73%), the 0.2% CNC–chitosan hydrogel (40% ± 0.82%) and so on. This observed trend was similar to the swelling test pattern of the hydrogels as indicated in Figure 4.10. When the hydrogel swelling ratio is high, a large amount of drug solution can be absorbed and retained in the hydrogel network, leading to an incremental increase in the drug loading efficiency. Therefore, we can conclude that the efficiency of drug loading in the hydrogel is dependent upon the swelling of the hydrogel in water. The p-value was used to test whether there is a relationship between nanocellulose content and entrapment efficiency. According to the p-value, there is a significant positive relationship between the nanocellulose content and the entrapment efficiency of the hydrogel ($r(8) = 0.87$, $p < 0.001$).

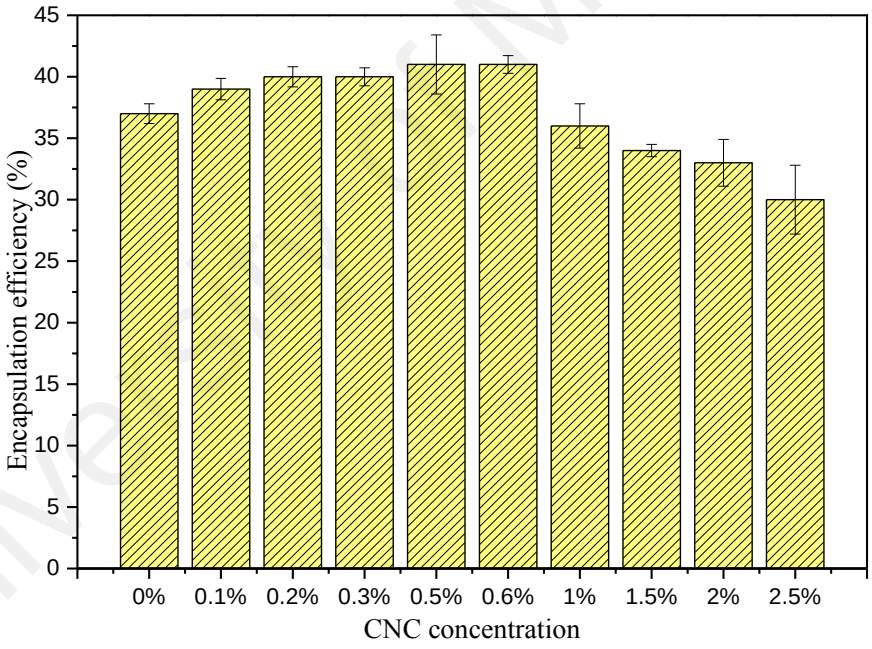

Figure 4.20: Encapsulation efficiency of curcumin for different hydrogels

As more CNC was added into the chitosan network, the voids in the chitosan network are gradually filled by CNC, forming a rigid structure and creating a barrier that would prevent the penetration of drug solution in to the hydrogel, which would cause a decrease in the drug loading efficiency.

4.2.1.3 In vitro drug release

The objective of this study is to improve the bioavailability of curcumin to increase absorption from acidic medium in a controlled manner, thereby avoiding wastage of the drug and achieving the desired treatment effect. As shown in Figure 4.21, the drug release pattern for all hydrogels investigated can be divided in to two phases: an initial burst release and a prolonged diffusion-controlled phase (Huang & Brazel, 2001). Rapid drug release in phase one of the test could be due to the presence of the drug on the surface of the hydrogel and the higher drug concentration gradient present at the beginning of the test. This higher concentration gradient could act as the driving force for the drug release from the hydrogel matrix. After the burst release, the releasing rates decline steadily with time, which may be due to the thickness of the hydrogel acting as a diffusion barrier (Fu & Kao, 2010).

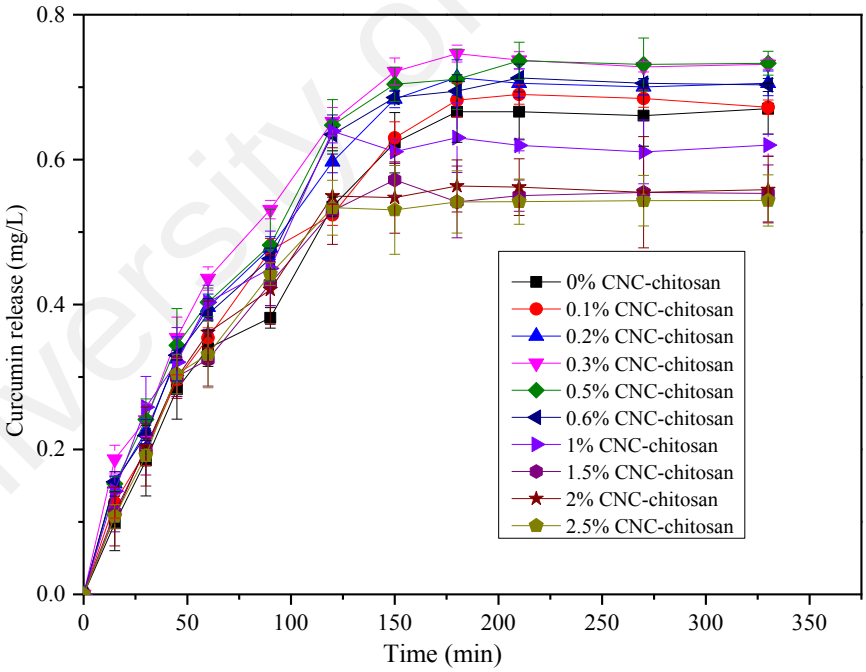

Figure 4.21: Curcumin release from different types of hydrogels

In general, the rate of drug release from hydrogel matrix is depend on the interaction between the drug and the polymer molecules, the solubility of the drug, and hydrogel swelling in aqueous media (Kim, Bae, & Okano, 1992). However, in this study, there is no indication for the presence of interaction between hydrogel and drug. Therefore, the

rate of drug release in this test depended only on the solubility of the drug and the swelling ratio of the hydrogel in aqueous media. It is clear that the drug release profiles of hydrogels are consistent with the data obtained from the swelling studies. The hydrogel with the higher swelling ratio achieved higher drug release percentages. In this study, the 0.5% CNC–chitosan hydrogel and 0.3% CNC-chitosan hydrogel had the highest drug release percentage, whereas the 2.5% CNC–chitosan hydrogel produced the lowest drug release percentage. A lower concentration of curcumin release from these hydrogels is attributed to the fact that curcumin has very poor solubility in water. It has been reported that curcumin has a solubility of around 2.67 μg/mL at pH 7.3 (Bajpai et al., 2015).

It is reported that the average gastric emptying times for healthy individuals at 1, 2, and 4 h are >90%, 60% and 10%, respectively (Jobe et al., 2013). Our results showed that all the hydrogels reached to a prolonged diffusion-controlled phase around 120 minutes. According to the drug release pattern of hydrogels, this drug delivery system can be suggested to improve the bioavailability of curcumin for the absorption from acidic medium during gastric residential time.

4.2.1.4 Drug release kinetics

The results of in-vitro drug release data can be plotted in various kinetic models, such as zero order, first order, Ritger-Peppas, Higuchi and Hixson–Crowell. The drug release mechanism from hydrophilic hydrogels is generally defined by diffusion of the drug from hydrogel matrix to the solution. In diffusion-based drug release systems, the drug release kinetics can be either Fickian or non-Fickian. Fickian diffusion describes the systems where the drug release rate is independent of its concentration.

Zero-order release kinetics describes the process of constant drug release from a drug delivery device. In its simplest form, the zero-order release kinetics can be described as Equation (4.1):

$$Q = Q_0 + K_0 t \tag{4.1}$$

Where Q is the cumulative amount of drug released or dissolved, Q_0 is the initial amount of drug in solution (it is usually zero) and K_0 is the apparent dissolution rate constant or zero-order release constant (Chime, Onunkwo, & Onyishi, 2013).

In non-Fickian diffusion, several factors can affect the drug release, and based on these factors, the release behavior can be predicted with several mathematical models as described below.

First-order model: The model describes the absorption and elimination of some drugs, although it is difficult to understand the mechanism on the theoretical basis. In typical first-order release kinetics, the drug release rate is directly proportional to the concentration of drug. First order model can be represented by the Equation (4.2):

$$Log\ Q_t = Log\ Q_0 - Kt/2.303 \tag{4.2}$$

Where Q_0 is the initial amount of drug in hydrogel, Q_t is the amount of drug released in time t and K is the first-order release constant (Chime et al., 2013).

Ritger-Peppas: Ritger and Peppas developed a simple, semi-emperical equation to describe drug release from polymeric matrix such as hydrogel. This model is generally applicable for pharmaceutical polymeric dosage forms when more than one type of release phenomena could be involved or release mechanism is not well known. Ritger-Peppas drug release model can be represented as Equation (4.3):

$$M_t/M_\infty = Kt^n \tag{4.3}$$

Where M_t/M_∞ is fraction of drug release at time t, K is the rate constant and n is release exponent (Chime et al., 2013).

Higuchi developed theoretical model to describe drug release from matrix drug delivery system involves both dissolution and diffusion. This is the most widely used model to describe drug release from different geometrics and porous system. Higuchi model is expressed as Equation (4.4):

$$Q_t = K_H t^{1/2} \quad (4.4)$$

Where Q_t is the amount of drug released in time t per unit area, K_H is the Higuchi release rate (Chime et al., 2013).

Hixson-Crowell: The model describes the release of the drug from systems where there is a change in surface area and diameter of particles or tablets. The equation shows that the drug release from the particle is proportional to the cubic root of its volume, and it can be described as Equation (4.5):

$$Q_0^{1/3} - Q_t^{1/3} = K_{HC} t \quad (4.5)$$

Where Q_0 is initial amount of drug in the hydrogel, Q_t is remaining amount of drug in hydrogel and K_{HC} is the rate constant for Hixson and Crowell equation (Chime et al., 2013).

In order to understand the in vitro drug release mechanism of the hydrogel, the released data were analyzed using zero order model, first order model, Hixson and Crowell model, Higuchi model and Ritger-Peppas model. The fitting results are shown in Table 4.1. These results revealed that the in vitro release profile of curcumin from hydrogel in simulated gastric fluid followed the Ritger- Peppas equation (According to R^2 values).

Table 4.1: Results of fitting models for in vitro release profile

Hydrogel Formulation	Zero-order R^2	First-order R^2	Higuchi R^2	Hixson-Crowell R^2	Ritger-Peppas R^2
0% CNC-chitosan	0.965	0.970	0.969	0.975	0.983
0.1% CNC-chitosan	0.935	0.942	0.985	0.960	0.993
0.2% CNC-chitosan	0.947	0.954	0.987	0.947	0.993
0.3% CNC-chitosan	0.930	0.939	0.988	0.926	0.989
0.5% CNC-chitosan	0.906	0.914	0.980	0.924	0.983
0.6% CNC-chitosan	0.907	0.914	0.976	0.928	0.981
1% CNC-chitosan	0.951	0.888	0.965	0.903	0.981
1.5% CNC-chitosan	0.949	0.851	0.974	0.955	0.986
2% CNC-chitosan	0.956	0.895	0.971	0.921	0.959
2.5% CNC-chitosan	0.962	0.884	0.966	0.922	0.957

Curcumin release kinetics was investigated using Ritger–Peppas model Equation (4.3). Where M_t/M_∞ is the ratio of curcumin release at time t to the equilibrium swollen state. K is the kinetic constant to measure velocity of release and geometrical parameters corresponding to drug–polymer system. *n* is the diffusion exponent related to transport mechanism. If $n < 0.5$, it indicates Fickian diffusion, or drug release that is diffusion-controlled and penetration of solvent into the hydrogel is much faster than the polymer chain relaxation. When $0.5 < n < 1$, diffusion and release of drug occur in a non-Fickian (anomalous) manner. This means that drug release followed both diffusion and erosion controlled mechanisms (Emami, Tajeddin, & Ahmadi, 2010). If $n = 1$, it indicates case II transport, where the release rate is constant and controlled by polymer relaxation. The values of *n*, *k* and R^2 of the present study are shown in Table 4.2. The n values range from 0.60–0.76 when curcumin released in simulated gastric fluid and drug release occurred in non-Fickian (anomalous) manner (Chime et al., 2013). If n is close to unity, it means solvent penetration controlled by relaxation of polymer chains rather than diffusion (Agnihotri & Aminabhavi, 2006). It appears that n value for 0% CNC–

chitosan hydrogel is closer to unity when compared with other hydrogels. This may be due to the fact that the 0% CNC–chitosan sample does not contain cellulose nanocrystals within the chitosan matrix. As the hydrogel does not contain the cellulose nanocrystals, there may be some relaxation of chitosan segments within the matrix. In this way, the curcumin release is not totally diffusion controlled but it is partly controlled by chain relaxation process also. On the other hand, there may probably be physical crosslinks between the surface hydroxyls of cellulose nanocrystals and –OH groups of chitosan molecules. The presence of H-bonding interactions between chitosan and cellulose restricts the relaxation of chitosan chains. Therefore, the n values for CNC reinforced chitosan hydrogels is lower than the n value of 0% CNC–chitosan hydrogel and drug release depends more on the diffusion rather than relaxation of polymer chains. Furthermore, a significant weight loss was not observed for the hydrogels when immersed in the simulated gastric fluid for 12 h. It may be due to the high degree of crosslinking (83.6%) of these hydrogels. This will further clarify that drug release is by diffusion driven, rather than erosion of the hydrogel. Figure 4.22 shows the Ritger–Peppas release profiles of curcumin from chitosan hydrogel and chitosan hydrogels reinforced with different concentrations of nanocellulose.

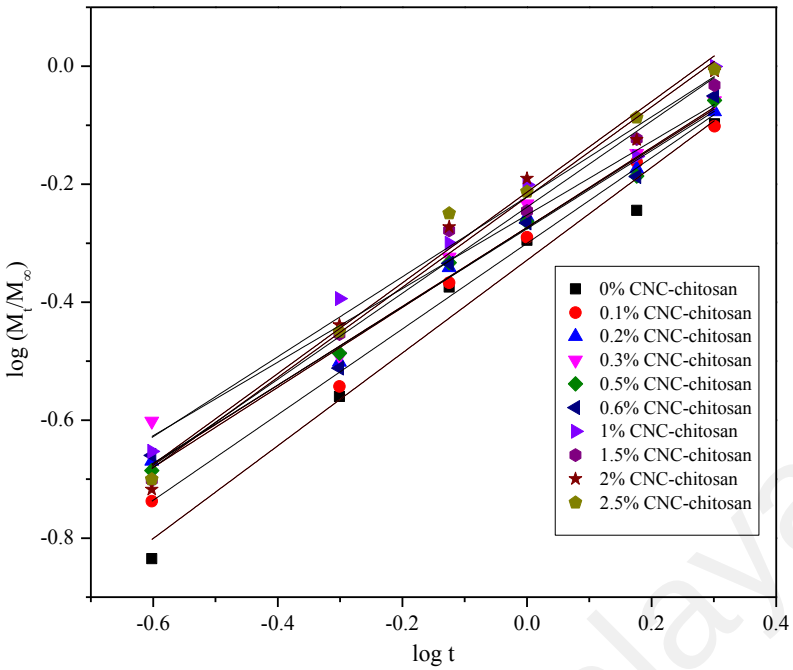

Figure 4.22: Ritger–Peppas release profiles of curcumin from different hydrogel

Table 4.2: Release kinetics of hydrogel in simulated gastric fluid

Hydrogel	***n***	***R*²**	***K***
0% CNC–chitosan	0.76	0.98	0.46
0.1% CNC-chitosan	0.69	0.99	0.49
0.2% CNC-chitosan	0.64	0.99	0.52
0.3% CNC-chitosan	0.60	0.99	0.55
0.5% CNC–chitosan	0.61	0.98	0.52
0.6% CNC- chitosan	0.61	0.98	0.52
1% CNC–chitosan	0.68	0.98	0.60
1.5% CNC–chitosan	0.70	0.99	0.57
2% CNC–chitosan	0.67	0.96	0.57
2.5% CNC–chitosan	0.66	0.96	0.57

The difference in *k* values indicates the difference in physical properties of hydrogel and difference in drug polymer interaction. In addition, the *k* values are smaller due to the less interaction between drug and polymers. In this study, Ritger–Peppas model was used to analyze the drug release kinetics. By using this model, regression coefficient

(R^2) was found very close to unity, and it suggested the release data best fit to Ritger–Peppas model.

4.2.2 Drug delivery studies of gas foamed hydrogels (Gas foamed at room temperature)

The release of the drug is usually controlled by diffusion and so the release profile can be easily modified by changing the material properties such as pore size or the overall pore surface area, pore connectivity and pore geometry (Gonzalez, Sagarzazu, & Zoltan, 2013). Larger pore size is suitable to load a high dose of drug molecules (Kwon et al., 2013). Due to the large pore size of hydrogels, a rapid initial burst release is typically observed. In this study, large-scale macroporous hydrogel with wide interconnected pores and large accessible surface area was obtained with using carbon dioxide gas foaming process. As shown in Figure 4.16, the pore size of hydrogel increased by more than tenfold after the gas foaming process. The increased pore size and pore interconnectivity act as a capillary system causing a rapid diffusion of drug solution through the hydrogel matrix.

4.2.2.1 Drug encapsulation efficiency

In this study, we fabricated the CNC–chitosan hydrogel using high pressure CO_2 at 10 bar, 30 and 50 bar in room temperature for two days. Slow depressurization (1 bar/min) was used as it helps to obtain large pore sizes in the hydrogel matrix. As shown in Figure 4.23, the encapsulation efficiency of all the hydrogels increased with increasing the pressure of gas foaming process. All the hydrogels, formed at 50 bar showed a highest drug encapsulation efficiency. This may be due to the formation of large interconnected pores at high pressure conditions. Similar results were reported by Nadzir, Mun, and Juan (2017) with the characterization studies of genipin- crosslinked gelatin hydrogel loaded with curcumin. According to their findings, the entrapment efficiency of curcumin increased with increasing the pore size of gelatin hydrogel. The

encapsulation efficiency of different hydrogels, formed at 50 bar is compared in Figure 4.24. It was observed that the drug encapsulation efficiency of 0.5% CNC–chitosan hydrogel increased from 41% to 50% with increasing the pressure of gas foaming process (from 1 bar to 50 bar). It also increased from 40% to 50% and from 40% to 50.1% for 0.3% CNC-chitosan hydrogel and 0.6% CNC-chitosan hydrogel, respectively. In addition, the encapsulation efficiency of gas foamed hydrogels increased with increasing the nanocellulose content from 0% to 0.6%. Further increase of nanocellulose resulted in a decrease of encapsulation efficiency. This trend observed is similar to that seen with the hydrogel formed at atmospheric condition.

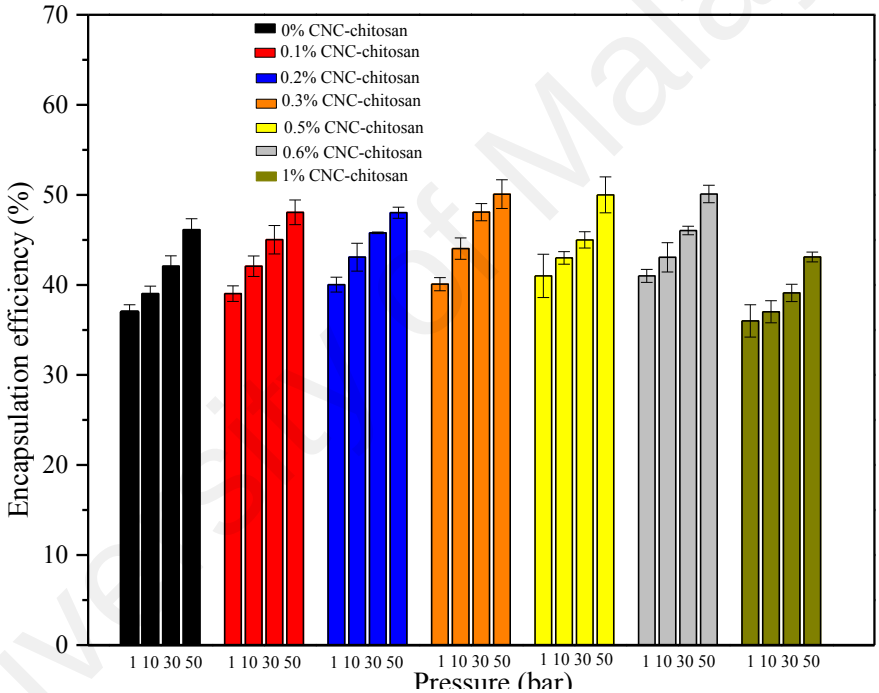

Figure 4.23: Encapsulation efficiency of curcumin for hydrogels formed at different pressure conditions

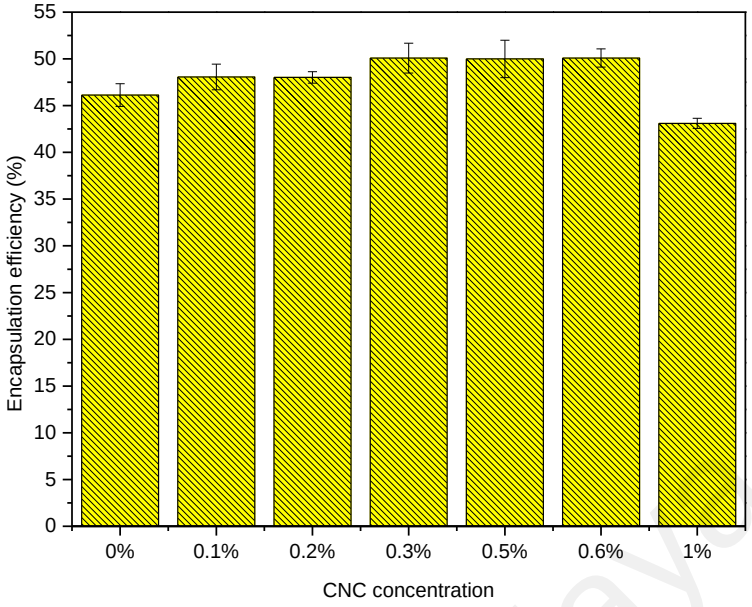

Figure 4.24: Encapsulation efficiency of hydrogels with different concentrations of nanocellulose and gas formed at 50 bar

4.2.2.2 Drug release

Due to the formation of large and highly interconnected open pore structures, a rapid release of drug and high amount of drug release was observed in the gas foamed hydrogels, as were typical of diffusion-controlled systems. The high-water content and large pore sizes of most hydrogels often result in relatively rapid drug release (Deepa, Thulasidasan, Anto, Pillai, & Kumar, 2012). The drug release rate and the amount of drug release of all the hydrogels increased with increasing the pressure of gas foaming process. As shown in Figure 4.25, the drug release of 0.5% CNC–chitosan hydrogel increased from 0.74 mg/L to 1.06 mg/L, when the pressure increased from 1 bar to 50 bar. Similarly, it increased from 0.67 mg/L to 0.89 mg/L, from 0.75 mg/L to 1.1 mg/L and from 0.71 mg/L to 0.99 mg/L for 0% CNC-chitosan hydrogel, 0.3% CNC-chitosan hydrogel and 0.6% CNC-chitosan hydrogel, respectively.

As can be seen from Figure 4.26, out of all the hydrogel processed at 50 bar, 0.3% CNC-chitosan hydrogel showed the highest drug release, followed by 0.5% CNC-chitosan hydrogel, 0.6% CNC-chitosan hydrogel, 0.2% CNC-chitosan hydrogel and

then 0% CNC-chitosan hydrogel. Finally, the lowest drug release was observed from the 1% CNC-chitosan hydrogel.

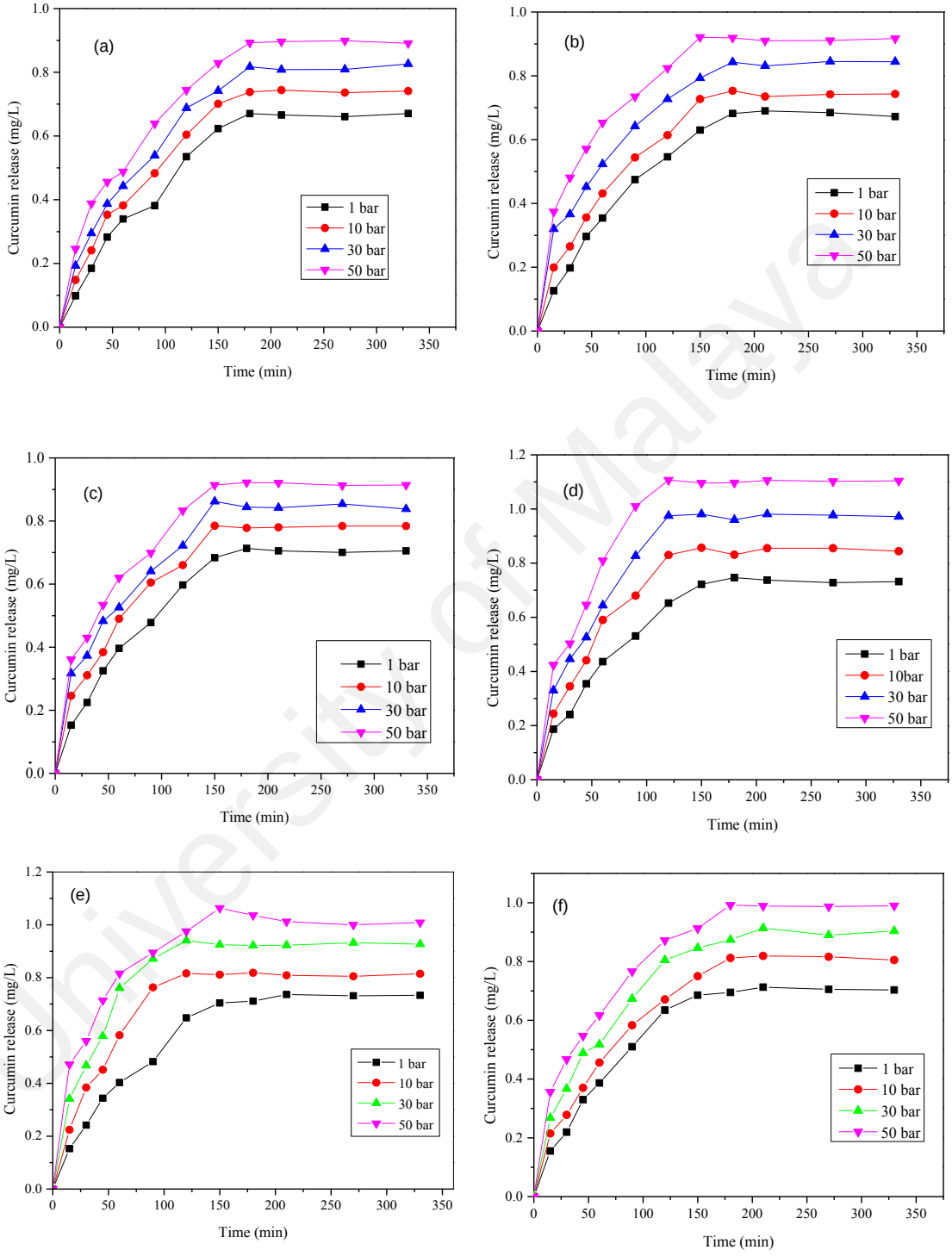

Figure 4.25 continued.

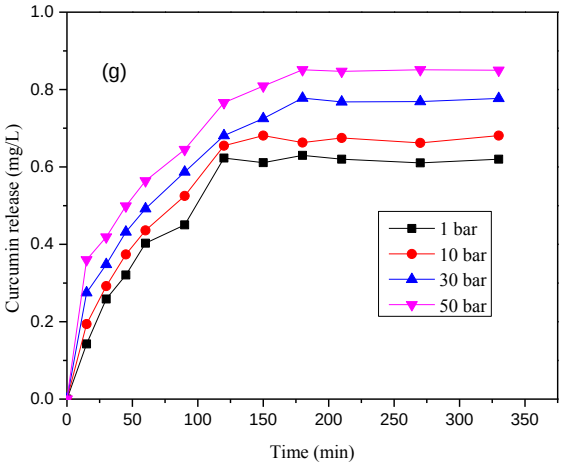

Figure 4.25: Curcumin release from: a) 0% CNC-chitosan hydrogel, (b) 0.1% CNC-chitosan hydrogel, (c) 0.2% CNC-chitosan hydrogel, (d) 0.3% CNC-chitosan hydrogel, (e) 0.5% CNC-chitosan hydrogel, (f) 0.6% CNC-chitosan hydrogel and (g) 1% CNC-chitosan hydrogel formed at different pressure conditions

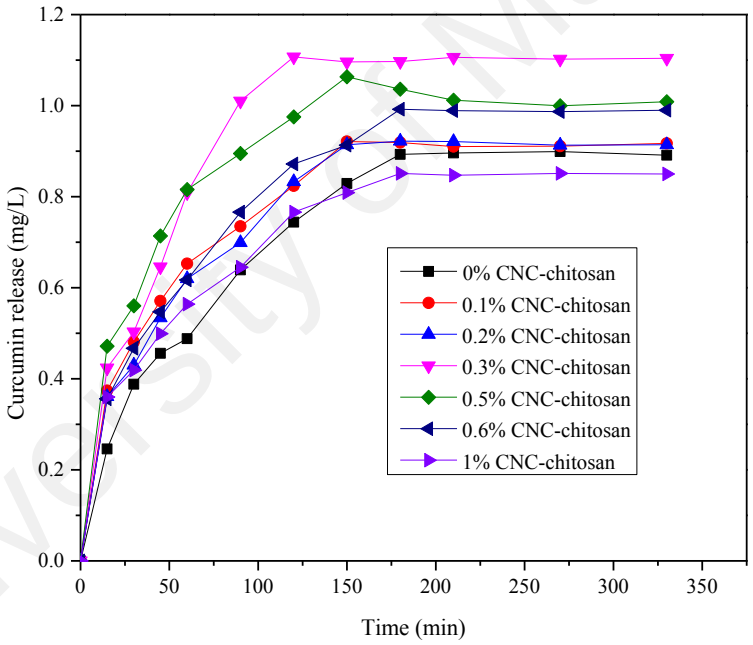

Figure 4.26: Curcumin release from different hydrogels formed at 50 bar

4.2.3 Drug delivery studies of gas foamed hydrogels (Gas foamed at 40 ^{0}C)

The processing temperature of the gas foaming process can significantly affect quality of porous structure. If the temperature is too lower, pore formation could be limited by the higher viscosity and lower diffusivity of the blowing agent. Increased temperature will lead to excess moisture loss during expansion. In this study, 0.3% CNC-chitosan hydrogel, 0.5% CNC-chitosan hydrogel, 0.6% CNC-chitosan hydrogel

and 1% CNC-chitosan hydrogel were gas foamed (at 30 bar and 40 °C) and compared their drug loading/releasing behavior with the hydrogels formed at 30 bar/27 °C, 1 bar/40 °C and 1 bar/27 °C.

4.2.3.1 Drug loading efficiency

As can be seen from Figure 4.27, the drug encapsulation efficiency of all the hydrogels increased with increasing the hydrogel formation temperature from 27 °C to 40 °C. 0.3% CNC-chitosan hydrogel showed an increase of encapsulation efficiency from 40% to 51% and 48% to 60% with increasing the temperature from 27 °C to 40 °C at 1 bar and 30 bar, respectively. Similarly, it increased from 41% to 52% and 45% to 68% for 0.5% CNC-chitosan hydrogel. The increase of encapsulation efficiency of hydrophobic drug (curcumin) in to the hydrogel matrix could be due to the improvement of crosslinking densities of the chitosan hydrogel at high temperature (Figueiredo, Alves, & Borges, 2009). Furthermore, as the reaction temperature is increased more stable Schiff bases are formed between amine groups of chitosan and carbonyl groups of glutaraldehyde (E-Thaher, Mekonnen, Mussone, Bressler, & Choi, 2013). Increase of crosslinking provides more hydrophobicity to chitosan hydrogel, which enhances the uptake of more curcumin (hydrophobic drug) to hydrogel matrix (Deepa et al., 2012). On the other hand, larger pores are formed by increasing the temperature of gas foaming process, as it increased the rate of diffusion of the gas, which allowed pore growth (Bhamidipati, Scurto, & Detamore, 2013). Nadzir et al. (2017) reported that gelatin hydrogel with largest pore sizes gave the highest entrapment efficiency for curcumin. These phenomenons might lead to higher drug encapsulation efficiency of the hydrogels, formed at 30 bar/40 °C, when compared to the other hydrogels, formed at 30 bar/ 27 °C, 1 bar/40 °C and 1 bar/27 °C.

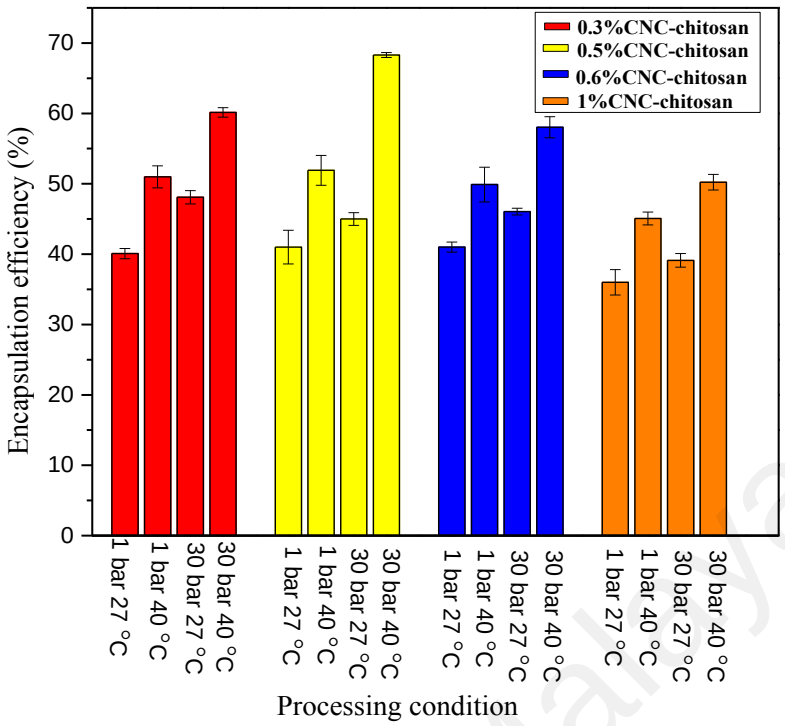

Figure 4.27: Encapsulation efficiency of hydrogel formed at different processing conditions

4.2.3.2 Drug release

As shown in Figure 4.28, hydrogels formed at 30 bar/40 °C showed higher and extended drug release when compared to the other hydrogels. Also, the hydrogel formed at 30 bar/27 °C showed higher drug release compared to the hydrogel formed at 1 bar/27 °C. However, the same result (obtained at 30 bar/27 °C) or bit higher improvement of drug release was observed with increasing the hydrogel formation temperature to 40 °C, but with pressure of 1bar. From the hydrogels formed at 30 bar and 40 °C, 0.5% CNC-chitosan hydrogel showed the highest drug release (1.61 mg/L). Further increase of nanocellulose caused decrease of drug release from the hydrogels (Figure 4.29). As described earlier, this may be due to the less swelling of the hydrogel because of the filling up the gaps of the hydrogel by nanocellulose. The extended release of the drug, from the hydrogels formed at 40 °C, might be due to the increase of crosslinking density of hydrogel. Increase of crosslinking provides more hydrophobicity to chitosan hydrogel. This will increase the hydrophobic interactions between hydrogel matrix and hydrophobic drug, thus exhibit a slower release profile (Lowe, Tenhu, &

Tylli, 1999). As shown in Figure 4.27 and Figure 4.29 the hydrogel formulations with increased drug loading, released much higher drug concentrations as expected.

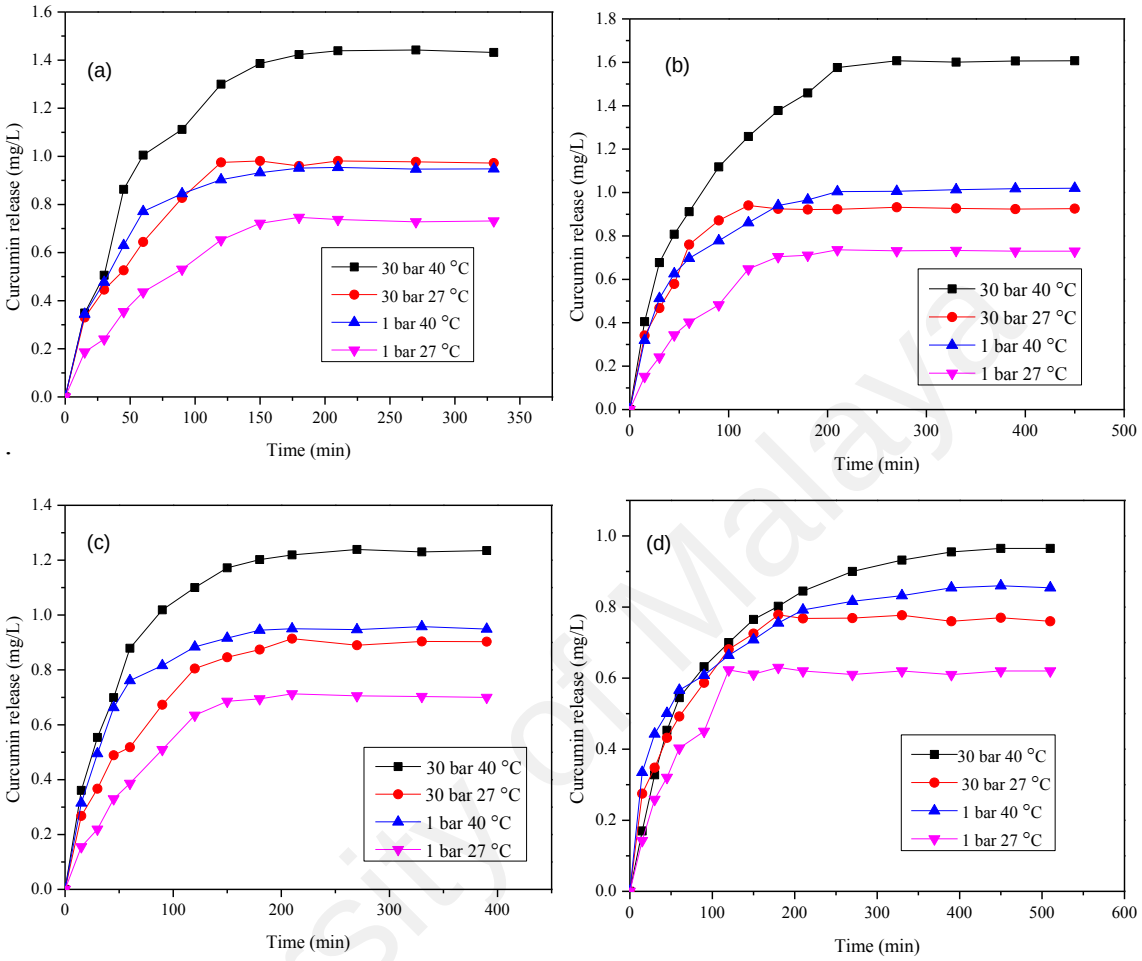

Figure 4.28: Curcumin release from: a) 0.3% CNC-chitosan hydrogel, (b) 0.5% CNC-chitosan hydrogel, (c) 0.6% CNC-chitosan hydrogel and (d) 1% CNC-chitosan hydrogel formed at different pressure and temperature conditions

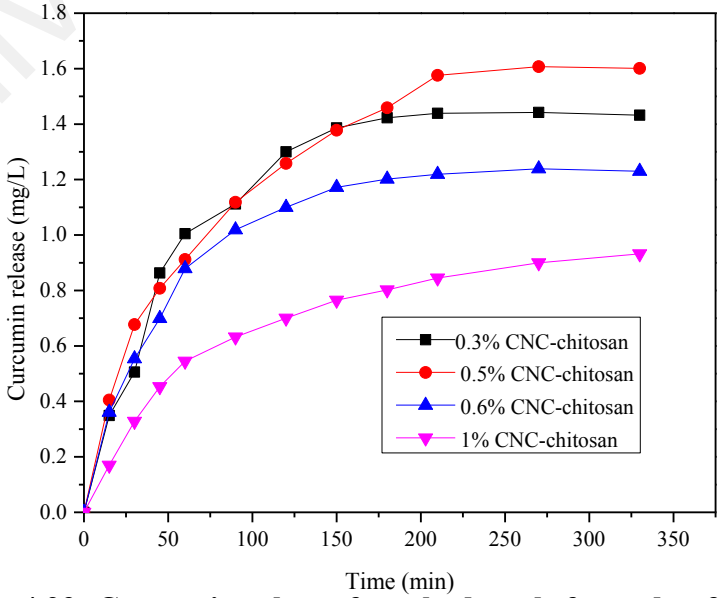

Figure 4.29: Curcumin release from hydrogels formed at 30 bar and 40 °C

4.2.4 **Drug activity**

After releasing, the chemical reactivity and biological activity of the drug are the most critical parameters in drug delivery systems (Bashir et al., 2016). For some drug delivery systems, drugs deteriorate due to the denaturation reactions with carrier and cause some detrimental effects after release. In order to prevent this, the carrier should not interact with the drug and able to be delivered into the body without any chemical transformation. In this study, the activity of curcumin before loading and after release was observed by comparison of UV visible spectra. The spectra of pure curcumin and in the release medium (SGF) were recorded. As shown in Figure 4.30, a significant difference was not observed for both spectra. This shows that the drug retained its chemical structure after release from the hydrogel.

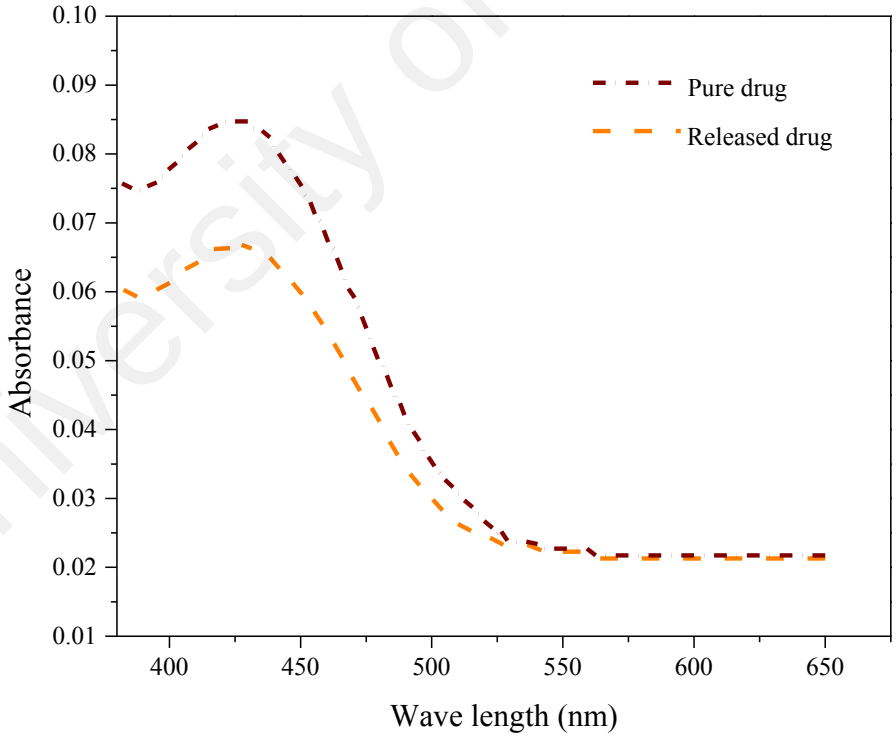

Figure 4.30: Chemical activity of pure curcumin and curcumin after release

4.2.5 **Investigation of the effect of a nonionic surfactant on the drug delivery behavior of the hydrogel (chitosan/nanocellulose/Tween 20 hydrogel)**

The objective of this study is to improve the bioavailability of curcumin by incorporating Tween 20 to 0.5% nanocellulose reinforced chitosan hydrogel. We extracted curcumin using turmeric powder and incorporated into hydrogel matrix with Tween 20, using in situ loading method. Previous cytotoxicity studies revealed that nonionic surfactants such as Tween have lower toxic effect than cationic, anionic and amphoteric ones (Cserháti, Forgács, & Oros, 2002). Due to the less cytotoxicity properties, a nonionic surfactant was selected for this study. Besides that, surfactants have a profound effect on the release rate of the drug from the encapsulated matrix. Using proper concentration of surfactant and a suitable HLB value, the cumulative release of the drug and rate of release can be controlled. According to the previous studies, the surfactants with lower HLB values such as Tween 80 caused lower release rates of hydrophobic drugs. This is because the surfactants having lower HLB values are more lipophilic and less water soluble. But with higher HLB values, hydrophobic drug release rate increased as these surfactants are more hydrophilic and water soluble (Sathali & Rajalakshmi, 2010). Tween 20 has a high HLB value (16.7) and it will help to improve the release of hydrophobic drug to a desired level. Tween 80 was also successfully applied in many hydrophobic drug delivery systems (Baig et al., 2016; Petchsomrit et al., 2013; Prabhakar, Afzal, Surender, & Kishan, 2013; Ren et al., 2009; Shahzad et al., 2017). However, the investigations on polysorbate-chitosan association by Picone and Cunha (2013) has shown that the longer hydrophobic polysorbate tail length of Tween 80 made it difficult to form homogeneous association with chitosan. Their further investigations had found that the shorter hydrophobic tail length of Tween 20 was more appropriated to form mixed surfactant–chitosan polymer systems. So, in this study, Tween 20, a less cytotoxic, nonionic, with shorter hydrophobic tail length

surfactant was used to improve the drug release of curcumin from nanocellulose reinforced chitosan hydrogel matrix.

4.2.5.1 FTIR analysis of curcumin (HIMEDIA Co.) and curcumin derived from turmeric

The FTIR spectra of curcumin (HIMEDIA Co.) and curcumin derived from turmeric powder are shown in Figure 4.31. The differences in the 3100-3600 cm^{-1} range may be attributed to the OH stretching of the methanol molecules adsorbed in the curcumin derived from turmeric powder. The appearance of strong peak at 1582 cm^{-1} and no peak at 1317 cm^{-1} in the derived curcumin as well as various displacements of the peaks may be due to different interactions between functional groups of curcumin. As shown in Figure 4.32, the chemical composition of the extracted curcumin is a mixture of curcuminoids (curcumin, demethoxycurcumin and bis-demethoxycurcumin).

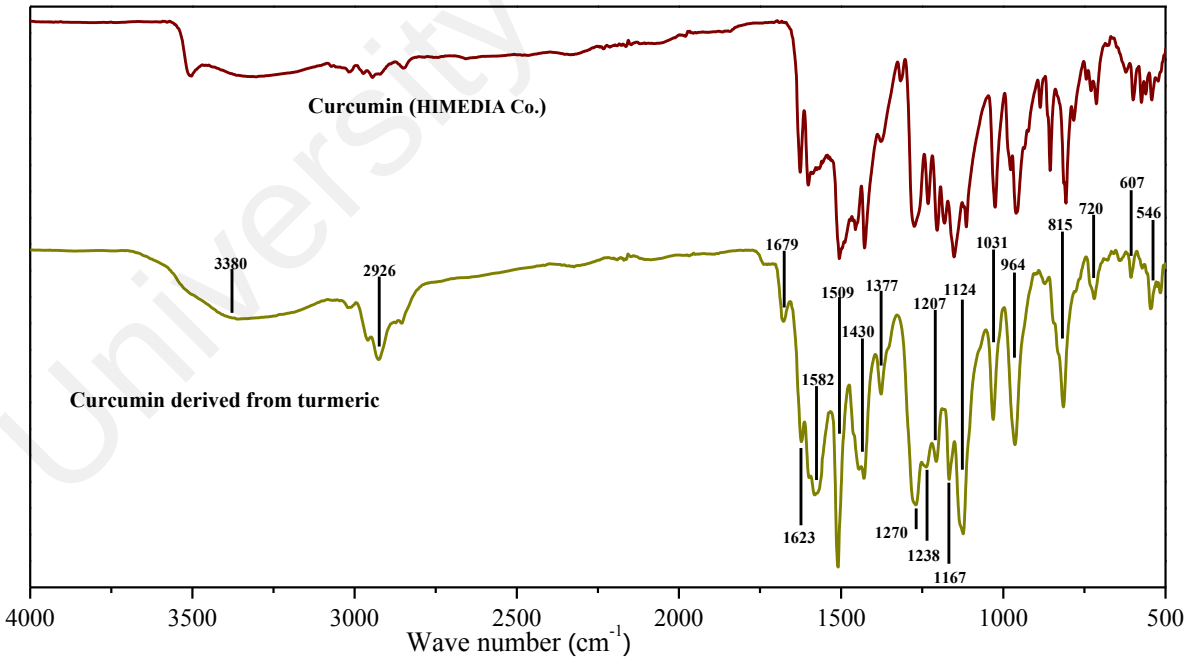

Figure 4.31: FTIR spectra of curcumin (HIMEDIA Co.) and curcumin derived from turmeric

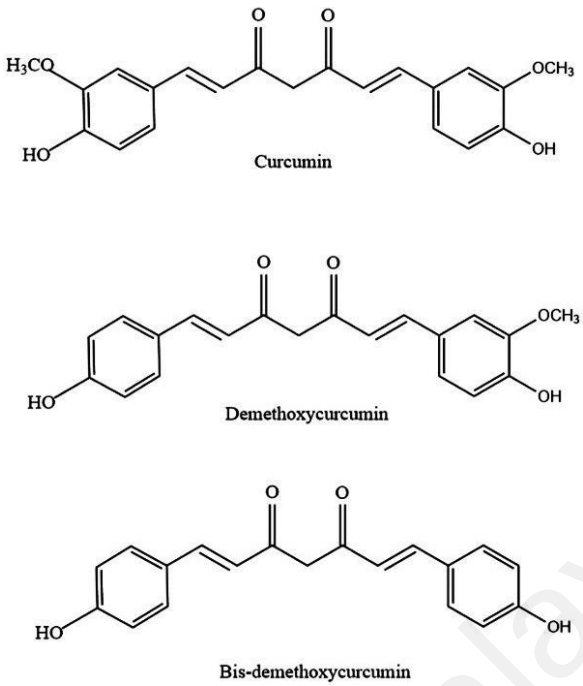

Figure 4.32: Curcuminoids present in turmeric powder

The IR spectrum of curcumin derived from turmeric is more similar to the IR spectrum of crystalline curcumin derived from turmeric powder (extracted using actone/ethanol/methanol), which was reported in previous studies (Bich et al., 2009; Fugita et al., 2012). A broad peak at 3380 cm^{-1} indicates the presence of OH. In the highest frequency region, phenolic vibrations of the curcumin has theoretical frequency at 3595 cm^{-1}, but in practice this band could be shifted downwards due to the intramolecular and intermolecular hydrogen bonds (Bich et al., 2009; Kolev, Velcheva, Stamboliyska, & Spiteller, 2005). The appearance of bands with low intensity in the region from 2700-3000 cm^{-1} can be attributed to the C–H stretches (Bich et al., 2009). The highest frequency bands observed within 2700-3000 cm^{-1} region are assigned to the aromatic C H stretches, while the lower frequency bands are attributed to the methyl group motions (Kolev et al., 2005). The peak at 1679 cm^{-1} appeared due to the C═O vibrations (Bich et al., 2009). The band at 1623 cm^{-1} can be assigned to the ν(C═C) of the benzene ring (Mohan, Sreelakshmi, Muraleedharan, & Joseph, 2012). The strong peak at 1582 cm^{-1} has a predominantly mixed ν(C═C) and ν(C═O) characteristic. The most prominent band in the IR spectrum is at 1509 cm^{-1}. This can be attributed to

highly mixed vibrations ($^{\nu}$C═O, $^{\delta}$CC^{10}C, $^{\delta}$CC═O) (Bich et al., 2009). The peaks at 1430 cm^{-1} appeared due to the asymmetric angular deformation vibrations of methyl groups (Kolev et al., 2005). The observed bands at 1377 cm^{-1} and 1207 cm^{-1} can be attributed to ν(C–O) and δ(C═C–H) of interring chain, respectively. One band and one shoulder at 1270/1238 cm^{-1} and peak at 1167 cm^{-1} are attributed to the in-plane deformation vibrations of (CCH) of phenyl rings and skeletal in-plane deformations, respectively. A prominent band at 1124 cm^{-1} is assigned also to the (C–O–C) vibrations (Bich et al., 2009). The peak at 1031 cm^{-1} appeared due to C–O stretching coupling with the adjacent C–C stretching vibrations (Fugita et al., 2012). The bands at 964 cm^{-1} and 815 cm^{-1} assigned to the ν(C–O) vibrations. The IR bands at 815 cm^{-1} and 720 cm^{-1} belongs to the ν(C–H) out of plane vibration of the aromatic ring (Kolev et al., 2005). In the range of 700-500 cm^{-1}, we could see deformation vibrations of both benzene rings and the out of plane vibrations of both OH groups, which are at 607 cm^{-1} and 546 cm^{-1} (Bich et al., 2009).

4.2.5.2 UV-Vis spectroscopic analysis of curcumin (HIMEDIA Co.) and extracted curcumin from turmeric

As shown in Figure 4.33, the UV-Vis spectra of curcumin (HIMEDIA Co.) and curcumin extracted from turmeric were obtained by scanning the drug solutions within the range of 350-800 nm using UV-Vis spectrophotometer.

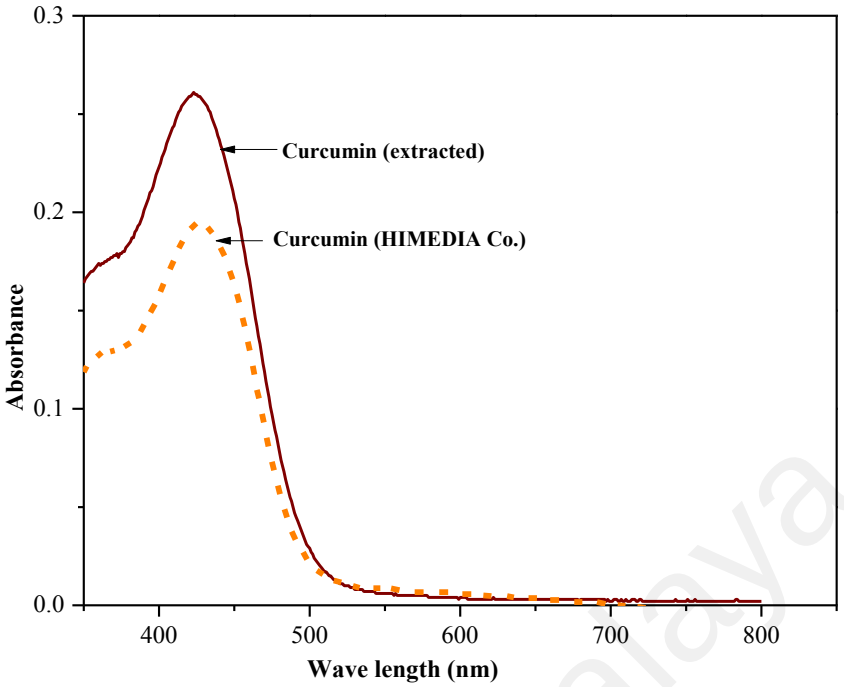

Figure 4.33: UV-Vis spectra of curcumin extracted from turmeric powder and curcumin (HIMEDIA Co.)

The UV-Vis spectra of curcumin represent the transition between the electronic energy levels. The maximum absorption wavelength of a compound is a measure of the difference between energy levels of the orbitals concerned. An isolated double bond/lone pair produces strong absorption maximum around 190 nm, whereas the presence of conjugation decreases the energy separation between orbitals and give rise to the absorption at longer wavelengths. In organic solvents enolization of diketone of curcumin conjugates between the π-electron clouds of the two vinylguaiacol parts leading to a common conjugated chromophore, resulted in decrease in energy. As a result of low-energy π- π* excitation of that chromophore, curcumin in organic solvents (primarily methanol or ethanol) typically absorbs around ~420 nm and appears in yellow color (Zsila, Bikádi, & Simonyi, 2004).

4.2.5.3 FTIR analysis of curcumin (extracted), Tween 20, 0.5% nanocellulose reinforced chitosan hydrogel and curcumin/Tween 20 incorporated hydrogel

Figure 4.34 displays the FTIR spectra of curcumin (extracted), Tween 20, and curcumin/Tween 20 incorporated hydrogel. From the spectrum of curcumin/Tween 20 incorporated hydrogel, it can be seen that the bands corresponded to the functional groups of Tween 20 are more prominent together with the bands assigned to the functional groups of the hydrogel. The sharper peaks related to the functional groups of curcumin are super imposed by the broader peaks of Tween 20 and hydrogel (in the spectrum of curcumin/Tween 20 incorporated hydrogel). Also, the drug concentration loaded to the hydrogel is very low when compared to Tween 20 concentration. Therefore, the peaks related to Tween 20 are more prominent in the spectrum of curcumin/Tween 20 incorporated hydrogel. However, there are no new peaks appeared in the spectrum of curcumin/Tween 20 incorporated hydrogel.

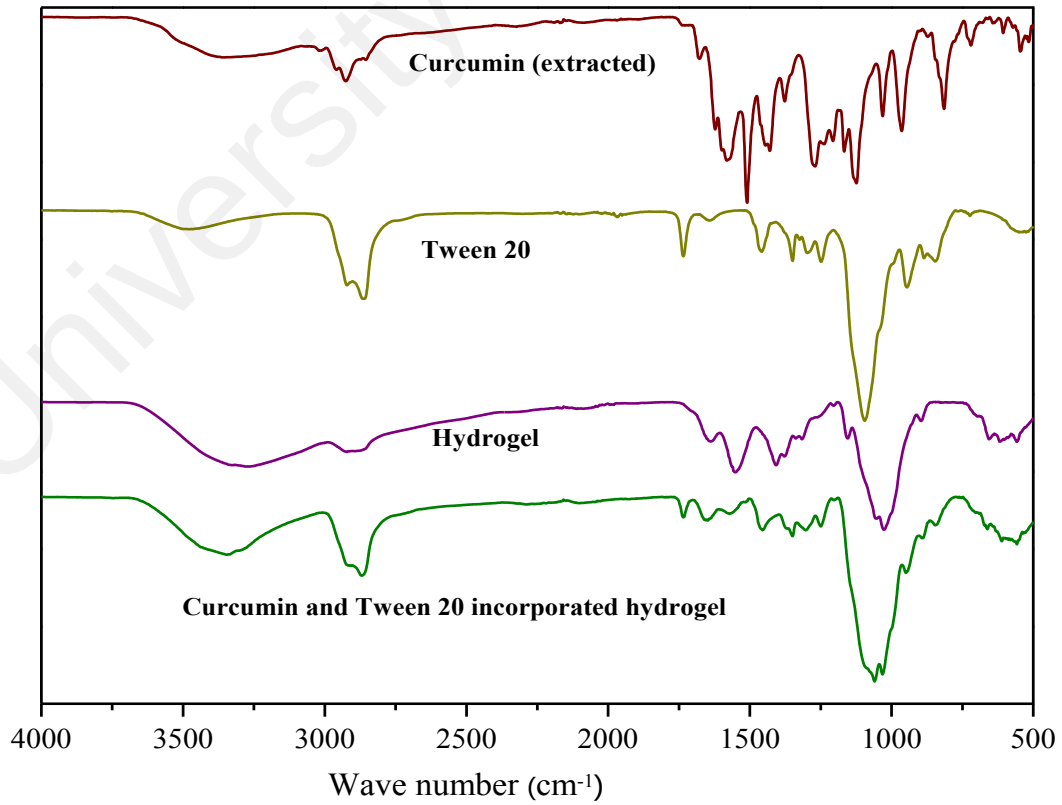

Figure 4.34: FTIR spectra of curcumin (extracted), Tween 20, nanocellulose reinforced chitosan hydrogel and curcumin /Tween 20 incorporated hydrogel

to 77.92% ± 0.70% with the addition of 5% (w/v) surfactant to the hydrogel. After that, it slightly decreased from 77.92% ± 0.70% to 70.21% ± 0.26% with increasing the surfactant concentration from 5% to 30% (w/v). The p-value was used to test whether there is a relationship between Tween 20 content and entrapment efficiency. According to the p-value, there is a significant positive relationship between the nanocellulose content and the entrapment efficiency of the hydrogel ($r(5) = 0.85$, $p < 0.05$).

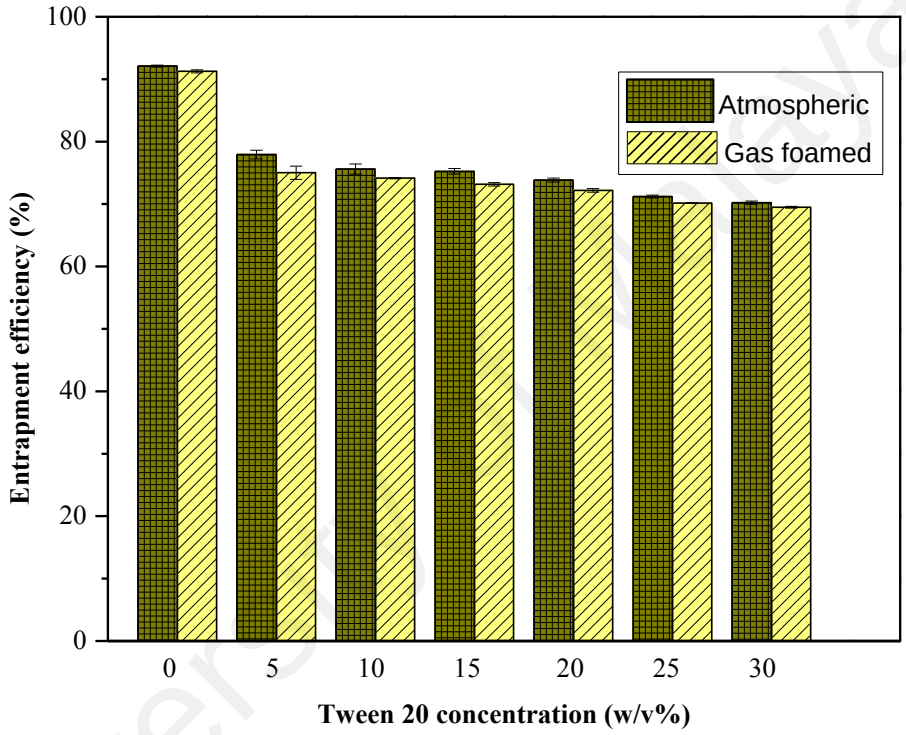

Figure 4.36: Entrapment efficiency of curcumin for gas foamed hydrogel and hydrogel formed at atmospheric condition

Similar result was obtained by Petchsomrit et al. (2013) for oil entrapped alginate bead formulation of curcumin. Tween 80 was used as the surfactant for their study and the entrapment efficiency of curcumin was found to decrease from 73.69% ± 2.04% to 40.28% ± 0.23% with increasing the Tween 80 content from 0% to 30%. From the study of variability of PLGA nanoparticles quality of protein loaded PLGA nanoparticles by Plackett–Burman design, Rahman, Zidan, Habib, and Khan (2010) described that the decreasing of entrapment efficiency with increasing the surfactant is due to the fact that the higher concentration of the emulsifier increases the partition of

the drug from internal to external phase due to the increased solubility of the drug in the external phase. In addition, the alkyl chain length influences the hydrophile–lipophile balance (HLB) value of the surfactant, which in turn directly affects the drug entrapment efficiency (El-Ridy et al., 2011). Non-ionic surfactants have hydrophilic and lipophilic properties and are characterized by their hydrophile–lipophile balance values. Low HLB value corresponds to high hydrophobicity. The higher HLB value the more water soluble the surfactant (Ag Seleci, Seleci, Walter, Stahl, & Scheper, 2016). The lower the HLB of the surfactant the higher will be the drug entrapment efficiency as in the case of niosomes prepared using Span 60 (HLB = 4.7), compared with Span 40 with a higher HLB of 6.7 (Bayindir & Yuksel, 2010; Guinedi, Mortada, Mansour, & Hathout, 2005; Nasr, Mansour, Mortada, & Elshamy, 2008). The HLB value of Tween 20 is 16.7. The higher HLB value represents higher hydrophilic property. According to Dinarvand, Moghadam, Sheikhi, and Atyabi (2005), the higher internal aqueous volume may increase the volume of water droplets in the hydrophobic phase. This will promote more contact and exchange (drug loss) to the external water phase. Polymer phase acts as a diffusion barrier against movement of drug molecules between the internal and external aqueous phases; the thickness of this layer decreases when the internal aqueous volume is increased. This may lead to reduced drug entrapment efficiency.

In this study, we have compared the drug delivery behavior of the gas foamed hydrogel with the hydrogel prepared at atmospheric condition. As can be seen from the Figure 4.36, the entrapment efficiency of curcumin in gas foamed hydrogel is slightly lower than that of the hydrogel formed at atmospheric condition. This result is different compared to our previous study, which has reported that the gas foamed hydrogel has higher drug entrapment efficiency compared to hydrogel formed in atmospheric condition. This may be caused by the different drug loading methods that have been applied in these two different studies (Fimantari & Budianto, 2018). In previous study,

the drug was encapsulated by post-loading method. However, we are applying in situ loading method in this study for the comparative study between the hydrogels prepared under gas foamed and atmospheric condition. In situ loading method helps to incorporate the surfactant together with the drug to the hydrogel matrix. However, the post-loading method does not provide the same. From the studies on the effects of different drug loading methods on drug delivery, Wong and Dodou (2017) reported that the drug is embedded within polymeric network when in situ loaded, instead of being deposited in microporous spaces of the hydrogel when post loaded. As can be seen from Figure 4.35, the hydrogel prepared at atmospheric condition composed of small pore structures when compared to the gas foamed hydrogel. The decrease of pore size of the hydrogel simply correlated with the higher hydrogel density, which contributing to more embedded drug in the hydrogel matrix and higher encapsulation efficiency. Therefore, in this study, the hydrogel prepared at atmospheric condition showed higher encapsulation efficiency compared to gas foamed hydrogel. Petchsomrit et al. (2017) also reported that the higher hydrogel density contributed to the increase of curcumin content on in situ drug loaded, alginate-based composite sponge.

Comparison between post loaded formulations from our previous study and in situ loaded formulations of this study, for all the hydrogels (gas foamed and hydrogel formed at atmospheric condition), it showed that the in situ loading method providing better drug entrapment efficiency within hydrogel network due to the specific interactions between polymer and drug molecules (Wong & Dodou, 2017).

4.2.5.6 Drug release from the hydrogels formed at atmospheric condition

The oral bio availability of a drug relies upon on its solubility and/or dissolution rate, and dissolution can be the rate determining step for the onset of drug action, hence there are numerous approaches available and reported in literature to enhance dissolution and

drug bioavailability of poorly water-soluble drugs. The use of surfactant to improve the solubility of hydrophobic/lipophilic drugs is a common practice in the industry and it has been extensively studied by many researchers. In this study, curcumin and Tween 20 were incorporated in to hydrogel matrix via in-situ loading method (Hydrogel network formulation and drug encapsulation are accomplished simultaneously).

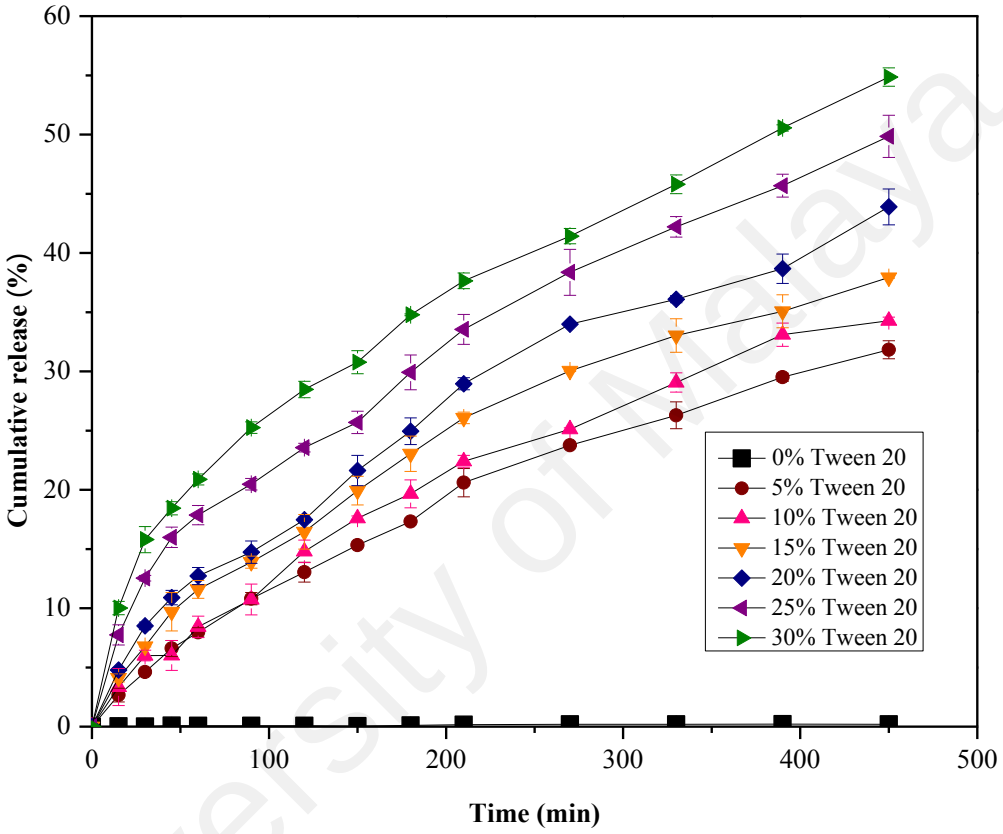

Figure 4.37: Curcumin release from the hydrogels containing different concentrations of Tween 20

The hydrogel discs (1.2 cm height and 1.8 cm diameter) containing 1.5 mg of drug with different concentrations of Tween 20 (5%, 10%, 15%, 20%, 25% and 30% (w/v)) were immersed in simulated gastric fluid and drug release was monitored over a period of 7.5 h. Since the solubility of curcumin is very low (Tønnesen & Karlsen, 1985), a large volume of the releasing medium was used to maintain a good sink condition (Cho, Lee, Lee, Huh, & Park, 2004). As can be seen in Figure 4.37, the cumulative release of curcumin increased from 0.21% ± 0.02% to 54.85% ± 0.77% with increasing the Tween 20 concentration from 0% to 30% (w/v), after 7.5 h immersion. Release studies

in the presence of Tween 20 show a burst release profile for curcumin, up to 20% of curcumin released in the first 60 min of the experiment. As shown in Figure 4.37, with the increase of Tween 20 concentration from 5-30% (w/v) at a fixed drug concentration, the amount of drug release increased from 31.82% ± 0.75% to 54.85% ± 0.77%, almost 1.7-fold increase after 7.5 h. During the time of monitoring, the formulations containing lower amount of Tween 20 produced an incomplete solubilization of curcumin, whereas complete solubilization showed at high concentration of Tween 20. Therefore, larger amount of surfactant produced a higher drug release. Ratanajiajaroen and Ohshima (2012) showed that the solubility of curcumin increased from 11 ng/mL to 0.767 mg/mL with Tween 20 at a concentration of 2% (v/v) in acetate buffer (pH 5.5). In addition, they found that the drug release rate increased from chitin beads as the Tween 20 concentration increased. O'Toole et al. (2012) investigated that the curcumin saturation point increased linearly with Tween 20 concentration throughout the range used in their experiments, with an upper limit of 294 μM curcumin with 0.05% (w/v) Tween 20. Further, they observed that curcumin can be released completely from the submicrometer spray-dried chitosan/Tween 20 particles in both 1% acetic acid and phosphate buffered saline solutions over a 2 h period.

Moreover, in terms of therapeutic applications for abdominal disorders, the doses of curcumin up to the healing levels should also been concerned. Considering the strong association of *H. pylori* and gastric cancer the authors of the study by Mahady et al. (2002) showed that both curcumin and methanolic extract of turmeric rhizome inhibited the growth of 19 different strains of *H. pylori.* They reported that curcumin, inhibited the growth of all the *H.pylori* strains by 100% at a concentration of 12.5 μg/mL, with a minimum inhibitory concentration from 6.25-12.5 μg/mL. De et al. (2009) investigated that the minimum inhibitory concentration of curcumin for *H.pylori* strains ranged from 5 μg/mL to 50 μg/mL and the majority of the strains (81%) showed a minimum

inhibitory concentration of either 10 μg/mL (23%) or 15 μg/mL (58%). In addition, curcumin is able to suppress the proliferation and survival of cancer cells by directly or indirectly binding to cellular molecular targets (Zang, Liu, Shi, & Qiao, 2014). Liu, Xiang, Wu, and Wang (2016) reported that curcumin inhibited the growth of gastric cancer cells in a concentration and a time-dependent manner. Their study showed that as compared to untreated cancer cells, the cell proliferation was significantly inhibited in the curcumin treated samples, after 48 h of treatment with 50 μM curcumin. In our study, the maximum concentration of curcumin released in the simulated gastric fluid was 3.98 μg/mL, after 7.5 h. Even so, we found that the drug release of the hydrogel increased (≥10 μg/mL) with increasing the initial concentration of the drug, which incorporated to the hydrogel (for same Tween 20 concentration). However, during the period of monitoring, with increasing the initial amount of drug, the percentage release of drug dramatically decreased. Therefore, in this study, 1.5 mg of drug per hydrogel disc (1.2 cm height and 1.8 cm diameter) was used for the encapsulation. However, the initial drug loading amount to the hydrogel can be varied in order to get the drug release to the extent desired (to reach the therapeutic levels) or to obtain the minimum inhibitory concentration. Finally, according to the results obtained from drug release studies, the nanocellulose reinforced chitosan/Tween 20 hydrogel can be suggested as a promising candidate for carrying curcumin for the absorption from stomach and upper intestinal tract.

4.2.5.7 Drug release from gas foamed hydrogel

Nanocellulose reinforced chitosan hydrogel was fabricated using gas foaming process. As shown in Figure 4.35, large-scale macroporous hydrogel with wide interconnected pores and large accessible surface area was obtained with using carbon dioxide gas foaming process. Like the previous study, due to the large pore size of hydrogels, a rapid initial burst release of drug was typically observed.

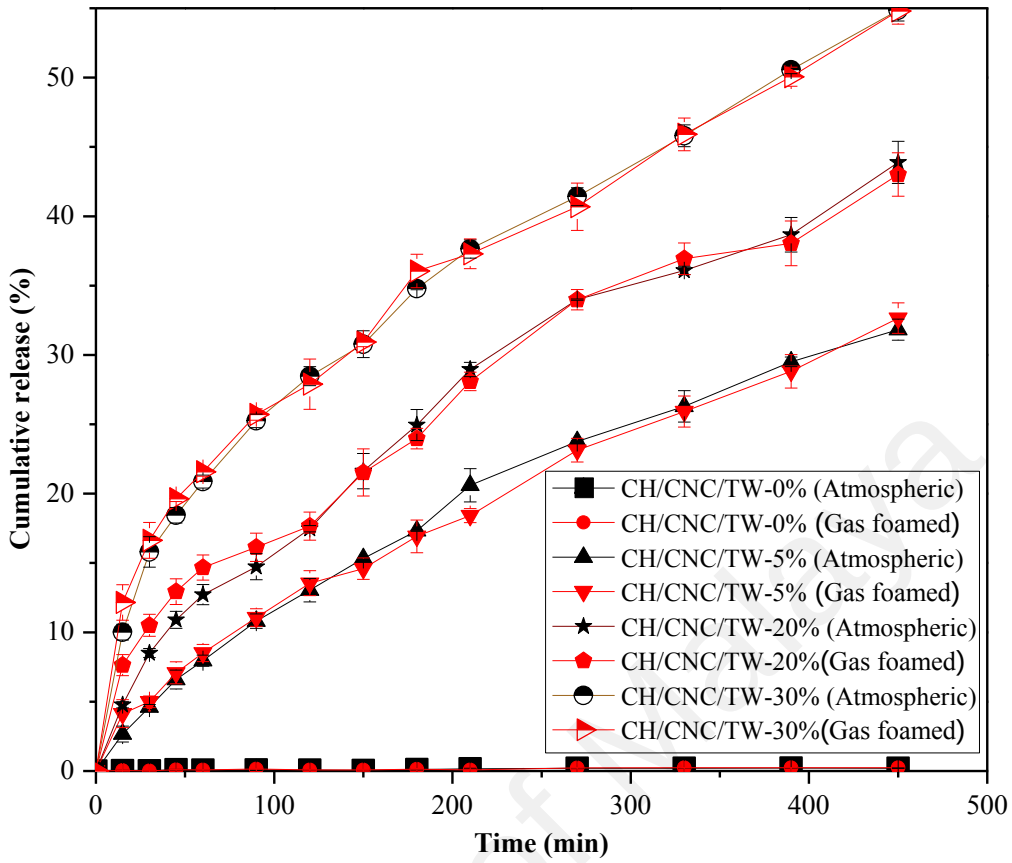

Figure 4.38: Curcumin release from gas foamed hydrogel and hydrogels formed at atmospheric condition with different concentrations of Tween 20

As shown in Figure 4.38, within the first 120 minutes, the concentration of released drug from gas foamed hydrogel was greater when compared to the hydrogel formed at atmospheric condition. The increased pore size and pore interconnectivity of gas foamed hydrogel act as a capillary system causing a rapid diffusion of drug solution through the hydrogel matrix. At 60 minutes, with 5% (w/v) Tween 20, the cumulative release of drug was 8.51% ± 0.61% and 7.95% ± 0.39% for gas foamed hydrogel and hydrogel formed at atmospheric condition respectively. For the hydrogels containing 30% (w/v) Tween 20, it was 21.58% ± 0.32% and 20.87% ± 0.46%. After the burst release, the rate of drug release of both types of hydrogels become almost similar.

From our previous study, the gas foamed hydrogel showed higher drug release when compared to the hydrogel formed at atmospheric condition. However, gas

foamed hydrogel did not show any improvement of the drug release over the hydrogel formed at atmospheric condition, in this study. This may be caused by the different drug loading methods used in these two different studies. The drug was encapsulated by post-loading method in the previous study and the in situ loading was applied in the current research study. Kawase et al. (1997) reported that the permeation rates of the drug from post-loaded formulations are generally more rapid compared to the in situ loaded ones. This may be due to drug being deposited in microporous spaces of the hydrogel when post-loaded, instead of being embedded within polymeric network when loaded in situ. In our previous study, gas foamed hydrogel with large and interconnected pore structures has allowed the drug deposited in the pore spaces of the hydrogel to be easily transported (Ullah, Kim, & Kim, 2018). Therefore, gas foamed hydrogel showed higher drug release compared to the hydrogel prepared at atmospheric condition in the previous study.

In the current research work, we have applied in situ loading method for the drug loading. The gas foamed hydrogel with larger interconnected pore structures would cause less impact on the drug release from the in situ loaded formulations (Fimantari & Budianto, 2018; Ullah et al., 2018; Wong & Dodou, 2017). Therefore, the gas foamed hydrogel did not show any improvement of the drug release over the hydrogel formed at atmospheric condition in this study.

4.2.5.8 Drug activity

After releasing, the chemical reactivity and biological activity of the drug are the most critical parameters in drug delivery systems (Bashir et al., 2016). Curcumin has three reactive functional groups which associated with its different biological activities: one diketone moiety, and two phenolic groups. The presence of C═O groups as hydrogen acceptors and C-4 as a hydrogen donor are most important for chemical reactions associated with its biological activities (Ahmed et al., 2017).

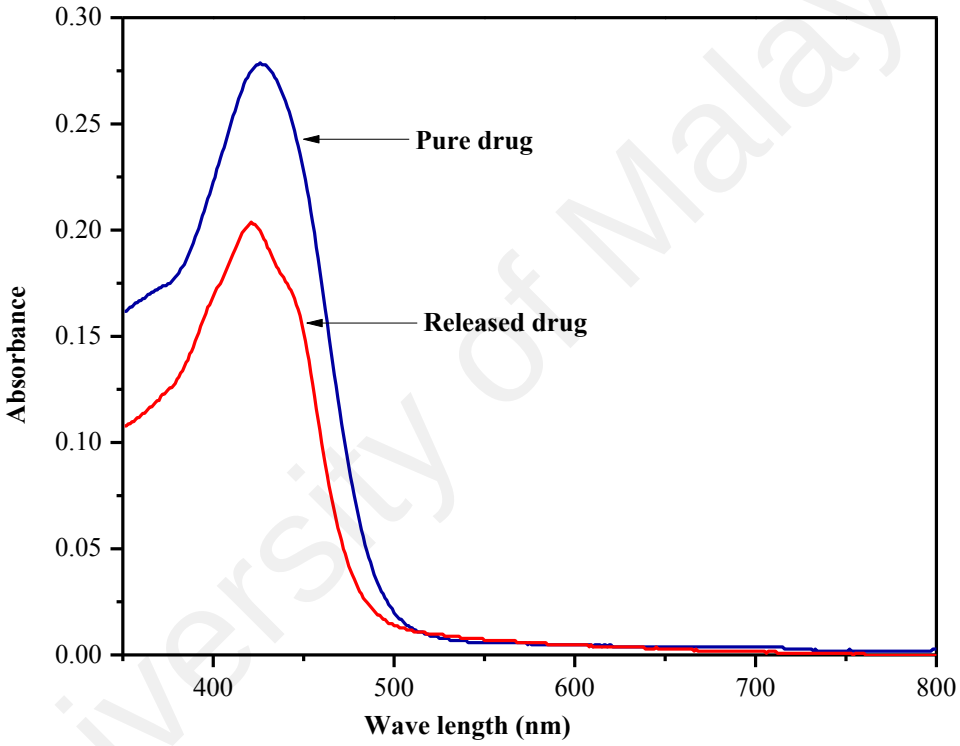

Figure 4.39: UV-Vis spectra of (a) pure drug and (b) released drug

As shown in Figure 4.39, both UV-Vis spectra indicate absorption peak around 427 nm, which can be assigned to the low-energy π- π* excitation of the chromophore, that formed due to the enolization of the diketone group and conjugation between the π-electron clouds of the two vinylguaiacol (Zsila et al., 2004). The presence of the absorption peak around 427 nm in both spectra revealed that the reactive functional groups, which associated with the biological activity of curcumin retained without any deterioration due to any denaturation reaction with the carrier molecules.

4.2.5.9 Solubility study

From our previous study, we observed lower drug release profiles of the hydrogel due to poor solubility of curcumin in simulated gastric fluid. To improve curcumin's solubility, Tween 20 was selected as potential solubilizing agent on known biocompatibility and previous successful application in curcumin drug delivery systems (O'Toole et al., 2012; Rahma, Munir, Prasetyo, Suendo, & Rachmawati, 2016; Ratanajiajaroen et al., 2012).

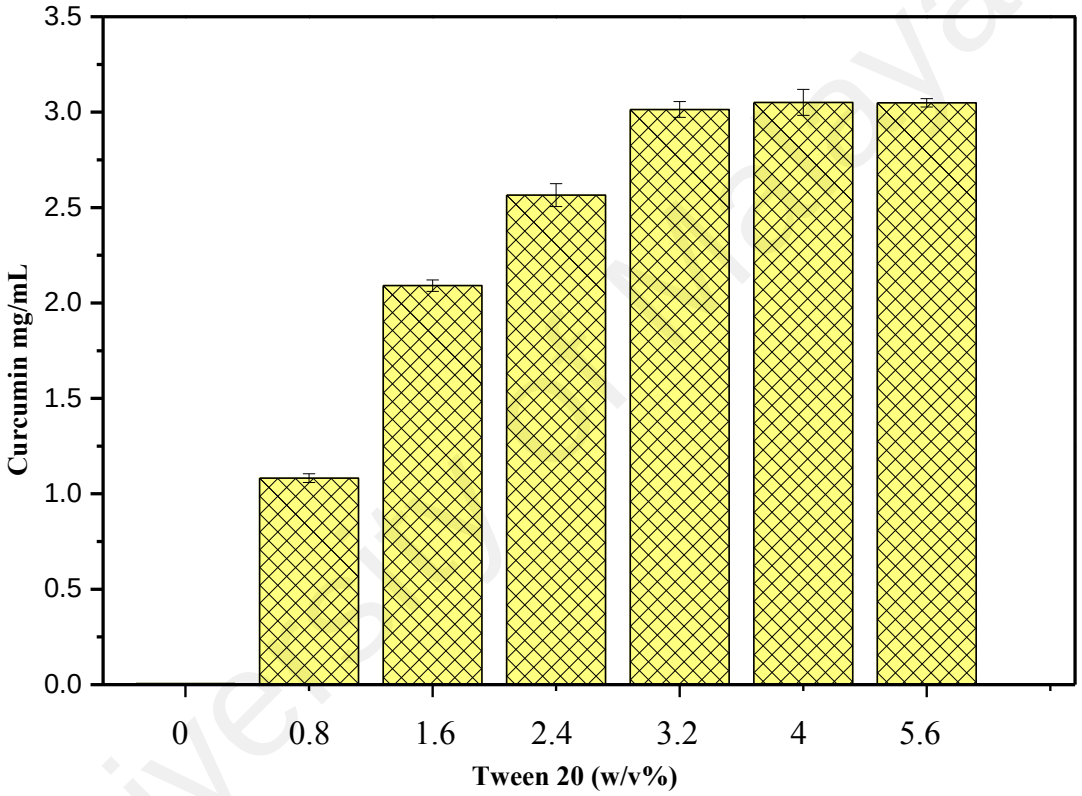

Figure 4.40: Solubility of curcumin in simulated gastric fluid with different concentrations of Tween 20

The ability of Tween 20 to solubilize curcumin in simulated gastric fluid was evaluated by measuring the curcumin concentration in curcumin-saturated simulated gastric fluid with varying amounts of Tween 20. As shown in Figure 4.40, the solubility of the drug gradually increased with increasing the concentration of nonionic surfactant (Tween 20), with an upper limit of 3.014 ± 0.041 mg/mL in the presence of 3.2% (w/v) Tween 20. Similar results were obtained from the studies on solubility of curcumin in aqueous polysorbate micelle, by Inchai, Ezure, Hongwiset, and Yotsawimonwat (2015).

Their studies showed that the solubility of curcumin increased up to 2.7 mg/mL in 20% aqueous solution of Tween 20. O'Toole et al. (2012) showed that the saturation point of curcumin increased linearly with increasing the Tween 20 concentration in 1% acetic acid medium. Their findings revealed that the solubility of curcumin increased with an upper limit of 294 μM (~0.108 mg/mL) with 0.05% (w/v) Tween 20.

In higher pH, curcumin degrades rapidly (on the timescale of minutes) and its solubility decreases rapidly with decreasing pH (Hung et al., 2008). In our study, the solubility of curcumin in simulated gastric medium was ~6 μg/mL (without addition of the surfactant). It showed a slight decrease when compared to the results obtained by Hung et al. (2008), which was 25 μM (~9.2 μg/mL) in pH 7 buffer solution. This may be due to the low pH of the simulated gastric fluid.

CHAPTER 5: CONCLUSION AND FUTURE WORK

5.1 Conclusion

Adequate mechanical strength is desirable for hydrogels as drug delivery systems. Improved mechanical strength can withstand the pressure during gastric contraction and prolong the gastric retention time. A unique biodegradable, superporous, swellable and pH sensitive nanocellulose reinforced chitosan hydrogel with dynamic mechanical properties was prepared for the enhancement of bioavailability of curcumin. Based on the characterization of the hydrogel and drug delivery studies, the following conclusions are made.

During the initial stage of this project, rod shaped CNCs with a length of 200–300 nm and width of 40–50 nm were extracted from microcrystalline cellulose, via sulfuric acid hydrolysis. The chitosan hydrogel and the chitosan hydrogels reinforced with different concentrations of CNCs were obtained using the chemical crosslinking method. The addition of CNCs (up to 2.5%) improved the maximum compression of the hydrogels from 25.9 ± 1kPa to 50.8 ± 3kPa. However, the maximum compression did not significantly increase with the addition of over 2.5% CNCs to the chitosan hydrogel. In the swelling test, the CNC-chitosan hydrogels exhibited excellent pH sensitivity and yielded maximum swelling ratios under an acidic condition (pH 4.01). The results showed that the maximum swelling ratio of the chitosan hydrogel at pH 4.01 was 222 ± 10%, and that of the chitosan hydrogel reinforced with 0.5% CNC was 188 ± 9%. The FTIR result confirmed the successful formation of an imine bond in the crosslinking structure with the appearance of a peak at 1548 cm^{-1}. Furthermore, the high crosslinking degree (83.6%) also confirmed stable gel formation. The FESEM images indicated that the CNC particles were in nanometer scale and were uniformly distributed within the chitosan matrix. The XRD patterns showed that adding CNCs induced a combination of amorphous and crystalline region in the hydrogel matrix. Nanocellulose

reinforced chitosan hydrogel showed higher stability compared to chitosan hydrogel, as it started to decompose at 304 °C. In vitro degradation of hydrogels was found dependent on the swelling ratio and the amount of CNC of the hydrogel.

Maximum compression of hydrogel decreased with increasing the pressure of gas foaming process. FESEM images showed that the pores of the hydrogel are around hundred micrometers and it increased more than tenfold after the gas foaming process (at 50 bar). Maximum swelling ratio in distilled water was obtained for 0.5% CNC–chitosan hydrogel and it decreased with increasing the CNC content. Gas foamed hydrogels swelled faster than the hydrogels prepared at atmospheric condition.

For the hydrogels formed at atmospheric condition, the drug encapsulation efficiency increased with increasing CNC content ranging from 0% to 0.6%. The maximum drug loading efficiency was observed in 0.5% and 0.6% CNC–chitosan hydrogel, which was 41% ± 2.4% and 41% ± 0.72%, respectively. The drug release profiles of hydrogels were consistent with the data obtained from the swelling studies. 0.5% CNC–chitosan hydrogel and 0.3% CNC-chitosan hydrogel showed the highest drug release percentage, whereas the 2.5% CNC–chitosan hydrogel produced the lowest drug release percentage. The kinetic parameters indicated that the drug diffusion through the hydrogel were in non-Fickian (anomalous) manner.

Higher drug loading ability was observed in gas foamed hydrogel when compared to the hydrogels formed at atmospheric condition. Results revealed that the encapsulation efficiency of hydrogels further increased with increasing the temperature of gas foaming process. The drug release rate and the amount of drug release of hydrogels increased with increasing the hydrogel processing pressure of gas foaming process. The hydrogels formed at high temperature showed extended drug release when compared to the hydrogels formed at room temperature.

At the later part of the research, curcumin was extracted from dried rhizomes of curcuma longa using methanol. Solubility studies showed that the saturation point of curcumin linearly increased with increasing the concentration of nonionic surfactant (Tween 20), with an upper limit of 3.014 ± 0.041 mg/mL in the presence of 3.2% (w/v) Tween 20. As similar to reported in previous studies, the entrapment efficiency of the hydrogels decreased with increasing the Tween 20 concentration. Furthermore, the in vitro drug release studies showed that the cumulative release of curcumin increased from 0.21% ± 0.02% to 54.85% ± 0.77%, with increasing the Tween 20 concentration from 0% to 30% (w/v), after 7.5 h.

Curcumin retained its structural integrity after release, which is critical requirement for preserving drug activity. On the basis of the findings of this study, we believe that mechanically improved nanocellulose reinforced chitosan hydrogel will provide a platform to overcome current problems associated with curcumin delivery.

5.2 Future work

The present study provides sufficient experimental evidence that nanocellulose reinforced chitosan hydrogel can be favorably applied to improve the bioavailability of poorly water-soluble drug, curcumin for the absorption from stomach and upper intestinal tract. After oral administration, stomach-site specific drug delivery systems would be retained in the stomach and release the drug in a sustainable manner. These drug delivery systems face major two challenges: the short gastric residence time and variable gastric emptying rates, which can result in incomplete release from the dosage form and cause decreased bio availability in the absorption zone. Therefore, it is desirable to produce site-specific formulations with additional gastric retention property to achieve the drug release in a controlled and prolonged manner, so that the drug could be supplied its absorption sites in the upper gastrointestinal tract for an extended period of

time. Various approaches have been adopted by previous researchers to enhance the gastric residence time of site-specific formulations to prolong the drug release in the upper gastrointestinal tract. Among different methods available, bioadhesive or mucoadhesive systems are highly used due to which they can prolong the intimate contact with the absorbing membrane (epithelial surface in the stomach) resulting in increased efficacy and plasma half-life. Different attempts have been taken to improve the mucoadhesive properties of chitosan. Several studies have reported that thiolation of chitosan showed significant improvement of mucoadhesive properties than neat chitosan, because of the covalent bonds formed between the thiol group and the mucin glycoprotein present in epithelial tissues are much stronger than the noncovalent bonds formed between chitosan and mucin glycoprotein. According to the previous studies, the mucoadhesion was linked to better bioavailability of drugs. Therefore, the modification of chitosan functional groups could be the next step towards the improvement of mucoadhesive properties of the nanocellulose reinforced chitosan hydrogel.

Furthermore, biocompatibility of the hydrogel system is a critical parameter for further applications. So, the future studies will be planned on the investigations of the cytotoxicity and biocompatibility of the hydrogel for in vivo drug delivery applications. There is however a need to further corroborates the findings of this study on living systems and therefore, in future investigations on disease models and clinical trials may be planned.

Previous studies have demonstrated that the drug (curcumin) found to possess promising anti-cancer properties and bear less side effects. Therefore, the enhancement of curcumin bioavailability using nanocellulose reinforced chitosan hydrogel shall be a great help to the suffering humanity.

REFERENCES

Abdelaal, O. A., & Darwish, S. M. (2011). Fabrication of tissue engineering scaffolds using rapid prototyping techniques. *International Journal of Mechanical, Aerospace, Industrial, Mechatronic and Manufacturing Engineering, 5*(11), 2317-2325.

Abou-Zeid, R. E., Hassan, E. A., Bettaieb, F., Khiari, R., & Hassan, M. L. (2015). Use of cellulose and oxidized cellulose nanocrystals from olive stones in chitosan bionanocomposites. *Journal of Nanomaterials, 16*(1), 172.

Adav, S. S., Chao, L. T., & Sze, S. K. (2012). Quantitative secretomic analysis of Trichoderma reesei strains reveals enzymatic composition for lignocellulosic biomass degradation. *Molecular & cellular proteomics, 11*(7), M111. 012419.

Ag Seleci, D., Seleci, M., Walter, J.-G., Stahl, F., & Scheper, T. (2016). Niosomes as nanoparticular drug carriers: fundamentals and recent applications. *Journal of Nanomaterials, 2016*.

Agarwal, S., Wendorff, J. H., & Greiner, A. (2008). Use of electrospinning technique for biomedical applications. *Polymer, 49*(26), 5603-5621.

Agnihotri, S. A., & Aminabhavi, T. M. (2006). Novel interpenetrating network chitosan-poly (ethylene oxide-g-acrylamide) hydrogel microspheres for the controlled release of capecitabine. *International journal of pharmaceutics, 324*(2), 103-115.

Ahmadi, F., Oveisi, Z., Samani, S. M., & Amoozgar, Z. (2014). Chitosan based hydrogels: characteristics and pharmaceutical applications. *Research in pharmaceutical sciences, 10*(1), 1-16.

Ahmed, E. M. (2015). Hydrogel: Preparation, characterization, and applications: A review. *Journal of advanced research, 6*(2), 105-121.

Ahmed, M., Qadir, M. A., Shafiq, M. I., Muddassar, M., Hameed, A., Arshad, M. N., & Asiri, A. M. (2017). Curcumin: Synthesis optimization and in silico interaction with cyclin dependent kinase. *Acta pharmaceutica, 67*(3), 385-395.

Ahuja, G., & Pathak, K. (2009). Porous carriers for controlled/modulated drug delivery. *Indian journal of pharmaceutical sciences, 71*(6), 599.

Akhlaghi, S. P., Berry, R. C., & Tam, K. C. (2013). Surface modification of cellulose nanocrystal with chitosan oligosaccharide for drug delivery applications. *Cellulose, 20*(4), 1747-1764.

Ali, M. S., Pandit, V., Jain, M., & Dhar, K. L. (2014). Mucoadhesive microparticulate drug delivery system of curcumin against Helicobacter pylori infection: Design, development and optimization. *Journal of advanced pharmaceutical technology & research, 5*(1), 48.

Alvarez, K., & Nakajima, H. (2009). Metallic scaffolds for bone regeneration. *Materials, 2*(3), 790-832.

Amin, S., Rajabnezhad, S., & Kohli, K. (2009). Hydrogels as potential drug delivery systems. *Scientific Research and Essays, 4*(11), 1175-1183.

Anand, P., Kunnumakkara, A. B., Newman, R. A., & Aggarwal, B. B. (2007). Bioavailability of curcumin: problems and promises. *Molecular pharmaceutics, 4*(6), 807-818.

Andersen, T., Auk-Emblem, P., & Dornish, M. (2015). 3D cell culture in alginate hydrogels. *Microarrays, 4*(2), 133-161.

Anitha, A., Maya, S., Deepa, N., Chennazhi, K., Nair, S., Tamura, H., & Jayakumar, R. (2011). Efficient water soluble O-carboxymethyl chitosan nanocarrier for the delivery of curcumin to cancer cells. *Carbohydrate Polymers, 83*(2), 452-461.

Annabi, N., Fathi, A., Mithieux, S. M., Weiss, A. S., & Dehghani, F. (2011). Fabrication of porous PCL/elastin composite scaffolds for tissue engineering applications. *The Journal of Supercritical Fluids, 59*, 157-167.

Annabi, N., Mithieux, S. M., Weiss, A. S., & Dehghani, F. (2009). The fabrication of elastin-based hydrogels using high pressure CO 2. *Biomaterials, 30*(1), 1-7.

Annabi, N., Mithieux, S. M., Weiss, A. S., & Dehghani, F. (2010). Cross-linked open-pore elastic hydrogels based on tropoelastin, elastin and high pressure CO 2. *Biomaterials, 31*(7), 1655-1665.

Annabi, N., Nichol, J. W., Zhong, X., Ji, C., Koshy, S., Khademhosseini, A., & Dehghani, F. (2010). Controlling the porosity and microarchitecture of hydrogels for tissue engineering. *Tissue Engineering Part B: Reviews, 16*(4), 371-383.

Annabi, N., Tsang, K., Mithieux, S. M., Nikkhah, M., Ameri, A., Khademhosseini, A., & Weiss, A. S. (2013). Highly elastic micropatterned hydrogel for engineering functional cardiac tissue. *Advanced functional materials, 23*(39), 4950-4959.

Anusha, J., & Fleming, A. T. (2016). Synthesis and characterization of chitosan nanoaggregates from gladius of Uroteuthis duvauceli. *International journal of biomaterials, 2016*.

Arya, P., & Pathak, K. (2014). Assessing the viability of microsponges as gastro retentive drug delivery system of curcumin: Optimization and pharmacokinetics. *International journal of pharmaceutics, 460*(1), 1-12.

Ashworth, J., Best, S., & Cameron, R. (2014). Quantitative architectural description of tissue engineering scaffolds. *Materials Technology, 29*(5), 281-295.

Auras, R., Harte, B., & Selke, S. (2004). An overview of polylactides as packaging materials. *Macromolecular bioscience, 4*(9), 835-864.

Ávila, H. M., Schwarz, S., Feldmann, E.-M., Mantas, A., von Bomhard, A., Gatenholm, P., & Rotter, N. (2014). Biocompatibility evaluation of densified bacterial nanocellulose hydrogel as an implant material for auricular cartilage regeneration. *Applied microbiology and biotechnology, 98*(17), 7423-7435.

Azimi, B., Nourpanah, P., Rabiee, M., & Arbab, S. (2014). Poly (lactide-co-glycolide) Fiber: An Overview. *Journal of Engineered Fabrics & Fibers (JEFF), 9*(1), 47-66.

Baig, M. S., Ahad, A., Aslam, M., Imam, S. S., Aqil, M., & Ali, A. (2016). Application of Box–Behnken design for preparation of levofloxacin-loaded stearic acid solid lipid nanoparticles for ocular delivery: Optimization, in vitro release, ocular tolerance, and antibacterial activity. *International journal of biological macromolecules, 85*, 258-270.

Bajpai, S., Chand, N., & Ahuja, S. (2015). Investigation of curcumin release from chitosan/cellulose micro crystals (CMC) antimicrobial films. *International journal of biological macromolecules, 79*, 440-448.

Bangyekan, C., Aht-Ong, D., & Srikulkit, K. (2006). Preparation and properties evaluation of chitosan-coated cassava starch films. *Carbohydrate Polymers, 63*(1), 61-71.

Bansal, S. S., Goel, M., Aqil, F., Vadhanam, M. V., & Gupta, R. C. (2011). Advanced drug delivery systems of curcumin for cancer chemoprevention. *Cancer prevention research, 4*(8), 1158-1171.

Bashir, S., Teo, Y. Y., Ramesh, S., & Ramesh, K. (2016). Synthesis, characterization, properties of N-succinyl chitosan-g-poly (methacrylic acid) hydrogels and in vitro release of theophylline. *Polymer, 92*, 36-49.

Bayindir, Z. S., & Yuksel, N. (2010). Characterization of niosomes prepared with various nonionic surfactants for paclitaxel oral delivery. *Journal of pharmaceutical sciences, 99*(4), 2049-2060.

Baziwane, D., & He, Q. (2003). Gelatin: the paramount food additive. *Food Reviews International, 19*(4), 423-435.

Bhamidipati, M., Scurto, A. M., & Detamore, M. S. (2013). The future of carbon dioxide for polymer processing in tissue engineering. *Tissue Engineering Part B: Reviews, 19*(3), 221-232.

Bhardwaj, N., & Kundu, S. C. (2010). Electrospinning: a fascinating fiber fabrication technique. *Biotechnology advances, 28*(3), 325-347.

Bhat, P. A., Dar, A. A., & Rather, G. M. (2008). Solubilization capabilities of some cationic, anionic, and nonionic surfactants toward the poorly water-soluble antibiotic drug erythromycin. *Journal of Chemical & Engineering Data, 53*(6), 1271-1277.

Bhattarai, N., Gunn, J., & Zhang, M. (2010). Chitosan-based hydrogels for controlled, localized drug delivery. *Advanced drug delivery reviews, 62*(1), 83-99.

Bich, V. T., Thuy, N. T., Binh, N. T., Huong, N. T. M., Yen, P. N. D., & Luong, T. T. (2009). Structural and spectral properties of curcumin and metal-curcumin complex derived from turmeric (Curcuma longa). *Physics and engineering of new materials*, 271-278.

Bode, F., da Silva, M. A., Drake, A. F., Ross-Murphy, S. B., & Dreiss, C. A. (2011). Enzymatically cross-linked tilapia gelatin hydrogels: physical, chemical, and hybrid networks. *Biomacromolecules, 12*(10), 3741-3752.

Bozsak, F., Gonzalez-Rodriguez, D., Sternberger, Z., Belitz, P., Bewley, T., Chomaz, J.-M., & Barakat, A. I. (2015). Optimization of drug delivery by drug-eluting stents. *PloS one, 10*(6), e0130182.

Bozzini, S., Giuliano, L., Altomare, L., Petrini, P., Bandiera, A., Conconi, M. T., . . . Tanzi, M. C. (2011). Enzymatic cross-linking of human recombinant elastin (HELP) as biomimetic approach in vascular tissue engineering. *Journal of Materials Science: Materials in Medicine, 22*(12), 2641-2650.

Brugnerotto, J., Lizardi, J., Goycoolea, F., Argüelles-Monal, W., Desbrieres, J., & Rinaudo, M. (2001). An infrared investigation in relation with chitin and chitosan characterization. *Polymer, 42*(8), 3569-3580.

Budianto, E., Muthoharoh, S. P., & Nizardo, N. M. (2015). Effect of crosslinking agents, pH and temperature on swelling behavior of cross-linked chitosan hydrogel. *Asian Journal of Applied Sciences, 3*(5), 581-588.

Caló, E., & Khutoryanskiy, V. V. (2015). Biomedical applications of hydrogels: A review of patents and commercial products. *European Polymer Journal, 65*, 252-267.

Carbinatto, F. M., de Castro, A. D., Evangelista, R. C., & Cury, B. S. (2014). Insights into the swelling process and drug release mechanisms from cross-linked pectin/high amylose starch matrices. *asian journal of pharmaceutical sciences, 9*(1), 27-34.

Carrillo, A. I., Bachl, J., Mayr, J., Plaza-González, P. J., Cátala-Civera, J. M., & Díaz, D. D. (2015). Non-invasive and continuous monitoring of the sol–gel phase transition of supramolecular gels using a fast (open-ended coaxial) microwave sensor. *Physical Chemistry Chemical Physics, 17*(9), 6212-6216.

Celebi, H., & Kurt, A. (2015). Effects of processing on the properties of chitosan/cellulose nanocrystal films. *Carbohydrate Polymers, 133*, 284-293.

Chandramohan, D., & Marimuthu, K. (2011). A review on natural fibers. *International Journal of Research and Reviews in Applied Sciences, 8*(2), 194-206.

Chang, C.-W., van Spreeuwel, A., Zhang, C., & Varghese, S. (2010). PEG/clay nanocomposite hydrogel: a mechanically robust tissue engineering scaffold. *Soft Matter, 6*(20), 5157-5164.

Chang, C., & Zhang, L. (2011). Cellulose-based hydrogels: present status and application prospects. *Carbohydrate Polymers, 84*(1), 40-53.

Chang, S.-W., Shefelbine, S. J., & Buehler, M. J. (2012). Structural and mechanical differences between collagen homo-and heterotrimers: relevance for the molecular origin of brittle bone disease. *Biophysical journal, 102*(3), 640-648.

Chatterjee, S., Lee, M. W., & Woo, S. H. (2009). Enhanced mechanical strength of chitosan hydrogel beads by impregnation with carbon nanotubes. *Carbon, 47*(12), 2933-2936.

Chavda, H., Modhia, I., Mehta, A., Patel, R., & Patel, C. (2013). Development of bioadhesive chitosan superporous hydrogel composite particles based intestinal drug delivery system. *BioMed research international, 2013*.

Chavda, H., & Patel, C. (2010). Chitosan superporous hydrogel composite-based floating drug delivery system: A newer formulation approach. *Journal of Pharmacy and Bioallied Sciences, 2*(2), 124.

Chen, C. H., Wang, F. Y., & Ou, Z. P. (2004). Deacetylation of β-chitin. I. Influence of the deacetylation conditions. *Journal of applied polymer science, 93*(5), 2416-2422.

Chen, R. H., Lin, J. H., & Yang, M. H. (1994). Relationships between the chain flexibilities of chitosan molecules and the physical properties of their casted films. *Carbohydrate Polymers, 24*(1), 41-46.

Chen, Y., Li, S., Li, X., Zhang, Y., Huang, Z., Feng, Q., . . . Yu, B. (2012). Noninvasive evaluation of injectable chitosan/nano-hydroxyapatite/collagen scaffold via ultrasound. *Journal of Nanomaterials, 2012*, 5.

Cheung, R. C. F., Ng, T. B., Wong, J. H., & Chan, W. Y. (2015). Chitosan: an update on potential biomedical and pharmaceutical applications. *Marine drugs, 13*(8), 5156-5186.

Chew, S., Wen, Y., Dzenis, Y., & Leong, K. W. (2006). The role of electrospinning in the emerging field of nanomedicine. *Current pharmaceutical design, 12*(36), 4751-4770.

Chhabra, P., Tyagi, P., Bhatnagar, A., Mittal, G., & Kumar, A. (2016). Optimization, characterization, and efficacy evaluation of 2% chitosan scaffold for tissue engineering and wound healing. *Journal of Pharmacy and Bioallied Sciences, 8*(4), 300.

Chikazu, D., Taguchi, T., Koyama, H., Hikiji, H., Fujihara, H., Suenaga, H., . . . Iino, M. (2010). Improvement in wound healing by a novel synthetic collagen-gel dressing in genetically diabetic mice. *Asian Journal of Oral and Maxillofacial Surgery, 22*(2), 61-67.

Chime, S., Onunkwo, G., & Onyishi, I. (2013). Kinetics and mechanisms of drug release from swellable and non swellable matrices: a review. *Research Journal of Pharmaceutical, Biological and Chemical Sciences, 4*(2), 97-103.

Chiono, V., Pulieri, E., Vozzi, G., Ciardelli, G., Ahluwalia, A., & Giusti, P. (2008). Genipin-crosslinked chitosan/gelatin blends for biomedical applications. *Journal of Materials Science: Materials in Medicine, 19*(2), 889-898.

Chirayil, C. J., Mathew, L., & Thomas, S. (2014). Review of recent research in nano cellulose preparation from different lignocellulosic fibers. *Reviews on advanced materials science, 37*, 20-28.

Chiu, Y.-C., Kocagöz, S., Larson, J. C., & Brey, E. M. (2013). Evaluation of physical and mechanical properties of porous poly (ethylene glycol)-co-(l-lactic acid) hydrogels during degradation. *PloS one, 8*(4), e60728.

Chivrac, F., Pollet, E., & Avérous, L. (2009). Progress in nano-biocomposites based on polysaccharides and nanoclays. *Materials Science and Engineering: R: Reports, 67*(1), 1-17.

Cho, M.-J., & Park, B.-D. (2011). Tensile and thermal properties of nanocellulose-reinforced poly (vinyl alcohol) nanocomposites. *Journal of Industrial and Engineering Chemistry, 17*(1), 36-40.

Cho, Y. W., Lee, J., Lee, S. C., Huh, K. M., & Park, K. (2004). Hydrotropic agents for study of in vitro paclitaxel release from polymeric micelles. *Journal of controlled release, 97*(2), 249-257.

Cox, S. C., Thornby, J. A., Gibbons, G. J., Williams, M. A., & Mallick, K. K. (2015). 3D printing of porous hydroxyapatite scaffolds intended for use in bone tissue engineering applications. *Materials Science and Engineering: C, 47*, 237-247.

Croisier, F., & Jérôme, C. (2013). Chitosan-based biomaterials for tissue engineering. *European Polymer Journal, 49*(4), 780-792.

Cserháti, T., Forgács, E., & Oros, G. (2002). Biological activity and environmental impact of anionic surfactants. *Environment international, 28*(5), 337-348.

Dahlin, R. L., Kasper, F. K., & Mikos, A. G. (2011). Polymeric nanofibers in tissue engineering. *Tissue Engineering Part B: Reviews, 17*(5), 349-364.

De Francesco, V., Bellesia, A., Ridola, L., Manta, R., & Zullo, A. (2017). First-line therapies for Helicobacter pylori eradication: a critical reappraisal of updated guidelines. *Annals of gastroenterology, 30*(4), 373.

De, R., Kundu, P., Swarnakar, S., Ramamurthy, T., Chowdhury, A., Nair, G. B., & Mukhopadhyay, A. K. (2009). Antimicrobial activity of curcumin against Helicobacter pylori isolates from India and during infections in mice. *Antimicrobial agents and chemotherapy, 53*(4), 1592-1597.

Deepa, G., Thulasidasan, A. K. T., Anto, R. J., Pillai, J. J., & Kumar, G. V. (2012). Cross-linked acrylic hydrogel for the controlled delivery of hydrophobic drugs in cancer therapy. *International journal of nanomedicine, 7*, 4077.

Dehghani, F., & Annabi, N. (2011). Engineering porous scaffolds using gas-based techniques. *Current opinion in biotechnology, 22*(5), 661-666.

Demirtaş, T. T., Irmak, G., & Gümüşderelioğlu, M. (2017). A bioprintable form of chitosan hydrogel for bone tissue engineering. *Biofabrication, 9*(3), 035003.

Dhandayuthapani, B., Yoshida, Y., Maekawa, T., & Kumar, D. S. (2011). Polymeric scaffolds in tissue engineering application: a review. *International Journal of Polymer Science, 2011*.

Dhivya, S., & Rajalakshmi, A. (2017). Curcumin Nano drug delivery systems: A Review on its type and therapeutic application. *PharmaTutor, 5*(12), 30-39.

Dhivya, S., Saravanan, S., Sastry, T., & Selvamurugan, N. (2015). Nanohydroxyapatite-reinforced chitosan composite hydrogel for bone tissue repair in vitro and in vivo. *Journal of nanobiotechnology, 13*(1), 40.

Dinarvand, R., Moghadam, S., Sheikhi, A., & Atyabi, F. (2005). Effect of surfactant HLB and different formulation variables on the properties of poly-D, L-lactide microspheres of naltrexone prepared by double emulsion technique. *Journal of microencapsulation, 22*(2), 139-151.

Dodds, W., Stutzman, L., & Sollami, B. (1956). Carbon dioxide solubility in water. *Industrial & Engineering Chemistry Chemical & Engineering Data Series, 1*(1), 92-95.

Dole, M. (1956). The melting range of semicrystalline polymers and copolymers. *Journal of Polymer Science Part A: Polymer Chemistry, 19*(92), 347-352.

Domingues, R. M., Silva, M., Gershovich, P., Betta, S., Babo, P., Caridade, S. G., . . . Gomes, M. E. (2015). Development of injectable hyaluronic acid/cellulose nanocrystals bionanocomposite hydrogels for tissue engineering applications. *Bioconjugate chemistry, 26*(8), 1571-1581.

Dubey, J., Verma, A., & Verma, N. (2015). Evaluation of chitosan based polymeric matrices for sustained stomach specific delivery of propranolol hydrochloride. *Indian Journal of Materials Science, 2015*.

Dufresne, A. (2003). Interfacial phenomena in nanocomposites based on polysaccharide nanocrystals. *Composite Interfaces, 10*(4-5), 369-387.

Dunphy, S. E., Bratt, J. A., Akram, K. M., Forsyth, N. R., & El Haj, A. J. (2014). Hydrogels for lung tissue engineering: Biomechanical properties of thin collagen–elastin constructs. *Journal of the mechanical behavior of biomedical materials, 38*, 251-259.

E-Thaher, N., Mekonnen, T., Mussone, P., Bressler, D., & Choi, P. (2013). Effects of electrolytes, water, and temperature on cross-linking of glutaraldehyde and hydrolyzed specified risk material. *Industrial & Engineering Chemistry Research, 52*(14), 4987-4993.

El-Mekawy, R. E., & Jassas, R. S. (2017). Recent trends in smart and flexible three-dimensional cross-linked polymers: synthesis of chitosan–ZnO nanocomposite hydrogels for insulin drug delivery. *Medicinal Chemistry Communications, 8*(5), 897-906.

El-Ridy, M. S., Abdelbary, A., Essam, T., Abd EL-Salam, R. M., & Aly Kassem, A. A. (2011). Niosomes as a potential drug delivery system for increasing the efficacy and safety of nystatin. *Drug development and industrial pharmacy, 37*(12), 1491-1508.

El-Sakhawy, M., Kamel, S., Salama, A., & Sarhan, H.-A. (2014). Carboxymethyl cellulose acetate butyrate: A review of the preparations, properties, and applications. *Journal of drug delivery, 2014*.

Eldin, M. S. M., Kamoun, E. A., Sofan, M. A., & Elbayomi, S. M. (2015). L-Arginine grafted alginate hydrogel beads: A novel pH-sensitive system for specific protein delivery. *Arabian Journal of Chemistry, 8*(3), 355-365.

Emami, J., Tajeddin, M., & Ahmadi, F. (2010). Preparation and in vitro evaluation of sustained-release matrix tablets of flutamide using synthetic and naturally occurring polymers. *Iranian Journal of pharmaceutical research*, 247-257.

Fernandes Queiroz, M., Melo, K. R. T., Sabry, D. A., Sassaki, G. L., & Rocha, H. A. O. (2014). Does the use of chitosan contribute to oxalate kidney stone formation? *Marine drugs, 13*(1), 141-158.

Fernandes, S. C., Freire, C. S., Silvestre, A. J., Neto, C. P., Gandini, A., Berglund, L. A., & Salmén, L. (2010). Transparent chitosan films reinforced with a high content of nanofibrillated cellulose. *Carbohydrate Polymers, 81*(2), 394-401.

Ferreira, A. M., Gentile, P., Chiono, V., & Ciardelli, G. (2012). Collagen for bone tissue regeneration. *Acta biomaterialia, 8*(9), 3191-3200.

Figueiredo, K., Alves, T. L., & Borges, C. P. (2009). Poly (vinyl alcohol) films crosslinked by glutaraldehyde under mild conditions. *Journal of applied polymer science, 111*(6), 3074-3080.

Fimantari, K., & Budianto, E. (2018). *Effect of drug loading method against drug dissolution mechanism of encapsulated amoxicillin trihydrate in matrix of semi-IPN chitosan-poly (N-vinylpyrrolidone) hydrogel with KHCO3 as pore forming agent in floating drug delivery system.* Paper presented at the AIP Conference Proceedings.

Foox, M., & Zilberman, M. (2015). Drug delivery from gelatin-based systems. *Expert opinion on drug delivery, 12*(9), 1547-1563.

French, A. D., & Cintrón, M. S. (2013). Cellulose polymorphy, crystallite size, and the Segal crystallinity index. *Cellulose, 20*(1), 583-588.

Friess, W. (1998). Collagen–biomaterial for drug delivery. *European Journal of Pharmaceutics and Biopharmaceutics, 45*(2), 113-136.

Fu, Y., & Kao, W. J. (2010). Drug release kinetics and transport mechanisms of non-degradable and degradable polymeric delivery systems. *Expert opinion on drug delivery, 7*(4), 429-444.

Fugita, R., Gálico, D., Guerra, R., Perpétuo, G., Treu-Filho, O., Galhiane, M., . . . Bannach, G. (2012). Thermal behaviour of curcumin. *Brazilian Journal of Thermal Analysis, 1*, 19-23.

Ganji, F., Vasheghani-Farahani, S., & Vasheghani-Farahani, E. (2010). Theoretical description of hydrogel swelling: a review. *Iranian polymer journal, 19*(5), 375-398.

Gavillon, R., & Budtova, T. (2007). Aerocellulose: new highly porous cellulose prepared from cellulose−NaOH aqueous solutions. *Biomacromolecules, 9*(1), 269-277.

Gemeinhart, R. A., Park, H., & Park, K. (2000). Pore structure of superporous hydrogels. *Polymers for advanced technologies, 11*(8-12), 617-625.

Gentile, P., Chiono, V., Carmagnola, I., & Hatton, P. V. (2014). An overview of poly (lactic-co-glycolic) acid (PLGA)-based biomaterials for bone tissue engineering. *International journal of molecular sciences, 15*(3), 3640-3659.

George, J., & Sabapathi, S. (2015). Cellulose nanocrystals: synthesis, functional properties, and applications. *Nanotechnology, science and applications, 8*, 45.

Ghose, T. (1987). Measurement of cellulase activities. *Pure and applied Chemistry, 59*(2), 257-268.

Ghosh, S., & Jassal, M. (2002). Use of polysaccharide fibres for modern wound dressings. *Indian Journal of Fibre and Textile Research, 27*(4), 434-452.

Giri, T. K., Thakur, A., Alexander, A., Badwaik, H., & Tripathi, D. K. (2012). Modified chitosan hydrogels as drug delivery and tissue engineering systems: present status and applications. *Acta Pharmaceutica Sinica B, 2*(5), 439-449.

Gonzalez, G., Sagarzazu, A., & Zoltan, T. (2013). Influence of microstructure in drug release behavior of silica nanocapsules. *Journal of drug delivery, 2013*.

González, K., Retegi, A., González, A., Eceiza, A., & Gabilondo, N. (2015). Starch and cellulose nanocrystals together into thermoplastic starch bionanocomposites. *Carbohydrate Polymers, 117*, 83-90.

Gowthamarajan, K., & Singh, S. K. (2010). Dissolution testing for poorly soluble drugs: a continuing perspective. *Dissolution Technologies, 17*(3), 24-32.

Goy, R. C., Britto, D. d., & Assis, O. B. (2009). A review of the antimicrobial activity of chitosan. *Polímeros, 19*(3), 241-247.

Grijalvo, S., Mayr, J., Eritja, R., & Díaz, D. D. (2016). Biodegradable liposome-encapsulated hydrogels for biomedical applications: a marriage of convenience. *Biomaterials science, 4*(4), 555-574.

Gritsch, L., Motta, F. L., Chirani, S., & Faré, S. (2015). History and applications of hydrogels. *Journal of biomedical sciences, 4*(2), 13.

Guillén, F., Martínez, M. J., Gutiérrez, A., & Del Rio, J. (2005). Biodegradation of lignocellu-losics: microbial, chemical, and enzymatic aspects of the fungal attack of lignin. *International Microbiology, 8*, 195-204.

Guinedi, A. S., Mortada, N. D., Mansour, S., & Hathout, R. M. (2005). Preparation and evaluation of reverse-phase evaporation and multilamellar niosomes as ophthalmic carriers of acetazolamide. *International journal of pharmaceutics, 306*(1), 71-82.

Guo, D., Xie, G., & Luo, J. (2013). Mechanical properties of nanoparticles: basics and applications. *Journal of Physics D: Applied Physics, 47*(1), 013001.

Gupta, G., & Singh, A. (2012). A short review on stomach specific drug delivery system. *International Journal of PharmTech Research, 4*(4), 1527-1545.

Gupta, K., & Kumar, M. N. (2001). Studies on semi-interpenetrating polymer network beads of chitosan–poly (ethylene glycol) for the controlled release of drugs. *Journal of applied polymer science, 80*(4), 639-649.

Gupta, N., & Aggarwal, N. (2008). Bioavailability enhancement and targeting of stomach tumors using gastro-retentive floating drug delivery system of curcumin—~~a~~ technical note". *American Association of Pharmaceutical Scientists Pharmscitech, 9*(3), 810-813.

Guzman-Villanueva, D., El-Sherbiny, I. M., Herrera-Ruiz, D., & Smyth, H. D. (2013). Design and in vitro evaluation of a new nano-microparticulate system for enhanced aqueous-phase solubility of curcumin. *BioMed research international, 2013*.

Habibi, Y., Lucia, L. A., & Rojas, O. J. (2010). Cellulose nanocrystals: chemistry, self-assembly, and applications. *Chemical reviews, 110*(6), 3479-3500.

Hamman, J. H. (2010). Chitosan based polyelectrolyte complexes as potential carrier materials in drug delivery systems. *Marine drugs, 8*(4), 1305-1322.

Han, J., Lei, T., & Wu, Q. (2014). High-water-content mouldable polyvinyl alcohol-borax hydrogels reinforced by well-dispersed cellulose nanoparticles: Dynamic rheological properties and hydrogel formation mechanism. *Carbohydrate Polymers, 102*, 306-316.

Hazra, K., Kumar, R., Sarkar, B. K., Chowdary, Y. A., Devgan, M., & Ramaiah, M. (2015). Uv-Visible Spectrophotometric estimation of curcumin in Nanoformulation. *International Journal of Pharmacognosy, 2*(3), 127-130.

He, X., Xiao, Q., Lu, C. H., Wang, Y. R., Zhang, X. F., Zhao, J. Q., . . . Deng, Y. L. (2014). Uniaxially aligned electrospun all-cellulose nanocomposite nanofibers reinforced with cellulose nanocrystals: scaffold for tissue engineering. *Biomacromolecules, 15*(2), 618-627.

Hejazi, R., & Amiji, M. (2002). Stomach-specific anti-H. pylori therapy. I: preparation and characterization of tetracyline-loaded chitosan microspheres. *International journal of pharmaceutics, 235*(1), 87-94.

Hernández, H. H., Benavides-Mendoza, A., Ortega-Ortiz, H., Hernández-Fuentes, A. D., & Juárez-Maldonado, A. (2017). Cu Nanoparticles in chitosan-PVA hydrogels as promoters of growth, productivity and fruit quality in tomato. *Emirates Journal of Food and Agriculture, 29*(8), 573-580.

Herrera, V., & Parsonnet, J. (2009). Helicobacter pylori and gastric adenocarcinoma. *Clinical Microbiology and Infection, 15*(11), 971-976.

Hesse, E., Hefferan, T. E., Tarara, J. E., Haasper, C., Meller, R., Krettek, C., . . . Yaszemski, M. J. (2010). Collagen type I hydrogel allows migration, proliferation, and osteogenic differentiation of rat bone marrow stromal cells. *Journal of Biomedical Materials Research Part A, 94*(2), 442-449.

Hilmi, A. B. M., Halim, A. S., Hassan, A., Lim, C. K., Noorsal, K., & Zainol, I. (2013). In vitro characterization of a chitosan skin regenerating template as a scaffold for cells cultivation. *Springerplus, 2*(1), 79.

Hoare, T. R., & Kohane, D. S. (2008). Hydrogels in drug delivery: progress and challenges. *Polymer, 49*(8), 1993-2007.

Hong, B., Chen, F., & Xue, G. (2016). Preparation and characterization of cellulose nanocrystals from bamboo pulp. *Cellulose Chemistry and Technology, 50*(2), 225-231.

Hoque, M. E., Chuan, Y. L., & Pashby, I. (2012). Extrusion based rapid prototyping technique: an advanced platform for tissue engineering scaffold fabrication. *Biopolymers, 97*(2), 83-93.

Hsieh, W.-C., Chang, C.-P., & Lin, S.-M. (2007). Morphology and characterization of 3D micro-porous structured chitosan scaffolds for tissue engineering. *Colloids and Surfaces B: Biointerfaces, 57*(2), 250-255.

Huang, X., & Brazel, C. S. (2001). On the importance and mechanisms of burst release in matrix-controlled drug delivery systems. *Journal of controlled release, 73*(2), 121-136.

Hung, B. P., Hutton, D. L., & Grayson, W. L. (2013). Mechanical control of tissue-engineered bone. *Stem cell research & therapy, 4*(1), 10.

Hung, W.-C., Chen, F.-Y., Lee, C.-C., Sun, Y., Lee, M.-T., & Huang, H. W. (2008). Membrane-thinning effect of curcumin. *Biophysical journal, 94*(11), 4331-4338.

Hussain, M. R., Iman, M., & Maji, T. K. (2013). Determination of degree of deacetylation of chitosan and their effect on the release behavior of essential oil from chitosan and chitosan-gelatin complex microcapsules. *International Journal of Advanced Engineering Applications, 6*(4), 4-12.

Inchai, N., Ezure, Y., Hongwiset, D., & Yotsawimonwat, S. (2015). Investigation on solubility and stability of curcumin in aqueous polysorbate micelle.

International Journal of Management and Applied Science (IJMAS), 3(4), 157-161.

Iviglia, G., Cassinelli, C., Torre, E., Baino, F., Morra, M., & Vitale-Brovarone, C. (2016). Novel bioceramic-reinforced hydrogel for alveolar bone regeneration. *Acta biomaterialia, 44*, 97-109.

Jameela, S., & Jayakrishnan, A. (1995). Glutaraldehyde cross-linked chitosan microspheres as a long acting biodegradable drug delivery vehicle: studies on the in vitro release of mitoxantrone and in vivo degradation of microspheres in rat muscle. *Biomaterials, 16*(10), 769-775.

Jamshidian, M., Tehrany, E. A., Imran, M., Jacquot, M., & Desobry, S. (2010). Polylactic acid: production, applications, nanocomposites, and release studies. *Comprehensive Reviews in Food Science and Food Safety, 9*(5), 552-571.

Jansirani, D., Saradha, R., Salomideborani, N., & Selvapriyadharshini, J. (2014). Comparative evaluation of various extraction methods of curcuminoids from Curcuma longa. *Journal of Chemical and Pharmaceutical Sciences*(4), 286-288.

Ji, C., Annabi, N., Khademhosseini, A., & Dehghani, F. (2011). Fabrication of porous chitosan scaffolds for soft tissue engineering using dense gas CO 2. *Acta biomaterialia, 7*(4), 1653-1664.

Jobe, B. A., Richter, J. E., Hoppo, T., Peters, J. H., Bell, R., Dengler, W. C., . . . Kahrilas, P. J. (2013). Preoperative diagnostic workup before antireflux surgery: An evidence and experience-based consensus of the esophageal diagnostic advisory panel. *Journal of the American College of Surgeons, 217*(4), 586-597.

Kaewnopparat, N., Kaewnopparat, S., Jangwang, A., Maneenaun, D., Chuchome, T., & Panichayupakaranant, P. (2009). Increased solubility, dissolution and physicochemical studies of curcumin-polyvinylpyrrolidone K-30 solid dispersions. *World academy of science, engineering and technology, 55*, 229-234.

Kaklamani, G., Cheneler, D., Grover, L. M., Adams, M. J., & Bowen, J. (2014). Mechanical properties of alginate hydrogels manufactured using external gelation. *Journal of the mechanical behavior of biomedical materials, 36*, 135-142.

Karnchanajindanun, J., Srisa-ard, M., & Baimark, Y. (2011). Genipin-cross-linked chitosan microspheres prepared by a water-in-oil emulsion solvent diffusion method for protein delivery. *Carbohydrate Polymers, 85*(3), 674-680.

Kaur, G., & Mehta, S. (2017). Developments of polysorbate (Tween) based microemulsions: Preclinical drug delivery, toxicity and antimicrobial applications. *International journal of pharmaceutics, 529*(1-2), 134-160.

Kavoosi, G., Dadfar, S. M. M., Dadfar, S. M. A., Ahmadi, F., & Niakosari, M. (2014). Investigation of gelatin/multi-walled carbon nanotube nanocomposite films as packaging materials. *Food science & nutrition, 2*(1), 65-73.

Kawase, M., Michibayashi, N., Nakashima, Y., Kurikawa, N., Yagi, K., & Mizoguchi, T. (1997). Application of glutaraldehyde-crosslinked chitosan as a scaffold for hepatocyte attachment. *Biological and Pharmaceutical Bulletin, 20*(6), 708-710.

Khan, A., Khan, R. A., Salmieri, S., Le Tien, C., Riedl, B., Bouchard, J., . . . Lacroix, M. (2012). Mechanical and barrier properties of nanocrystalline cellulose reinforced chitosan based nanocomposite films. *Carbohydrate Polymers, 90*(4), 1601-1608.

Khoo, R., Ismail, H., & Chow, W. (2016). Thermal and morphological properties of poly (lactic acid)/nanocellulose nanocomposites. *Procedia Chemistry, 19*, 788-794.

Khurma, J. R., Rohindra, D. R., & Nand, A. V. (2006). Synthesis and properties of hydrogels based on chitosan and poly (vinyl alcohol) crosslinked by genipin. *Journal of Macromolecular Science, Part A: Pure and Applied Chemistry, 43*(4-5), 749-758.

Kildeeva, N., Perminov, P., Vladimirov, L., Novikov, V., & Mikhailov, S. (2009). About mechanism of chitosan cross-linking with glutaraldehyde. *Russian journal of bioorganic chemistry, 35*(3), 360-369.

Kim, J. F., Kim, J. H., Lee, Y. M., & Drioli, E. (2016). Thermally induced phase separation and electrospinning methods for emerging membrane applications: A review. *American Institute of Chemical Engineers Journal, 62*(2), 461-490.

Kim, S. J., Yang, D. H., Chun, H. J., Chae, G. T., Jang, J. W., & Shim, Y. B. (2013). Evaluations of chitosan/poly (D, L-lactic-co-glycolic acid) composite fibrous scaffold for tissue engineering applications. *Macromolecular Research, 21*(8), 931-939.

Kim, S. W., Bae, Y. H., & Okano, T. (1992). Hydrogels: swelling, drug loading, and release. *Pharmaceutical Research, 9*(3), 283-290.

Kolev, T. M., Velcheva, E. A., Stamboliyska, B. A., & Spiteller, M. (2005). DFT and experimental studies of the structure and vibrational spectra of curcumin. *International Journal of Quantum Chemistry, 102*(6), 1069-1079.

Krishnamachari, P., Hashaikeh, R., Chiesa, M., & Gad El Rab, K. (2012). Effects of acid hydrolysis time on cellulose nanocrystals properties: nanoindentation and thermogravimetric studies. *Cellulose Chemistry and Technology, 46*(1), 13.

Kumar, A., Negi, Y. S., Choudhary, V., & Bhardwaj, N. K. (2014). Characterization of cellulose nanocrystals produced by acid-hydrolysis from sugarcane bagasse as agro-waste. *Journal of Materials Physics and Chemistry, 2*(1), 1-8.

Kumar, G. P., & Rajeshwarrao, P. (2011). Nonionic surfactant vesicular systems for effective drug delivery—an overview. *Acta Pharmaceutica Sinica B, 1*(4), 208-219.

Kumar, K., & Rai, A. (2012). Development and evaluation of floating microspheres of curcumin. *Tropical journal of pharmaceutical research, 11*(5), 713-719.

Kumar, P. T. S., Praveen, G., Raj, M., Chennazhi, K. P., & Jayakumar, R. (2014). Flexible, micro-porous chitosan–gelatin hydrogel/nanofibrin composite bandages for treating burn wounds. *RSC Advances, 4*(110), 65081-65087. doi:10.1039/c4ra11969j

Kuo, C. K., & Ma, P. X. (2001). Ionically crosslinked alginate hydrogels as scaffolds for tissue engineering: part 1. Structure, gelation rate and mechanical properties. *Biomaterials, 22*(6), 511-521.

Kwon, S., Singh, R. K., Perez, R. A., Neel, E. A. A., Kim, H.-W., & Chrzanowski, W. (2013). Silica-based mesoporous nanoparticles for controlled drug delivery. *Journal of tissue engineering, 4*, 2041731413503357.

La Carrubba, V., Pavia, F. C., Brucato, V., & Piccarolo, S. (2008). PLLA/PLA scaffolds prepared via thermally induced phase separation (TIPS): tuning of properties and biodegradability. *International Journal of Material Forming, 1*(1), 619-622.

Lam, C. X. F., Mo, X., Teoh, S.-H., & Hutmacher, D. (2002). Scaffold development using 3D printing with a starch-based polymer. *Materials Science and Engineering: C, 20*(1), 49-56.

Laulicht, B., Tripathi, A., Schlageter, V., Kucera, P., & Mathiowitz, E. (2010). Understanding gastric forces calculated from high-resolution pill tracking. *Proceedings of the National Academy of Sciences, 107*(18), 8201-8206.

Leceta, I., Guerrero, P., & De la Caba, K. (2013). Functional properties of chitosan-based films. *Carbohydrate Polymers, 93*(1), 339-346.

Lee, H., Hamid, S., & Zain, S. (2014). Conversion of lignocellulosic biomass to nanocellulose: structure and chemical process. *The Scientific World Journal, 2014*.

Lee, J. S., Lee, H. K., Kim, J. Y., Hyon, S. H., & Kim, S. C. (2003). Thermally induced phase separation in poly (lactic acid)/dialkyl phthalate systems. *Journal of applied polymer science, 88*(9), 2224-2232.

Lee, K. Y., & Mooney, D. J. (2012). Alginate: properties and biomedical applications. *Progress in polymer science, 37*(1), 106-126.

Lee, M., Dunn, J. C., & Wu, B. M. (2005). Scaffold fabrication by indirect three-dimensional printing. *Biomaterials, 26*(20), 4281-4289.

Lee, S. J., Kim, S. S., & Lee, Y. M. (2000). Interpenetrating polymer network hydrogels based on poly (ethylene glycol) macromer and chitosan. *Carbohydrate Polymers, 41*(2), 197-205.

Leppiniemi, J., Lahtinen, P., Paajanen, A., Mahlberg, R., Mets -Kortelainen, S., Pinomaa, T., . . . Hyt nen, V. P. (2017). 3D-printable bioactivated nanocellulose–alginate hydrogels. *ACS applied materials & interfaces, 9*(26), 21959-21970.

Lestari, H., Martono, S., Wulandari, R., & Rohman, A. (2017). Simultaneous analysis of Curcumin and demethoxycurcumin in Curcuma xanthorriza using FTIR spectroscopy and chemometrics. *International Food Research Journal, 24*(5).

Li, B., Shan, C.-L., Zhou, Q., Fang, Y., Wang, Y.-L., Xu, F., . . . Xie, G.-L. (2013). Synthesis, characterization, and antibacterial activity of cross-linked chitosan-glutaraldehyde. *Marine drugs, 11*(5), 1534-1552.

Li, B., Wang, L., Hao, Y., Wei, D., Li, Y., Feng, Y., . . . Zhou, Y. (2015). Ultraviolet-crosslinkable and injectable chitosan/hydroxyapatite hybrid hydrogel for critical size calvarial defect repair in vivo. *Journal of Nanotechnology in Engineering and Medicine, 6*(4), 041001.

Li, D., Krantz, W. B., Greenberg, A. R., & Sani, R. L. (2006). Membrane formation via thermally induced phase separation (TIPS): Model development and validation. *Journal of membrane science, 279*(1), 50-60.

Li, F., Mascheroni, E., & Piergiovanni, L. (2015). The potential of nanocellulose in the packaging field: a review. *Packaging Technology and Science, 28*(6), 475-508.

Li, G., Wen, Q., Zhang, T., & Ju, Y. (2013). Synthesis and properties of silver nanoparticles in chitosan-based thermosensitive semi-interpenetrating hydrogels. *Journal of applied polymer science, 127*(4), 2690-2697.

Li, L., Ding, S., & Zhou, C. (2004). Preparation and degradation of PLA/chitosan composite materials. *Journal of applied polymer science, 91*(1), 274-277.

Li, X., Cui, R., Sun, L., Aifantis, K. E., Fan, Y., Feng, Q., . . . Watari, F. (2014). 3D-printed biopolymers for tissue engineering application. *International Journal of Polymer Science, 2014*.

Lim, J. I., Lee, Y.-K., Shin, J.-S., & Lim, K.-J. (2011). Preparation of interconnected porous chitosan scaffolds by sodium acetate particulate leaching. *Journal of Biomaterials Science, Polymer Edition, 22*(10), 1319-1329.

Lim, S. L., Ahmad, I., & Lazim, A. M. (2015). PH sensitive hydrogel based on poly (acrylic acid) and cellulose nanocrystals. *Sains Malaysiana, 44*(6), 779-785.

Lin, C.-C., & Metters, A. T. (2006). Hydrogels in controlled release formulations: network design and mathematical modeling. *Advanced drug delivery reviews, 58*(12), 1379-1408.

Lin, N., G ze, A., Wouessidjewe, D., Huang, J., & Dufresne, A. (2016). Biocompatible double-membrane hydrogels from cationic cellulose nanocrystals and anionic alginate as complexing drugs codelivery. *ACS applied materials & interfaces, 8*(11), 6880-6889.

Liu, G., Xiang, T., Wu, Q. F., & Wang, W. X. (2016). Curcumin suppresses the proliferation of gastric cancer cells by downregulating H19. *Oncology letters, 12*(6), 5156-5162.

Liu, X., & Ma, P. X. (2004). Polymeric scaffolds for bone tissue engineering. *Annals of biomedical engineering, 32*(3), 477-486.

Liu, Y., Cai, Y., Jiang, X., Wu, J., & Le, X. (2016). Molecular interactions, characterization and antimicrobial activity of curcumin–chitosan blend films. *Food Hydrocolloids, 52*, 564-572.

Lowe, T. L., Tenhu, H., & Tylli, H. (1999). Effect of hydrophobicity of a drug on its release from hydrogels with different topological structures. *Journal of applied polymer science, 73*(6), 1031-1039.

Lu, J., Li, X., Yang, R., Zhao, J., & Qu, Y. (2013). Tween 40 pretreatment of unwashed water-insoluble solids of reed straw and corn stover pretreated with liquid hot

water to obtain high concentrations of bioethanol. *Biotechnology for biofuels, 6*(1), 159.

Luo, H., Xiong, G., Li, Q., Ma, C., Zhu, Y., Guo, R., & Wan, Y. (2014). Preparation and properties of a novel porous poly (lactic acid) composite reinforced with bacterial cellulose nanowhiskers. *Fibers and Polymers, 15*(12), 2591-2596.

Lynd, L. R., Weimer, P. J., Van Zyl, W. H., & Pretorius, I. S. (2002). Microbial cellulose utilization: fundamentals and biotechnology. *Microbiology and molecular biology reviews, 66*(3), 506-577.

Ma, J., Li, X., & Bao, Y. (2015). Advances in cellulose-based superabsorbent hydrogels. *RSC Advances, 5*(73), 59745-59757.

Ma, N., Liu, D., Liu, Y., & Sui, G. (2015). Extraction and characterization of nanocellulose from xanthoceras sorbifolia husks. *International Journal of Nanoscience and Nanoengineering, 2*(6), 43-50.

Madhavi, D., & Kagan, D. (2014). Bioavailability of a sustained release formulation of curcumin. *Integrative Medicine: A Clinician's Journal, 13*(3), 24.

Mahady, G., Pendland, S., Yun, G., & Lu, Z. (2002). Turmeric (Curcuma longa) and curcumin inhibit the growth of Helicobacter pylori, a group 1 carcinogen. *Anticancer research, 22*(6C), 4179-4181.

Mahattanadul, S. (2016). Floating gellan gum-based in situ gels containing curcumin for specific delivery to the stomach. *Thai Journal of Pharmaceutical Sciences (TJPS), 40*.

Maitra, J., & Shukla, V. K. (2014). Cross-linking in hydrogels-a review. *American Journal of Polymer Science, 4*(2), 25-31.

Maji, K., Dasgupta, S., Pramanik, K., & Bissoyi, A. (2016). Preparation and evaluation of gelatin-chitosan-nanobioglass 3D porous scaffold for bone tissue engineering. *International journal of biomaterials, 2016*.

Majithiya, R. J., & Murthy, R. S. (2005). Chitosan-based mucoadhesive microspheres of clarithromycin as a delivery system for antibiotic to stomach. *Current drug delivery, 2*(3), 235-242.

Makadia, H. K., & Siegel, S. J. (2011). Poly lactic-co-glycolic acid (PLGA) as biodegradable controlled drug delivery carrier. *Polymers, 3*(3), 1377-1397.

Mallick, S., Tripathi, S., & Srivastava, P. (2015). Advancement in scaffolds for bone tissue engineering: A review. *IOSR Journal of Pharmacy and Biological Sciences, 10*, 37-54.

Mariano, M., El Kissi, N., & Dufresne, A. (2016). Cellulose nanocrystal reinforced oxidized natural rubber nanocomposites. *Carbohydrate Polymers, 137*, 174-183.

Martins, A. F., Facchi, S. P., Monteiro, J. P., Nocchi, S. R., Silva, C. T., Nakamura, C. V., . . . Muniz, E. C. (2015). Preparation and cytotoxicity of N, N, N-trimethyl chitosan/alginate beads containing gold nanoparticles. *International journal of biological macromolecules, 72*, 466-471.

Mascheroni, E., Rampazzo, R., Ortenzi, M. A., Piva, G., Bonetti, S., & Piergiovanni, L. (2016). Comparison of cellulose nanocrystals obtained by sulfuric acid hydrolysis and ammonium persulfate, to be used as coating on flexible food-packaging materials. *Cellulose, 23*(1), 779-793.

Mattioli-Belmonte, M., Zizzi, A., Lucarini, G., Giantomassi, F., Biagini, G., Tucci, G., . . . Morganti, P. (2007). Chitin nanofibrils linked to chitosan glycolate as spray, gel, and gauze preparations for wound repair. *Journal of bioactive and compatible polymers, 22*(5), 525-538.

Medina-Gonzalez, Y., Camy, S., & Condoret, J.-S. (2012). Cellulosic materials as biopolymers and supercritical CO2 as a green process: chemistry and applications. *International Journal of Sustainable Engineering, 5*(1), 47-65.

Mehta, S., Kaur, G., & Bhasin, K. (2010). Tween-embedded microemulsions—physicochemical and spectroscopic analysis for antitubercular drugs. *American Association of Pharmaceutical Scientists Pharmscitech, 11*(1), 143-153.

Mi, F.-L., Tan, Y.-C., Liang, H.-C., Huang, R.-N., & Sung, H.-W. (2001). In vitro evaluation of a chitosan membrane cross-linked with genipin. *Journal of Biomaterials Science, Polymer Edition, 12*(8), 835-850.

Miao, X., & Sun, D. (2009). Graded/gradient porous biomaterials. *Materials, 3*(1), 26-47.

Migneault, I., Dartiguenave, C., Bertrand, M. J., & Waldron, K. C. (2004). Glutaraldehyde: behavior in aqueous solution, reaction with proteins, and application to enzyme crosslinking. *Biotechniques, 37*(5), 790-806.

Mikos, A. G., & Temenoff, J. S. (2000). Formation of highly porous biodegradable scaffolds for tissue engineering. *Electronic Journal of Biotechnology, 3*(2), 23-24.

Mirahmadi, F., Tafazzoli-Shadpour, M., Shokrgozar, M. A., & Bonakdar, S. (2013). Enhanced mechanical properties of thermosensitive chitosan hydrogel by silk fibers for cartilage tissue engineering. *Materials Science and Engineering: C, 33*(8), 4786-4794.

Mirzaei B, E., Ramazani SA, A., Shafiee, M., & Danaei, M. (2013). Studies on glutaraldehyde crosslinked chitosan hydrogel properties for drug delivery systems. *International Journal of Polymeric Materials and Polymeric Biomaterials, 62*(11), 605-611.

Mirzaei, E., Faridi-Majidi, R., Shokrgozar, M. A., & Asghari Paskiabi, F. (2014). Genipin cross-linked electrospun chitosan-based nanofibrous mat as tissue engineering scaffold. *Nanomedicine Journal, 1*(3), 137-146.

Mogilevskaya, E., Akopova, T., Zelenetskii, A., & Ozerin, A. (2006). The crystal structure of chitin and chitosan. *Polymer Science Series A, 48*(2), 116-123.

Mohammed, N., Grishkewich, N., Berry, R. M., & Tam, K. C. (2015). Cellulose nanocrystal–alginate hydrogel beads as novel adsorbents for organic dyes in aqueous solutions. *Cellulose, 22*(6), 3725-3738.

Mohammed, N. A., & Habil, N. Y. (2015). Evaluation of antimicrobial activity of curcumin against two oral bacteria. *Automation, Control and Intelligent Systems, 3(2-1)*, 18-21.

Mohan, P. K., Sreelakshmi, G., Muraleedharan, C., & Joseph, R. (2012). Water soluble complexes of curcumin with cyclodextrins: Characterization by FT-Raman spectroscopy. *Vibrational Spectroscopy, 62*, 77-84.

Moon, R. J., Martini, A., Nairn, J., Simonsen, J., & Youngblood, J. (2011). Cellulose nanomaterials review: structure, properties and nanocomposites. *Chemical Society Reviews, 40*(7), 3941-3994.

Murphy, C. M., & O'Brien, F. J. (2010). Understanding the effect of mean pore size on cell activity in collagen-glycosaminoglycan scaffolds. *Cell adhesion & migration, 4*(3), 377-381.

Muzzarelli, R. A. (2009). Genipin-crosslinked chitosan hydrogels as biomedical and pharmaceutical aids. *Carbohydrate Polymers, 77*(1), 1-9.

Myung, D., Waters, D., Wiseman, M., Duhamel, P. E., Noolandi, J., Ta, C. N., & Frank, C. W. (2008). Progress in the development of interpenetrating polymer network hydrogels. *Polymers for advanced technologies, 19*(6), 647-657.

Nadzir, M. M., Mun, L. S., & Juan, C. P. (2017). Characterization of genipin-crosslinked gelatin hydrogel loaded with curcumin. *Journal of Engineering and Applied Sciences, 12*(9), 2294-2298.

Naito, H., Yoshimura, M., Mizuno, T., Takasawa, S., Tojo, T., & Taniguchi, S. (2013). The advantages of three-dimensional culture in a collagen hydrogel for stem cell differentiation. *Journal of Biomedical Materials Research Part A, 101*(10), 2838-2845.

Nasr, M., Mansour, S., Mortada, N. D., & Elshamy, A. (2008). Vesicular aceclofenac systems: a comparative study between liposomes and niosomes. *Journal of microencapsulation, 25*(7), 499-512.

Ng, T. K., & Zeikus, J. (1981). Comparison of extracellular cellulase activities of Clostridium thermocellum LQRI and Trichoderma reesei QM9414. *Applied and environmental microbiology, 42*(2), 231-240.

Nguyen, K. T., & West, J. L. (2002). Photopolymerizable hydrogels for tissue engineering applications. *Biomaterials, 23*(22), 4307-4314.

Nguyen, T. T. T., Chung, O. H., & Park, J. S. (2011). Coaxial electrospun poly (lactic acid)/chitosan (core/shell) composite nanofibers and their antibacterial activity. *Carbohydrate Polymers, 86*(4), 1799-1806.

Novo, L. P., Bras, J., García, A., Belgacem, N., & Curvelo, A. A. (2015). Subcritical water: a method for green production of cellulose nanocrystals. *ACS Sustainable Chemistry & Engineering, 3*(11), 2839-2846.

Nwe, N., Furuike, T., & Tamura, H. (2009). The mechanical and biological properties of chitosan scaffolds for tissue regeneration templates are significantly enhanced by chitosan from Gongronella butleri. *Materials, 2*(2), 374-398.

O'brien, F. J. (2011). Biomaterials & scaffolds for tissue engineering. *Materials today, 14*(3), 88-95.

O'Toole, M. G., Henderson, R. M., Soucy, P. A., Fasciotto, B. H., Hoblitzell, P. J., Keynton, R. S., . . . Gobin, A. S. (2012). Curcumin encapsulation in submicrometer spray-dried chitosan/Tween 20 particles. *Biomacromolecules, 13*(8), 2309-2314.

Ooi, S. Y., Ahmad, I., & Amin, M. C. I. M. (2016). Cellulose nanocrystals extracted from rice husks as a reinforcing material in gelatin hydrogels for use in controlled drug delivery systems. *Industrial Crops and Products, 93*, 227-234.

Othman, S. H. (2014). Bio-nanocomposite materials for food packaging applications: types of biopolymer and nano-sized filler. *Agriculture and Agricultural Science Procedia, 2*, 296-303.

Ozdemir, E., Sendemir-Urkmez, A., & Yesil-Celiktas, O. (2013). Supercritical CO 2 processing of a chitosan-based scaffold: Can implantation of osteoblastic cells be enhanced? *The Journal of Supercritical Fluids, 75*, 120-127.

Ozioko, P., Ikeyi, A., & Ugwu, O. (2013). Review article cellulases their substrates activity and assay methods. *The Experiment, 12*(2), 778-785.

Pandit, R. S., Gaikwad, S. C., Agarkar, G. A., Gade, A. K., & Rai, M. (2015). Curcumin nanoparticles: physico-chemical fabrication and its in vitro efficacy against human pathogens. *3 Biotech, 5*(6), 991-997.

Parize, A. L., Stulzer, H. K., Laranjeira, M. C. M., Brighente, I. M. d. C., & Souza, T. C. R. d. (2012). Evaluation of chitosan microparticles containing curcumin and crosslinked with sodium tripolyphosphate produced by spray drying. *Química Nova, 35*(6), 1127-1132.

Park, M., Lee, D., & Hyun, J. (2015). Nanocellulose-alginate hydrogel for cell encapsulation. *Carbohydrate Polymers, 116*, 223-228.

Patel, V., Prajapati, B., & Patel, M. (2007). Design and characterization of chitosan-containing mucoadhesive buccal patches of propranolol hydrochloride. *Acta pharmaceutica, 57*(1), 61-72.

Patel, V. R., & Amiji, M. M. (1996). Preparation and characterization of freeze-dried chitosan-poly (ethylene oxide) hydrogels for site-specific antibiotic delivery in the stomach. *Pharmaceutical Research, 13*(4), 588-593.

Patil, S. V., Patil, S. A., & Pratap, A. P. (2016). Diester-containing zwitterionic gemini surfactants with different spacer and its impact on micellization properties and viscosity of aqueous micellar solution. *Journal of oleo science, 65*(9), 759-773.

Paula, E. L. d., Mano, V., Duek, E. A. R., & Pereira, F. V. (2015). Hydrolytic degradation behavior of plla nanocomposites reinforced with modified cellulose nanocrystals. *Química Nova, 38*(8), 1014-1020.

Pauly, M., & Keegstra, K. (2008). Cell-wall carbohydrates and their modification as a resource for biofuels. *The Plant Journal, 54*(4), 559-568.

Pawar, H., Karde, M., Mundle, N., Jadhav, P., & Mehra, K. (2014). Phytochemical evaluation and curcumin content determination of turmeric rhizomes collected

from Bhandara District of Maharashtra (India). *Medicinal Chemistry, 4*, 588-591.

Peltola, S. M., Melchels, F. P., Grijpma, D. W., & Kellomäki, M. (2008). A review of rapid prototyping techniques for tissue engineering purposes. *Annals of medicine, 40*(4), 268-280.

Pendekal, M. S., & Tegginamat, P. K. (2012). Development and characterization of chitosan-polycarbophil interpolyelectrolyte complex-based 5-fluorouracil formulations for buccal, vaginal and rectal application. *DARU Journal of Pharmaceutical Sciences, 20*(1), 67.

Peng, L., Cheng, X. R., Wang, J. W., Xu, D. X., & Wang, G. (2006). Preparation and evaluation of porous chitosan/collagen scaffolds for periodontal tissue engineering. *Journal of bioactive and compatible polymers, 21*(3), 207-220.

Petchsomrit, A., Sermkaew, N., & Wiwattanapatapee, R. (2013). Effect of alginate and surfactant on physical properties of oil entrapped alginate bead formulation of curcumin. *World Academy of Science, Engineering and Technology, International Journal of Medical, Health, Biomedical, Bioengineering and Pharmaceutical Engineering, 7*(12), 864-868.

Petchsomrit, A., Sermkaew, N., & Wiwattanapatapee, R. (2017). Alginate-based composite sponges as gastroretentive carriers for curcumin-loaded self-microemulsifying drug delivery systems. *Scientia pharmaceutica, 85*(1), 11.

Picone, C. S. F., & Cunha, R. L. (2013). Formation of nano and microstructures by polysorbate–chitosan association. *Colloids and Surfaces A: Physicochemical and Engineering Aspects, 418*, 29-38.

Piraino, F., & Selimović, Š. (2015). A current view of functional biomaterials for wound care, molecular and cellular therapies. *BioMed research international, 2015*.

Potdar, S., Grossi, F., Singh, M., Sullivan, E., Vega, C., Zhang, Z., . . . Olson, P. (2008). Collagen-based gel as a potential transscleral drug delivery system for age-related macular degeneration. *Investigative Ophthalmology & Visual Science, 49*(13), 1816-1816.

Poursamar, S. A., Hatami, J., Lehner, A. N., da Silva, C. L., Ferreira, F. C., & Antunes, A. P. M. (2015). Gelatin porous scaffolds fabricated using a modified gas foaming technique: Characterisation and cytotoxicity assessment. *Materials Science and Engineering: C, 48*, 63-70.

Prabhakar, K., Afzal, S. M., Surender, G., & Kishan, V. (2013). Tween 80 containing lipid nanoemulsions for delivery of indinavir to brain. *Acta Pharmaceutica Sinica B, 3*(5), 345-353.

Prasad, S., Tyagi, A. K., & Aggarwal, B. B. (2014). Recent developments in delivery, bioavailability, absorption and metabolism of curcumin: the golden pigment from golden spice. *Cancer research and treatment: official journal of Korean Cancer Association, 46*(1), 2-18.

Qin, Y. (2004). Absorption characteristics of alginate wound dressings. *Journal of applied polymer science, 91*(2), 953-957.

Raafat, A. I. (2010). Gelatin based pH-sensitive hydrogels for colon-specific oral drug delivery: Synthesis, characterization, and in vitro release study. *Journal of applied polymer science, 118*(5), 2642-2649.

Rahma, A., Munir, M. M., Prasetyo, A., Suendo, V., & Rachmawati, H. (2016). Intermolecular interactions and the release pattern of electrospun curcumin-polyvinyl (pyrrolidone) fiber. *Biological and Pharmaceutical Bulletin, 39*(2), 163-173.

Rahman, Z., Zidan, A. S., Habib, M. J., & Khan, M. A. (2010). Understanding the quality of protein loaded PLGA nanoparticles variability by Plackett–Burman design. *International journal of pharmaceutics, 389*(1), 186-194.

Rahmani, A. H., Alsahli, M. A., Aly, S. M., Khan, M. A., & Aldebasi, Y. H. (2018). Role of curcumin in disease prevention and treatment. *Advanced biomedical research, 7*.

Rahmi, Fathurrahmi, Irwansyah, & Purnaratrie, A. (2015). Comparative adsorption of Fe(III) and Cd(II) ions on glutaraldehyde crosslinked chitosan–coated cristobalite. *Oriental Journal of Chemistry, 31*(4), 2071-2076.

Rao, K. K., Naidu, B. V. K., Subha, M., Sairam, M., & Aminabhavi, T. (2006). Novel chitosan-based pH-sensitive interpenetrating network microgels for the controlled release of cefadroxil. *Carbohydrate Polymers, 66*(3), 333-344.

Rashmi. (2014). *Development of oral colon targeted drug delivery systems for treatment of inflammatory bowel disease characterization and evaluation (doctoral dissertation).* Shoolini University, Solan, India.

Ratanajiajaroen, P., & Ohshima, M. (2012). Synthesis, release ability and bioactivity evaluation of chitin beads incorporated with curcumin for drug delivery applications. *Journal of microencapsulation, 29*(6), 549-558.

Ratanajiajaroen, P., Watthanaphanit, A., Tamura, H., Tokura, S., & Rujiravanit, R. (2012). Release characteristic and stability of curcumin incorporated in β-chitin non-woven fibrous sheet using Tween 20 as an emulsifier. *European Polymer Journal, 48*(3), 512-523.

Ravindra, S., Mulaba-Bafubiandi, A. F., Rajinikanth, V., Varaprasad, K., Reddy, N. N., & Raju, K. M. (2012). Development and characterization of curcumin loaded silver nanoparticle hydrogels for antibacterial and drug delivery applications. *Journal of Inorganic and Organometallic Polymers and Materials, 22*(6), 1254-1262.

Reddy, N., Reddy, R., & Jiang, Q. (2015). Crosslinking biopolymers for biomedical applications. *Trends in biotechnology, 33*(6), 362-369.

Ren, T., Xu, N., Cao, C., Yuan, W., Yu, X., Chen, J., & Ren, J. (2009). Preparation and therapeutic efficacy of polysorbate-80-coated amphotericin B/PLA-b-PEG nanoparticles. *Journal of Biomaterials Science, Polymer Edition, 20*(10), 1369-1380.

Ridhima, D., Shweta, P., & Upendra, K. (2012). Formulation and evaluation of floating microspheres of curcumin. *International Journal of Pharmacy and Pharmaceutical Sciences, 4*, 334-336.

Risbud, M. V., Hardikar, A. A., Bhat, S. V., & Bhonde, R. R. (2000). pH-sensitive freeze-dried chitosan–polyvinyl pyrrolidone hydrogels as controlled release system for antibiotic delivery. *Journal of controlled release, 68*(1), 23-30.

Rizwan, M., Yahya, R., Hassan, A., Yar, M., Azzahari, A. D., Selvanathan, V., . . . Abouloula, C. N. (2017). pH sensitive hydrogels in drug delivery: Brief history, properties, swelling, and release mechanism, material selection and applications. *Polymers, 9*(4), 137.

Rodrigues, I. R., de Camargo Forte, M. M., Azambuja, D. S., & Castagno, K. R. (2007). Synthesis and characterization of hybrid polymeric networks (HPN) based on polyvinyl alcohol/chitosan. *Reactive and Functional Polymers, 67*(8), 708-715.

Rohindra, D. R., Nand, A. V., & Khurma, J. R. (2004). Swelling properties of chitosan hydrogels. *The South Pacific Journal of Natural and Applied Sciences, 22*(1), 32-35.

Roozbahani, F., Sultana, N., Almasi, D., & Naghizadeh, F. (2015). Effects of chitosan concentration on the protein release behaviour of electrospun poly (-caprolactone)/chitosan nanofibers. *Journal of Nanomaterials, 2015*, 11.

Rubentheren, V., Ward, T. A., Chee, C. Y., & Nair, P. (2015). Physical and chemical reinforcement of chitosan film using nanocrystalline cellulose and tannic acid. *Cellulose, 22*(4), 2529-2541.

Saber-Samandari, S., & Gazi, M. (2015). Pullulan based porous semi-IPN hydrogel: Synthesis, characterization and its application in the removal of mercury from aqueous solution. *Journal of the Taiwan Institute of Chemical Engineers, 51*, 143-151.

Sachlos, E., & Czernuszka, J. (2003). Making tissue engineering scaffolds work. Review: the application of solid freeform fabrication technology to the production of tissue engineering scaffolds. *Eur Cell Mater, 5*(29), 39-40.

Sadeghifar, H., Filpponen, I., Clarke, S. P., Brougham, D. F., & Argyropoulos, D. S. (2011). Production of cellulose nanocrystals using hydrobromic acid and click reactions on their surface. *Journal of materials science, 46*(22), 7344-7355.

Salernitano, E., & Migliaresi, C. (2003). Composite materials for biomedical applications: a review. *Journal of Applied Biomaterials & Biomechanics, 1*(1), 3-18.

Sarkar, A., De, R., & Mukhopadhyay, A. K. (2016). Curcumin as a potential therapeutic candidate for Helicobacter pylori associated diseases. *World journal of gastroenterology, 22*(9), 2736.

Sathali, A. A. H., & Rajalakshmi, G. (2010). Evaluation of transdermal targeted niosomal drug delivery of terbinafine hydrochloride. *Int J Pharm Tech Res, 2*(3), 2081-2089.

Sethi, S., Datta, A., Gupta, B. L., & Gupta, S. (2013). Optimization of cellulase production from bacteria isolated from soil. *ISRN biotechnology, 2013*.

Shahzad, Y., Saeed, S., Ghori, M. U., Mahmood, T., Yousaf, A. M., Jamshaid, M., . . . Rizvi, S. A. (2017). Influence of polymer ratio and surfactants on controlled drug release from cellulosic microsponges. *International journal of biological macromolecules*.

Shapiro, J. M., & Oyen, M. L. (2013). Hydrogel composite materials for tissue engineering scaffolds. *The Journal of The Minerals, Metals & Materials Society, 65*(4), 505-516.

She, Z., Jin, C., Huang, Z., Zhang, B., Feng, Q., & Xu, Y. (2008). Silk fibroin/chitosan scaffold: preparation, characterization, and culture with HepG2 cell. *Journal of Materials Science: Materials in Medicine, 19*(12), 3545-3553.

Shen, X., Shamshina, J. L., Berton, P., Gurau, G., & Rogers, R. D. (2016). Hydrogels based on cellulose and chitin: fabrication, properties, and applications. *Green Chemistry, 18*(1), 53-75.

Shi, X., Zhou, W., Ma, D., Ma, Q., Bridges, D., Ma, Y., & Hu, A. (2015). Electrospinning of nanofibers and their applications for energy devices. *Journal of Nanomaterials, 2015*, 122.

Shivashankar, M., & Mandal, B. K. (2012). A review on interpenetrating polymer network. *International Journal of Pharmacy and Pharmaceutical Sciences, 4*(5), 1-7.

Shoulders, M. D., & Raines, R. T. (2009). Collagen structure and stability. *Annual review of biochemistry, 78*, 929.

Singh, V., & Singh, D. (2014). An overview on the preparation, characterization and properties of electrodeposited-metal matrix nanocomposites. *Nanoscience & Technology, 1*(3), 1-20.

Sivashankari, P., & Prabaharan, M. (2016). Prospects of chitosan-based scaffolds for growth factor release in tissue engineering. *International journal of biological macromolecules, 93*, 1382–1389.

Sobral, J. M., Caridade, S. G., Sousa, R. A., Mano, J. F., & Reis, R. L. (2011). Three-dimensional plotted scaffolds with controlled pore size gradients: effect of scaffold geometry on mechanical performance and cell seeding efficiency. *Acta biomaterialia, 7*(3), 1009-1018.

Spagnol, C., Rodrigues, F. H., Pereira, A. G., Fajardo, A. R., Rubira, A. F., & Muniz, E. C. (2012). Superabsorbent hydrogel composite made of cellulose nanofibrils and chitosan-graft-poly (acrylic acid). *Carbohydrate Polymers, 87*(3), 2038-2045.

Stanek, M., Manas, D., Manas, M., Navratil, J., Kyas, K., Senkerik, V., & Skrobak, A. (2012). Comparison of different rapid prototyping methods. *International journal of mathematics and computers in simulation, 6*, 550-557.

Subramanian, A., & Lin, H. Y. (2005). Crosslinked chitosan: its physical properties and the effects of matrix stiffness on chondrocyte cell morphology and proliferation. *Journal of Biomedical Materials Research Part A, 75*(3), 742-753.

Sullivan, E. M., Moon, R. J., & Kalaitzidou, K. (2015). Processing and characterization of cellulose nanocrystals/polylactic acid nanocomposite films. *Materials, 8*(12), 8106-8116.

Sultana, N., & Wang, M. (2008). Fabrication of HA/PHBV composite scaffolds through the emulsion freezing/freeze-drying process and characterisation of the scaffolds. *Journal of Materials Science: Materials in Medicine, 19*(7), 2555-2561.

Sultana, N., & Wang, M. (2012). Fabrication of tissue engineering scaffolds using the emulsion freezing/freeze-drying technique and characteristics of the scaffolds. *Integrated Biomaterials in Tissue Engineering*, 63-89.

Sundararaghavan, H. G., Metter, R. B., & Burdick, J. A. (2010). Electrospun fibrous scaffolds with multiscale and photopatterned porosity. *Macromolecular bioscience, 10*(3), 265-270.

Synytsya, A., & Novak, M. (2014). Structural analysis of glucans. *Annals of translational medicine, 2*(2), 17-17.

Szymańska, E., & Winnicka, K. (2015). Stability of chitosan—a challenge for pharmaceutical and biomedical applications. *Marine drugs, 13*(4), 1819-1846.

Tan, X. Y., Hamid, S. B. A., & Lai, C. W. (2015). Preparation of high crystallinity cellulose nanocrystals (CNCs) by ionic liquid solvolysis. *Biomass and Bioenergy, 81*, 584-591.

Tanpichai, S., & Oksman, K. (2016). Cross-linked nanocomposite hydrogels based on cellulose nanocrystals and PVA: Mechanical properties and creep recovery. *Composites Part A: Applied Science and Manufacturing, 88*, 226-233.

Thakur, A., Monga, S., & Wanchoo, R. (2014). Sorption and drug release studies from semi-interpenetrating polymer networks of chitosan and xanthan gum. *Chemical and Biochemical Engineering Quarterly, 28*(1), 105-115.

Tian, Z., Liu, W., & Li, G. (2016). The microstructure and stability of collagen hydrogel cross-linked by glutaraldehyde. *Polymer Degradation and Stability, 130*, 264-270.

Tønnesen, H. H., & Karlsen, J. (1985). Studies on curcumin and curcuminoids. *Zeitschrift für Lebensmittel-Untersuchung und Forschung, 180*(5), 402-404.

Torabi, K., Farjood, E., & Hamedani, S. (2014). Rapid prototyping technologies and their applications in prosthodontics, a review of literature. *Journal of Dentistry, Shiraz University of Medical Sciences, 1*(1), 1-9.

Treesinchai, S., Puttipipatkhachorn, S., Pitaksuteepong, T., & Sungthongjeen, S. (2016). Development of curcumin floating tablets based on low density foam powder. *asian journal of pharmaceutical sciences, 11*(1), 130-131.

Ullah, A., Kim, C. M., & Kim, G. M. (2018). Porous polymer coatings on metal microneedles for enhanced drug delivery. *Royal Society open science, 5*(4), 171609.

Usov, I., Nyström, G., Adamcik, J., Handschin, S., Schütz, C., Fall, A., . . . Mezzenga, R. (2015). Understanding nanocellulose chirality and structure-properties relationship at the single fibril level. *Nature communications, 6*.

Van Toan, N., & Hanh, T. T. (2013). Application of chitosan solutions for rice production in Vietnam. *African Journal of Biotechnology, 12*(4).

Vasconcelos, A., Gomes, A. C., & Cavaco-Paulo, A. (2012). Novel silk fibroin/elastin wound dressings. *Acta biomaterialia, 8*(8), 3049-3060.

Vazquez, O. R., Avila, I. O., Díaz, J. C. S., & Hernandez, E. (2016). An overview of mechanical tests for polymeric biomaterial scaffolds used in tissue engineering. *Journal of Research Updates in Polymer Science, 4*(4), 168-178.

Venkatesan, J., Jayakumar, R., Mohandas, A., Bhatnagar, I., & Kim, S.-K. (2014). Antimicrobial activity of chitosan-carbon nanotube hydrogels. *Materials, 7*(5), 3946-3955.

Verma, D., Gope, P., Maheshwari, M., & Sharma, R. (2012). Bagasse fiber composites-A review. *Journal of Materials and Environmental Science, 3*(6), 1079-1092.

Vroman, I., & Tighzert, L. (2009). Biodegradable polymers. *Materials, 2*(2), 307-344.

Wang, H., & Roman, M. (2011). Formation and properties of chitosan− cellulose nanocrystal polyelectrolyte− macroion complexes for drug delivery applications. *Biomacromolecules, 12*(5), 1585-1593.

Wang, X., Sang, L., Luo, D., & Li, X. (2011). From collagen–chitosan blends to three-dimensional scaffolds: the influences of chitosan on collagen nanofibrillar structure and mechanical property. *Colloids and Surfaces B: Biointerfaces, 82*(1), 233-240.

Wang, Z., Hu, Q., & Cai, L. (2010). Chitin fiber and chitosan 3D composite rods. *International Journal of Polymer Science, 2010*.

Wegiel, L. A., Zhao, Y., Mauer, L. J., Edgar, K. J., & Taylor, L. S. (2014). Curcumin amorphous solid dispersions: the influence of intra and intermolecular bonding on physical stability. *Pharmaceutical development and technology, 19*(8), 976-986.

Wei, G., & Ma, P. X. (2004). Structure and properties of nano-hydroxyapatite/polymer composite scaffolds for bone tissue engineering. *Biomaterials, 25*(19), 4749-4757.

Wen, Y., Li, F., Li, C., Yin, Y., & Li, J. (2017). High mechanical strength chitosan-based hydrogels cross-linked with poly (ethylene glycol)/polycaprolactone micelles for the controlled release of drugs/growth factors. *Journal of Materials Chemistry B, 5*(5), 961-971.

Weng, L., Chen, X., & Chen, W. (2007). Rheological characterization of in situ crosslinkable hydrogels formulated from oxidized dextran and N-carboxyethyl chitosan. *Biomacromolecules, 8*(4), 1109-1115.

Whang, K., Thomas, C., Healy, K., & Nuber, G. (1995). A novel method to fabricate bioabsorbable scaffolds. *Polymer, 36*(4), 837-842.

Wong, R. S. H., & Dodou, K. (2017). Effect of drug loading method and drug physicochemical properties on the material and drug release properties of poly (ethylene oxide) hydrogels for transdermal delivery. *Polymers, 9*(7), 286.

Xing, Q., Yates, K., Vogt, C., Qian, Z., Frost, M. C., & Zhao, F. (2014). Increasing mechanical strength of gelatin hydrogels by divalent metal ion removal. *Scientific reports, 4*, 4706.

Yadav, K. H., Satish, C., & Shivakumar, H. (2007). Preparation and evaluation of chitosan-poly (acrylic acid) hydrogels as stomach specific delivery for amoxicillin and metronidazole. *Indian journal of pharmaceutical sciences, 69*(1), 91.

Yadav, V. R., Suresh, S., Devi, K., & Yadav, S. (2009). Effect of cyclodextrin complexation of curcumin on its solubility and antiangiogenic and anti-inflammatory activity in rat colitis model. *American Association of Pharmaceutical Scientists Pharmscitech, 10*(3), 752.

Yan, H., Huang, D., Chen, X., Liu, H., Feng, Y., Zhao, Z., . . . Lin, Q. (2017). A novel and homogeneous scaffold material: preparation and evaluation of alginate/bacterial cellulose nanocrystals/collagen composite hydrogel for tissue engineering. *Polymer Bulletin*, 1-16.

Yang, H. C., Wu, Q. Y., Liang, H. Q., Wan, L. S., & Xu, Z. K. (2013). Thermally induced phase separation of poly (vinylidene fluoride)/diluent systems: Optical microscope and infrared spectroscopy studies. *Journal of Polymer Science Part B: Polymer Physics, 51*(19), 1438-1447.

Yang, J., Han, C.-R., Duan, J.-F., Ma, M.-G., Zhang, X.-M., Xu, F., . . . Xie, X.-M. (2012). Studies on the properties and formation mechanism of flexible nanocomposite hydrogels from cellulose nanocrystals and poly (acrylic acid). *Journal of Materials Chemistry, 22*(42), 22467-22480.

Yang, J. M., & Su, W. Y. (2011). Preparation and characterization of chitosan hydrogel membrane for the permeation of 5-Fluorouracil. *Materials Science and Engineering: C, 31*(5), 1002-1009.

Yang, S., Leong, K.-F., Du, Z., & Chua, C.-K. (2001). The design of scaffolds for use in tissue engineering. Part I. Traditional factors. *Tissue engineering, 7*(6), 679-689.

Yang, X., Bakaic, E., Hoare, T., & Cranston, E. D. (2013). Injectable polysaccharide hydrogels reinforced with cellulose nanocrystals: morphology, rheology, degradation, and cytotoxicity. *Biomacromolecules, 14*(12), 4447-4455.

Yao, K. D., Liu, J., Cheng, G. X., Zhao, R. Z., Wang, W. H., & Wei, L. (1998). The dynamic swelling behaviour of chitosan-based hydrogels. *Polymer international, 45*(2), 191-194.

Yassin, A. E. B., Alsarra, I. A., & Al-Mohizea, A. M. (2006). Chitosan beads as a new gastroretentive system of verapamil. *Scientia pharmaceutica, 74*(4), 175.

Yi, H., Wu, L.-Q., Bentley, W. E., Ghodssi, R., Rubloff, G. W., Culver, J. N., & Payne, G. F. (2005). Biofabrication with chitosan. *Biomacromolecules, 6*(6), 2881-2894.

Youn, D. K., No, H. K., & Prinyawiwatkul, W. (2013). Preparation and characteristics of squid pen β-chitin prepared under optimal deproteinisation and demineralisation condition. *International Journal of Food Science & Technology, 48*(3), 571-577.

Yuan, Y., Chesnutt, B. M., Haggard, W. O., & Bumgardner, J. D. (2011). Deacetylation of chitosan: Material characterization and in vitro evaluation via albumin adsorption and pre-osteoblastic cell cultures. *Materials, 4*(8), 1399-1416.

Zali, H., Rezaei-Tavirani, M., & Azodi, M. (2011). Gastric cancer: prevention, risk factors and treatment. *Gastroenterology and Hepatology from bed to bench, 4*(4), 175.

Zamani, A., & Taherzadeh, M. J. (2012). Production of superabsorbents from fungal chitosan. *Iranian polymer journal, 21*(12), 845-853.

Zang, S., Liu, T., Shi, J., & Qiao, L. (2014). Curcumin: a promising agent targeting cancer stem cells. *Anti-Cancer Agents in Medicinal Chemistry (Formerly Current Medicinal Chemistry-Anti-Cancer Agents), 14*(6), 787-792.

Zeng, Q., Desai, M. S., Jin, H.-E., Lee, J. H., Chang, J., & Lee, S.-W. (2016). Self-healing elastin–bioglass hydrogels. *Biomacromolecules, 17*(8), 2619-2625.

Zhang, P., Chen, L., Zhang, Q., & Hong, F. F. (2016). Using in situ dynamic cultures to rapidly biofabricate fabric-reinforced composites of chitosan/bacterial nanocellulose for antibacterial wound dressings. *Frontiers in microbiology, 7*.

Zhang, Y., Feng, Y., Huang, Z., Ramakrishna, S., & Lim, C. T. (2006). Fabrication of porous electrospun nanofibres. *Nanotechnology, 17*(3), 901-908.

Zhang, Y. N., Avery, R. K., Vallmajo-Martin, Q., Assmann, A., Vegh, A., Memic, A., . . . Khademhosseini, A. (2015). A highly elastic and rapidly crosslinkable elastin-like polypeptide-based hydrogel for biomedical applications. *Advanced functional materials, 25*(30), 4814-4826.

Zhang, Z., Wu, Q., Song, K., Lei, T., & Wu, Y. (2015). Poly (vinylidene fluoride)/cellulose nanocrystals composites: rheological, hydrophilicity, thermal and mechanical properties. *Cellulose, 22*(4), 2431-2441.

Zhao, X., Lang, Q., Yildirimer, L., Lin, Z. Y., Cui, W., Annabi, N., . . . Khademhosseini, A. (2016). Photocrosslinkable gelatin hydrogel for epidermal tissue engineering. *Advanced healthcare materials, 5*(1), 108-118.

Zhao, Z., Xie, M., Li, Y., Chen, A., Li, G., Zhang, J., . . . Li, S. (2015). Formation of curcumin nanoparticles via solution-enhanced dispersion by supercritical CO2. *International journal of nanomedicine, 10*, 3171.

Zhou, T., Wang, X., Gu, M., & Xiong, D. (2009). Study on mechanical, thermal and electrical characterizations of nano-SiC/epoxy composites. *Polymer journal, 41*(1), 51-57.

Zhou, Y., Fu, S., Zhang, L., Zhan, H., & Levit, M. V. (2014). Use of carboxylated cellulose nanofibrils-filled magnetic chitosan hydrogel beads as adsorbents for Pb (II). *Carbohydrate Polymers, 101*, 75-82.

Zhu, N., Li, M., Cooper, D., & Chen, X. (2011). Development of novel hybrid poly (L-lactide)/chitosan scaffolds using the rapid freeze prototyping technique. *Biofabrication, 3*(3), 034105.

Zorofchian Moghadamtousi, S., Abdul Kadir, H., Hassandarvish, P., Tajik, H., Abubakar, S., & Zandi, K. (2014). A review on antibacterial, antiviral, and antifungal activity of curcumin. *BioMed research international, 2014*.

Zsila, F., Bikádi, Z., & Simonyi, M. (2004). Circular dichroism spectroscopic studies reveal pH dependent binding of curcumin in the minor groove of natural and synthetic nucleic acids. *Organic & biomolecular chemistry, 2*(20), 2902-2910.

LIST OF PUBLICATIONS AND PAPERS PRESENTED

Sampath, U. G., Ching, Y. C., Chuah, C. H., Sabariah, J. J., & Lin, P.-C. (2016). Fabrication of porous materials from natural/synthetic biopolymers and their composites. *Materials, 9*(12), 991.

Sampath, U. T. M., Ching, Y. C., Chuah, C. H., Singh, R., & Lin, P.-C. (2017). Preparation and characterization of nanocellulose reinforced semi-interpenetrating polymer network of chitosan hydrogel. *Cellulose, 24*(5), 2215-2228.

Udeni Gunathilake, T. M. S., Ching, Y. C., & Chuah, C. H. (2017). Enhancement of curcumin bioavailability using nanocellulose reinforced chitosan hydrogel. *Polymers, 9*(2), 64.

Udeni Gunathilake, T.; Ching, Y.C.; Ching, K.Y.; Chuah, C.H.; Abdullah, L.C. (2017). Biomedical and microbiological applications of bio-based porous materials: A review. *Polymers*, *9*, 160.

Gunathilake, T. M. S. U., Ching, Y. C., Chuah, C. H., Illias, H. A., Ching, K. Y., Singh, R., & Nai-Shang, L. (2018). Influence of a nonionic surfactant on curcumin delivery of nanocellulose reinforced chitosan hydrogel. International journal of biological macromolecules, 118, 1055-1064.

Gunathilake, T. M. S. U., Ching, Y. C., Chuah, C. H. (2016, October). *Some studies of nanocellulose reinforcement in chitosan hydrogel*. Poster session presented at the Oils and Fat International Congress, Kuala Lumpur, Malayasia.